Melt-rock interactions and melt-assisted deformation in the Lherz peridodite, with implications for the structural, chemical and isotopic evolution of the lithospheric mantle

Véronique Le Roux

UNIVERSITÉ MONTPELLIER II
SCIENCES ET TECHNIQUES DU LANGUEDOC

THÈSE

Pour obtenir le grade de

DOCTEUR DE L'UNIVERSITÉ MONTPELLIER II

Discipline : Structure et évolution de la Terre et des autres planètes
École Doctorale : SIBAGHE

Présentée et soutenue publiquement

Par

VÉRONIQUE LE ROUX

Le 7 novembre 2008

MELT-ROCK INTERACTIONS AND MELT-ASSISTED DEFORMATION IN THE LHERZ PERIDOTITE, WITH IMPLICATIONS FOR THE STRUCTURAL, CHEMICAL AND ISOTOPIC EVOLUTION OF THE LITHOSPHERIC MANTLE

JURY

M. Jean-Louis Bodinier	Directeur de Recherche (CNRS UMII)	Directeur de thèse
M. Alain Vauchez	Maître de Conférences (UM II)	Co-directeur de thèse
Mme Suzanne Y. O'Reilly	Professeur (Macquarie University)	Co-directrice de thèse
M. Michel Grégoire	Chargé de Recherche (Obs. Midi. Pyr.)	Rapporteur
M. Ben Holtzman	Docteur (Columbia University)	Rapporteur
Mme Andréa Tommasi	Directeur de Recherche (CNRS UMII)	Examinateur
M. Francis Albarède	Professeur (ENS Lyon)	Examinateur
M. Jean-Pierre Lorand	Directeur de Recherche (Muséum, Paris)	Examinateur

The most exciting phrase to hear in science, the one that heralds new discoveries, is not “Eureka!” (I've found it!), but “That's funny...”

Isaac Asimov

TABLE OF CONTENTS

ABSTRACT

Differentiation of the lithospheric mantle occurred principally through partial melting and extraction of basaltic melt. In this scheme, harzburgites are widely considered as refractory mantle residues left after extraction of a basaltic component, whereas fertile lherzolites are regarded as pristine mantle only weakly affected by partial melting. However, a part of tectonically-emplaced mantle rocks displays local evidence of melt percolation and have been ascribed to igneous refertilization of refractory peridotites. In this context, the present work re-investigates the nature of the Lherz spinel lherzolites (French Pyrenees), from the type-locality of lherzolites, described as a piece of preserved fertile mantle. Structural and geochemical data presented in this study show that the Lherz lherzolites are not pristine but formed through a refertilization reaction between MORB-like ascending partial melts and a depleted lithosphere from which the Lherz harzburgites are the remnants. As the type locality of lherzolites, the Lherz peridotites were partly used to infer the composition of the primitive upper mantle and these results may have important implications for the nature of the late veneer. Additionally, the analysis of crystal-preferred orientations (CPO) of minerals from Lherz peridotites highlight a strong feedback between percolation of basaltic melts and deformation under near-solidus conditions at the lithosphere-asthenosphere boundary, suggesting that refertilization may be a major process involved in the rejuvenation of the lithosphere. Variations in CPO patterns and intensity record the relative contribution of dislocation glide and diffusion processes, ruled by a balance between instantaneous melt fraction and local strain rate. These results also suggest that the pervasive websteritic layering that formed synchronous to the refertilized lherzolites may result from deformation-assisted melt segregation due to decreasing permeability in the system. Finally, this work investigated the effect of melt percolation on Hf, Nd and Sr isotopic variations. Isotope systematics of the Lherz peridotites shows that a strong isotopic decoupling may arise at the melt percolation front between depleted harzburgite and refertilized lherzolite. The one-dimensional modelling used shows that these decoupled signatures are generated by porous flow and governed by critical parameters such as the concentrations of the elements in the melt to the matrix, chemical diffusivities or efficiency of isotopic homogenization. We observe that, under certain circumstances, melt-rock interactions can generate enriched, “intraplate-like” isotopic signatures in the transition zone between upwelling partial melts and lithospheric mantle. These results suggest that a part of isotopic signatures of mantle-related rocks could be generated by diffusional processes associated with melt transport.

DECLARATION

This thesis is a cotutelle work carried out in University of Montpellier II, France, and in Macquarie University, Australia, over the period October 2005 to October 2008. I hereby declare that all data and interpretations presented in this thesis are my own work except for information cited from published or unpublished work of others that has been fully acknowledged. No part of this thesis has been submitted at any other university than Macquarie University.

Veronique Le Roux

1st of December 2008

Acknowledgments

This thesis results from the collaboration between Geosciences Montpellier (France) and GEMOC ARC National Key Centre (Australia). This work has been supported by INSU DYETI Program, University of Montpellier II, Macquarie University, ARC Discovery project grants, the French Ministry of Research and 'Bourses Lavoisier cotutelle'.

I want to thank all the people who have been implicated in my work during these three years, and particularly my official supervisors Jean-Louis Bodinier, Alain Vauchez and Suzanne O'Reilly. I am also grateful to Andrea Tommasi and Olivier Alard who were involved in some parts of my project.

Thanks a lot to the staff in Geosciences Montpellier (particularly Claude Merlet, Olivier Bruguier and Simone Pourtales) and in GEMOC ARC National Key Centre (particularly Peter Wieland and Norman Pearson) for their help on technical and analytical aspects.

Last but not least I want to thank all the PhD students, post-docs and researchers in Montpellier and in Sydney for the good moments that I spent in their company, and my family and my friends for their support.

~

I finally want to thank the jury who accepted to evaluate this work.

Remerciements

Par ces quelques lignes je tiens à remercier les principales personnes qui ont contribué à ce travail de recherche, et ceux qui m'ont soutenue et encouragée durant ces trois années.

Je pense tout d'abord à **Jean-Louis Bodinier**. Je le remercie pour son enseignement, pour m'avoir accordé sa confiance en me permettant de réaliser ce travail, et pour m'avoir laissé une grande liberté d'expression.

Je remercie très chaleureusement **Alain Vauchez** et **Andréa Tommasi** pour leurs conseils, leur efficacité et leur soutien. La confiance qu'ils m'ont accordée au fil du temps a été une vraie récompense en soi.

Pour nos discussions et pour son aide, je tiens à remercier **Olivier Alard**, toujours d'une grande disponibilité.

Je remercie également techniciens, ingénieurs et secrétaires. Je pense particulièrement à **Christophe Nevado**, **Doriane Delmas**, **Olivier Bruguier**, **Simone Pourtalès** et **Claude Merlet**. Je repense également à ces moments de réconfort apportés par 'maman' **Bernadette Marie** et au sourire radieux de **Marie-France Roch**.

La présence dans le laboratoire de **Marion Drouin**, **Andreas Wüstefeld** et **Riccardo Vassallo** a été un soutien énorme au quotidien et ils savent à quel point je tiens à eux. Je pense également à **Nicolas Le Moigne, Sébastien Van Gorp**, **Mary-Alix Kaczmarek**, **Stéphanie Bordelais** et **Caroline Dewonck** pour tous les bons moments partagés au cours de cette période montpelliéraine. Bien entendu un grand merci à tous les thésards et ingénieurs de Géosciences (**Fab**, **Lyd**, **Flo**, **les Mickaël**, **Eric**, **Tom**, **Titou**, **Bruno** etc.) pour avoir partagé les repas

gastronomiques du RU et les diverses soirées ensemble. Un merci à **Vio** pour ces moments de co-bureau bien sympas…

Par la même occasion, il m'est indispensable de remercier **Jean-Marie Dautria** et **Michel Lopez**, avec qui j'ai partagé avec grand plaisir les principales heures d'enseignement de mon monitorat.

Je n'oublierai pas non plus les Ariégeois, qui m'ont accueillie lors de mes missions terrain, je pense particulièrement à **Pascale & Camille Coutanceau** et à **Catherine & Denis Mange**, les tenanciers de la mythique 'Auberge du Gypaète Barbu' (à Biert, pour la pub).

Mon séjour en Australie aura duré un peu plus de 6 mois, durant lesquels j'ai pu m'initier aux joies de la géochimie isotopique et apprécier l' « Australian way of life ». Je remercie ceux qui m'ont aidé financièrement à savoir le laboratoire GEMOC ARC National Key Centre en les personnes de **Suzanne O'Reilly** et **Bill Griffin**, les Bourses Lavoisier Cotutelle et le Ministère de la Recherche. Je remercie Sue et Bill pour leur accueil et pour m'avoir laissé une grande liberté d'action sur les machines. Pour tous les aspects techniques de mon travail, j'ai une grande reconnaissance envers **Peter Wieland** qui m'a initiée à la chimie des isotopes en salle blanche. Je remercie très amicalement **Norman Pearson** pour son aide sur les aspects analytiques et pour sa gentillesse. Pour avoir partagé la bière du vendredi soir et de nombreuses soirées poker ou BBQ, je remercie **Lee & Cara Donnelly**, **Alan & Melissa Kobussen**, **Weiqiang Li**, **Marek Locmelis**, **Olivia Wang**. Sans oublier la « french connection » et particulièrement **Alex Corgne** pour son aide au tout début de mon séjour et **June Chevet** pour sa bonne humeur permanente.

Je veux remercier mes amis de Nantes, et particulièrement **Maud Rajeau** et **Elsa Jourd'heuil** pour leur soutien. Un énorme merci à mes amis des années fac de Nantes, qui m'ont permis de me 'couper' des préoccupations de ma thèse: **Benjamin Bonnefoy**, **Aurélien Delaunay**, **Hélène & Sébastien Dulais**, **Antoine Lucas**, **Sabrina Havard**, **Samuel Toucanne**.

Egalement issu de la promo de Nantes et oreille attentive de tous les instants, je me dois de faire un special highlight sur **François Deschamps**, un ami inclassable avec qui j'ai dû battre le record du monde du papotage au téléphone.

Je remercie évidemment mes grands-parents, **Guéna**, mes grands frères **Stéphane** et **Damien,** ainsi que mes parents pour leurs encouragements à distance et leur soutien lorsque j'en ai eu besoin.

Finally, I want to thank the man who shares my life and supports me whatever it happens.

~

Je tiens par ailleurs à remercier mon jury qui a accepté d'évaluer ce travail.

Chapter I: Introduction

1. General Introduction

Mantle rocks that outcrop at the Earth's surface provide a direct source of information on the composition and evolution of the Earth's upper mantle. Until recently, the fertile lherzolites were generally regarded as pristine mantle, only weakly affected by partial melting (Frey et al., 1985; McDonough and Frey, 1989). Therefore, they have been used to infer the composition of the Earth's primitive mantle, i.e. the Earth's mantle before the extraction of the crust (Goldschmidt, 1929; Jagoutz et al., 1979; McDonough and Sun, 1995; Palme and O'Neill, 2003; Ringwood, 1975). Together with chondrites, the Lherz lherzolites have therefore contributed to the debate on Earth composition and differentiation.

However, some of the tectonically-emplaced mantle rocks are actually ascribed to igneous refertilization of refractory peridotites rather than to partial melting (Elthon, 1992; Müntener et al., 2004; Nicolas and Dupuy, 1984; Rampone et al., 1994). The refertilization process is a process whereby refractory mantle rocks previously depleted in basaltic components - during one or several melt extraction events - are re-enriched (re-fertilized) by basaltic melt percolation (Menzies et al., 1987). The refertilization process may either be viewed as melt entrapment followed by solidification (i.e. "impregnation") or as a melt-rock reaction at decreasing melt mass between peridotite and percolating melt. The refertilization may also be considered as a form of mantle metasomatism. However, the word "metasomatism" is more widely used to define mantle processes involving strong chemical disequilibrium between melt and fluids, marked by a selective enrichment in certain major or trace elements like Fe, Ti (Menzies, 1983), LILE, and LREE (Dawson, 1984), or in accessory minerals such as amphibole, mica or rutile (Harte, 1983).

Textural or chemical evidence for local refertilization has been mainly observed in plagioclase peridotites from ophiolitic (Barth et al., 2003; Dijkstra et al., 2001; Takazawa et al., 2003), abyssal (Elthon, 1992; Luguet et al., 2001; Paulick et al., 2006; Seyler et al., 2001) and orogenic mantle suites (Müntener et al., 2004; Nicolas and Dupuy, 1984; Piccardo et al., 2004; Rampone et al., 1997; Rampone et al., 1994; Saal et al., 2001). Refertilization was less commonly observed in spinel and garnet peridotites. In the Ronda massif (Spain), a significant part of the spinel lherzolites has been ascribed to the refertilization of subcontinental lithosphere by kilometer-scale porous melt flow (Garrido and Bodinier, 1999; Lenoir et al., 2001; Van der Wal and Bodinier, 1996). Rampone et al. (2008) also recently showed that spinel and plagioclase peridotites from the Mt. Maggiore (Corsica) underwent melt-rock reaction and melt impregnation, respectively, depending on the lithospheric depths at which interaction occurred. Likewise, garnet peridotites from the Western Gneiss Region (Norway) were recently reinterpreted as formed by refertilization of a dunitic Archean lithospheric mantle (Beyer et al., 2004; Beyer et al., 2006). In addition to tectonically-emplaced mantle rocks, an increasing set of observations on mantle xenoliths further strengthen the hypothesis that the refertilization process may be widespread in the mantle (Carlson et al., 2004; Downes et al., 2006; Tang et al., 2008).

In the large Ronda massif (300 km2), the refertilization is associated to a melting front, that led to asthenospherization and attenuation of the lithospheric mantle (Garrido and Bodinier, 1999; Vauchez and Garrido 2001; Lenoir et al., 2001; Van der Wal and Bodinier, 1996). Likewise, the refertilization in Lanzo has been ascribed to the ‘asthenospherization’ of subcontinental lithospheric mantle by upwelling asthenospheric melts during the early stages of oceanisation (Müntener et al., 2004). Some authors have suggested that the presence of melt can weaken the lower lithosphere and accommodate its removal by mantle convection, initiating feedback processes and involving further thermo-chemical erosion.

The coexistence of depleted and fertile mantle rocks can be explained by different processes such as partial melting (e.g. Frey et al.,1985), melt-rock reactions (e.g. Downes 1991; Kelemen, 1995) or convective mingling (Bodinier and Godard, 2003). The Lherz massif, type-locality of lherzolites, has been described as a piece of preserved fertile mantle. However, the structural and chemical constraints provided by previous studies were insufficient to assess the mode of formation of the lherzolites-harzburgites alternations. The present work aims to re-investigate the Lherz massif peridotites, located in the French Pyrenees. At the end of 18th century, De La Méthérie proposed the term "lherzolite", though he did not know at that time the precise mineralogical composition of the rock. The Lherz lherzolites were then successively investigated by Lacroix (1917), Ave Lallemant (1967) and Conquéré (1978). For many decades the massif has been an inspiring source of debates, notably concerning melt processes in the mantle (Bodinier et al., 1988; Bodinier et al., 1987a; Bodinier et al., 2004; Bodinier et al., 1990; Burnham et al., 1998; Chaussidon and Lorand, 1990; Deloule et al., 1991; Downes et al., 1991; Fabriès et al., 1998; Fabriès et al., 1991; Hamelin and Allègre, 1988; Lorand, 1989; Lorand, 1991; Loubet and Allègre, 1982; McPherson et al., 1996; Mukasa et al., 1991; Pattou et al., 1996; Polvé and Allègre, 1980; Reisberg and Lorand, 1995; Woodland et al., 1996; Zanetti et al., 1996). So far, the Lherz lherzolites were traditionally considered as pristine rocks, close to the primitive mantle. The pristine origin of the lherzolites was commonly accepted and the chemical trends from lherzolites to harzburgites were generally attributed to partial melting. However in the Lherz massif, fertile lherzolites and depleted harzburgites are intermingled at the scale of tens of meters (Avé Lallemant, 1967; Conquéré, 1978; Conquéré and Fabriès, 1984; Fabriès et al., 1991) but show distinct isotopic signatures that are not consistent with a simple partial melting process (Bodinier and Godard, 2003; Downes et al., 1991). Downes et al. (1991) proposed that the harzburgites were selectively percolated by enriched melts whereas

Bodinier and Godard (2003) interpreted the harzburgites as lithospheric strips incompletely mixed with pristine asthenospheric lherzolites during thermo-mechanical erosion of the lithosphere by upwelling mantle. However, previous structural maps of the Lherz massif did not detail the inner deformation structures of harzburgites and lherzolites (Avé Lallemant, 1967; Conquéré, 1978). Thus to examine the different hypotheses, the first step of this study consisted in a detailed structural mapping of the Lherz ultramafic complex. This was the starting point of this work.

2. Geological setting of the Lherz massif

The Pyrenean peridotite massifs occur as restricted bodies scattered across Mesozoic sediments along the North Pyrenean Fault (NPF; Fig. 1). More than 40 peridotite massifs have been listed in the Pyrenees, with dimensions varying from several m^2 to 1 km^2 for the Lherz massif (Fabriès et al., 1991; Monchoux, 1971). Additionally, some large massifs (2 x 3 km) crop out farther to the west (Fabriès et al., 1998). The Pyrenean orogenic peridotites are distributed in seven groups. To the east, the Salvezines, Prades-Bestiac, Vicdessos-Lherz, and Castillon groups form the eastern Pyrenean massifs. The Tuc Desse-Arguenos, Avezac-Moncaut and Turon de Técouère-Col d'Urdach groups form the central and western Pyrenean peridotite massifs

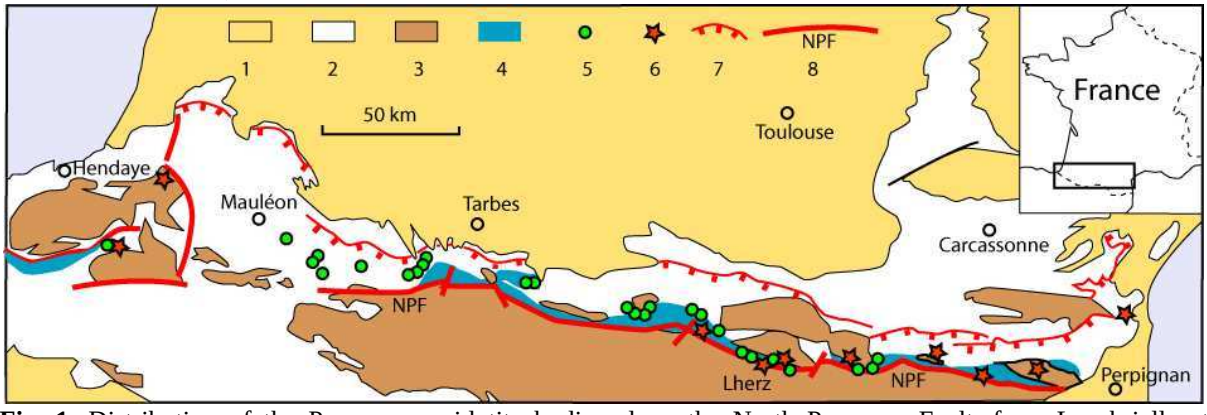

Fig. 1: Distribution of the Pyrenean peridotite bodies along the North Pyrenean Fault, from Lagabrielle et Bodinier (2008) after Choukroune (1978). 1: Oligocene and post-Oligocene sediments; 2: Mesozoic and Eocene sediments; 3: Paleozoic basement; 4: area of LP-HT Pyrenean metamorphism; 5: lherzolite bodies; 6: granulites; 7: main thrusts external zones; 8: North Pyrenean Fault.

Pyrenean peridotites are generally embedded in sedimentary basins made of voluminous detrital formations (flyschs) related to tectonic instabilities and sedimentary transport. The North Pyrenean Metamorphic Zone (NPMZ) is a narrow (0-5 km wide) band of Mesozoic carbonate sediments of Jurassic to Aptian age (Fig. 3) affected by a low pressure – high temperature metamorphism (Golberg and Leyreloup, 1990) dated between 110 and 85 Ma, with a peak at 95Ma (Albarède and Michard-Vitrac, 1978; Golberg and Maluski, 1988; Golberg et al., 1986; Montigny et al., 1986). The NPMZ also contains lenses of granulites (Azambre and Ravier, 1978; Vielzeuf and Kornprobst, 1984), breccias, and granulated agglomerates that contain a large variety of metamorphic minerals such as kornerupine, sapphirine, corundum, phlogopite or cordierite (Monchoux, 1972).

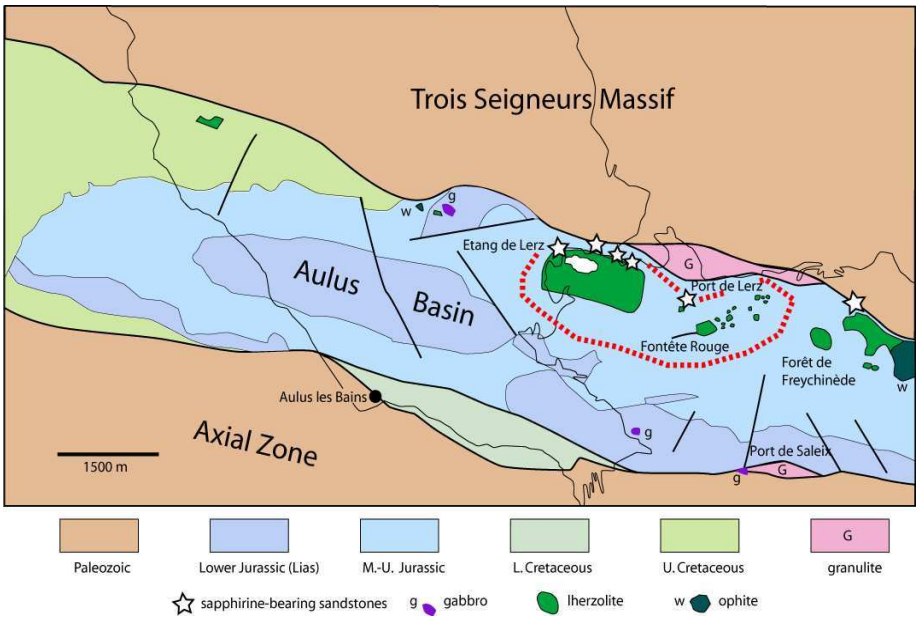

Fig. 2: Simplified geological map of the Aulus-Lherz region redrawn by Lagabrielle and Bodinier (2008) after Vielzeuf and Kornprobst (1984) and Colchen et al. (1997). Thick dotted line delineates the region of polymictic debris-flow deposits (Lagabrielle and Bodinier, 2008). Hatched area represents the region north of the main ultramafic bodies, where strongly deformed Mesozoic sediments are exposed, and where rare sedimentary clastic deposits have been observed.

Exhumation of Pyrenean peridotites is usually ascribed to lithospheric thinning associated with successive opening and closing of elongated, asymmetrical pull-apart basins in response to the dominantly transcurrent motion of the Iberian plate relative to the European plate in the

mid-Cretaceous (Choukroune and Mattauer, 1978; Debroas, 1987; Vielzeuf and Kornprobst, 1984).

The crustal emplacement of the central and eastern peridotite massifs has been dated at 110-105 by Ar-Ar and Sm-Nd methods on amphiboles and whole-rocks, respectively, from Lherz and Caussou (Henry et al., 1998) but is probably older (109-117 Ma) in the western Pyrenees (Fabriès et al., 1998). Previous models of emplacement suggested purely tectonic mechanisms such as solid intrusion of mantle rocks into the sediments (Minnigh et al., 1980; Vielzeuf and Kornprobst, 1984). On the other hand, Choukroune (1973), Fortané (1986) and more recently Lagabrielle and Bodinier (2008) proposed tectono-sedimentary models involving disintegration and transport of mantle rocks exhumed on the sea-floor (Fig. 4).

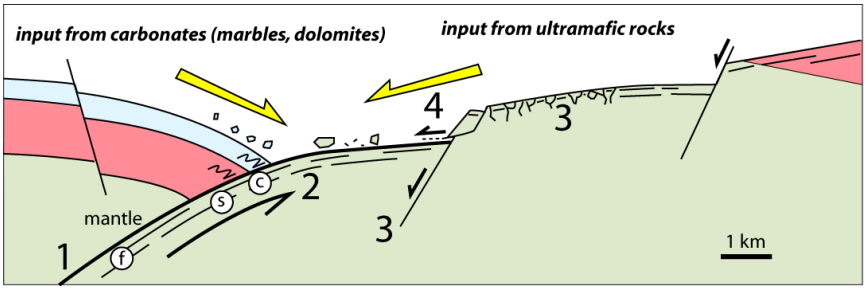

Fig. 3: Possible geological setting and mode of emplacement of the ultramafic bodies and associated clastic rocks (Lagabrielle and Bodinier, 2008). Blue: Jurassic platform carbonates; pink: continental crust; green: mantle; 1: detachment leaving late foliation in mantle rocks; 2: LT shear zone(s), cataclasites (c) and exhumation to seafloor; 3: late normal faulting, weathering and brecciation; 4: gravity sliding and sedimentary reworking.

Meter-scale low-temperature mylonitic bands also cross-cut the massif; they are more common at the borders and are probably related to the emplacement of the massif in the crust (Costa and Maluski, 1988).

2.1 Lithologies

The Pyrenean peridotite massifs are mostly composed of layered spinel lherzolites where the layering is defined by ubiquitous cm- to dm-thick parallel bands of websterite. The Pyrenean peridotites are equilibrated either in the Ariege subfacies (garnet in mafic layers) or

in the Seiland subfacies (mafic layers devoid of garnet) defined by O'Hara (1967) and Obata (1980). Eastern and Central Pyrenean peridotites are equilibrated either in the Ariege or Seiland spinel subfacies. The Lherz massif peridotites are equilibrated in the Ariege spinel subfacies and show petrological and geochemical characteristics typical of sub-continental lithosphere: equilibration temperatures of 800-900°C (Fabriès et al., 1991); old osmium ages (Reisberg and Lorand, 1995); metasomatic features comparable to those observed in mantle xenoliths (Bodinier et al., 1988; Bodinier et al., 1990; Downes et al., 1991). Besides, they are never associated with large gabbro or pillow-lavas formations of MORB affinity suggesting that they do not represent typical oceanic lithosphere. Western Pyrenean peridotites are equilibrated in the Seiland spinel subfacies and locally show incipient recrystallization in the plagioclase stability field (Fabriès et al., 1998). They are also more serpentinized than the Eastern bodies (Fabriès et al., 1991). This suggests that the westernmost Pyrenean peridotites reached a very shallow level in oceanic basins. They are considered to be transitional between the Lherz peridotites, which represent the subcontinental mantle, and the ocean-continent transition peridotites generally equilibrated at lower pressure, higher temperature and more affected by serpentinization (e.g. Lanzo).

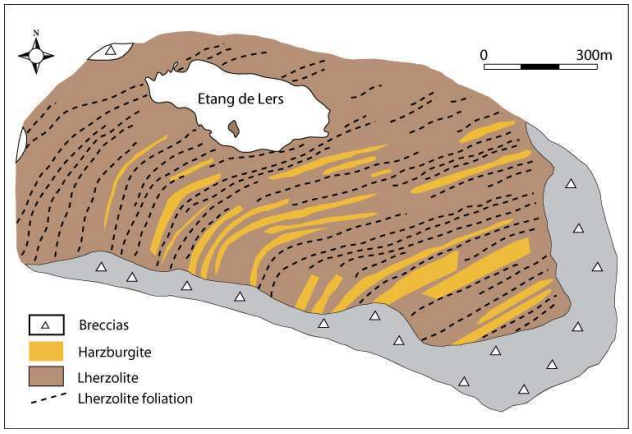

Fig. 4: Cartography of the lherzolites and harzburgites of the Lherz massif from Conquéré (1978).

The Lherz massif is mostly constituted of spinel peridotites (around 80% lherzolite and 20% harzburgite; Fig. 5). Harzburgites "bands" attain thicknesses up to some 20m (Avé Lallemant, 1967; Conquéré, 1978). The websteritic layering locally shows small,

asymmetrical and isoclinal folds but more open folds are observed, especially in thick pyroxenite layers which have a higher resistance to deformation (Fabriès et al., 1991).

Fig. 5: (a) small websteritic "disk-like" pockets in depleted harzburgites; (b) the size of the websteritic pockets increases when approaching the contact with lherzolites; (c) Cr-rich websteritic bands close to a harzburgite-lherzolite contact; (d) a harzburgite-lherzolite contact underlined by a thin websteritic banding; (e) pervasive websteritic layering in the lherzolites; (f) some websteritic bands may locally attain tens of centimeters; (g) amphibole-pyroxenite dykes; (h) hornblendite veins; (i) carbonate-peridotite breccias.

The Lherz ultramafic complex is cross-cut by a late generation of amphibole-pyroxenite dykes (Bodinier et al., 1987b; Conquéré, 1971; Vétil et al., 1988) considered as high-pressure – high-temperature crystal segregates from alkaline basalts that migrated through the Pyrenean lithospheric mantle in the Cretaceous (Bodinier et al., 1990; Fabriès et al., 1991; Golberg et al., 1986; Loubet and Allègre, 1982; Rossy et al., 1992) . Hornblendites veins ("lherzites") were also emplaced at a slightly later stage. They were ascribed to the segregation of volatile-rich, evolved melts after crystallization of anhydrous garnet

pyroxenites from the alkaline basalt (Bodinier et al., 1988; Wilshire et al., 1980; Woodland et al., 1996).

2.2 Sampling

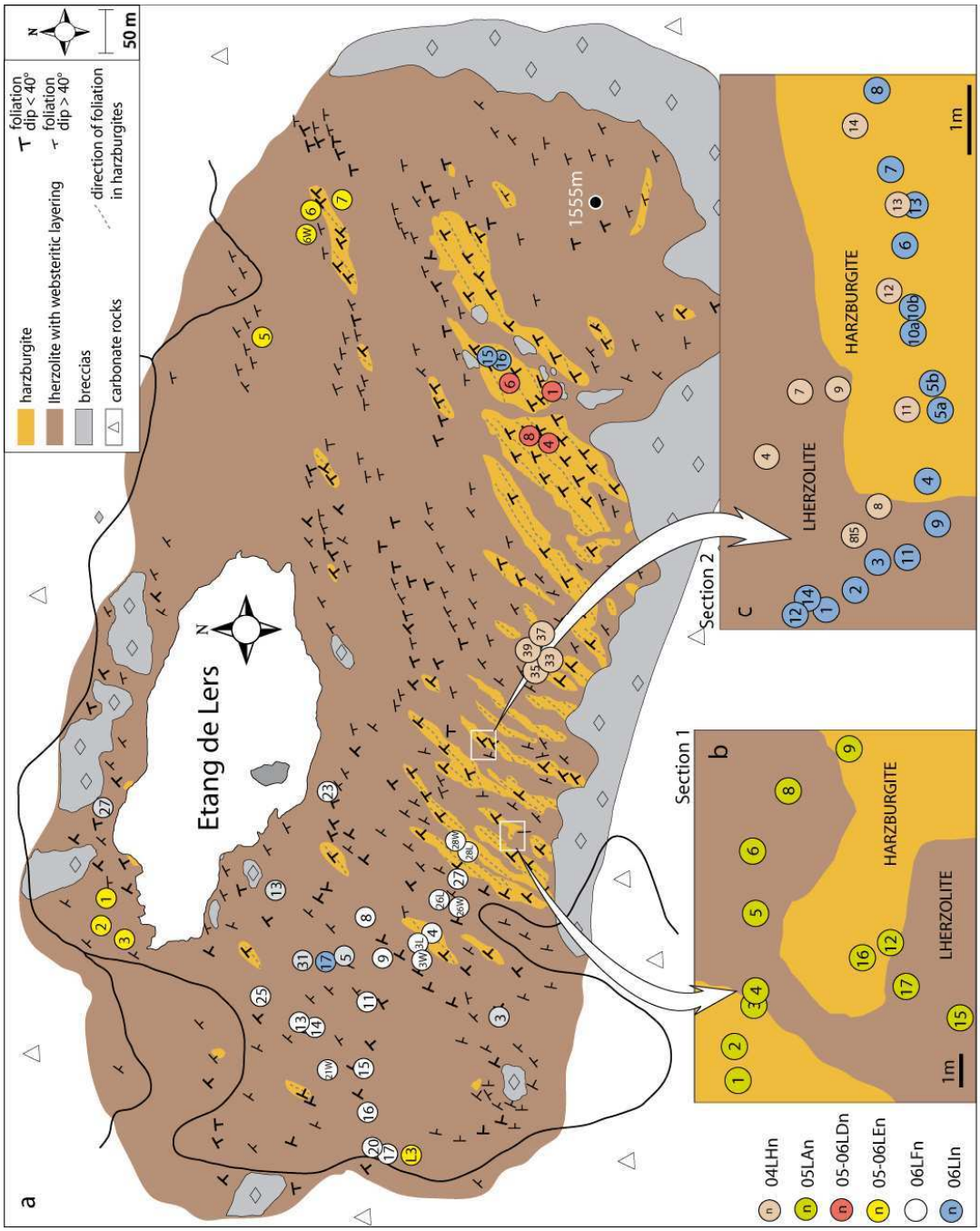

Fig. 6: (a) Map of the Lherz massif realized during this study (Le Roux et al., 2007) presenting the location of the harzburgites, lherzolites and websterites sampled during this study, and used for microstructural, petrophysical, geochemical and isotopic analyses; (b) detail of the section 1. The samples are part of the 05LA sampling series; (c) detail of the section 2. The grey samples are part of the 04LH sampling series; the white samples are part of the 06LI sampling series.

The Lherz peridotites have been sampled in different locations. Sampling restricted to the harzburgite-lherzolite contacts aim to observe small-scale variations whereas profiles along the massif provide information on larger-scale processes.

3. Presentation of the chapters

Following the introduction, the second chapter presents a combined structural and geochemical survey of the Lherz peridotites. The main conclusion of this chapter is that the lherzolites from the type-locality do not represent pristine asthenospheric material, as assumed in previous studies, but are secondary and formed through a refertilization process at the expense of an ancient harzburgitic protolith (Le Roux et al., 2007; published in EPSL).

In the last decade, the relationships between melt percolation and deformation have been studied mostly using an experimental approach. Based on the new model on the formation of the Lherz lherzolites developed in the second chapter, the Lherz massif has become an exceptional area to study interactions between percolation and deformation in mantle rocks of a natural system. Thus, chapter three develops the geodynamical implications of a refertilization episode, through a detailed microstructural and petrophysical study of the refertilized lherzolites. The main conclusion of this chapter is that the lherzolites record a feedback between melt percolation and deformation, leading to a contemporaneous localization of the deformation / percolation (Le Roux et al., 2008; published in EPSL). This feedback might play a significant role in the structuration of the lithospheric mantle.

Additionally, the consequences of magma transport on chemical/isotopic variations in the mantle are usually neglected. The third part of this work (fourth chapter) consists in a detailed investigation of Hf, Nd and Sr isotopic variations in the Lherz massif through a frozen melt percolation front materialized by the harzburgite-lherzolite contacts. The main conclusion of this chapter is that melt percolation through mantle rocks may produce transient isotopic signatures that do not reflect a simple mixing between the two source components. Thus, part

of mantle rocks isotopic variability could be generated by diffusional processes associated with melt transport rather than by mixing between individual reservoirs (Le Roux et al., 2008a; accepted to EPSL). Finally, the fifth chapter summarizes the main conclusions of this study, discusses some remaining, open questions and suggests work perspectives.

For reader's convenience, all references are compiled at the end of this manuscript. Details on the technical work are given at the beginning of supplementary material. Two published articles and a fourth article in preparation are also presented in this last section.

Chapter II:

The Lherz spinel lherzolite: refertilized rather than pristine mantle

Article published in Earth and Planetary Science Letters **259** (2007), 599-612.

V. Le Roux[1,2], J.-L. Bodinier[1], A. Tommasi[1], O. Alard[1], J.-M. Dautria[1], A. Vauchez[1], A.J.V. Riches[3]

[1] Géosciences Montpellier, Université de Montpellier 2 and CNRS, Cc 060, Place E. Bataillon, 34095 Montpellier cedex 5 France

[2] GEMOC, Department of Earth & Planetary Sciences, Macquarie University NSW 2109 AUSTRALIA

[3] The Open University, Department of Earth Sciences, Walton Hall, Milton Keynes, MK7 6AA UNITED KINGDOM

VLR's contribution in this paper: analyses, interpretations, writing.

Abstract

Differentiation of the Earth's mantle and formation of continental and oceanic crust occur principally through partial melting and extraction of basaltic melt. Among the mantle rocks occurring at the Earth's surface, as tectonically-emplaced massifs, abyssal peridotites or xenoliths, the harzburgites (<5% clinopyroxene) are widely considered as refractory mantle residues left after extraction of a basaltic component. In contrast, the most fertile lherzolites (≥15% clinopyroxene) are generally regarded as pristine mantle, only weakly affected by partial melting. In this paper we present new convergent structural and geochemical data from the Lherz massif, the type-locality of lherzolite, indicating that the lherzolites from Lherz do not represent pristine mantle. Detailed structural mapping clearly shows that the lherzolites are secondary rocks formed at the expense of the harzburgites. Variations of major, minor and trace elements through the harzburgite-lherzolite contacts indicate that the lherzolites were formed through a refertilization process involving interaction of refractory, lithospheric mantle with upwelling asthenospheric partial melts. Combined with previously published indications of refertilization in orogenic peridotites, our new observations in Lherz suggest that most lherzolite massifs represent secondary (refertilized) rather than pristine mantle. Together with geochemical data on mantle xenoliths, this indicates that melt transport and melt-rock reaction play a key role on the rejuvenation and erosion of the lithospheric mantle.

Keywords: Lherz; refertilization; melt-rock reaction; erosion of the lithospheric mantle

1. Introduction

Chemical variations observed in mantle rocks are classically ascribed to variable degrees of partial melting and melt extraction: the most fertile lherzolites (≥15% clinopyroxene) are interpreted as pristine mantle only weakly affected by partial melting whereas harzburgites (<5% clinopyroxene) record high degrees of melt extraction (Bodinier, 1988; Frey et al., 1985). Together with chondritic meteorites, these fertile lherzolites were used to infer the composition of the Earth's primitive mantle (McDonough and Sun, 1995). In this scheme, tectonically-emplaced peridotites massifs equilibrated in the plagioclase (Lanzo, Italy (Bodinier, 1988; Boudier and Nicolas, 1977); Othris, Greece (Menzies and Allen, 1974); Horoman, Japan (Frey et al., 1991)), spinel (Ronda, Spain (Dickey Jr, 1970; Frey et al., 1985); Lherz, France (Bodinier et al., 1988); Ivrea, Italy (Hartmann and Wedephol, 1993)) and garnet fields (Western Gneiss Region, Norway (Carswell, 1968)) were widely considered as residual mantle containing sparse remnants of pristine material. However, an increasing set of observations shows that lherzolites may also form by combined processes of partial melting and igneous refertilization. Plagioclase lherzolites, in particular, are interpreted as products of impregnation of previously depleted peridotites by percolating melts (Nicolas and Dupuy, 1984; Piccardo et al., 2004; Rampone et al., 1997; Rampone et al., 1994; Saal et al., 2001). Müntener et al. (2004) have ascribed the formation of plagioclase peridotites in western Alps and Apennines to a reaction between extending lithosphere from embryonic ocean basins and upwelling asthenospheric melts. Spinel lherzolites from the Ronda Massif (S Spain) have also been ascribed to refertilization of subcontinental lithosphere (Lenoir et al., 2001; Van der Wal and Bodinier, 1996) . In Ronda, this process was coupled with thermal erosion and extensive melting of deeper lithospheric levels (Garrido and Bodinier, 1999; Lenoir et al., 2001). Finally, Beyer et al. (2006) recently interpreted garnet peridotites and pyroxenites from the Western Gneiss Region (Norway) as formed by refertilization of a dunitic Archean lithospheric mantle.

The Lherz Massif in the Central Pyrenees, France, which is the type-locality of lherzolite, shows a decametric-scale intermingling of highly refractory harzburgites and fertile spinel lherzolites. This km-scale orogenic peridotite is therefore a natural laboratory to study the relations between depleted and fertile mantle

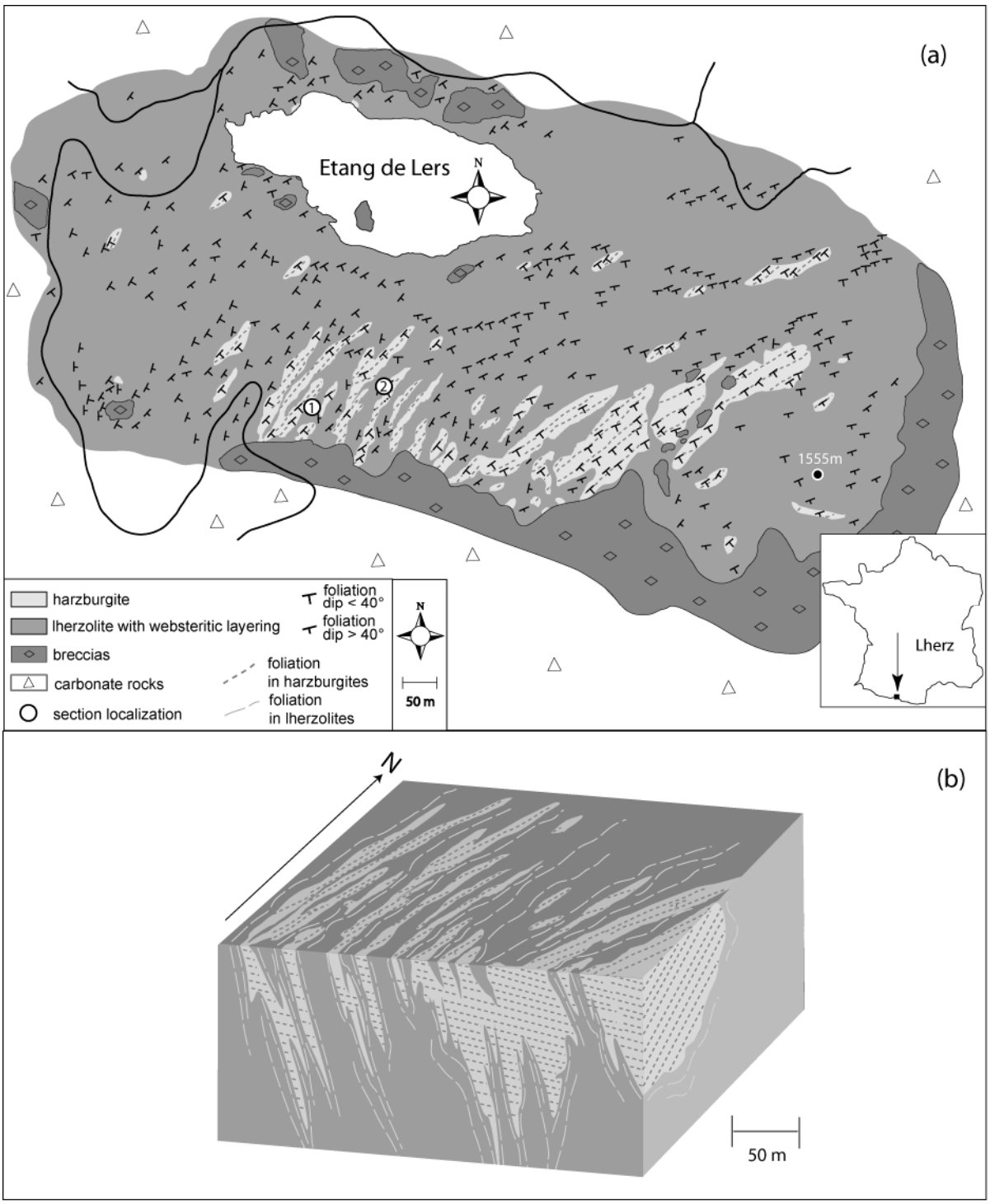

Fig. 1: (a) Geological map of the Lherz peridotite massif showing anastomosed fertile lherzolites enclosing irregularly-shaped refractory harzburgite bodies. Foliation in harzburgites shows a constant N40-N60 orientation with a gentle southward dip, while lherzolite foliation and websterite layering show variable directions and a steep southward dip. Right insert: localization of the massif. (b) 3-D bloc diagram of the upper part of the massif made after the dips of websterite layering at the contact

rocks. We present here a detailed structural mapping of this massif combined with petrophysical and geochemical (major and trace elements) analyses performed along

two distinct, 7-8m-long sections across harzburgite-lherzolite contacts (11 harzburgites and 8 lherzolites). Additionally, 2 harzburgites and 2 lherzolites collected away from the contacts (>20m) were studied for comparison. Our results provide a unique set of convergent structural and geochemical arguments indicating that the Lherz spinel lherzolites were formed by a refertilization reaction between a refractory harzburgitic-dunitic protolith and ascending basaltic melts. Combined with previous studies on worldwide mantle rocks, these results allow us to discuss the extent of the refertilization process and its implications for the rejuvenation and erosion of the lithospheric mantle.

2. Geological background

The Pyrenean orogenic peridotites comprise about 40 distinct ultramafic bodies mainly composed of layered spinel lherzolites, with dimensions varying from a few m^2 to 1 km^2 in Lherz (Fabriès et al., 1991). Most massifs are spatially associated with crustal granulites (Azambre and Ravier, 1978; Vielzeuf and Kornprobst, 1984) and are embedded within carbonate rocks of Jurassic to Aptian age affected by a low pressure high temperature metamorphism (the 'North Pyrenean Metamorphic Zone') (Golberg and Leyreloup, 1990; Montigny et al., 1986). Exhumation of mantle rocks is generally ascribed to transcurrent movement of the Iberian plate relative to Europe in the mid-Cretaceous, which resulted in crustal thinning associated with successive opening and closing of elongated, asymmetrical pull-apart basins (Choukroune and Mattauer, 1978; Debroas, 1987).

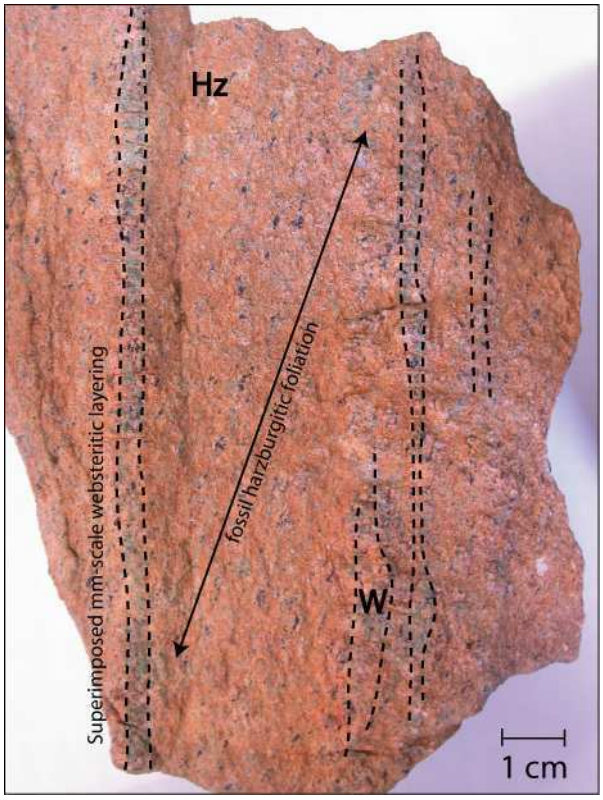

Fig. 2: Print of the fossil harzburgitic foliation in harzburgites (Hz) close to the contact, cross-cut by a latter mm-scale websteritic layering (W) related to the refertilization. The thin layering superimposed to the harzburgitic foliation initiates the development of cm-scale websteritic veins.

The Lherz massif is predominantly composed of spinel lherzolites which are intermingled with metric to decametric bodies of highly refractory harzburgites in the upper part of the massif (Fig 1). The

lherzolites contain numerous cm- to 10 cm-scale spinel-websterite layers and some thicker (10-50 cm) tabular garnet pyroxenites. The harzburgites often contain mm- to cm-thick websterite layers near the contact with lherzolites. Shortly before the exhumation, the massif was cross-cut by a late generation of amphibole pyroxenite dykes considered to represent trans-lithospheric melt conduits for Cretaceous alkaline magmatism in Pyrenees (Bodinier et al., 1987a; Conquéré, 1971; Montigny et al., 1986; Vétil et al., 1988) .

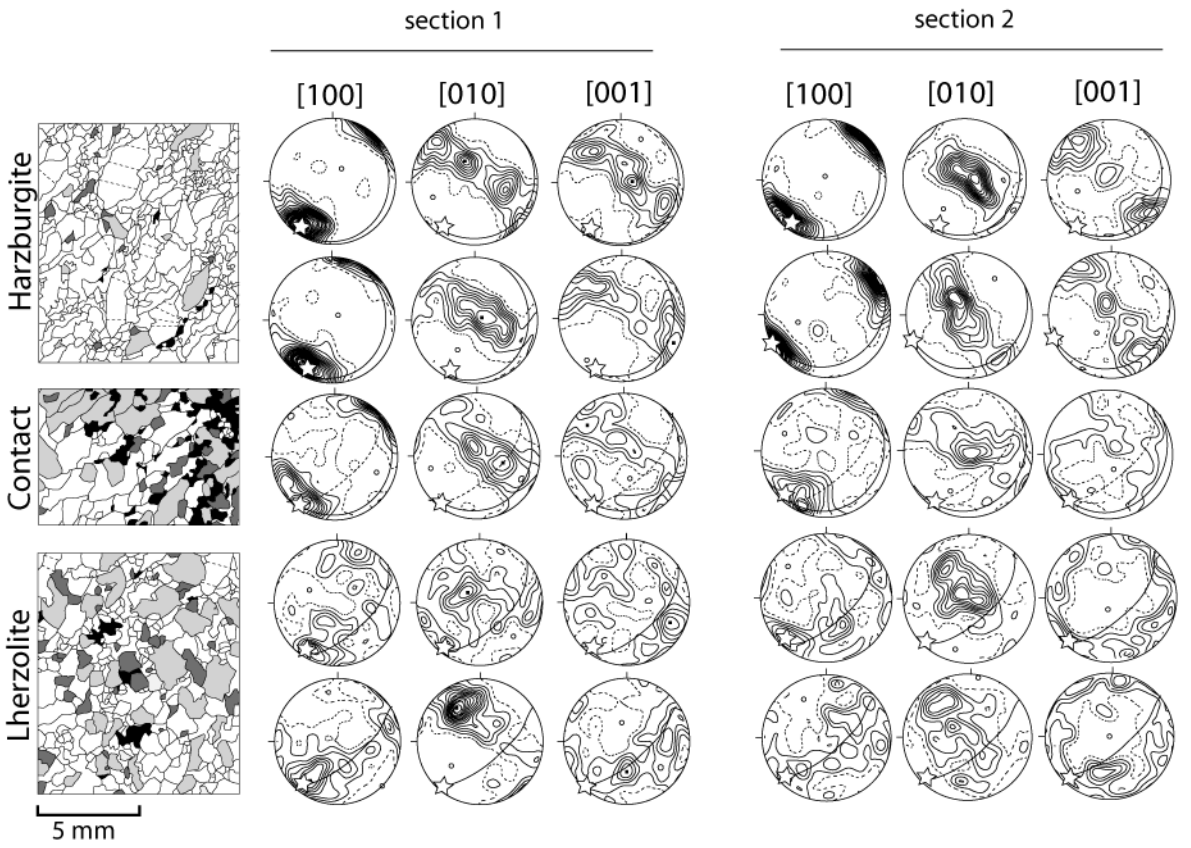

Fig. 3: Change in microstructure (left), from high-temperature porphyroclastic to coarse-granular, and associated weakening of olivine crystallographic preferred orientations (right) across two harzburgite–lherzolite contacts (sections 1 and 2). The presented CPO are representative of all measured CPO through the contacts. Microstructures are from samples collected within 1m from the contact, marked by cm-scale websterite banding. Microstructures were hand-drawn from thin sections; white: olivine, dashed lines mark subgrain boundaries; light grey: enstatite, dark grey: clinopyroxene; black: spinel. Olivine CPO are presented as lower-hemisphere equal area stereographic projections in a geographic reference frame (top to North); >130 individual grain measurements; contours at 0.5 multiple of a uniform distribution intervals. Solid lines: foliation; dashed lines: websterite layering; empty stars: lineation.

Narrow metasomatized dyke wall rocks and hornblendites veins record limited melt infiltration in host peridotites (Bodinier et al., 2004; Bodinier et al., 1990). The final emplacement of the peridotites is marked by extensive brecciation in the outer rim of the Lherz body and in the host limestones.

3. Structural and microstructural data

Previous structural maps of the Lherz Massif showed the harzburgites as elongated strips parallel to the high-temperature foliation of the lherzolites. However the present detailed mapping reveals that the harzburgite bodies form elongated, but irregularly-shaped bodies within anastomosed lherzolites (Fig. 1). All harzburgites, even those forming small isolated bodies, show a penetrative shallowly-dipping foliation with a constant N40-60°E orientation which is marked by elongated spinels and olivine porphyroclasts. The contact with the lherzolites is often sharp and steep, and underlined by a cm-scale websteritic layering. Near the contact (<1m) with harzburgites, the lherzolites are generally coarse-grained and show a weak foliation. This foliation is variable in orientation (N10 to N80), steeply dipping towards the east or south, and generally oblique on the harzburgite foliation (Figs. 1&2). Both layering and foliation in the lherzolites tend to wrap the contact with the harzburgite bodies. Away from the contact, fertile lherzolites display a steeply dipping foliation, dominantly N40-N80, marked by alignment of spinel aggregates that parallels the cm-scale websteritic layering.

At the thin-section scale, harzburgites display a porphyroclastic microstructure, characteristic of deformation by dislocation creep (Fig. 3). Foliation and lineation are marked by elongated spinels and olivine porphyroclasts with curvilinear grain boundaries, undulose extinction, and closely-spaced (100) subgrain boundaries. Orthopyroxenes, as well as small clinopyroxenes (<1mm), show irregular shapes and undulose extinction. Close to the contact, websterites and Cpx-poor lherzolites have coarser, more equant grains, but intracrystalline deformation features are still observed in olivine crystals. Spinels are interstitial and display no shape-preferred orientation. Farther from the contact, lherzolites display large (2-4mm), equant clino- and orthopyroxenes. Elongate olivine porphyroclasts show a strong undulose extinction. Alignment of interstitial, holy-leaf spinels defines a clear lineation and foliation.

Crystallographic orientations (Fig. 3) were measured by indexation of Electron Back Scattered Diffraction (EBSD) patterns using the SEM-EBSD system of Geosciences Montpellier (France).

Table 1
Whole-rock major- and trace-element contents, and modal compositions, of Lherz peridotites collected along two sections across harzburgite-lherzolite contacts and in distal peridotites

Section 1

Sample	05LD1 Distal harz.	05LD4 Distal harz.	05LA2 harz.	05LA1 harz.	05LA16 harz.	05LA9 harz.	05LA12 harz.	05LA3 harz.	05LA4 harz.	05LA5 lherz.	05LA6 lherz.	05LA8 lherz.	05LA15 lherz.
Distance from contact	>20m	>20m	4.5m	3.5m	1m	1m	10cm	10cm	5cm	1.5m	3m	5m	5m
SiO2	39,2	42,1	44,7	43,1	42,3	41,9	42,2	41,4	41,5	46,2	44,8	45,4	46,9
Al2O3	0,170	0,920	1,87	0,880	0,640	0,980	2,46	1,26	0,700	4,97	3,01	3,53	4,03
Cr2O3	0,094	0,437	0,796	0,293	0,304	0,299	1,06	0,596	0,230	0,463	0,341	0,394	0,386
FeO	7,82	7,59	7,31	7,43	7,94	6,85	7,80	7,85	7,84	7,43	8,63	8,26	7,29
MgO	45,5	43,1	41,9	43,9	44,4	40,8	40,5	42,0	43,0	34,9	38,6	37,2	36,4
CaO	0,280	0,610	0,730	0,500	0,320	0,580	1,90	0,470	0,440	4,70	2,20	3,42	3,31
MnO	0,120	0,120	0,130	0,120	0,120	0,120	0,120	0,120	0,120	0,130	0,140	0,140	0,130
NiO	0,370	0,313	0,263	0,296	0,290	0,283	0,267	0,297	0,299	0,232	0,246	0,243	0,209
Na2O	0,050	0,060	0,090	0,070	0,080	0,060	0,160	0,070	0,070	0,360	0,200	0,290	0,260
TiO2	0,030	0,020	0,040	0,060	0,050	0,030	0,060	0,050	0,040	0,200	0,100	0,140	0,160
LOI	6,44	4,46	2,93	3,85	3,48	7,83	3,41	5,95	5,73	0,480	1,33	1,04	0,820
TOTAL	100,1	99,6	100,8	100,5	99,9	99,8	100,0	100,0	99,9	100,0	99,6	100,1	99,8
Modal composition													
Ol %	94,0	79,5	66,8	76,9	79,5	71,4	69,1	75,3	79,6	45,5	57,3	54,4	47,1
Opx %	4,6	16,8	27,7	20,3	18,4	25,7	16,7	20,8	17,9	28,5	29,5	28,4	34,4
Cpx %	1,2	2,4	3,1	2,1	1,5	2,3	10,7	2,2	1,9	22,7	10,9	15,2	15,7
Spl %	0,2	1,2	2,5	0,7	0,6	0,6	3,5	1,7	0,6	3,3	2,3	2,0	2,8
Mg#	92,0	91,8	91,9	92,1	91,7	92,2	91,1	91,4	91,6	90,3	89,8	89,9	90,8

Section 2

Sample	04LH13 harz.	04LH12 harz.	04LH14 harz.	04LH11 harz.	04LH08 lherz.	04LH815 lherz.	04LH07 lherz.	04LH04 lherz.	05L3 lherz.	05LE3 lherz.
Distance from contact	2m	1.5m	1.2m	1m	10cm	50cm	80cm	1.5m	>20m	>20m
SiO2	41,3	41,5	41,5	41,9	43,9	43,8	40,9	44,3	44,1	44,4
Al2O3	0,439	0,450	0,444	0,539	2,10	3,40	1,87	3,15	2,99	2,95
Cr2O3	0,287	0,252	0,223	0,274	0,461	0,356	0,547	0,377	0,342	0,353
FeO	7,70	7,71	7,88	7,87	7,65	7,57	7,72	7,87	7,91	7,79
MgO	43,8	43,4	43,8	44,2	41,9	38,3	40,2	39,3	38,7	39,6
CaO	0,358	0,351	0,319	0,382	2,18	3,26	2,01	2,66	2,69	2,46
MnO	0,118	0,118	0,119	0,121	0,125	0,129	0,124	0,132	0,130	0,130
NiO	0,296	0,298	0,299	0,292	0,260	0,243	0,284	0,240	0,260	0,251
Na2O	0,048	0,040	0,045	0,058	0,219	0,290	0,185	0,216	0,210	0,200
TiO2	0,010	0,012	0,016	0,017	0,124	0,153	0,082	0,131	0,130	0,120
LOI	4,81	5,23	4,49	4,10	0,680	0,350	1,23	1,75	2,62	1,43
TOTAL	99,1	99,4	99,1	99,7	99,7	97,9	95,1	100,1	100,0	99,7
Modal composition										
Ol %	82,0	82,9	84,1	80,4	59,9	72,6	61,6	68,8	63,6	60,9
Opx %	15,9	15,3	14,1	17,6	26,3	16,2	20,8	19,9	22,7	25,6
Cpx %	1,5	1,4	1,4	1,5	11,7	9,3	14,9	9,7	12,0	11,3
Spl %	0,6	0,4	0,4	0,5	2,1	1,9	2,7	1,6	1,7	2,2
Mg#	91,8	91,8	91,7	91,8	90,8	91,2	90,9	91,6	90,6	91,0

harz. = harzburgite; harz.* = harzburgite with thin (~mm) websterite layers; lherz. = lherzolite. LOI = loss on ignition; Mg# = Mg/Mg+Fe cationic ratio.

Measurements were performed manually (i.e. indexing of every crystal was verified by the operator) on grain by grain basis along 2 mm-spacing profiles parallel to the long axis of the thin section. The change in microstructure is associated with a variation in both orientation and strength of olivine crystal-preferred orientations (CPO). Harzburgites exhibit a strong olivine CPO, characterized by alignment of [100] axes close to the lineation and a girdle distribution of [010] and [001] with a maximum of [010] normal to the foliation. At the contact, olivine CPO in the lherzolites is weaker but the orientation of the 3 maxima is preserved. In the lherzolites close to the contact, the weakening of the CPO is stronger, with a strong dispersion of [100] parallel to the layering but the orientation of [010] and [001] maxima is similar to the one in the harzburgites. Farther the contact, [010] axes are reoriented and the maximum concentration is normal to the lherzolite foliation.

Elements	Harzburgites				Lherzolites			
	Ol	Opx	Cpx	Spl	Ol	Opx	Cpx	Spl
SiO_2 (wt. %)	40.7-41.8	56.5-57.5	53.5-54.4	0.074-0.195	40.6-41.4	54.8-57.2	51.7-52.8	0.100-0.145
Al_2O_3	-	1.65-2.81	2.48-5.06	26.1-43.2	-	1.9-4.43	5.99-7.45	46.4-61.3
Cr_2O_3	-	0.331-0.562	0.937-1.79	25.7-41.6	-	0.197-0.403	0.602-1.30	6.74-21.4
FeO	8.45-9.09	5.51-6.17	1.84-2.10	13.7-19.6	9.13-10.75	6.11-6.86	1.99-2.37	11.1-14.6
MgO	48.7-49.3	33.7-34.3	14.4-16.3	11.9-16.8	47.3-49.2	31.3-34.0	13.7-14.4	16.5-20.0
CaO	0.008-0.017	0.331-0.505	20.6-23.2	-	0.006-0.022	0.282-1.324	20.3-21.5	-
MnO	0.119-0.141	0.133-0.175	0.066-0.088	0.182-0.316	0.126-0.155	0.146-0.164	0.065-0.090	0.105-0.190
NiO	0.416-0.436	0.069-0.090	0.026-0.075	0.074-0.198	0.375-0.450	0.049-0.089	0.028-0.065	0.227-0.462
Na_2O	-	0.021-0.049	0.705-2.19	-	-	0.023-0.217	1.85-2.18	-
TiO_2	-	0.014-0.098	0.051-0.321	0.018-0.172	-	0.103-0.193	0.550-0.772	0.025-0.083
Mg#	90.5-91.5				89.0-89.9			
Cr#				0.28-0.41				0.069-0.104

Table 2
Compositional ranges in major and minor elements of olivine (Ol), orthopyroxene (Opx), clinopyroxene (Cpx) and spinel (Spl) for harzburgites and lherzolites, and ranges of Mg# in olivine (= Mg/Mg+Fe cationic ratio) and Cr# in spinel (=Cr/Cr+Al cationic ratio).

4. Geochemical data

Major elements, Ti, Cr and Ni in whole rocks were analyzed by X-ray fluorescence at Geosciences Laboratories (Canada) and Open University (UK). Major and minor elements in olivine, orthopyroxene, clinopyroxene and spinel were analyzed by electron probe at Microsonde Sud facility, Montpellier (France), and Rare Earth Elements (REE) in clinopyroxene by laser-ablation plasma-mass spectrometry (LAM-ICP-MS) at Geosciences Montpellier. Whole-rock analyses are reported in table 1, compositional ranges in major and minor elements of minerals in table 2 and representative REE analyses of clinopyroxene in table 3.

Sample	05LD4			04LH11					04LH8						05LE3		
	Harzburgite			Harzburgite					Lherzolite						Lherzolite		
Distance from contact	>20m			95cm					10cm						>20m		
	cpx1	cpx2	cpx3	cpx1	cpx2	cpx3	cpx4	cpx5	cpx1	cpx2	cpx3	cpx4	cpx5	cpx6	cpx1	cpx2	cpx3
La (ppm)	0.857	0.584	0.676	7.81	7.59	7.18	5.78	6.58	1.74	1.59	1.57	1.39	1.63	1.64	0.933	0.918	0.893
Ce	1.70	1.19	1.75	14.4	13.9	14.2	11.7	12.6	5.99	5.63	5.47	5.19	5.59	5.66	3.69	3.50	3.33
Pr	0.241	0.180	0.239	1.51	1.45	1.48	1.29	1.34	1.23	1.16	1.11	1.09	1.13	1.11	0.661	0.634	0.625
Nd	1.11	1.16	1.37	5.83	5.70	5.73	5.07	5.26	7.87	7.30	6.94	6.94	7.25	7.14	3.96	3.91	3.93
Sm	0.340	0.337	0.388	1.32	1.37	1.34	1.22	1.29	2.85	2.73	2.61	2.62	2.72	2.71	1.69	1.54	1.70
Eu	0.103	0.103	0.107	0.458	0.466	0.465	0.434	0.458	1.08	1.06	1.01	1.02	1.03	1.03	0.726	0.674	0.700
Gd	0.369	0.365	0.407	1.47	1.52	1.50	1.45	1.54	3.77	3.51	3.35	3.28	3.50	3.55	2.41	2.56	2.44
Tb	0.050	0.054	0.058	0.245	0.246	0.247	0.238	0.249	0.613	0.560	0.541	0.525	0.560	0.558	0.433	0.451	0.466
Dy	0.353	0.341	0.369	1.74	1.71	1.65	1.76	1.82	3.97	3.69	3.72	3.61	3.79	3.72	3.33	3.44	3.53
Ho	0.076	0.075	0.072	0.373	0.349	0.351	0.389	0.383	0.795	0.719	0.708	0.703	0.724	0.722	0.674	0.753	0.753
Er	0.259	0.259	0.243	1.09	1.05	1.04	1.23	1.14	2.15	1.96	1.96	1.93	1.94	1.99	2.16	2.30	2.32
Yb	0.409	0.403	0.295	1.16	1.07	1.04	1.37	1.21	1.79	1.76	1.72	1.75	1.76	1.77	2.15	2.24	2.18
Lu	0.063	0.067	0.058	0.171	0.155	0.163	0.208	0.180	0.251	0.244	0.248	0.247	0.234	0.254	0.279	0.304	0.302

Table 3
REE compositions of clinopyroxene in four representative peridotites: a harzburgite and a lherzolite distal from harzburgites-lherzolites contacts, and the same rock types adjacent to a contact (section 2 in table 1).

Modal compositions calculated by linear inversion of whole-rock and mineral compositions for major elements are given in table 1. They range from 94% Ol, 4.6% Opx, 1.2% Cpx and <1% Spl in harzburgites to 62% Ol, 21% Opx, 15% Cpx and >2% Spl in lherzolites. Major and minor elements in whole rocks display a wide range of variation from highly refractory (e.g., 45.53 wt% MgO and 0.17 wt% Al_2O_3) to very fertile compositions (34.85 wt% MgO and 4.97 wt% Al_2O_3). Harzburgites collected in the vicinity of lherzolites (< 5m) are more fertile on average than more distal harzburgites. Their modal and major-element compositions partly overlap the composition of lherzolites (e.g., in the range 2-2.5 wt% Al_2O_3 -Table 1; Fig. 4). This feature reflects the presence of mm-scale websterite layers that are abundant near the contact with lherzolites. This is the case, for instance, in sample 05LA12 which is lherzolitic in terms of major-element and modal composition (10.7 % Cpx). However, this sample is distinguished from the "true" lherzolites from Lherz by lower Ti and much higher Cr contents (Fig. 4) and by mineral compositions typical of harzburgites (Table 2, Annex 1). It is therefore referred to as a harzburgite throughout this study.

Similar to the majority of mantle peridotite suites worldwide, the harzburgites and lherzolites from Lherz display chemical covariations such as decreasing MgO with

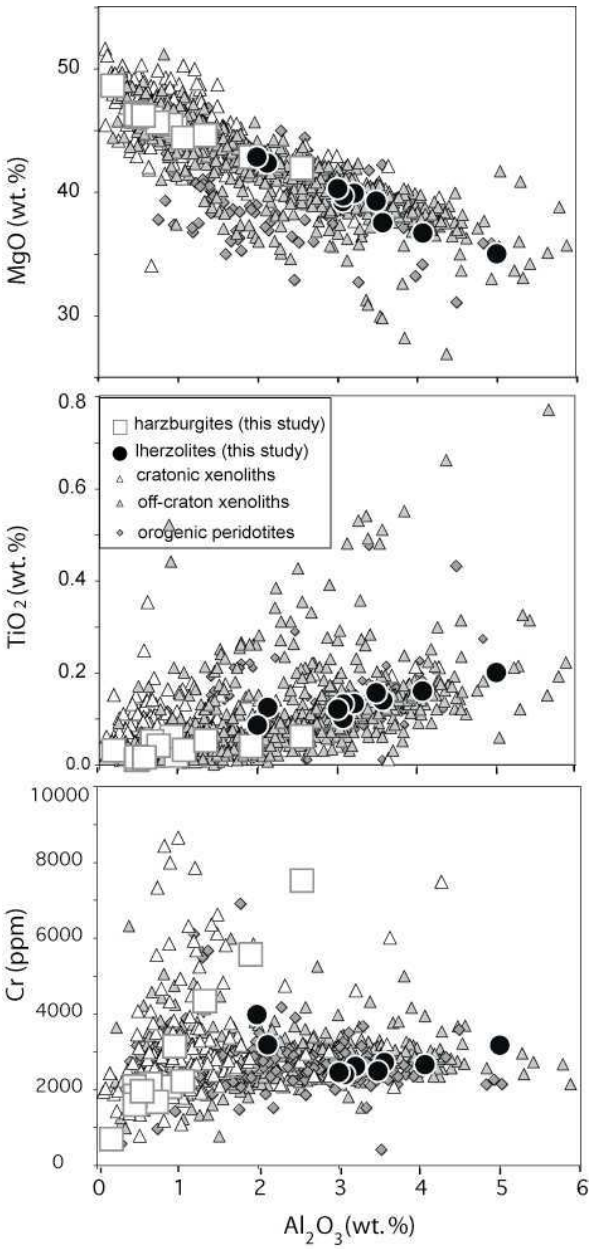

FIG. 4: MgO, TiO_2 and Cr *vs.* Al_2O_3 concentrations in whole-rock harzburgites and lherzolites from Lherz (table 1) compared with literature data for mantle xenoliths and orogenic peridotites (Canil, 2004). Empty squares = harzburgites; full circles = lherzolites. The variations observed within a few meters across harzburgite-lherzolite contacts in Lherz encompass almost the whole range of mantle peridotites worldwide.

increasing Al_2O_3 traditionally ascribed to partial melting (Fig. 4). A more detailed analysis shows however that harzburgites and lherzolites tend to define distinct covariations trends, notably for minor

elements. For instance the lherzolites are distinguished by slightly higher Ti contents at a given Al_2O_3 value (Fig. 4). On a Cr *vs.* Al_2O_3 diagram, the difference between the harzburgite and lherzolite trends is striking: while the harzburgites show a steep, steady positive correlation, the lherzolites display a

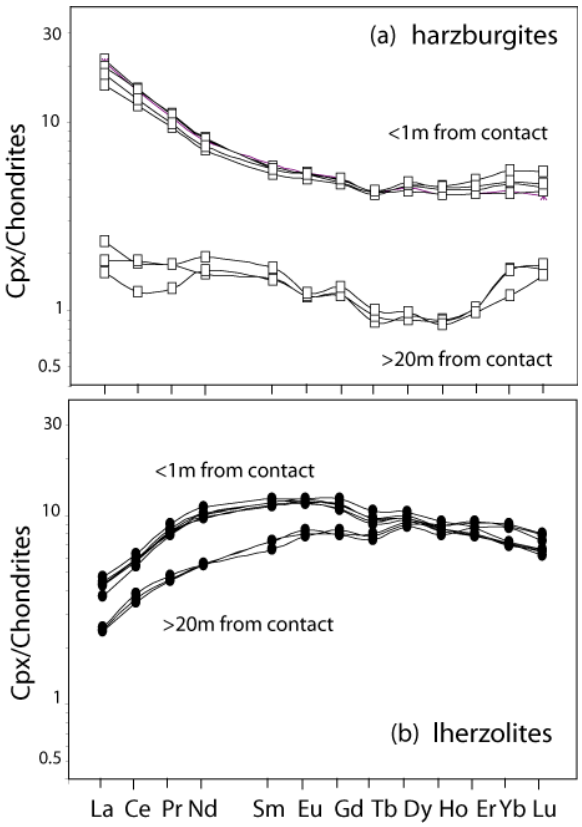

Fig. 5: Chondrite-normalized (Sun and McDonough, 1989) REE patterns of clinopyroxenes in four representative peridotites, including harzburgites and lherzolites, both distal and adjacent to a harzburgite-lherzolite contact (table 2).

curved trajectory trending towards a gentle, positive correlation in the most fertile samples (Fig. 4). From their wide range of Cr contents (600 to 7400ppm) and low Al_2O_3 values (< 2.5%), the harzburgites resemble cratonic xenoliths, notably those equilibrated at shallow depth, in the stability field of spinel (Canil, 2004). Conversely, the lherzolites show a narrow range of Cr contents (2400-4000ppm) and higher Al_2O_3 comparable to the composition of other orogenic peridotites and off-craton mantle xenoliths.

The existence of two different trends for Cr in covariation diagrams is a reflection of the markedly distinct Cr contents in minerals from harzburgites and lherzolites (Table 2). The Cr# number (= Cr/Cr+Al cationic ratio) of spinel, for instance, is in the range 0.28-0.41 in harzburgites compared with 0.069-0.104 in lherzolites. This bimodal distribution of mineral compositions is also observed for Mg# (= Mg/Mg+Fe cationic ratio) in olivine and minor elements such as Ti in pyroxenes. The forsterite value of olivine (Fo) is 0.905-0.915 in harzburgites, compared with 0.890-0.899 in lherzolites, and TiO_2 in clinopyroxene is 0.02-0.06 wt% in harzburgites, compared with 0.12-0.20 wt% in for lherzolites.

Rare earth elements (REE) in clinopyroxene display a wide range of concentrations and variable chondrite-normalized REE patterns (Table 3; Fig. 5). In the core of the thickest harzburgite bodies (> 10m), clinopyroxene shows strongly depleted, U-shaped REE patterns. These REE patterns mimic the whole-rock patterns previously reported for harzburgites unrelated to pyroxenite dykes and lherzolites (Bodinier et al., 1988; Bodinier et al., 2004).

In lherzolites away from contacts (> 20 m), clinopyroxene displays the classic, N-MORB, REE pattern observed in orogenic lherzolites worldwide (McDonough and Frey, 1989). This pattern is relatively enriched in heavy REE but selectively depleted in light REE. Within a few meters from the contact, both lherzolite and harzburgite show more LREE-enriched clinopyroxenes than their distal counterparts. The variations observed in harzburgites are especially striking: the REE content of clinopyroxene increases by a factor of 5 (heavy REE) to 10 (light REE) from the core of the harzburgite bodies to the contacts.

5. Discussion

5.1. Structural relationships between harzburgitic protolith and secondary lherzolites

The constant orientation of the foliation and lineation in harzburgite bodies throughout the Lherz Massif (Fig. 1) strongly suggests that all harzburgites were once part of a single and continuous unit. This, together with the observation that the steeply dipping lherzolite foliation and websterite layering cross-cut the shallowly dipping harzburgite foliation, indicates that the deformation of the harzburgites predates the formation of the lherzolites and websterites. Such structural relationships between harzburgites and lherzolites, visible throughout the intermingled zone and at the massif-scale (Fig. 1), clearly indicate that the lherzolites are secondary rocks compared to harzburgites. The harzburgite bodies represent the remnants of a highly refractory mantle protolith largely replaced by the lherzolites.

Analysis of microstructures and olivine CPO suggest deformation of harzburgites by dislocation creep with activation of the high-temperature, low-stress (010) [100] slip system. The formation of the lherzolites and websterites modifies both the microstructure and the CPO of the harzburgitic protolith. However, while the change in microstructure, marked by grain growth, occurs at the contact, the re-orientation of the [100] and [010] axis of olivine, parallel to the lineation and perpendicular to the lherzolite foliation respectively, is only observed at some distance from the contact (>1-2m). At the contact, lherzolites show larger and more equant grains and olivine CPO are quite similar to harzburgites, but weaker. The increase in grain size and the dispersion of the olivine CPO in lherzolites through harzburgite-lherzolite contacts may be due to static recrystallization and crystallization of new randomly-oriented olivine crystals during melt-rock reactions (Tommasi et al., 2004). The more pronounced growth of Opx and Cpx together with the increase in their modal proportions

suggest that they represent the main crystallization products of the reaction. Far from the contact, olivine microstructures and CPO are consistent with the steeply-dipping foliations and sub-horizontal lineations observed at the macroscopic scale. These observations suggest that melt percolation and melt-rock reactions started at static conditions, leading to changes in modal composition, grain growth and dispersion of olivine CPO. This percolation produced an anastomosed lherzolite network in which the later deformation producing the steeply dipping foliations was localised.

Our structural observations preclude therefore the formation of the harzburgite-lherzolite intercalations by mechanical dispersion by small-scale convection at the base of the lithosphere (Bodinier and Godard, 2003), since this deformation would result in transposition of both harzburgites (lithospheric material) and lherzolites (asthenospheric material) foliations. The structural observations are on the other hand consistent with the formation of lherzolites by a near-solidus refertilization reaction between harzburgite and basaltic melts leading to precipitation of pyroxene, spinel, minor amphibole and sulphide phase, which started under static conditions and was followed by a deformation stage.

5.2. Formation of the lherzolites by refertilization reaction

Covariations of modal and major-element compositions in the Lherz peridotites are comparable to those observed in several suites of mantle rocks worldwide. These covariations were generally ascribed to variable degrees of partial melt extraction (Bodinier, 1988; Canil, 2004; Frey et al., 1985), although in most cases variable degrees of refertilization of a refractory protolith would also account for the observed modal and chemical trends (Beyer et al., 2006). In the case of Lherz, the partial melting model is precluded by structural observations that show that the harzburgite predate the lherzolites. Formation of harzburgite-lherzolite intercalations by variable degrees of melting is also ruled out by variations of minor and trace elements in peridotites and/or their constituent minerals.

Chromium, for instance, shows two features at odds with the partial melting model. First, although highly compatible during mantle melting (Liu and O'Neill, 2004), this element tends to be negatively correlated with MgO and positively correlated with Al_2O_3 (Fig. 4). Second, harzburgites and lherzolites form two different trends on Cr *vs.* major-element correlation diagrams, a feature that reflects the bimodal distribution of the Cr content in minerals, notably spinel. In contrast with

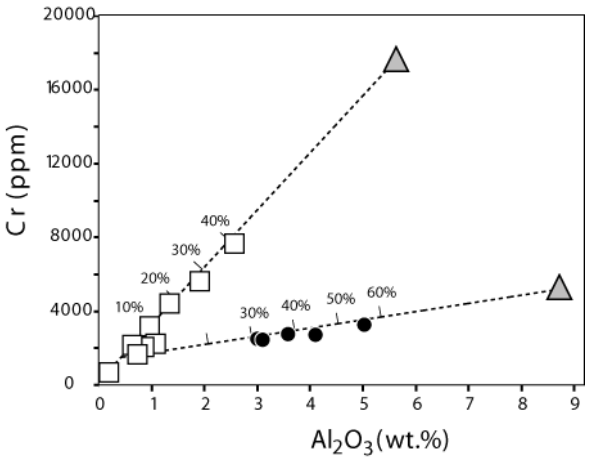

FIG. 6: Cr vs. Al_2O_3 diagram for the peridotites of section 1 and distal samples (table 1), emphasizing the two distinct covariations trends observed in lherzolites and harzburgites, respectively. The symbols for the samples are the same as in figure 4. The dashed lines represent mixing between a refractory harzburgite (intersection of the harzburgite and lherzolite trends) and variable proportions (in percent) of two distinct websterite components (grey triangles). The compositions of the websterite components were calculated from modal and mineral compositions. Modal compositions estimated by extrapolating those of the peridotites towards 0 % olivine are roughly identical for harzburgites and lherzolites (60% Opx, 34% Cpx and 6% Sp). Websterite mineral compositions were measured in thin (<1cm) websterite layers hosted by harzburgites and lherzolites. In both cases, the mineral compositions are similar in websterites and in their host peridotites, but they differ markedly between harzburgites and lherzolites. As a result, the two websterite components show distinct compositions, the one related to harzburgites being much more enriched in Cr than the one related to lherzolites.

melt extraction, refertilization of a refractory protolith involving precipitation of Cr- and Al-bearing minerals, mostly spinel and pyroxenes, can explain both the positive Cr *vs.* Al_2O_3 correlations and the existence of distinct Cr arrays for harzburgites and lherzolites (Fig. 6). In this model, the intersection of the harzburgite and lherzolite trends at low (<1%) Al_2O_3 content indicates the composition of the refractory protolith before refertilization. The lherzolite trend is interpreted as a linear mixing line between the depleted protolith composition and 30-60 wt% of an aluminous websterite component (60% Opx, 34% Cpx, 6% Spl). Mineral compositions in the websterite are identical to those in lherzolites, as it is the case for thin (<10 cm) websterite layers in Lherz (Fabriès et al., 1991) and other orogenic lherzolites (Shervais and Mukasa, 1991). The harzburgite trend is defined by harzburgite samples collected within a few meters from the contact with lherzolites and containing thin (~ mm) websterite seams (section 1 in table 1). These samples may be accounted for by mixing of the refractory protolith with 10-40 wt% of a Cr-rich websterite component comparable to the harzburgites in term of mineral compositions. These harzburgites were probably slightly refertilized by Cr-rich (harzburgite-buffered) small volume melts infiltrated beyond the main refertilization front represented by the harzburgite-lherzolite contact. The inferred variation in percolating melt composition, also reflected by bimodal Cr contents in minerals, may be explained by chromatographic fractionation of Cr due to cation exchange between the peridotite and the percolating melt (Navon and Stolper, 1987). The coincidence of the Cr chromatographic front with the

harzburgite-lherzolite contact indicates a significant drop in the melt fraction across the reaction front as a result of partial melt consumption by the reaction (Bodinier et al., 2004).

Titanium differs from chromium in showing closely spaced, almost aligned covariation trends for harzburgites and lherzolites on the TiO_2 *vs.* Al_2O_3 diagram (Fig. 4). Hence the two arrays may be overlooked and viewed as a single correlation recording variable degrees of partial melting. However, the distribution of Ti in Cpx precludes this process. It is roughly constant in lherzolites and drops abruptly in harzburgites, whereas melting models predict a gradual decrease of Ti contents in both whole rocks and minerals (Fig. 7). When recalculated for near-solidus, high-temperature conditions (1250°C), the bimodal distribution of Ti in Cpx is less pronounced but the discrepancy with the melting models remains significant. As shown on figure 7, the distribution of Ti can be successfully reproduced with a numerical simulation of refertilization involving a pyroxene- and spinel-forming reaction (Vernières et al., 1997). Based on the intersections of the harzburgite and lherzolites trends on Cr vs. modal and major-element composition diagrams (e.g., Fig 6), the protolith is assumed to be a highly refractory harzburgite (1.5% Cpx, 0.02 wt% TiO_2). The Ti content of the infiltrated melt was derived from the composition of clinopyroxene in the most fertile lherzolite

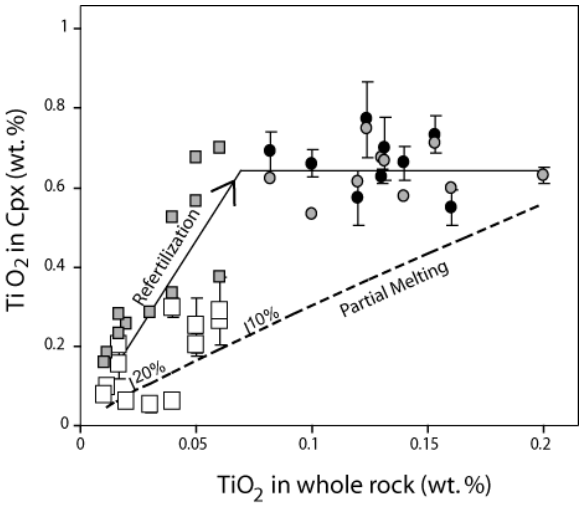

Fig. 7: TiO_2 concentrations in clinopyroxene *vs.* whole rocks for the harzburgites and lherzolites (same symbols as in Fig. 4). Error bars indicate the variation in Cpx composition at the sample scale. Grey symbols represent Cpx compositions recalculated for near-solidus temperature (1250°C) using inter-mineral partition coefficients derived from Wood and Blundy (2003). Numerical models of TiO_2 variations during partial melting and magmatic refertilization are shown for comparison. For the melting model, we used the modal composition of the most fertile lherzolite, and its TiO_2 content in Cpx and whole rock, as the source composition. The melting reaction was taken from Walter et al. (1995) and the mineral/melt partition coefficients from Wood and Blundy (2003). The results reported here were calculated with the fractional melting model. However, changing the melting model (e.g. for batch or incremental melting) does not significantly modify the variation trend of TiO_2 in Cpx *vs.* whole rock. Magmatic refertilization was simulated with the Plate Model of Vernières et al. (Vernières et al., 1997) applied to the following melt-rock reaction: $f_i.melt_i + x_{ol}.Ol \rightarrow f_r.melt_r + x_{opx}.Opx + x_{cpx}.Cpx + x_{spl}.Spl$, where $melt_i$ and $melt_r$ stand for the infiltrated and residual melts, respectively, f_i and f_r for the corresponding melt mass fractions, x_{ol} for the mass fraction of dissolved olivine, and x_{opx}, x_{cpx} and x_{spl} for the mass fractions of crystallized Opx, Cpx, and Spl. Reaction parameters f_i, f_r, x_{ol}, x_{opx}, x_{cpx} and x_{sp} were adjusted to reproduce the modal variations and the Ti contents in Cpx and whole-rocks. The protolith is a highly refractory harzburgite (83% Ol, 15% Opx, 1.5% Cpx, 0.5% Spl, 0.02 wt.% TiO_2 in whole rock and 0.05 wt.% TiO_2 in Cpx). The Ti content of the infiltrated melt (TiO_2 = 2 wt.%) was derived from the composition of clinopyroxene in the most fertile lherzolite and Cpx/melt partition coefficients (Wood and Blundy, 2003).

and Cpx/melt partition coefficients (Wood and Blundy, 2003). The results indicate constant Ti concentration in clinopyroxene of refertilized peridotites, which have their mineral compositions governed by incoming melt. Downstream of the Ti chromatographic front, Ti in Cpx rapidly decreases in the more refractory harzburgites, which mostly preserve the mineral compositions of the protolith.

Finally, REE enrichments observed at the harzburgite-lherzolite contacts also cannot be explained by partial melting model and provide further evidence for the refertilization process. Strong enrichment of highly incompatible elements (HIE, including REE) at melt infiltration fronts is indeed predicted by theoretical modelling of melt-consuming reactions combined with melt transport (Vernières et al., 1997). This enrichment results from the segregation of HIE- and volatile-rich small melt fractions moving ahead of melt-consuming reaction fronts. This mechanism, also referred to as "percolative fractional crystallization" (Harte et al., 1993), was advocated to explain enriched HIE compositions in "cryptically" metasomatized mantle xenoliths (Bedini et al., 1997) and in tens of centimetres-thick wall-rocks of alkaline dykes in Lherz (Bodinier et al., 1990). In the case of the harzburgite-lherzolite contacts, the REE variation in harzburgite Cpx indicates that small melt fractions residual after the refertilization reaction migrated in the harzburgite protolith several meters (< 20 meters) ahead of the main reaction front. Behind the reaction front, clinopyroxene REE compositions in lherzolites reflect the initial melt composition, which is depleted in LREE relative to HREE (i.e., similar to N-MORB).

5.3. Refertilization and isotopic variations

A striking feature of Pyrenean and several other orogenic peridotites is the existence of correlations between Os-Sr-Nd radiogenic isotopes and peridotite fertility (Bodinier and Godard, 2003; Downes et al., 1991; Reisberg and Lorand, 1995). In the Pyrenees, the positive correlation between $^{187}Os/^{188}Os$ and Al_2O_3 has been ascribed to a ~ 2.5 Ga-old depletion event considered to record partial melting and stabilization of lithospheric mantle in the Archean (Reisberg and Lorand, 1995). However, this hypothesis does not account for the negative correlation of $^{87}Sr/^{86}Sr$ and the positive correlation of $^{143}Nd/^{144}Nd$ with Al_2O_3. These covariations were ascribed either to selective percolation of enriched melts through the harzburgites (Downes et al., 1991) or to incomplete mixing of lithospheric strips (harzburgites) into asthenospheric material (lherzolites) during thermo-mechanical erosion of lithosphere by upwelling mantle

(Bodinier and Godard, 2003). However, the first alternative implies unrealistically enriched melt compositions (Bodinier and Godard, 2003) and the second is denied by our structural observations. In contrast the refertilization process suggested in this paper provides a coherent explanation for the isotopic variations observed in Pyrenean peridotites. The correlations of $^{87}Sr/^{86}Sr$ and $^{143}Nd/^{144}Nd$ with Al_2O_3 indicate that the refractory protolith was isotopically enriched - due to radiogenic decay following ancient enrichment – while the percolating melt had a DMM (Depleted MORB Mantle) composition. The refertilization process may also account for the positive correlation between $^{187}Os/^{188}Os$ and Al_2O_3, as previously suggested for the Horoman orogenic peridotite in Japan (Saal et al., 2001).

5.4. Refertilization fronts, a moving lithosphere-asthenosphere boundary?

In the light of our convergent structural and geochemical arguments we suggest that the Lherz massif is a fossil lithosphere-asthenosphere boundary, where a >2 Ga-old (Reisberg and Lorand, 1995) and refractory lithospheric mantle, from which the harzburgites are the remnants, was infiltrated and reacted with asthenospheric melts. The irregularly-shaped lherzolite-harzburgite contacts represent therefore a convoluted melt-rock reaction front formed by coalescence of porous melt infiltration channels. All lithospheric structures and geochemical signatures were efficiently erased within a few meters across the front. The ubiquitous websterite layers record higher melt/rock ratios and suggest small-scale anisotropic variations in the melt flux. A possible origin for the websterite layering is refraction and channelling of percolating melts against the freezing horizon represented by eroded lithosphere (Rabinowicz and Ceuleneer, 2005; Sparks and Parmentier, 1991; Spiegelman, 1993). This hypothesis is consistent with the systematic parallelism of websterite layers and harzburgite-lherzolite contacts. It was already suggested for replacive websterite layers related to lithospheric thermal erosion in the Ronda peridotite (Garrido and Bodinier, 1999). The low equilibrium temperatures recorded by pyroxene compositions in the Lherz peridotites (Fabriès et al., 1991) imply that thermal relaxation occurred between the refertilization episode and the emplacement of the massif in the crust, in the Cretaceous. Refertilization is thus probably related to the late-Variscan, post-collisional thermal event responsible for granulitic metamorphism in western Pyrenees (Pin and Vielzeuf, 1983), which has been interpreted as the result of the destabilization of the thickened orogenic lithosphere.

Is the refertilization process specific to Lherz? This is the first study showing convergent structural and geochemical data for extensive rejuvenation of refractory lithospheric mantle by refertilization. However, textural or chemical evidence for igneous refertilization has been reported from tectonically-emplaced plagioclase lherzolites in New Caledonia (Nicolas and Dupuy, 1984), western Alps (Müntener et al., 2004; Rampone et al., 1994), Horoman (Saal et al., 2001), and from Cpx-poor lherzolites at the base of the Oman ophiolite (Godard et al., 2000). Recently Beyer et al. (2006) suggested the transformation of highly refractory (dunitic) Archean lithospheric mantle via igneous refertilization, producing garnet peridotites and pyroxenites. An association between refertilization and lithospheric thinning was proposed for the orogenic lherzolites of Ronda and Lanzo (Lenoir et al., 2001; Müntener et al., 2004). The Ronda massif displays a narrow (<400m) refertilization front which separates a spinel tectonite domain interpreted as an old lithospheric mantle and a granular domain deeply modified by melting processes (Lenoir et al., 2001; Van der Wal and Bodinier, 1996). The refertilization front of the Lherz massif may have been associated with such a melting front below.

In the Cr *vs* Al_2O_3 diagram, several suites of mantle rocks show variations comparable to those observed in the Lherz massif (Fig. 4). These variations are hardly consistent with partial melting and may suggest that the majority of lherzolites observed at the Earth surface record refertilization processes. The refertilization mechanism also provides a key to understand the paradoxical association of LREE-enriched harzburgites with LREE-depleted lherzolites often observed in mantle xenoliths and in tectonically-emplaced peridotites (McDonough and Frey, 1989). Although recognized for at least two decades, this association, which is inconsistent with partial melting, was never given a satisfactory explanation.

6. Conclusions

The Lherz Massif, lithotype of the lherzolite, is an exceptional area for studying the structural and geochemical evolution of the sub-continental lithospheric mantle. Detailed structural mapping reveals that the Lherz spinel lherzolites are secondary rocks formed at the expense of harzburgites, which represent remnant bodies of an old (>2Ga) and highly refractory protolith. Petrological and geochemical data show that the lherzolite-websterite suite has been formed by a near-solidus refertilization reaction involving crystallization of pyroxene and spinel, and dissolution of olivine. The irregular-shaped harzburgite-lherzolite contact thus materializes an anastomosed

refertilization front formed by coalescence of melt infiltration channels. This evolution starts under static conditions but is followed by localization of the deformation in the refertilized domains. Upwelling of basaltic partial melts through the lithospheric mantle was associated with the migration of an important refertilization front. At a larger-scale, the Ronda Massif (S Spain) also displays a refertilization front which is tightly linked to a partial melting domain below (Lenoir et al., 2001; Van der Wal and Bodinier, 1996). We can thus imagine that the refertilization front observed in the Lherz Massif also moved ahead of a melting front related to thermo-mechanical erosion of the lithosphere.

There is a growing body of evidence indicating that the chemical variations observed in tectonically-emplaced mantle rocks result from igneous refertilization superimposed onto previous depletion events. An important implication is that fertile lherzolites from peridotite massifs cannot be straightforwardly used to infer primitive mantle compositions. In this perspective, it is logic to wonder whether the fertile mantle xenoliths represent refertilized or pristine mantle. Several authors have ascribed the chemical stratification of cratonic lithosphere and/or its temporal evolution to metasomatic refertilization (Griffin et al., 2003; Kopylova and Russell, 2000; Lee and Rudnick, 1999). In this scheme, fertile (predominantly lherzolitic), off-craton lithosphere may be viewed as the ultimate transformation of cratonic lithosphere after one or several cycles of igneous refertilization. Extensive refertilization in the Western Alps and Betic peridotites is intrinsically related to the lithospheric thinning processes that led to mantle exhumation (Lenoir et al., 2001; Müntener et al., 2004; Piccardo et al., 2004), which may suggest that large-scale refertilization is specific of tectonically-emplaced, orogenic peridotites. However, the Lherz massif illustrates a situation where refertilization and exhumation are related to distinct events, separated in time by thermal relaxation of the subcontinental mantle lithosphere. Several suites of spinel peridotite xenoliths compositionally comparable to the Lherz peridotites (i.e., formed of LREE-depleted lherzolites associated with subordinate, LREE-enriched harzburgites) might also record magmatic refertilization of a previously depleted lithospheric mantle.

Magmatic refertilization probably plays a key role in the rejuvenation and erosion of the lithospheric mantle. Seismological data suggest that the lithospheric mantle is strongly thinned in extensional environments (Bastow et al., 2005) and above mantle plumes (Li et al., 2004). Numerical models, however, predict that thermo-mechanical processes, like small-scale convective

destabilization, only produce limited thinning (<30km) (Thoraval et al., 2006), due to the strong temperature dependence of the viscosity and slow heat conduction in the lithospheric mantle. Refertilization of the lithospheric mantle by asthenospheric melts may reconcile these contrasting observations. Deformation experiments show that the presence of even a small fraction of basaltic melt results in a marked decrease of olivine-rich rocks strength (Hirth and Kohlstedt, 1995). Progression of the melt infiltration front producing the refertilization will therefore reduce the viscosity and favor the destabilization and removal of the lithospheric mantle.

Acknowledgements

This study was supported by the DyETI programme of INSU-CNRS and the Laboratoire de Tectonophysique, Montpellier. We thank Fred Frey for his comments on an earlier version of this paper, and Martin Menzies and Cin-Ty Lee for their constructive reviews. We are grateful to Christophe Nevado and Doriane Delmas for providing high-quality thin sections, to Claude Merlet for his help with electron probe analyses, and to Olivier Bruguier and Simone Pourtales for their assistance during LA-ICPMS analyses.

References: end of thesis manuscript.

Chapter III:

Feedback between melt percolation and deformation in an exhumed lithosphere-asthenosphere boundary

Article published in Earth and Planetary Science Letters **274** (2008), 401-413.

V. Le Roux[1,2], A. Tommasi[1], A. Vauchez[1]

[1] Géosciences Montpellier, Université de Montpellier 2 and CNRS, Cc 060, Place E. Bataillon, 34095 Montpellier cedex 5 France

[2] GEMOC, Department of Earth & Planetary Sciences, Macquarie University NSW 2109 AUSTRALIA

VLR's contribution in this paper: analyses, interpretations, writing.

Abstract

Interactions between deformation and melt percolation yield important consequences for the evolution of the mantle lithosphere, controlling its composition and mechanical behavior. In the Lherz massif (Pyrenees, France), the analysis of structural relationships between harzburgites, lherzolites and pyroxenites and of the crystal-preferred orientations (CPO) of olivine and pyroxenes highlights a strong feedback between percolation of basaltic melts and deformation under near-solidus conditions at the lithosphere-asthenosphere boundary. Elongated harzburgite bodies up to tens of meters wide, which are the remnants of an old lithospheric mantle, preserve a constant foliation. This foliation is locally outlined by cm-scale flattened websteritic lenses. At the contact with the enclosing lherzolites, the harzburgite foliation is crosscut by the lherzolites foliation and by cm-wide websterite bands parallel to the contact. Strain intensity in the lherzolites increases with distance to the harzburgites. Based on these observations, we propose that reactive percolation was synchronous to the deformation and propose that variations in instantaneous melt fraction, due to pyroxenes and spinel crystallization during reactive melt transport, guided strain localization. Accordingly, the observed decrease in olivine CPO intensity and change in CPO patterns from harzburgites to distal lherzolites are interpreted as recording changes in the relative contribution of dislocation glide and diffusion processes, which is ruled by a balance between the instantaneous melt fraction and the local strain rate. We also propose that the pervasive websteritic layering in the refertilized lherzolites may result from deformation-assisted melt segregation in a system with decreasing permeability due to refertilization reactions. Finally, we discuss the possible timing and geodynamical context of the refertilization episode.

Keywords: melt percolation; strain localization; mantle lithosphere; olivine; pyroxene; crystal-preferred orientation; dislocation creep; diffusion; refertilization reactions, lherzolites; websterites; harzburgites; melt segregation

1. Introduction

The evolution of the upper mantle is strongly associated with partial melting and refertilization processes. Recent studies have shown that percolating melts may react with the mantle lithosphere, inducing enrichment in fusible components, i.e., refertilization via the crystallization of pyroxenes and spinel (Beyer et al., 2006; Le Roux et al., 2007; Lenoir et al., 2001; Müntener et al., 2004; Rampone et al., 1994; Tommasi et al., 2004). Experimental deformation of partially molten assemblages shows that the presence of melt, even in low fractions, leads to a strong decrease in viscosity (Hirth and Kohlstedt, 1995; Rosenberg and Handy, 2005; Takei, 2005). Additionally, deformation may produce a higher transient permeability and facilitate melt segregation (Holtzman et al., 2003; Rosenberg and Handy, 2000). This feedback between melt percolation and deformation, observed experimentally, has also been proposed, on the basis of structural observations, as responsible for the development of shear zones in the middle and the lower crust (Brown and Solar, 1998; Kisters et al., 1998; Tommasi et al., 1994; Vauchez and Tommasi, 2003) and in the shallow mantle (Kelemen and Dick, 1995). At the plate scale, it has also been suggested, based on geodynamical models and seismic anisotropy data, that magmas play an essential role in the initiation of rifting (Buck, 2006; Kendall et al., 2006) and in the erosion of the lithosphere above mantle plumes (Thoraval et al., 2006). Interactions between melt percolation and deformation in the mantle are thus major processes in the evolution of the lithosphere, controlling its composition and mechanical behavior. In this article we document still poorly understood feedback processes between melt percolation and deformation in a complex natural system: a propagating lithosphere-asthenosphere boundary.

The Lherz Massif (Pyrenees, France) is an ideal location to study interactions between percolation and deformation in mantle rocks. It is composed of refertilized spinel lherzolites containing frequent cm-scale websteritic layers that surround metric to decametric-scale bodies of depleted harzburgite in the southern part of the massif. Detailed structural mapping and geochemical analysis show that the lherzolites formed at the expense of the harzburgites during a near-solidus refertilization reaction coeval with deformation of the lherzolites (Le Roux et al., 2007). The Lherz massif represents therefore an outcrop of a frozen lithosphere-asthenosphere boundary where the percolation of basaltic melts deeply modified the structure and the composition of the

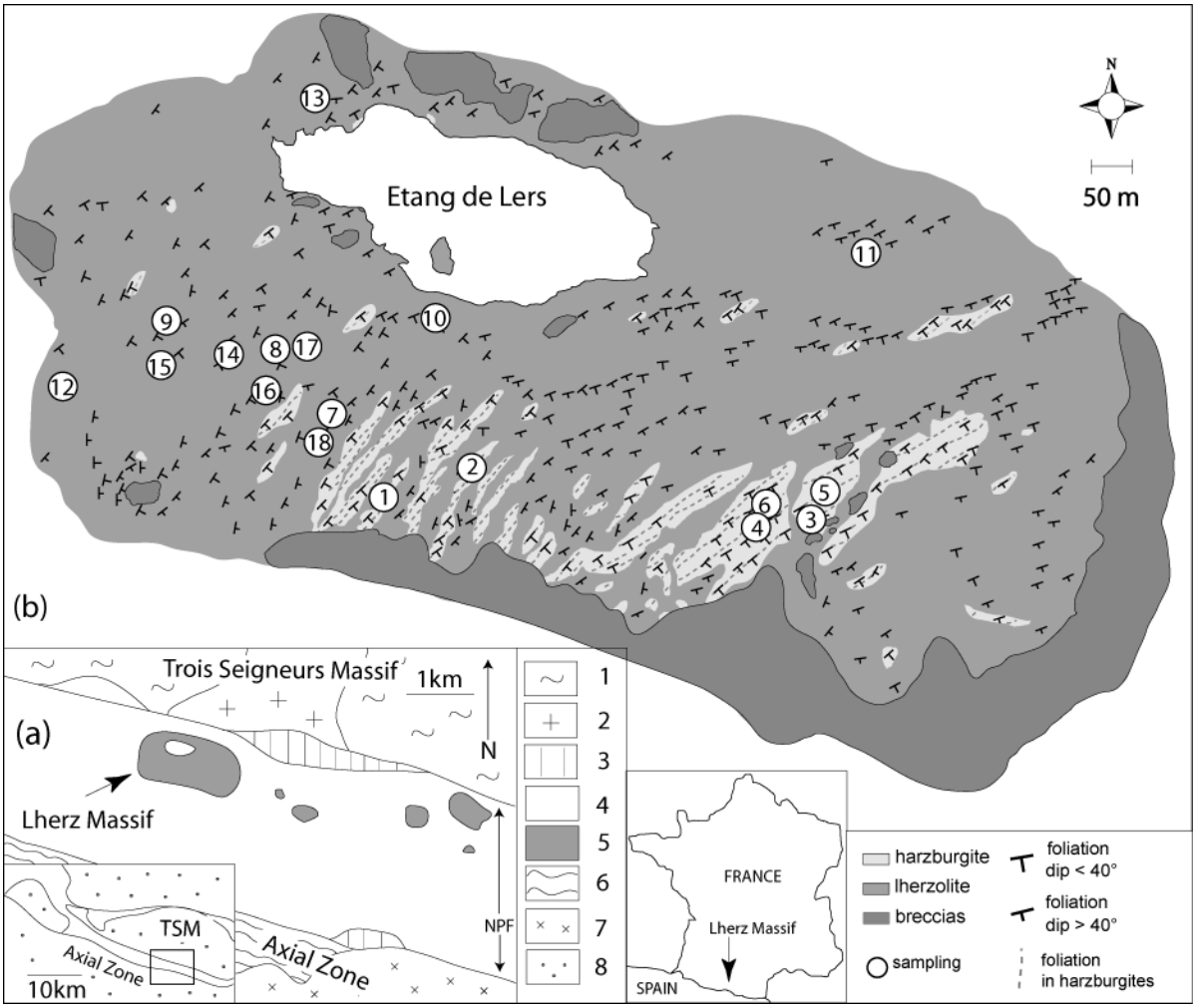

Fig. 1: (a) Localization and geological context of the Lherz Massif (Azambre and Ravier, 1978; Kornprobst and Vielzeuf, 1984; Monchoux, 1970; Vielzeuf, 1980). 1- Schists; 2- Mesozoic and Cenozoic rocks; 3- Granulites; 4- Metamorphic Mesozoic rocks; 5- Peridotites; 6- Granulite occurrences; 7- Hercynian basement; 8- Late Tertiary sediments. (b) Geological map of the Lherz Massif (Le Roux et al., 2007) with the location of analyzed samples.

mantle lithosphere.

We present a detailed study of the lithological distribution and deformation structures from the massif to the thin section scale, combined with analyses of olivine and pyroxenes crystal-preferred orientations (CPO) in harzburgites, refertilized lherzolites and websterites from the Lherz massif. These observations associated with previous data on the refertilization process (Le Roux et al., 2007) highlight a strong feedback between reactive melt percolation and deformation during refertilization. This results in both strain localization, which allowed the preservation of the pre-existing structure in the harzburgite lenses, and melt segregation, which lead to the formation of the websterites. Finally, we discuss the possible timing and geodynamical context for the refertilization episode.

2. The Lherz peridotitic massif (Pyrenees, France)

The Lherz Massif, type-locality of the lherzolite, is one of the largest of the 40 ultramafic bodies that outcrop along the North Pyrenean Fault (NPF; Pyrenees, France; Fig. 1a). The Pyrenean peridotite massifs, which dimensions vary from several m^2 to a few km^2, with ~ 1 km^2 for the Lherz massif (Fabriès et al., 1991; Monchoux, 1971), are mainly composed of layered spinel lherzolites. Exhumation of Pyrenean peridotites is usually ascribed to lithospheric thinning associated with successive opening and closing of elongated, asymmetrical pull-apart basins in response to the dominantly transcurrent motion of the Iberian plate relative to the European plate in the mid-Cretaceous (Choukroune and Mattauer, 1978; Debroas, 1987; Vielzeuf and Kornprobst, 1984). Most ultramafic massifs outcrop within carbonate rocks of Jurassic to Aptian age affected by a low pressure-high temperature metamorphism that characterizes the 'North Pyrenean Metamorphic Zone' (Golberg and Leyreloup, 1990), and they are generally associated with crustal granulites (Azambre and Ravier, 1978; Pin and Vielzeuf, 1983; Vielzeuf and Kornprobst, 1984).

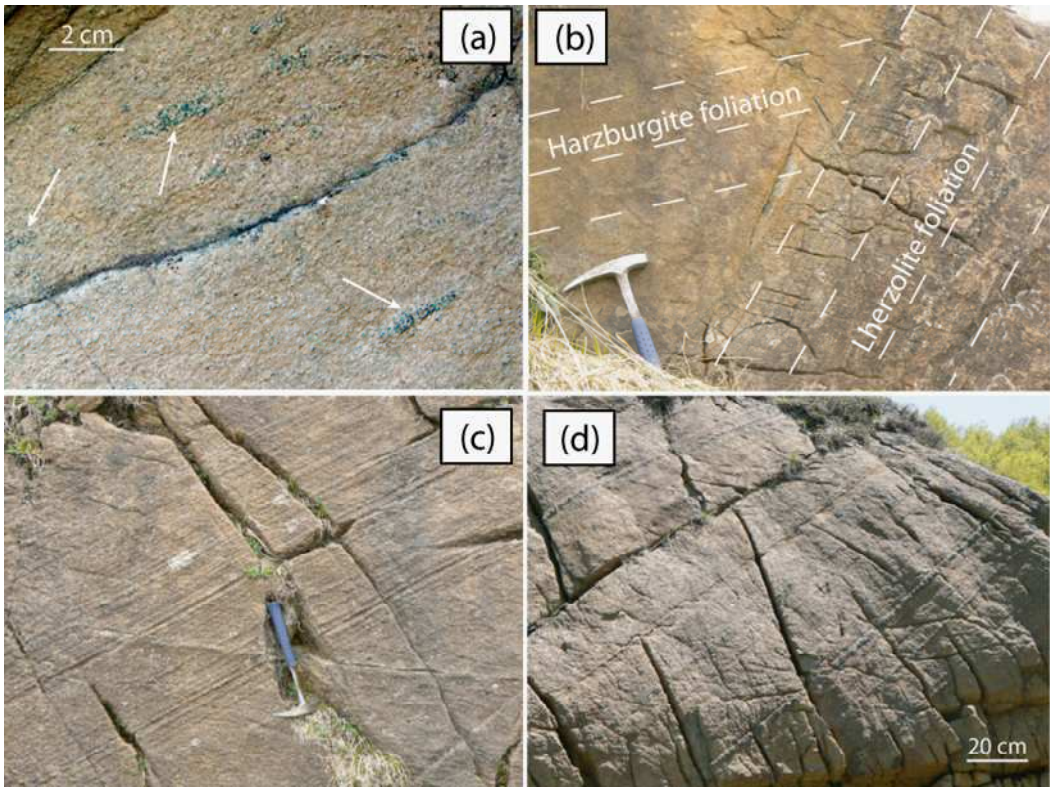

Fig. 2: Photographs of (a) fertile pockets in harzburgites; (b) a contact between harzburgite and lherzolite underlined by a thin websteritic layering. The foliations of harzburgites and lherzolites and the direction of the websteritic layering measured on the field are reported on the photograph as dashed lines; (c), (d) pervasive websteritic layering in distal lherzolites.

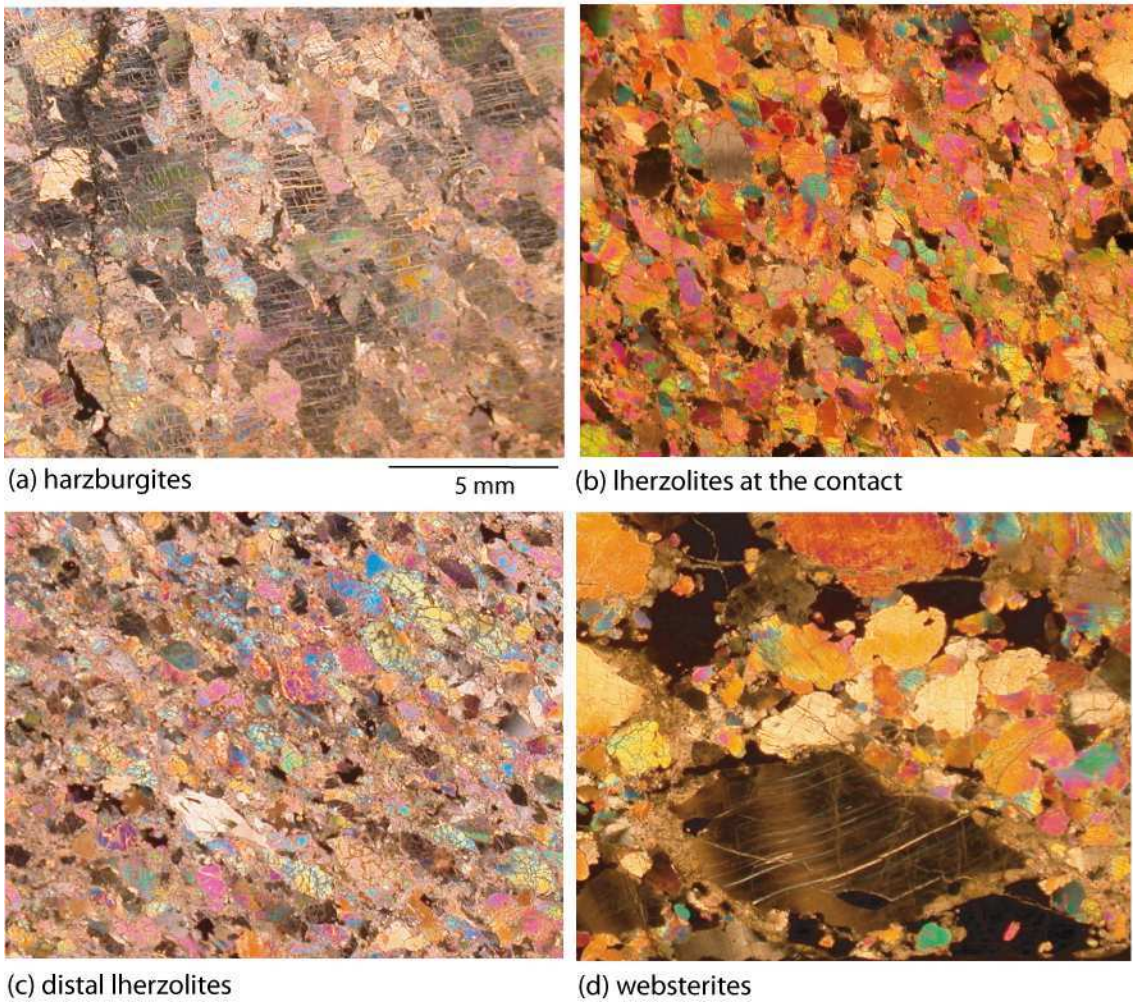

Fig. 3: Polarized-light photomicrographs showing: (a) the porphyroclastic texture in harzburgites; (b) the granular texture in lherzolites at the contact with an incipient foliation; (c) the porphyroclastic texture in distal lherzolites with well-developed foliation and lineation, marked by the elongation of spinel (Spl) and olivine (Ol) crystals; and (d) the coarse-granular texture in websterites with large deformed orthopyroxenes (Opx).

Emplacement of the ultramafic rocks in the crust has been dated at 105-110 Ma (Henry et al., 1998). In the Lherz massif, the last stage of exhumation of the peridotites is marked by extensive brecciation in the outer rim of the peridotite body and in the host limestones that show structures typical of sedimentary reworking (Lagabrielle and Bodinier, 2008).

Although mainly composed of refertilized spinel lherzolites that form ca. 75% of the massif (Fig. 1b), the Lherz massif displays metric to decametric-scale intermingling of secondary lherzolites and highly refractory harzburgites in its topographically higher, southern part (Le Roux et al., 2007). The northern part of the massif is essentially composed of refertilized lherzolites containing a pervasive cm-scale websteritic layering (Fig. 2c,d). The websteritic bands are numerous in lherzolites, whereas harzburgites are devoid

of them, except at the contact between the two lithologies. The entire massif is crosscut by a later generation of amphibole-bearing pyroxenite dykes and hornblendite veins, related to alkaline magmatism during the Cretaceous (Bodinier et al., 1987a; Golberg et al., 1986; Loubet and Allègre, 1982; Vétil et al., 1988). Meter-scale low-temperature mylonitic bands cross-cut the massif; they are more common at its borders and are probably related to the emplacement of the massif in the crust (Costa and Maluski, 1988).

The harzburgites generally occur as elongated bands a few meters to tens of meters-wide within the lherzolites. All harzburgites show a penetrative shallowly-dipping foliation with a constant N40-N60°E orientation and SW-NE sub-horizontal lineation, marked by elongated spinels and elongated olivine porphyroclasts. Throughout the massif, harzburgites display a homogeneous coarse-grained porphyroclastic microstructure (Fig. 3a), characteristic of deformation by dislocation creep under high-temperature, low-stress conditions (T >1100° C). Large olivine porphyroclasts (up to 5 mm long) are usually elongated; aspect ratios may attain up to 1:4. They display curvilinear grain boundaries, wavy extinction, and closely-spaced (100) subgrain boundaries. Orthopyroxenes and rare clinopyroxenes are smaller (2-3 mm and < 1 mm on average, respectively) and show irregular shapes and wavy extinction.

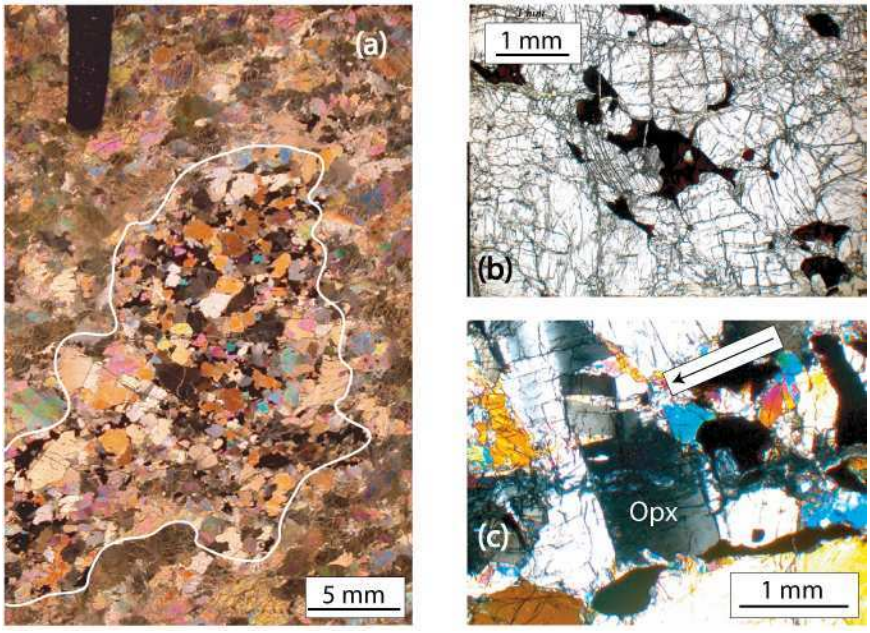

Fig. 4: (a) Photomicrograph parallel to the foliation plane of a porphyroclastic harzburgite showing a orthopyroxene-clinopyroxene-spinel rich websteritic lens with a coarse granular texture. Detail photomicrographs of the lens showing (b) irregularly-shaped interstitial spinels (Spl) and (c) a strongly deformed orthopyroxene (Opx) with en-echelon fractures normal to the kink bands filled with clinopyroxene.

Harzburgites often contain cm-scale disk-like pockets enriched in orthopyroxene-clinopyroxene-spinel flattened parallel to the foliation (Fig. 2a, 4a). In these fertile pockets, orthopyroxene is strongly deformed with common kink bands that locally evolve into fractures filled with clinopyroxene (Fig. 4c). Clinopyroxene deformation varies from grain to grain, some crystals show wavy extinction whereas others do not display any intracrystalline deformation features. Spinels display irregular interstitial shapes, which evolve into thin films along grain boundaries (Fig. 4b). Preservation of these delicate interstitial crystallization morphologies, marked by the crystallographic continuity between crystals within triple junctions and thin films along grain boundaries indicate that these crystals have not been deformed. In addition, some irregularly-shaped spinels, which surround the pyroxenes, may have formed by exsolution from the pyroxenes at even lower temperatures during cooling. According to their compositions, minerals constituting these pockets are in equilibrium with the harzburgitic matrix and represent accumulated newly-formed crystals. Approaching the contact with the lherzolites, these websteritic pockets become larger and more numerous and evolve to irregular or vein-like shapes oblique to the harzburgite foliation, but sub-parallel to the contact.

The contact between harzburgites and lherzolites is often sharp, steeply-dipping and marked by cm-scale websteritic layers (Fig. 2b) that crosscut the harzburgite foliation (Fig. 1, 2b). However, a progressive transition within some meters from harzburgite to clinopyroxene-poor lherzolites and to lherzolite may be locally observed. In the lherzolites close to the contact, the foliation is marked by a weak alignment of interstitial, irregularly-shaped spinels. This foliation is incipient close to the contact (<1m), but it strengthens away from it, where it is marked by alignment of spinels and elongation of olivine and pyroxene crystals (Fig. 3b). It is variable in orientation (N10 to N80) and dips either eastward or southward. It is usually oblique to the harzburgite foliation and parallel to the lherzolite-harzburgite contacts. At the contact, lherzolites often display a mm- to cm-scale websteritic layering parallel to the foliation. Proximal lherzolites show coarse pyroxene grains: orthopyroxenes are 2-3 mm large on average, but may attain up to 5mm, and clinopyroxenes are 1-2 mm large on average. Most pyroxenes are undeformed, but some display a faint wavy extinction. Olivine porphyroclasts (3-4 mm on average) are associated with smaller olivine grains (<1 mm). All olivine grains display wavy extinction and subgrains and they are more elongated with increasing distance to the contact.

Farther from the contact with the harzburgite bodies (>30m), distal refertilized

lherzolites are associated with a pervasive mm- to tens of cm-scale websteritic layering that parallels the foliation plane. Distal lherzolites are characterized by a well-developed, steeply-dipping foliation, dominantly oriented N40-N80, and defined by the alignment of spinel aggregates and the shape preferred orientation of olivine porphyroclasts (Fig. 3c). These lherzolites display both elongated olivine porphyroclasts (3-4 mm on average) with marked wavy extinction and closely-spaced subgrain boundaries, and smaller deformed olivine grains (<1 mm). Clinopyroxenes and orthopyroxenes are equant, 2-4 mm wide, and show wavy extinction. The thickest websterite bands (>10 cm wide) are locally folded or boudinaged, suggesting that they behaved as stiffer layers during the late stages of deformation. Generally, websterite layers contain small and equant olivine grains (<1 mm) showing wavy extinction. Clinopyroxenes and orthopyroxenes are 3-4 mm on average, but orthopyroxene may attain up to 1 cm (Fig. 3d). The largest orthopyroxene and clinopyroxene crystals usually show strong wavy extinction and subgrains. Spinels display irregular shapes.

3. Evolution of CPO through the Lherz Massif

3.1. Sampling and Methods

To investigate the evolution of the deformation in refertilized lherzolites and associated websterites through the Lherz massif, we sampled harzburgite-lherzolite contacts, proximal lherzolites close to the contacts with harzburgites (<30m), distal lherzolites (> 30m from the contact) and their associated websterites in the western part of the massif where they dominate (Fig. 1b).

Crystal-preferred orientations (CPO) of olivine, orthopyroxene and clinopyroxene were measured by indexing of Electron Back Scattered Diffraction (EBSD) patterns using the SEM-EBSD system at Geosciences Montpellier (France). Indexing was performed either manually or automatically. Manual measurements consisted of grain-by-grain indexing along 2 mm-spacing profiles parallel to the long axis of the thin section. For each thin section, except in the websterites, ≥ 200 olivine grains were indexed to obtain a statistically representative sampling of the CPO (Ben Ismaïl and Mainprice, 1998). The automatic mapping used a regular grid step of 85µm, which is in average 10-11 times smaller than the largest observed grains, over the whole thin section. Raw maps are characterized by 50-60% indexed surface. Non-indexed pixels are linked to serpentinization, polishing defects, grain boundaries and non-indexed minor phases like spinels. Post-acquisition data treatment allowed to further increase the

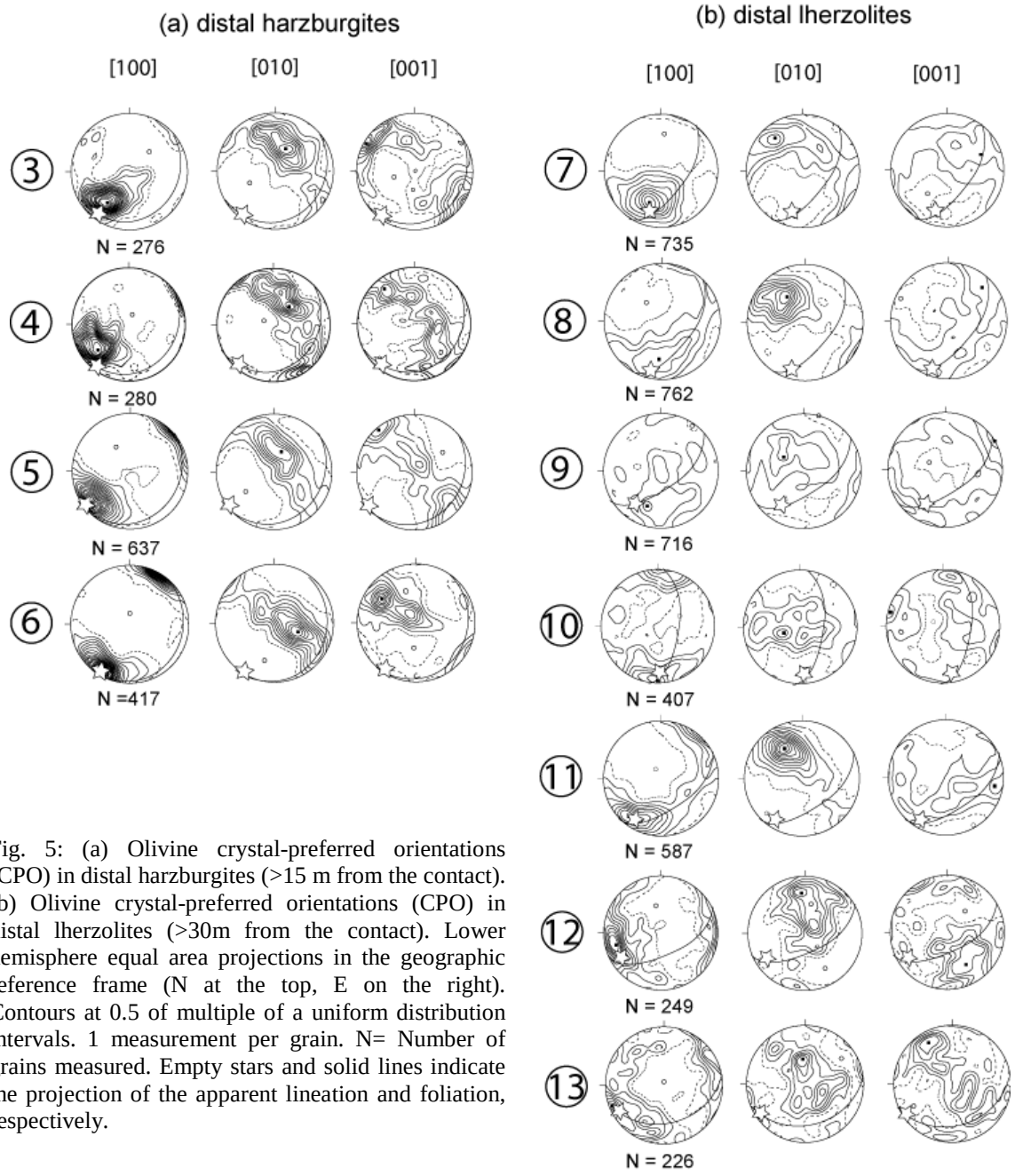

Fig. 5: (a) Olivine crystal-preferred orientations (CPO) in distal harzburgites (>15 m from the contact). (b) Olivine crystal-preferred orientations (CPO) in distal lherzolites (>30m from the contact). Lower hemisphere equal area projections in the geographic reference frame (N at the top, E on the right). Contours at 0.5 of multiple of a uniform distribution intervals. 1 measurement per grain. N= Number of grains measured. Empty stars and solid lines indicate the projection of the apparent lineation and foliation, respectively.

indexing rate by (i) filling the non-indexed pixels that have up to 8 identical neighbors with this orientation, (ii) repeating this operation using respectively 7, 6, and 5 identical neighbors, (iii) identifying the grains, i.e. continuous domains characterized by an internal misorientation <15°, and (iv) within each olivine crystal, searching and correcting for systematic indexing errors due to the olivine hexagonal pseudo-symmetry, which results in similar diffraction patterns for orientations differing by a rotation of 60° around [100]. At each step, the resulting orientation maps were checked to avoid over-extrapolation of the data. In addition, the microstructure and average grain size estimated from the EBSD crystal orientation

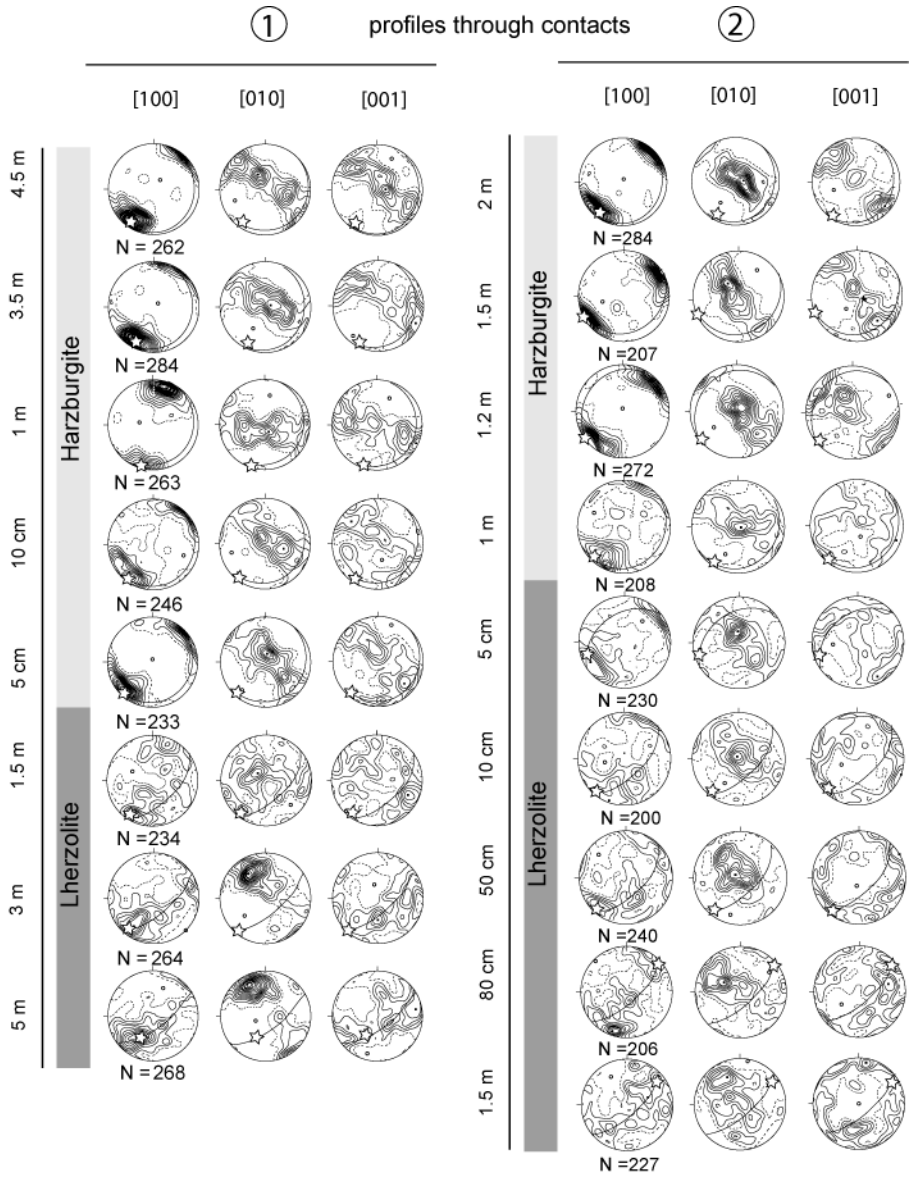

Fig. 6: Evolution of olivine crystal-preferred orientations (CPO) across two harzburgite-lherzolite contacts. Lower hemisphere equal area projections in the geographic reference frame (N at the top, E on the right). Contours at 0.5 of multiple of an uniform distribution intervals. 1 measurement per grain. N= Number of grains measured. Empty stars and solid lines indicate the projection of the apparent lineation and foliation, respectively.

maps were constrained by comparison to those observed by optical microscopy.

Pole figures are represented using average Euler angles for each grain instead of individual measurements to avoid over-representation of larger grains on the thin section. In addition we set up a minimum grain area of 36125μm^2 (5 contiguous measurement points) to avoid over-representing poorly indexed grains. This minimum area is small enough not to lose information on the orientation of the smaller grains, which are on average 1mm-wide. We obtained >400 indexed olivine grains and >200 indexed pyroxenes for each thin section, with exception of the websterites where fewer olivine grains could be measured.

The fabric strength is quantified by the J index, which is the volume-averaged integral of the squared orientation densities and hence is sensitive to peaks in the orientation distribution function (Bunge, 1982). J is dimensionless; it is 1 for a random distribution and infinity for a single crystal orientation. It usually ranges between 2 to 20 for natural peridotites (Ben Ismaïl and Mainprice, 1998).

3.2. Weakening of CPO associated with the refertilization process

Harzburgites display a clear [100]-fiber olivine CPO throughout the massif (Figs. 5a, 6 & 7). This olivine CPO pattern is characterized by alignment of [100] axes close to the lineation and a girdle distribution of [010] and [001] with a maximum of [010] normal to the foliation. It is typical of deformation by dislocation creep with activation of the high temperature, low stress (0kl)[100] slip systems, with (010) as the dominant slip plane (Tommasi et al., 2000). The orientation of the olivine CPO in the harzburgites is consistent throughout the massif. Its intensity, characterized by J_{ol} (Table 1) varies from point to point; CPO are strong (J_{ol} >8) away from the contacts, but more variable (J_{ol} varying from 10 to 4, with an average close to 7) within 10m of the contacts (Fig. 7). Orthopyroxene CPO in the

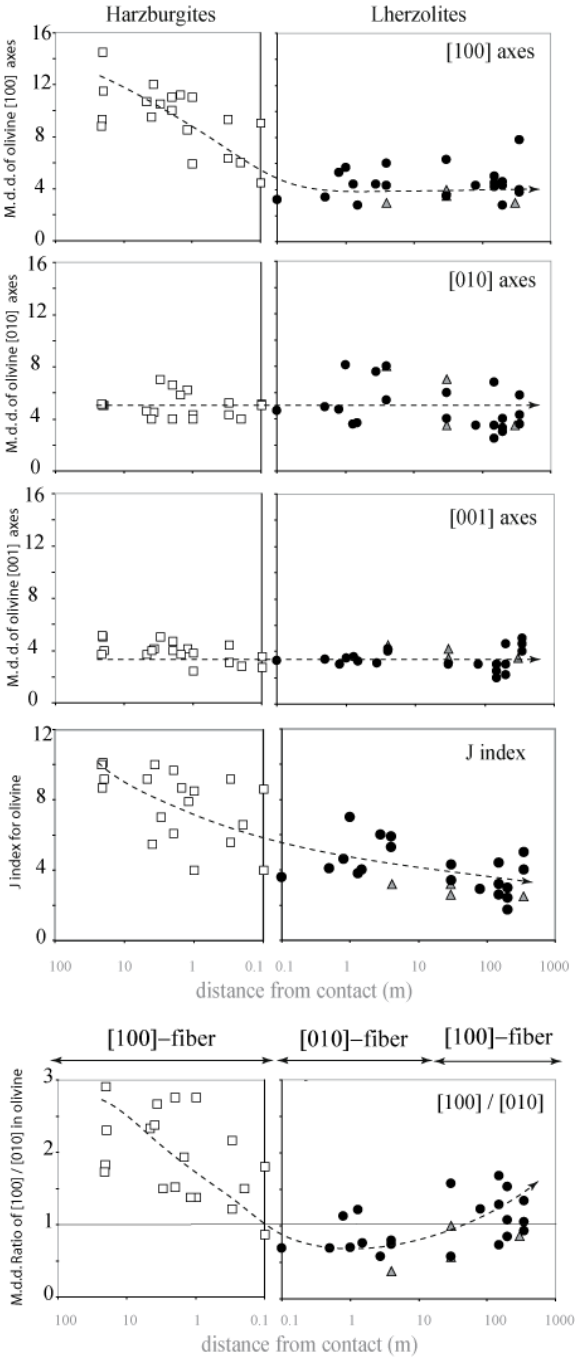

Fig. 7: Evolution of olivine CPO as function of the distance to the harzburgite-lherzolite contacts. (a) CPO strength, represented by the J index. (b), (c), and (d) Maximum density of distribution of [100], [010], and [001] axes of olivine, respectively. (e) Ratio of maximum density of distribution of [100] axes relative to the one of [010] axes. This plot highlights the transition from strong [100]-fiber patterns in harzburgites to ([010]-fiber patterns in lherzolites close to the contact, and finally to weak [100]-fiber patterns in lherzolites far from the contact. Empty squares: harzburgites; solid circles: lherzolites; grey triangles: websterites. Dotted lines outline the general evolution of the olivine CPO from the harzburgites to the lherzolites far from the contacts.

Sampling site	Sample type	Distance from contact	J index of olivine	fiber	Modal composition Ol	Opx	Cpx	Spl
1	harzburgite	5 cm	8.6	[100]	79.6	17.9	1.9	0.6
1	harzburgite	10 cm	6.6	[100]	75.3	20.8	2.2	1.7
1	harzburgite	1 m	8.5	[100]	71.4	25.7	2.3	0.6
1	harzburgite	3.5 m	9.2	[100]	76.9	20.3	2.1	0.7
1	harzburgite	4.5 m	10	[100]	66.8	27.7	3.1	2.5
1	lherzolite	1.5 m	3.8	[100]	45.5	28.5	22.7	3.3
1	lherzolite	3 m	6	[010]	57.3	29.5	10.9	2.3
1	lherzolite	5 m	7	[010]	54.4	28.4	15.2	2.0
2	harzburgite	1 m	4	[100]	80.4	17.6	1.5	0.5
2	harzburgite	1.2 m	7.9	[100]	84.1	14.1	1.4	0.4
2	harzburgite	1.5 m	8.7	[100]	82.9	15.2	1.4	0.4
2	harzburgite	2 m	9.7	[100]	82	16	1.5	0.6
2	lherzolite	5 cm	4	[010]	78	16	5	1
2	lherzolite	10 cm	3.6	[010]	68.8	19.9	9.7	1.6
2	lherzolite	50 cm	4.6	[100]	61.6	20.8	14.9	2.7
2	lherzolite	80 cm	4.1	[010]	72.6	16.1	9.3	1.9
2	lherzolite	1.5 m	4	[010]	59.9	26.3	11.7	2.1
3	harzburgite	> 15 m	8.7	[100]	94.0	4.6	1.2	0.2
4	harzburgite	> 15 m	10	[100]	79.5	16.8	2.4	1.2
5	harzburgite	> 15 m	9.2	[100]	78.0	19.0	2.0	1.0
6	harzburgite	> 15 m	10.1	[100]	76.0	21.0	2.0	1.0
7	lherzolite	30 m	4.3	[100]	61.0	25.0	11.5	2.5
8	lherzolite	50 m	3.4	[010]	46.0	35.0	15.0	2.0
9	lherzolite	60 m	1.75	[010]	46.0	32.0	20.0	2.0
10	lherzolite	70m	2.6	[100]	46.0	29.0	20.0	5.0
11	lherzolite	150 m	4.4	[010]	63.0	19.0	15.0	3.0
12	lherzolite	150 m	3	[100]	63.6	22.7	12.0	1.7
13	lherzolite	350 m	4	[100]	62.0	24.0	12.0	2.0
14	lherzolite	80 m	2.9	[100]	78.0	16.0	5.0	1.0
15	lherzolite	80 m	3.2	[100]	60.0	25.0	12.5	2.5
16	websterite	10 m	3.6	[010]	5.0	46.5	38.5	10.0
17	websterite	30 m	2.3	[010]	30.0	39.0	27.0	4.0
18	websterite	30 m	3.5	[010]	12.0	34.0	45.0	9.0

Table 1: Modal composition and olivine CPO pattern and intensity (J index) of the studied samples, according to their distance to the nearest harzburgite-lherzolite contact. The localization of the samples is given in Fig. 1; Ol = olivine, Opx = orthopyroxene, Cpx = clinopyroxene, Spl = spinel. Modal compositions were calculated by inversion of whole-rock chemical compositions based on mineral compositions obtained by microprobe analysis (Le Roux et al., 2007).

harzburgites display strong [001]-fiber patterns (Fig. 8a), characterized by alignment of [001] axes close to the lineation and a weaker concentration of [100] axes normal to the foliation (Fig. 8a). This CPO is typical of high-temperature deformation of orthopyroxene with dominant activation of the (100)[001] slip system. The correlation between olivine and orthopyroxene CPO, marked by parallelism of the dominant high-temperature Burgers vectors [100] and [001] respectively, suggests a coherent deformation of these two mineral phases. Although more dispersed, clinopyroxenes CPO are similar to that of the orthopyroxenes (Fig. 8a).

The harzburgite-lherzolite contacts are marked by a significant decrease of the olivine CPO from the harzburgites to the lherzolites with J_{ol} varying from 7 on

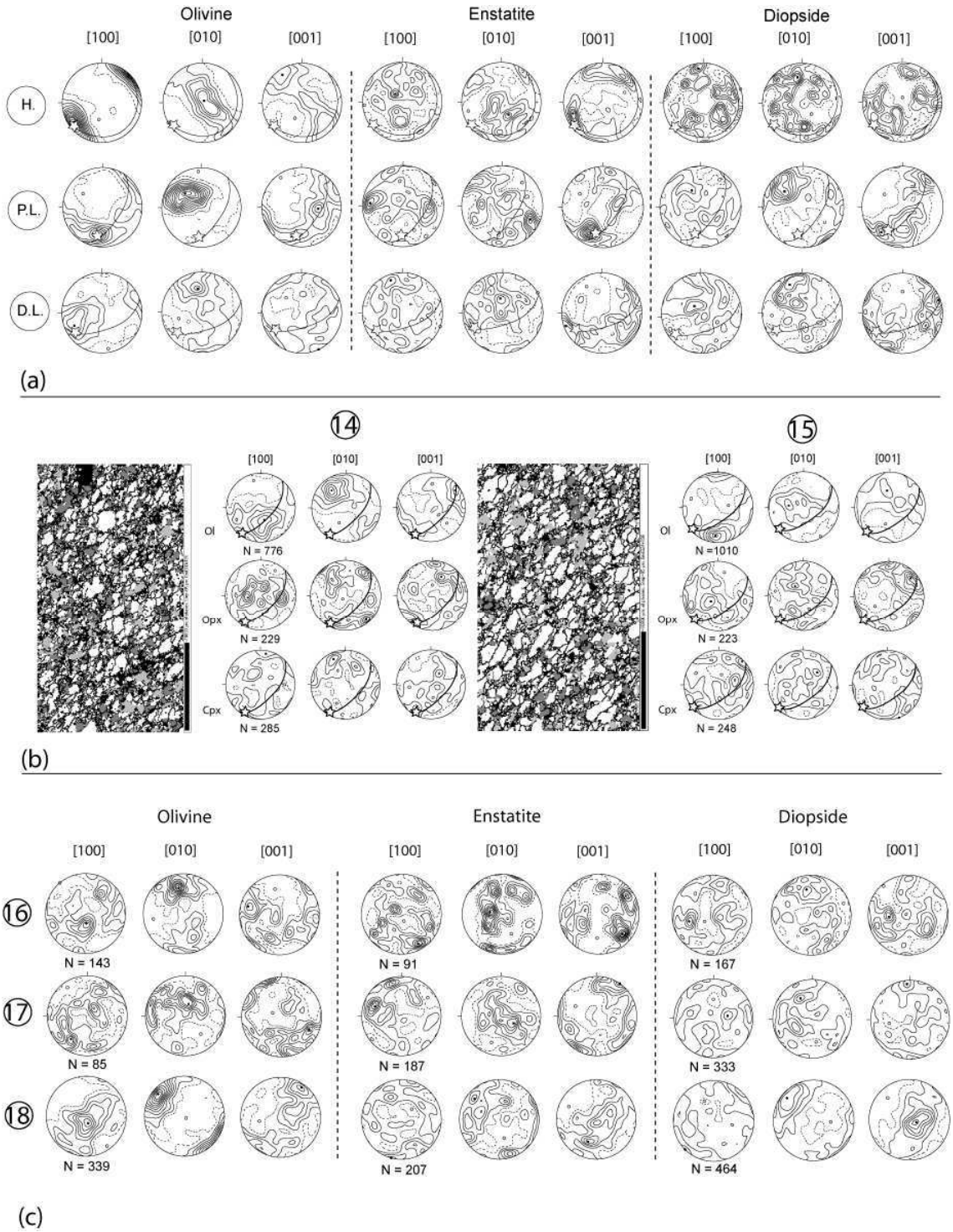

Fig. 8: (a) Representative crystal-preferred orientations (CPO) of olivine, enstatite and diopside in harzburgites (H.), proximal lherzolites (P.L.) and distal lherzolites (D.L.). Lower hemisphere equal area projections in the geographic reference frame (N at the top, E on the right). Contours at 0.5 of multiple of a uniform distribution intervals. 1 measurement per grain. N= Number of grains measured. Empty stars and solid lines indicate the projection of the average lineation and foliation of representative samples. (b) Shape- and crystal-preferred orientations (CPO) of olivine (Ol, white), orthopyroxene (Opx, light gray) and clinopyroxene (Cpx, dark gray) measured by crystal orientation mapping with a 85µm grid step in two 'abnormal' distal lherzolites. Empty stars and solid lines indicate the projection of the apparent lineation and foliation respectively. The lineation, marked by the elongation of olivine crystals, is not parallel to the maximum concentration of [100] axes of olivine, but it is parallel to the maximum concentration of [001] axes of pyroxenes. (c) Crystal-preferred orientations (CPO) of olivine, enstatite and diopside in cm-scale websterite layers within lherzolites. Dotted lines represent the orientation of the websteritic layer.

average in harzburgites to 4 in lherzolites within a few meters (Table 1; Fig. 7). Most lherzolites at the contact have a weak [010]-fiber olivine CPO pattern (Figs. 6 & 7). Surprisingly, in lherzolites within 1m from the contact, olivine (010) planes and pyroxenes (100) planes are not parallel to the incipient foliation measured in the field; they are rather aligned with the foliation and the olivine CPO in the neighboring harzburgites. Farther away from the contact (>1m), the olivine CPO becomes consistent with the lineation and foliation observed in the lherzolites at both field and thin-section scales (Fig. 6). The re-alignment of the crystallographic axes in the newly-developed foliation seems thus belated compared to the change in modal composition in response to the refertilization process, suggesting a weak deformation at the contact. Pyroxenes CPO in proximal lherzolites is weak, but orthopyroxenes show a clear [001] maximum parallel to the lineation, whereas clinopyroxenes tend to show a weak [010] maximum and a girdle distribution of [001] normal and parallel to the foliation, respectively (Fig. 8a).

In the distal (> 30m from the contact), layered lherzolites that outcrop in the northern and western part of the Lherz massif, olivine CPO is always weak: J_{ol} ranges between 4.4 and 1.7 (J_{ol} =3 on average; Table 1 & Fig. 7). These lherzolites dominantly display [100]-fiber olivine CPO patterns (Figs. 5b & 7). [100] axes of olivine are aligned close to the lineation, whereas [010] and [001] display a girdle distribution with a maximum of [010] normal to the foliation. This crystallographic fabric is consistent with activation of (0kl)[100] slip systems with dominant slip on (010) planes. Some distal lherzolites display [010]-fiber olivine CPO, similar to those observed close to the harzburgite bodies (Figs. 5b & 7). Orthopyroxene CPO in distal lherzolites are also weak, but well-correlated with the olivine CPO (Fig. 8a). Finally, some distal lherzolites from the western part of the massif, show an olivine CPO uncorrelated to the olivine shape preferred orientation that marks a clear foliation and lineation (Fig. 8b). In these peculiar lherzolites, the maximum concentration of [100] axes of olivine is oblique (ca. 40-50°) to the elongation of olivine crystals. In contrast, pyroxenes CPO show a good correlation with the olivine shape preferred orientation; [001] axes of clino- and orthopyroxenes are preferentially aligned parallel to the direction of elongation of olivine crystals (Fig. 8b).

Distal lherzolites are always associated with cm-scale websteritic layers in which olivine and pyroxene display a weak CPO (Fig. 8c). Olivine CPO is usually characterized by [010]-fiber patterns and J_{ol} varying from 3.6 to 1.7 (J_{ol} =2.6 on average; Table 1). [100] axes of olivine and [001] axes of pyroxenes are parallel to the

direction of elongation of pyroxenes while [010] axes of olivine and [010] and [100] axes of clino- and orthopyroxene, respectively, are normal to the layering measured in the field.

4. Discussion

4.1. Evolution of percolation-deformation feedback mechanisms from harzburgites to lherzolites

In the Lherz massif, lherzolites formed through a refertilization process involving interaction of refractory mantle lithosphere (harzburgites) with upwelling asthenospheric melts (Le Roux et al., 2007). Detailed structural mapping shows that the orientation of the foliation and the lineation in harzburgites is consistent at the scale of the massif even though many harzburgites are small, isolated bodies enclosed in the lherzolites. On the other hand, the direction of the foliation and lineation in lherzolites varies throughout the massif. The lherzolites steeply-dipping foliation locally moulds the harzburgite bodies and often crosscuts their steady shallowly-dipping foliation. In addition, within the lherzolites, an increase in the deformation away from the contact with harzburgites is suggested by the progressive development of a shape-preferred orientation of olivine crystals and a better alignment of spinels, which results in an evolution in the field from an incipient to a well-developed foliation with increasing distance to the contacts. Stronger deformation in the distal lherzolites is also suggested by boudinage and folding of the websteritic layering that are not observed close to the contacts. These observations support that the harzburgites preserve structures related to an episode of deformation prior to the formation of the lherzolites, and that subsequent deformation was localized in the lherzolites. The important change in the deformation kinematics, characterized by sub-horizontal foliations in harzburgites to steeply-dipping foliations in lherzolites, suggests two distinct deformation episodes rather than a continuum. In the following paragraphs we discuss the relations between melt percolation and deformation that vary throughout the massif, from the harzburgites to the distal lherzolites.

The numerous cm-scale websteritic lenses in the harzburgites (Fig. 2a) were probably formed by partial crystallization of small volumes of melt injected in the harzburgite. Coexistence of strongly deformed orthopyroxene crystals showing wavy extinction, kink bands, local ‘en echelon’ fractures and moderately to undeformed clinopyroxenes and undeformed spinels (Fig. 4) suggests syn-kinematic crystallization where strain rate progressively decreased with increasing

crystal fraction. Fractures normal to kink bands in large deformed orthopyroxene crystals filled by small undeformed clinopyroxene crystals (Fig. 4c) may have resulted from crystal-scale hydraulic fracturing in the harzburgites caused by local overpressure due to the presence of melts.

Far from the harzburgite-lherzolite contacts, these websteritic lenses are systematically parallel to the harzburgites foliation. In contrast, close to the contacts, they are larger and more numerous and they are often oblique to the harzburgite foliation and parallel to the contact. Because of their minerals composition similar to those of the host matrix, it seems difficult to chemically discriminate whether these pockets are linked or not to the refertilization event. Although a possible formation of these websteritic lenses during an older melt percolation event cannot be ruled out, we favor, based on our structural observations, the hypothesis that they represent the early stage of the melt percolation event that formed the lherzolites. In this scenario, the foliation-parallel websterite lenses represent the initial stages of melt percolation that were accompanied by an incipient deformation of the harzburgites. Alignment of the melt lenses in the foliation implies that the percolation of these small melt volumes was guided by the preexistent anisotropic structure of the harzburgites (Tommasi et al., 2008; Waff and Faul, 1992). The strong olivine CPO in the harzburgites resulted in a mechanical anisotropy (Tommasi and Vauchez, 2001) that probably also controlled the incipient stages of deformation. Close to the contact with lherzolites, the structural control by the harzburgite foliation was probably overwhelmed by the external solicitation (imposed kinematics), which is better expressed in lherzolites. Finally, coexistence of deformed and undeformed minerals in these lenses suggests that partial crystallization and refertilization reactions in the melt pockets led to a stop of the deformation and transfer of strain to domains with a larger proportion of melt and hence a lower dynamic viscosity.

With increasing distance to the contacts with harzburgites, lherzolites display an evolution of macroscopic structures and crystal preferred orientations that may be explained by variations in finite strain and in the melt fraction present during deformation. The tectonic fabric of the lherzolites strengthens with increasing distance to the contact. Within 1m from contact, the lherzolites show an incipient foliation marked by the alignment of interstitial spinels and a cm-scale websterite banding, but their olivine CPO is still parallel to the harzburgite one. This suggests that, in this narrow contact zone, strain was not high enough to erase the crystallographic fabric inherited from harzburgites. Within 30m from the contacts, proximal lherzolites show

a weak but clearly developed foliation and lineation, to which is associated a weak olivine CPO with a dominant [010]-fiber pattern, characterized by a point maximum of [010] normal to the foliation and dispersion of [100] in the foliation plane.

[010]-fiber olivine patterns similar to those observed in the proximal lherzolites have been observed in peridotites world-wide, for instance in the Ronda massif (Vauchez and Garrido, 2001), in alkali-basalt xenoliths from Siberia (Tommasi et al., 2008), in cratonic xenoliths (Ben Ismaïl and Mainprice, 2001; Vauchez et al., 2005) and in mantle xenoliths from oceanic islands (Bascou et al., 2008). The development of such patterns has been explained by: (i) axial shortening or 3D transpressive deformation (Bascou et al., 2008; Tommasi et al., 1999), (ii) activation of multiple glide directions (Mainprice et al., 2005; Tommasi et al., 2000), (iii) static recrystallization (Tommasi et al., 2008), and (iv) deformation in presence of melt (Holtzman et al., 2003). The alignment of [001] axes of orthopyroxene forming a point maximum close to the lineation does not support a transpressive deformation, which would also result in dispersion of the orthopyroxene [001] axes in the foliation plane, as observed for instance in the Kerguelen Islands mantle (Bascou et al., 2008). The present microstructural observations indicate that the Lherz peridotites were deformed in the shallow mantle (in the spinel stability field) at near-solidus conditions. The pressure/stress conditions that prevailed during the deformation are therefore too low for activation of [001] glide (Couvy et al., 2004; Jung and Karato, 2001; Mainprice et al., 2005; Vauchez et al., 2005). Indeed, analysis of crystallographic orientation maps shows that subgrain boundaries in these lherzolites are dominantly (100) tilt boundaries, implying dominant activation of [100] glide. Finally, the absence of annealing features in olivine does not support static recrystallization. Thus we favor the latter hypothesis, i.e., a simple shear deformation in presence of melt to explain [010]-fiber olivine patterns in the proximal lherzolites. This suggests that deformation mechanisms similar to those in the laboratory experiments were activated even though natural deformation conditions were very different from the experimental ones, in particular the grain sizes (10 microns versus several mm in natural conditions) and the strain rates.

Farther from the contact (>30m), the distal lherzolites have a well-developed foliation and lineation marked by the alignment of spinel aggregates and flattening of olivine, which suggest a larger finite strain. This interpretation is corroborated by the observation of local boudinage or folding of the pervasive websteritic layering. Paradoxically, the distal lherzolites display olivine CPO with a dominant [100]-fiber

pattern (Fig. 5b), but that are significantly weaker than those in the proximal lherzolites. Higher finite strain in the distal lherzolites may have favored a better orientation of [100] parallel to the lineation. The association of a strong foliation and lineation with weak CPO might be explained by an increase of diffusion accommodated creep and/or grain boundary sliding at the expense of dislocation creep. Diffusion processes are favored by higher temperatures, lower deviatoric stresses, and the presence of fluids. An important temperature or stress gradient is unrealistic at the tens of meters scale. However the greater abundance of websteritic layers, locally up to tens of cm-wide, suggests that this zone may have experienced a higher melt flux than the proximal lherzolites, even though the porosity probably never exceeded 2-3%. Larger instantaneous melt fractions may have favored melt-assisted grain boundary sliding (Rosenberg and Handy, 2001; Scott and Kohlstedt, 2006). The average olivine grain size decreases from harzburgites to refertilized lherzolites. Smaller grains have a larger surface/volume ratio which, when deformation occurs in the presence of melt, favors an accommodation by melt-assisted grain boundary sliding. Furthermore, Wark and Watson (2000) have shown that when coarse- and fine-grained domains are in chemical communication, melt is focused in the fine-grained domains, resulting in a permeability that matches or exceeds that of coarser grained domains. Thus if grain size refinement preceded melt percolation, both melt percolation and deformation may have localized within the fine-grained domains. Finally, some distal lherzolites have a maximum concentration of [100] axes at 40-50° to the lineation marked by the elongation of the olivine crystals, which is nevertheless parallel to the enstatite [001] maximum (Fig. 8b). We speculate that the observed lack of correlation between the shape- and crystallographic fabric of olivine might be related to partitioning of deformation with a higher contribution of diffusion and dislocation creep in melt-rich and melt-poor domains, respectively (Holtzman et al., 2003) or to local transtension.

Structural data in the Lherz massif points to a direct correlation between strain intensity and percolating melt volume fraction as illustrated in Fig. 9. Increasing deformation tends to favor melt segregation (Holtzman et al., 2003), which, by a feedback effect, leads to further strain localization. In the Lherz massif however, the progressive crystallization of the magmas during the refertilization reaction might have been a limitant parameter for this feedback between deformation and percolation, resulting in transfer of strain towards new melt-rich zones.

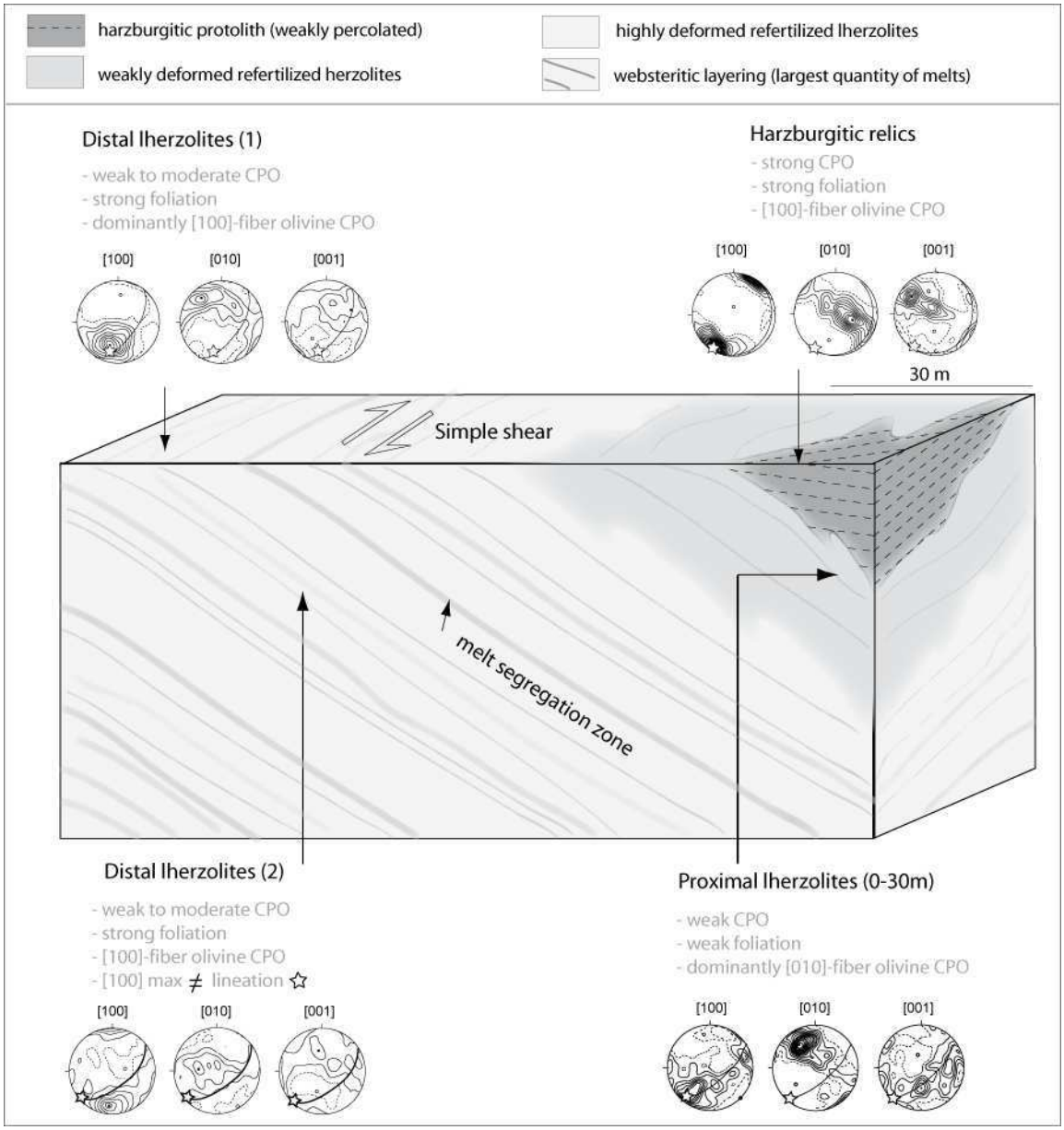

Fig. 9: Sketch summarizing the evolution of microstructures and olivine CPO in harzburgites and lherzolites from the Lherz massif according to their distance to the harzburgite-lherzolite contacts.

4.2. Formation of a pervasive websteritic layering in refertilized lherzolites

The refertilization process in the Lherz massif resulted in the formation of both massive lherzolites and of mm- to tens of cm-scale websteritic layers parallel to the foliation of the lherzolites. The websteritic layering is pervasive in the distal lherzolites, but cm-wide websteritic bands are also often observed at the harzburgite-lherzolite contacts. The chemical composition of these websterites shows that they do not represent simple crystallized trapped melts (Bodinier et al., 1987b). We interpret therefore these websteritic layers as zones of melt segregation, favored by strain, where higher melt fractions resulted in more developed

refertilization reactions (dissolution of larger volumes of olivine and crystallization of larger amounts of pyroxenes and spinels). However, the actual volume of melts needed to form these layers cannot be assessed accurately.

Holtzman et al. (2003) showed that in olivine + basalt + chromite or FeS, anorthite + basalt, and in olivine + albite melt samples deformed under simple shear, melt segregates into a network of melt-rich bands. Analysis of these results as well as numerical models suggest that segregation is controlled by pressure gradients and depends therefore on the compaction length of the system, which is a function of the permeability and of the solid and fluid viscosities (Hofmann, 2003; Rabinowicz and Ceuleneer, 2005; Spiegelman, 1993). In the Lherz massif, pyroxenes and spinel crystallization during refertilization reactions resulted in a reduction of porosity, plugging the melt network and hence favoring the segregation of melts. The coexistence of cm-scale strongly deformed orthopyroxenes and moderately to undeformed clinopyroxenes suggests that the deformation slowed progressively as the newly-formed crystals plugged the porosity, likely localizing further in less crystallized domains. The websteritic layers in the Lherz massif thus probably represent multiple “frozen” timesteps of a dynamic melt transport system.

4.3. Geodynamic environment of the refertilization process

In this paper we suggest that the refertilization of the old harzburgitic mantle lithosphere was coeval with a deformation dominated by simple shear under subsolidus temperature conditions. During the evolution of the Pyrenean domain, two major events have tightly associated magmatism and deformation: 1) the Cretaceous deformation and 2) the Hercynian orogeny. The emplacement of the Lherz massif in the crust during the Cretaceous (Henry et al., 1998) might have produced such a deformation. However amphibole-pyroxenite dykes considered to represent trans-lithospheric melt conduits for Cretaceous alkaline magmatism (Bodinier et al., 1987a; Golberg et al., 1986; Loubet and Allègre, 1982; Vétil et al., 1988) crosscut at high angle the foliations of both the harzburgites and refertilized lherzolites, suggesting that the refertilization event occurred before the Cretaceous. Moreover Pyrenean peridotites record equilibrium conditions of 8-17 kb at ~950°C suggesting an isobaric cooling stage from ~1200°C to ~900°C during a ~20My thermal relaxation episode (Fabriès et al., 1991; Sautter and Fabriès, 1990). This long thermal relaxation rules out the idea that the refertilization episode occurred during the emplacement of the massif in the crust, since this later is inferred to have occurred in

<5m.y. throughout the Pyrenees (Fabriès et al., 1998; Fabriès et al., 1991; Schärer et al., 1995).

Seismic anisotropy measurements in the Pyrenees led Barruol et al. (1998) to suggest that the retrieved S-wave polarization anisotropy is largely inherited from the deformation of the mantle lithosphere during the Hercynian orogeny. Indeed, shear-wave splitting measurements yield a consistent ~N100E polarization of the fast S-wave and rather large splitting, suggesting a lithospheric fabric mostly due to transcurrent motions. This anisotropy is observed in all domains of the Pyrenean belt, even in the southern and northern external domains where the ECORS seismic profile has shown that only the uppermost crust was involved in the Pyrenean tectonics (Choukroune, 1988). An Hercynian orogenic fabric therefore appears as the best candidate to explain the observed S-wave anisotropy (Barruol et al., 1998; Vauchez and Barruol, 1996). The late stages of the Hercynian orogeny in the Pyrenees are characterized by emplacement of syncinematic granites at the scale of the belt. Based on the analysis of the magmatic flow fabric of these granites and of the tectonic fabric in the host rocks, Gleizes et al. (1997) suggested that the whole Pyrenean belt behaved as a large, lithospheric-scale "shear-zone" during the last stage of the Variscan orogeny. We suggest therefore that the Variscan event may represent an adequate context for the syn-orogenic refertilization episode of an older lithosphere, remnants of which have been preserved in Lherz massif.

5. Conclusions

Based on a detailed study of the relationships between deformation and melt percolation in harzburgites, refertilized lherzolites and websteritic layers in the Lherz massif we propose that:

(a) Reactive percolation of basaltic melts in the harzburgitic Pyrenean lithosphere was synchronous to a lithospheric-scale simple shear deformation, which led to the development of a new foliation in the refertilized, secondary lherzolites and associated websterites. Some remnants of the harzburgitic protolith avoided most of this deformation and form elongated lenses within the refertilized and deformed lherzolites.

(b) There is a continuum in the deformation, which started in the harzburgites and progressively localized in the refertilized lherzolites. The deformation intensity increases with increasing distance from the harzburgites and increasing volume of percolating melts. We suggest that feedback between deformation and melt percolation produced the observed structures: larger melt fractions favored strain localization and larger strain favored

melt percolation through a higher dynamic porosity. This feedback is probably a major process in the compositional and structural rejuvenation of the subcontinental mantle lithosphere.

(c) The response of the rocks' texture to deformation depends on a subtle balance between two parameters: the strain intensity and the volume of percolating melts. In the Lherz massif, this led to coexistence of [100]-fiber and [010]-fiber olivine CPO. [100]-fiber olivine CPO developed where strain dominated the evolution (very low melt fractions as in the harzburgites or high strain as in the distal lherzolites). On the other hand, [010]-fiber olivine CPO developed where melt played an equally important or dominant part in the evolution (low melt fraction and incipient strain in proximal lherzolites or large melt fractions in the websterites).

(e) The formation of the websterites layers was synchronous of that of the lherzolites, due to melt segregation that was probably favored by the refertilization reactions, which plugged the melt network, reducing the permeability and producing small-scale pressure gradients.

(e) The deformation-refertilization event observed in the Lherz massif probably records the evolution of the Pyrenean mantle lithosphere during the late stage of the Variscan orogeny during the Carboniferous, when abundant magmatism coeval with orogen-parallel transcurrent faulting was emplaced throughout the Pyrenean domain. This shearing produced a large-scale anisotropic structure in the mantle lithosphere, which may explain the belt-parallel polarization of the fast split shear wave observed in the Pyrenees.

Acknowledgments

We thank Ben Holtzman and Günter Suhr for their constructive reviews. D. Mainprice provided softwares for analysing/plotting CPO data and C. Nevado and D. Delmas supplied high quality polished thin sections for EBSD measurements. This study was partially funded by the Institut National des Sciences de l'Univers (CNRS/INSU) program 'Dynamique et Evolution de la Terre Interne' (DyETI). This is contribution no 544 from the GEMOC ARC National Key Centre.

References: end of thesis manuscript.

Chapter IV:

Isotopic decoupling during porous melt flow: a case-study in the Lherz peridotite

Article accepted to Earth and Planetary Science Letters

V. Le Roux[1,2], J.-L. Bodinier[1], O. Alard[1,2], S.Y. O'Reilly[2], W.L. Griffin[2]

[1] Géosciences Montpellier, Université de Montpellier 2 and CNRS, Cc 060, Place E. Bataillon, 34095 Montpellier cedex 5 France

[2] GEMOC, Department of Earth & Planetary Sciences, Macquarie University NSW 2109 AUSTRALIA

VLR's contribution in this paper: analyses, interpretations, writing.

Abstract

Most peridotite massifs and mantle xenoliths show a wide range of isotopic variations, often involving significant decoupling between Hf, Nd and Sr isotopes. These variations are generally ascribed either to mingling of individual components of contrasted isotopic compositions or to time integration of parent-element enrichment by percolating melts/fluids, superimposed onto previous depletion event(s). However, strong isotopic decoupling may also arise during porous flow as a result of daughter-elements fractionation during solid-liquid interaction. Although porous flow is recognized as an important process in mantle rocks, its effects on mantle isotopic variability have been barely investigated so far. The peridotites of the Lherz massif (French Pyrenees) display a frozen melt percolation front separating highly refractory harzburgites from refertilized lherzolites. Isotopic signatures observed at the melt percolation front show a strong decoupling of Hf from Nd and Sr isotopes that cannot be accounted for by simple mixing involving the harzburgite protolith and the percolating melt. Using one dimensional percolation-diffusion and percolation-reaction modeling, we show that these signatures represent transient isotopic compositions generated by porous flow. These signatures are governed by a few critical parameters such as daughter element concentrations in melt and peridotite, element diffusivity, and efficiency of isotopic homogenization rather than by the chromatographic effect of melt transport and the refertilization reaction. Subtle variations in these parameters may generate significant inter-isotopic decoupling and wide isotopic variations in mantle rocks.

Keywords: isotopic decoupling; mantle rocks; melt transport; metasomatism; diffusion; Lherz

1. Introduction

Mantle rocks that outcrop at the Earth's surface provide a direct source of information on the composition and evolution of the Earth's mantle. Isotopes systematics observed in most peridotite massifs (Reisberg and Zindler, 1986; Downes et al., 1991; Pearson and Nowell, 2004) and mantle xenoliths (Deng and Mcdougall, 1992; Witt-Eickschen and Kramm, 1997; Bizimis et al., 2003;Wittig et al., 2007) show a wide range of variations compared with single suites of mantle-derived lavas. Some of the isotopic variations observed in peridotite massifs are correlated with lithologies, e.g. pyroxenites vs. peridotites (Reisberg and Zindler, 1986; Pearson and Nowell, 2004) and have been ascribed to convective mingling of subducted material with pristine material (Allègre and Turcotte, 1986; Becker, 1996). Other, small scale heterogeneities are ascribed to isotopic enrichment by metasomatizing fluids/melts superimposed onto ancient depletion due to melt extraction (Downes et al., 1991; Bizimis et al., 2003; Wittig et al., 2007). The time integration of both depletion and enrichment of parent elements is often considered as the primary cause of isotopic variations in lithospheric peridotites.

However, few studies have tackled the relationships between isotopic variations and metasomatic processes (e.g. Ionov et al., 2002; Bodinier et al. 2004). Therefore, the mechanisms of isotopic enrichment and inter-isotopes decoupling during mantle metasomatism are still barely understood. Additionally, the "instantaneous" (as opposed to "time-integrated") effect of melt transport on isotopes systematics is usually neglected, although it may theoretically generate drastic fractionation of daughter elements from different isotopic systems (Navon and Stolper, 1987). Further complexity may also arise from solid-liquid disequilibrium during fluid/melt-rock interaction. Van Orman (2001) showed that REE (Rare-Earth Elements) diffusion in clinopyroxene at magmatic temperatures may be slower than first envisioned. For instance, Sneeringer et al. (1984) obtained a diffusion rate of $\sim 5.10^{-15}$ $cm^2.s^{-1}$ for Sm in diopside at 1250°C and 1.4 Gpa while Van Orman et al. (2001) showed that Yb, one of the fastest REE, did not diffuse faster than $5\text{-}6.10^{-16}$ $cm2.s^{-1}$ at the same pressure-temperature conditions. The high mantle temperature and the relatively slow rate of mantle melting may not guarantee isotopic equilibrium between the solid residue and the extracted molten fractions when the mantle source is isotopically heterogeneous.

In the lower temperature conditions of the lithosphere-asthenosphere transition, diffusional processes may be even slower, and therefore chemical and isotopic equilibrium between minerals and percolating melts may not be reached.

Recent studies in the Lherz massif, the type-locality of lherzolites exposed in the French Pyrenees, suggest that the Lherz lherzolites formed through a near-solidus refertilization reaction between a harzburgitic protolith and ascending partial melts (Le Roux et al., 2007). The transition zone between the remnants of the harzburgitic protolith and the refertilized material represents a frozen melt-percolation "front", tens of meters wide that moved through the subcontinental mantle lithosphere. Thus, the massif offers a unique opportunity to trace Hf, Nd and Sr isotopic variations related to melt transport. We used a one-dimensional percolation-diffusion model (Vasseur et al., 1991) modified to include isotopic homogenization and a percolation-reaction model (Vernières et al., 1997) to assess the effects of mineralogical reactions on isotopic variations. We show that transient, decoupled, isotopic signatures may develop in a melt percolation front. These signatures are highly sensitive to parameters such as daughter-element concentrations in peridotite and melt, element diffusivity, mineral grain size and efficiency of isotopic reequilibration. The variations observed in the Lherz peridotites are more readily governed by diffusional peridotite-melt disequilibrium than by the chromatographic effect of melt transport and the refertilization reaction.

2. Background and sampling

The Lherz massif is one of the largest peridotite massifs in the Pyrenees (France), exhumed from the mantle around 105 Ma ago (Henry et al. 1998) and exposed within sedimentary basins of Cretaceous age. Pyrenean peridotites usually outcrop embedded in metamorphized carbonate sediments of Jurassic to Aptian age (Golberg and Leyreloup, 1990) scattered in small groups along the North Pyrenean Fault (Monchoux, 1971; Fabriès et al., 1991; Fig. 1a). The Lherz massif is mostly constituted of fertile spinel lherzolites associated with websteritic layers, intermingled with elongated bodies of depleted spinel harzburgites (Avé Lallemant, 1967; Conquéré, 1978; Fabriès et al., 1991; Le Roux et al., 2007; Fig.1b).

Recent work yielded convergent structural and geochemical evidence demonstrating that the melt-extraction hypothesis, which regards depleted harzburgites as derived through partial meting of the fertile lherzolites, was not consistent with structural and chemical observations (Le Roux et al., 2007). Harzburgites bodies show a consistent

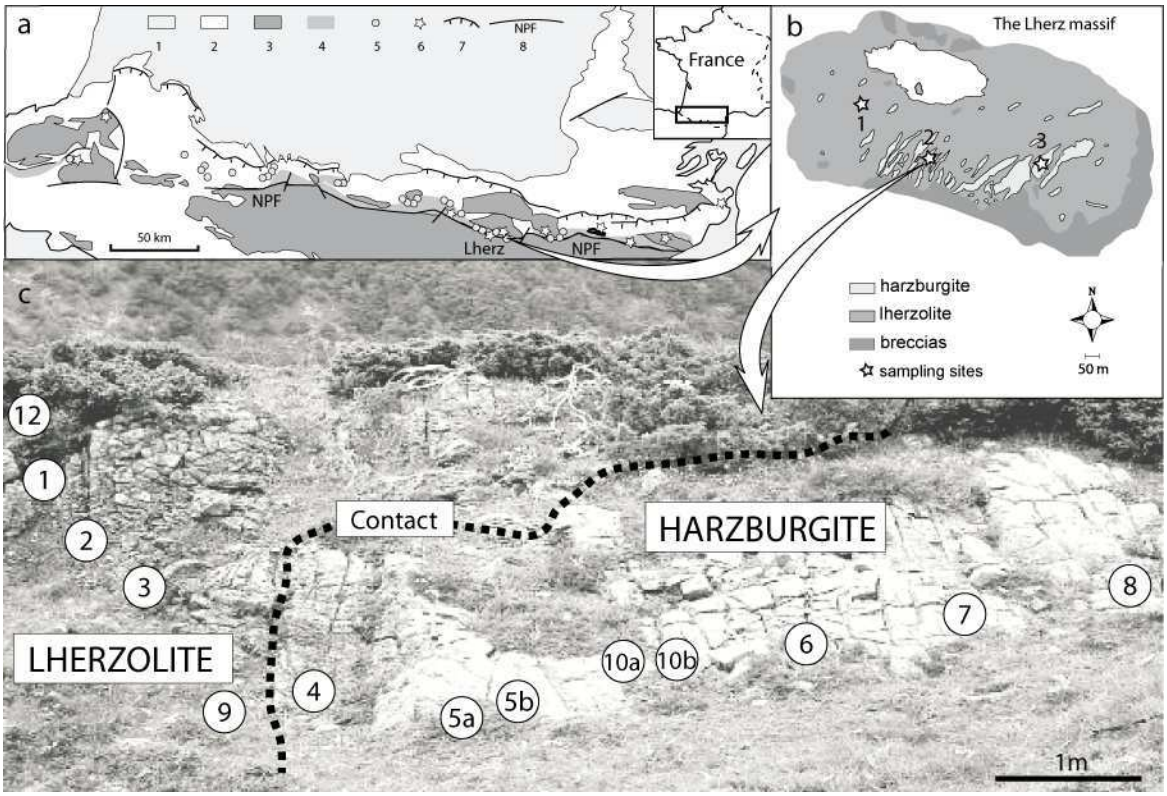

Fig. 1**:** (a) Distribution of the Pyrenean peridotite bodies along the North Pyrenean Fault (NPF), from Lagabrielle and Bodinier (2008) after Choukroune (1978). 1: Oligocene and post-Oligocene sediments; 2: Mesozoic and Eocene sediments; 3: Paleozoic basement; 4: area of LP-HT Pyrenean metamorphism; 5: lherzolite bodies; 6: granulites; 7: main thrusts external zones; 8: North Pyrenean Fault. (b) Harzburgites and lherzolites intermingling in the Lherz massif (Le Roux et al., 2007); the location of the sampling sites are indicated on the map, 1: distal lherzolite; 2: profile through a contact; 3: distal harzburgites. (c) Detailed sampling site 2 through a harzburgite-lherzolite contact.

sub-horizontal foliation throughout the massif that is crosscut by the lherzolite foliation and the websteritic layering. This suggests that the harzburgite bodies once formed a single continuous unit and that the deformation of harzburgites predates the formation of the lherzolites and websterites. Microstructural and petrophysical data indicate that the deformation of the lherzolite-websterite suite was enhanced by the presence of melts. By feedback effect, larger melt fractions favored strain localization and larger strain favored melt percolation through a higher dynamic porosity (Le Roux et al., 2008). Besides, major and minor elements correlations, as well as the association of LREE-enriched harzburgites and LREE-depleted lherzolites, are not consistent with partial melting, but can be explained by melt-rock reaction. Thus the Lherz lherzolites probably formed during a refertilization episode via a near-solidus reaction at the expense of a harzburgite protolith (Le Roux et al., 2007). Therefore the transition zone between the harzburgitic protolith and the refertilized material represents a frozen, anastomosed, melt-percolation "front", tens of meters wide that

moved through the subcontinental mantle lithosphere.

Within the transition zone we sampled 8 harzburgites and 5 lherzolites along a ~ 10m profile across one contact between harzburgite and lherzolite (Fig. 1c). The new samples come from the same location than samples from section 2 in Le Roux et al. (2007). The sampled zone is not cross-cut by dykes and/or veins related to the alkaline magmatism that affected the Lherz massif during Cretaceous time. Three 'distal' peridotites have also been sampled, outside of the transition zone at more than 15m from a contact, to characterize the lithospheric protolith and the refertilized mantle.

We present here the Hf, Nd and Sr isotopic compositions of clinopyroxene separates, considered to have similar isotopic signatures to the whole-rocks, and their rare-earth elements compositions obtained during this study.

3. Samples preparation and analytical methods

Rare Earth Elements (REE) were obtained by Laser ablation inductively coupled plasma-mass spectrometer (LA-ICP-MS) at GEMOC ARC National Key Centre (Australia), using a Agilent 7500 ICPMS coupled with a frequency quintupled Nd:YAG UV laser from New Wave/Merchantek laser microprobes. Ablation was performed under a pure He atmosphere, Typical spot sizes were ca. 70 µm, energy density about 10 $J.cm^{-2}$ and the repetition rate was set at 10Hz. The oxide production was kept low ($^{248}ThO/^{232}Th<1\%$). Data reduction was carried out using the GLITTER software (Van Achtebergh et al., 2001). The CaO content of clinoyroxenes (Cpx), obtained by electron microprobe (Cameca SX 100, GEMOC ARC National Key Centre), was used as internal standard. Data in Table 1 are averages of ''n'' analyses of different Cpx grains from the same sample.

Aliquots of the crushed samples were ground in agate mortars to produce whole-rocks powders. Cpx fractions were obtained for the same samples by magnetic pre-concentration (using a Frantz magnetic separator), further purification was achieved through careful handpicking under a binocular microscope. The final 16 pure clinopyroxene fractions (weights ranging between 102 to 222mg) have been leached prior to dissolution to remove possible contamination from grain surfaces and cracks. Cpx mineral were leached in 2N two-bottle distilled HCl for 30 minutes in an ultrasonic bath and then rinsed three times with MQ-H_2O. This procedure was repeated twice.

Hf, Nd and Sr isotopes analyses, including samples dissolution, chemical separation and measurements were carried

out at the GEMOC ARC National Key Centre (Macquarie University, Australia). Chemical separation of Sr and Nd were performed using standard dissolution and column procedures described by Mukasa et al. (1991) and by Pin and Zalduegui (1997) for Nd-specific columns. Hf chemical separation was carried out following the protocol of Blichert-Toft (2001). The sixteen Sr and nine Nd isotopic ratios of clinopyroxene separates were obtained on a Thermo Finnigan Triton thermal ionization mass spectrometer (TIMS). $^{87}Sr/^{86}Sr$ and $^{143}Nd/^{144}Nd$ ratios were corrected for instrumental mass fractionation by normalizing to $^{86}Sr/^{88}Sr=0.1194$ and $^{146}Nd/^{144}Nd=0.7219$, respectively. Seven replicate analyses of the BHVO-2 standard yielded $^{87}Sr/^{86}Sr$ of 0.703491 ± 8 (2SD; typical internal precision was about 5.10^{-6}) and $^{143}Nd/^{144}Nd$ of = 0.512971 ± 5 (2SD; typical internal precision was about 4.10^{-6}). These values are well within the accepted-published values (Weis et al., 2005). The sixteen Hf and seven Nd isotopic ratios of clinopyroxene separates were measured on a Nu Plasma high resolution multi-collector inductively-coupled plasma mass spectrometer (MC-ICPMS). All measured Hf isotope ratios were corrected for W and Ta, and Lu and Yb interferences at masses 180 and 176, respectively, by monitoring the isotopes ^{182}W, ^{181}Ta, ^{175}Lu, and ^{173}Yb, and normalized for mass fractionation to $^{179}Hf/^{177}Hf$ of 0.7325 using an exponential law. In order to asses the daily performance of the MC-ICP-MS, JMC475 (≈50 ppb) and JMC321 (≈50 ppb) were used as internal standards for Hf and Nd respectively and yield $(^{176}Hf/^{177}Hf)_{JMC475}$= 0.282173 ± 15 (2SD; n= 18; typical internal precision is c.a 3.10^{-6}) and $(^{143}Nd/^{144}Nd)_{JMC321}$= 0.511008 ± 20 (2SD; n= 5; typical internal precision is c.a 5.10^{-6}). Four standards BHVO-2 gave a $^{176}Hf/^{177}Hf$ of 0.283107 ± 20 (2SD; typical internal precision is c.a 8.10^{-6}) and $^{143}Nd/^{144}Nd$ of 0.512961 ± 9 (2SD; typical internal precision is c.a. 6.10^{-6}). These values are well within the accepted-published values (Barrat and Nesbitt, 1996; Blichert-Toft and Albarede, 1997; Weis et al., 2005;). Procedural blanks were as follow: $[Sr]_{blank}$ = 139±61 pg (n=2); $[Nd]_{blank}$ = 26 pg (n=1); $[Hf]_{blank}$ = 64±31 pg (n=3). The results are given in Table 1.

4. Results

REE obtained in clinopyroxenes from the sixteen peridotites sampled for this work (Table 1) show strongly depleted, U-shaped patterns in distal harzburgite bodies with La_N=0.5 and $(La/Sm)_N$~2 (normalized to chondrites after Sun and McDonough, 1989) and classic, N-MORB, REE pattern in the distal lherzolite (La_N=2.3; $(La/Sm)_N$~0.3), as observed in orogenic lherzolites worldwide (McDonough and Frey, 1989). At the

CPX	dist. (m)	weight (mg)	$^{87}Rb/^{86}Sr$	2σ	$^{87}Sr/^{86}Sr$	2σ	$^{147}Sm/^{144}Nd$	2σ	$^{143}Nd/^{144}Nd$	2σ	ENd	$^{176}Lu/^{177}Hf$	2σ	$^{176}Hf/^{177}Hf$	2σ	Ehf	TDM (Hf)
Spinel lherzolites																	
06LI1	1.5	202	0.0036	*5.E-04*	0.70281	*2.E-05*	0.2657	*0.0851*	0.51278	*2.E-05*	2.86	0.046	*0.016*	0.283029	*5.E-06*	9.09	1.22
06LI2	2	171	0.0010	*1.E-04*	0.70318	*1.E-05*	0.2469	*0.0517*	0.51280	*2.E-05*	3.09	0.022	*0.002*	0.282996	*6.E-06*	7.93	-
06LI3	1	180	0.0013	*2.E-04*	0.70297	*2.E-05*	0.1859	*0.0600*	0.51285	*1.E-05*	4.22	0.022	*0.002*	0.282996	*8.E-06*	7.91	1.14
06LI9	0.3	136	0.0006	*1.E-04*	0.70313	*1.E-05*	0.1739	*0.0352*	0.51280	*1.E-05*	3.20	0.026	*0.002*	0.283019	*4.E-06*	8.73	-
06LI12	2	167	0.0054	*6.E-04*	0.70280	*4.E-05*	0.2859	*0.0610*	0.51282	*1.E-05*	3.59	0.032	*0.002*	0.28293	*1.E-05*	5.45	1.52
06LI17	50	134	0.0018	*2.E-04*	0.70256	*2.E-05*	0.3233	*0.0822*	0.51309	*1.E-05*	8.75	0.041	*0.003*	0.28329	*2.E-05*	18.30	1.60
Harzburgites																	
06LI4	0.3	135	0.0006	*1.E-04*	0.702981	*5.E-06*	0.1655	*0.0344*	0.51285	*1.E-05*	4.08	0.026	*0.002*	0.28316	*1.E-05*	13.69	2.23
06LI5a*	1.3	136	0.00040	*9.E-05*	0.702950	*6.E-06*	0.1149	*0.0248*	0.51271	*1.E-05*	1.34	0.039	*0.003*	0.28283	*2.E-05*	2.11	0.12
06LI5b*	1.5	102	0.00029	*8.E-05*	0.702901	*6.E-06*	0.1026	*0.0210*	0.512724	*6.E-06*	1.68	0.033	*0.002*	0.28349	*1.E-05*	25.44	0.95
06LI6*	1.8	109	0.0004	*1.E-04*	0.703276	*6.E-06*	0.1508	*0.0318*	0.512551	*5.E-06*	-1.69	0.025	*0.002*	0.283051	*9.E-06*	9.86	2.66
06LI7*	2	132	0.0009	*2.E-04*	0.702875	*6.E-06*	0.1620	*0.0510*	0.512818	*6.E-06*	3.52	0.038	*0.004*	0.28407	*2.E-05*	45.81	1.39
06LI8*	2.5	125	0.0006	*1.E-04*	0.703024	*6.E-06*	0.1630	*0.0350*	0.512788	*6.E-06*	2.92	0.056	*0.005*	0.283434	*7.E-06*	23.41	0.71
06LI10a*	1	148	0.0007	*2.E-04*	0.702923	*8.E-06*	0.1934	*0.0569*	0.512665	*5.E-06*	0.52	0.040	*0.004*	0.283323	*7.E-06*	19.48	3.69
06LI10b*	1.3	151	0.00064	*9.E-05*	0.70296	*1.E-05*	0.1000	*0.0245*	0.512715	*5.E-06*	1.50	0.015	*0.002*	0.283108	*7.E-06*	11.88	0.91
06LI15*	15	222	0.00638	*1.E-03*	0.703046	*5.E-06*	0.1633	*0.0661*	0.51264	*2.E-05*	0.11	0.084	*0.008*	0.2888	*1.E-04*	214.36	2.14
06LI16*	15	178	0.0009	*1.E-04*	0.702944	*6.E-06*	0.1471	*0.0341*	0.512763	*7.E-06*	2.43	0.085	*0.009*	0.28546	*3.E-05*	95.15	3.13
BHVO-2 TIMS*				N=4	0.703491	*8.0E-06*		N=4	0.512971	*5.E-06*							
BHVO-2 MC-ICPMS								N=3	0.512961	*9.E-06*			N= 3	0.28311	*2.0E-05*		
BHVO-2 published					0.70348	*8.E-05*			0.51297	*1.E-05*				0.28310	*2.0E-05*		
JMC 475 MC-ICPMS													N= 18	0.28217	*1.5E-05*		
JMC475 published														0.282163	*9.0E-06*		
JMC 321MC-ICPMS								N= 5	0.51101	*2.E-05*							
JMC 321 published									0.511123	-							

CPX (ppm)	Rb	Sr	Hf	La	Ce	Pr	Nd	Sm	Eu	Gd	Tb	Dy	Ho	Er	Tm	Yb	Lu
06LI1	0.0713	55.2	0.951	0.561	3.19	0.730	4.68	1.97	0.887	2.85	0.532	3.92	0.850	2.40	0.340	2.26	0.315
	0.0062	*5.1*	*0.114*	*0.061*	*0.390*	*0.086*	*0.525*	*0.225*	*0.101*	*0.350*	*0.062*	*0.460*	*0.097*	*0.285*	*0.041*	*0.265*	*0.042*
06LI2	0.0297	81.7	1.49	1.37	4.79	0.929	5.34	2.09	0.855	2.75	0.478	3.29	0.701	1.92	0.266	1.72	0.238
	0.0039	*5.2*	*0.138*	*0.127*	*0.445*	*0.079*	*0.385*	*0.159*	*0.065*	*0.240*	*0.047*	*0.260*	*0.063*	*0.164*	*0.027*	*0.149*	*0.025*
06LI3	0.0482	105.6	1.34	2.29	8.94	1.53	7.61	2.25	0.950	2.49	0.417	2.79	0.581	1.60	0.225	1.57	0.216
	0.0067	*9.7*	*0.159*	*0.240*	*1.085*	*0.178*	*0.855*	*0.260*	*0.108*	*0.310*	*0.050*	*0.330*	*0.067*	*0.196*	*0.028*	*0.182*	*0.030*
06LI9	0.0260	113.3	1.23	2.97	10.96	1.84	8.87	2.45	0.930	2.49	0.407	2.69	0.576	1.65	0.236	1.59	0.229
	0.0043	*7.2*	*0.109*	*0.247*	*0.927*	*0.143*	*0.613*	*0.181*	*0.069*	*0.206*	*0.037*	*0.207*	*0.049*	*0.137*	*0.023*	*0.135*	*0.023*
06LI12	0.0966	50.1	1.41	0.460	2.67	0.674	4.61	2.09	0.875	3.09	0.563	4.05	0.879	2.43	0.339	2.32	0.329
	0.0092	*3.2*	*0.111*	*0.035*	*0.186*	*0.048*	*0.320*	*0.169*	*0.065*	*0.235*	*0.042*	*0.305*	*0.062*	*0.182*	*0.028*	*0.180*	*0.028*
06LI17	0.0344	55.1	0.904	0.847	3.79	0.732	3.21	1.65	0.734	2.25	0.411	3.06	0.662	1.87	0.272	1.87	0.265
	0.0038	*4.0*	*0.082*	*0.064*	*0.265*	*0.055*	*0.315*	*0.134*	*0.056*	*0.185*	*0.033*	*0.240*	*0.053*	*0.160*	*0.024*	*0.160*	*0.025*
06LI4	0.029	128.6	1.30	3.81	13.93	2.36	11.12	2.92	1.06	2.91	0.471	3.00	0.636	1.73	0.247	1.69	0.240
	0.004	*8.21*	*0.107*	*0.245*	*0.860*	*0.155*	*0.730*	*0.235*	*0.079*	*0.230*	*0.037*	*0.235*	*0.048*	*0.141*	*0.021*	*0.143*	*0.022*
06LI5a	0.021	144.6	0.566	8.23	19.12	2.09	6.81	1.24	0.466	1.21	0.202	1.42	0.318	0.963	0.149	1.05	0.160
	0.005	*9.23*	*0.050*	*0.525*	*1.170*	*0.137*	*0.445*	*0.107*	*0.036*	*0.101*	*0.016*	*0.115*	*0.025*	*0.079*	*0.013*	*0.087*	*0.014*
06LI5b	0.017	168.2	0.601	8.66	22.73	2.66	8.94	1.46	0.516	1.29	0.196	1.34	0.304	0.876	0.135	0.966	0.144
	0.004	*11.1*	*0.054*	*0.610*	*1.490*	*0.192*	*0.585*	*0.115*	*0.041*	*0.104*	*0.018*	*0.110*	*0.026*	*0.076*	*0.012*	*0.088*	*0.013*
06LI6	0.018	132.3	0.626	7.18	14.56	1.60	6.30	1.51	0.481	1.36	0.206	1.28	0.260	0.700	0.106	0.733	0.112
	0.003	*8.83*	*0.059*	*0.530*	*0.985*	*0.122*	*0.430*	*0.121*	*0.039*	*0.112*	*0.020*	*0.109*	*0.024*	*0.067*	*0.011*	*0.074*	*0.012*
06LI7	0.024	77.9	0.318	4.66	6.98	0.633	2.51	0.646	0.257	0.725	0.111	0.697	0.147	0.455	0.069	0.540	0.086
	0.005	*4.91*	*0.044*	*0.295*	*0.440*	*0.046*	*0.202*	*0.088*	*0.028*	*0.086*	*0.017*	*0.090*	*0.017*	*0.061*	*0.010*	*0.073*	*0.013*
06LI8	0.026	127.4	0.367	3.03	10.24	1.68	7.97	2.06	0.768	1.91	0.287	1.84	0.378	0.993	0.149	1.03	0.147
	0.004	*7.96*	*0.044*	*0.192*	*0.650*	*0.109*	*0.545*	*0.171*	*0.059*	*0.159*	*0.026*	*0.166*	*0.031*	*0.098*	*0.015*	*0.105*	*0.016*
06LI10a	0.016	62.4	0.283	3.73	5.73	0.508	2.03	0.625	0.220	0.644	0.102	0.683	0.148	0.449	0.075	0.540	0.081
	0.003	*3.97*	*0.037*	*0.235*	*0.380*	*0.037*	*0.159*	*0.078*	*0.024*	*0.075*	*0.015*	*0.081*	*0.015*	*0.053*	*0.010*	*0.065*	*0.011*
06LI10b	0.040	174.8	1.17	10.81	27.24	3.31	11.86	1.884	0.621	1.46	0.189	1.30	0.250	0.742	0.111	0.843	0.128
	0.005	*11.9*	*0.112*	*0.720*	*1.765*	*0.220*	*0.835*	*0.189*	*0.058*	*0.153*	*0.024*	*0.144*	*0.027*	*0.092*	*0.016*	*0.108*	*0.018*
06LI15	0.033	14.6	0.080	0.228	0.522	0.066	0.286	0.077	0.031	0.080	0.016	0.128	0.035	0.138	0.028	0.256	0.043
	0.006	*0.95*	*0.011*	*0.019*	*0.037*	*0.007*	*0.035*	*0.026*	*0.008*	*0.022*	*0.006*	*0.029*	*0.006*	*0.023*	*0.005*	*0.035*	*0.006*
06LI16	0.059	181.5	0.112	2.92	9.98	1.54	6.97	1.63	0.594	1.39	0.184	1.05	0.193	0.478	0.065	0.452	0.068
	0.005	*11.7*	*0.019*	*0.225*	*0.735*	*0.119*	*0.550*	*0.138*	*0.049*	*0.130*	*0.018*	*0.101*	*0.019*	*0.054*	*0.008*	*0.053*	*0.009*

Table 1: $^{87}Sr/^{86}Sr$, $^{143}Nd/^{144}Nd$ and $^{176}Hf/^{177}Hf$ isotopic ratios in the 16 clinopyroxenes separates from a harzburgite-lherzolite transition zone in the Lherz massif as well as in distal samples (06LI15: harzburgitic protolith; 06LI17 distal lherzolite), obtained by TIMS and MC-ICP-MS techniques at the GEMOC ARC National Key Centre (Australia). The associated $^{87}Rb/^{86}Sr$, $^{147}Sm/^{144}Nd$ and $^{176}Lu/^{177}Hf$ were calculated from Rb, Sr, Sm, Nd, Lu and Hf concentrations in clinopyroxenes obtained by LA-ICPMS. dist. (m) is the distance to the contact between harzburgites and lherzolites. Meaningless T_{CHUR} model ages have not been reported. * denotes that Nd isotopes ratios obtained by TIMS. BHVO-2 values are from Weis et al. (2005), JMC475 values are from Blichert-Toft and Albarede, (1997) and JMC321 values are from Barrat and Nesbitt (1996). The clinopyroxene REE compositions (ppm) in harzburgites and lherzolites are from the transition zone and the distal (>15m from a contact) peridotites. Errors are twice the standard deviations. At least 5 clinopyroxenes have been lasered in each thin section, and all individual clinopyroxenes have been lasered twice.

contact, lherzolite and harzburgite show more Light-REE-enriched clinopyroxenes than their distal counterparts, especially in harzburgites which display strong enrichment in LREE relative to Heavy REE (HREE) and/or Medium REE (MREE) with La_N up to 29 and $(La/Sm)_N$~3.6 (Fig. 2). These patterns are similar to the representative REE patterns at the massif-scale obtained on more than 50 samples in Le Roux et al. (2007). Thus the harzburgite-lherzolite contact sampled for this study can be considered as a representative transition zone between harzburgites and lherzolites.

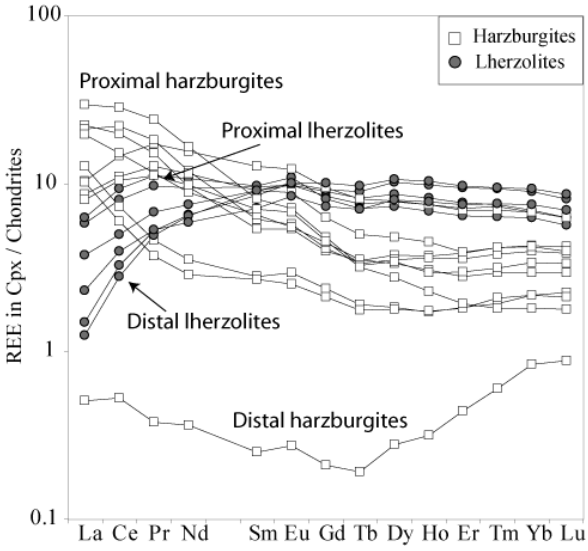

Fig. 2: Chondrite-normalized (Sun and McDonough, 1989) clinopyroxenes REE patterns in the sixteen peridotites analyzed in this study, including distal harzburgites and lherzolites (> 15m from the contact), and samples adjacent to the contact ('proximal').

The association of LREE-enriched harzburgites with LREE-depleted lherzolites observed at the harzburgite-lherzolite contact in the Lherz massif are actually predicted by theoretical modeling of melt-consuming reactions combined with melt transport (Vernières et al., 1997) and were attributed to small melt fractions residual after the refertilization reaction which migrated in the harzburgite protolith several meters ahead of the main reaction front (Le Roux et al., 2007). We consider that the U-shaped patterns observed in the distal harzburgites are related to an older metasomatic event, distinct from the refertilization episode that affected the Lherz peridotites (Le Roux et al. 2007). The models presented in this study aim to reproduce the effect of the refertilization episode.

Hf, Nd and Sr isotopic compositions of the 16 clinopyroxene separates from harzburgites and lherzolites of the Lherz massif are presented in figure 3. The isotopic signatures of the Lherz peridotites are widely scattered. Hf isotopes describe a large range of variations ($2< \varepsilon_{Hf} \leq 214$) that encompasses a significant part of the variability seen in cratonic and off-craton peridotites worldwide (Fig. 3a). $^{87}Sr/^{86}Sr$ ratios also vary between 0.702562 and 0.703276 and ε_{Nd} ranges between -1.7 and 8.8 (Fig 3b). The harzburgitic protolith and the distal refertilized lherzolites have distinctive isotopic signatures that define two different poles. One is a highly refractory lithosphere characterized by a time-integrated high Lu/Hf and Rb/Sr and low Sm/Nd ($\varepsilon_{Hf} \approx 214$; $\varepsilon_{Nd} \approx 0$; $^{87}Sr/^{86}Sr= 0.703046$). Calculations of the T_{CHUR} Hf model age gave a value of ~

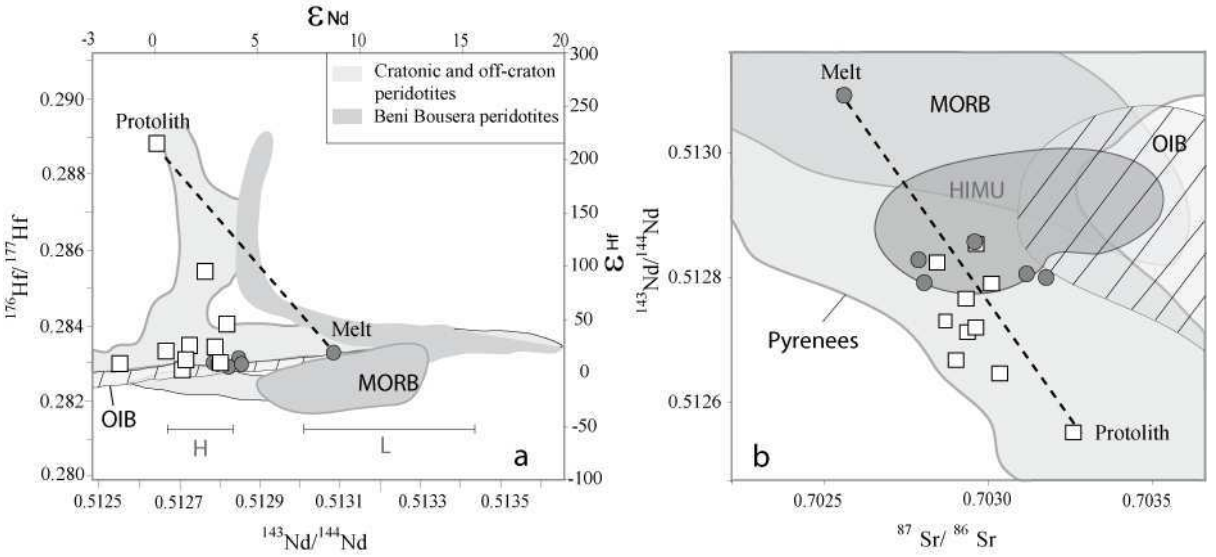

Fig. 3: (a) $^{176}Hf/^{177}Hf$ (and ε_{Hf}) versus $^{143}Nd/^{144}Nd$ (and ε_{Nd}) for 16 clinopyroxene separates from Lherz harzburgites (open squares) and lherzolites (solid circles), compared with the fields of Beni Bousera peridotites (Pearson and Nowell, 2004), cratonic and off-craton peridotites (Pearson and Nowell, 2004), MORB (Vervoort et al., 1999; Nowell et al. 1998) and Ocean-Island Basalts - OIB - (Salters and White, 1998). . ε_{Nd} and ε_{Hf} are defined as (($^{143}Nd/^{144}Nd_{sample}$ / $^{143}Nd/^{144}Nd_{CHUR}$)-1)*10000 and (($^{176}Hf/^{177}Hf_{sample}$ / $^{176}Hf/^{177}Hf_{CHUR}$)-1)*10000 respectively (e.g. Blichert-Toft and Albarede, 1997). ε_{Nd} and ε_{Hf} are present-day values.The Nd isotopic ranges of Pyrenean harzburgites (H) and lherzolites (L) (Downes et al., 1991) are also shown for comparison. (b) $^{143}Nd/^{144}Nd$ versus $^{87}Sr/^{86}Sr$ for the same clinopyroxene separates compared with the fields of Pyrenean peridotites (Downes, 1991), MORB, OIB and HIMU (Hofmann, 1997; Zindler and Hart, 1986 and reference therein). The isotopic data for this study have been measured by TIMS and MC-ICP-MS techniques and corrected to 105 Ma, the age of exhumation. The differences between corrected and non-corrected isotopic ratios range between $1*10^{-6}$ to $5*10^{-6}$.

2.1Ga on the protolith sample (06LI15), slightly younger than the ~2.2 Ga previously published Re depletion model ages (Reisberg and Lorand, 1995) and ~2.5 Ga in-situ Os model age (Alard et al., 2008). However, giving the variations of T_{CHUR} Hf model ages in harzburgitic samples, uncertainty on this age is probably high. The 'distal' harzburgitic sample which combines a U-shaped, highly REE-depleted signature (Fig. 2) and the most enriched isotopic composition is considered to be the closest to the depleted protolith before refertilization. The second pole is represented by a distal refertilized lherzolite characterized by a MORB-like isotopic signature ($\varepsilon_{Hf} \approx 18$; $\varepsilon_{Nd} \approx 9$; $^{87}Sr/^{86}Sr = 0.702562$) and a LREE-depleted signature (Fig. 2). Other Pyrenean lherzolites that contain no visible harzburgites are isotopically comparable to the distal Lherz lherzolite (Downes et al., 1991; Mukasa et al., 1991; Fig. 3), suggesting a similar origin by regional magmatic refertilization.

Harzburgites and lherzolites from the transition zone differ markedly from the distal ones with respect to their isotopic signatures. Their compositions plot close to the field of intraplate basalts (Ocean-Island Basalts and HIMU) and a simple mixing between the two poles defined by the distal

peridotites particularly fail to account for their Hf-Nd isotopic signatures (Fig. 3).

5. Discussion

5.1. Contrasted isotopic compositions of lherzolites and harzburgites in the Pyrenees

Previous works have revealed that fertile lherzolites and depleted harzburgites in eastern Pyrenean peridotites show markedly distinct Os-Sr-Nd isotopic signatures (Downes et al., 1991; Reisberg and Lorand, 1995; Burnham et al., 1998). The positive correlation of $^{187}Os/^{188}Os$ with Al_2O_3 wt% has been ascribed to an old (Proterozoic) depletion event (Reisberg and Lorand, 1995; Burnham et al., 1998). However, $^{87}Sr/^{86}Sr$ and $^{143}Nd/^{144}Nd$ show, respectively, negative and positive correlations with Al_2O_3 wt% in whole-rocks, a feature which is not consistent with partial melting (Downes et al., 1991; Bodinier and Godard, 2003). Downes et al. (1991) proposed that the Lherz harzburgites were selectively percolated by enriched melts whereas Bodinier and Godard (2003) interpreted them as lithospheric strips incompletely mixed with pristine asthenospheric lherzolites during thermo-mechanical erosion of the lithosphere by upwelling mantle. Recently, Le Roux et al. (2007) suggested that the refertilization scenario was the most likely to explain, at the same time, the positive correlation of $^{187}Os/^{188}Os$ vs. Al_2O_3, and the negative and positive correlations of $^{87}Sr/^{86}Sr$ and $^{143}Nd/^{144}Nd$, respectively, vs. Al_2O_3.

The Nd and Sr isotopic variations observed in this study, from the harzburgitic protolith to the refertilized lherzolites, are consistent with previously published data in the Pyrenees (Downes et al., 1991). We obtained a Nd-Sr negative correlation which can be roughly accounted for by mixing between a low-Nd/high-Sr harzburgite protolith and a melt in equilibrium with the high-Nd/low-Sr distal lherzolite (Fig. 3b). However, at the harzburgite-lherzolite contacts, the Hf isotopes are strongly decoupled from Nd (Fig. 3a) and Sr (not shown). In contrast with the Nd-Sr isotopic covariation, the Hf-Nd isotopic signatures observed at the harzburgite-lherzolite contact cannot be accounted for by mixing between the harzburgite protolith and a melt in equilibrium with the distal lherzolites (Fig. 3a). In a mixing scheme, these isotopic signatures would require a third, unradiogenic Hf-Nd component. However, this would necessitate the circulation of intraplate-type melt strictly confined to the sharp and convoluted contact between harzburgites and lherzolites, which is very unlikely according to chemical and structural constraints. A more likely alternative is that these isotopic signatures formed at the melt percolation front through a particular

chemical/physical process that led to the decoupling of Hf from Nd and Sr.

5.2. Modeling of isotopic reequilibration during melt percolation

We have evaluated the influence of melt percolation on isotopic reequilibration between peridotite and an infiltrated melt using a one-dimensional percolation-diffusion model (Vasseur et al., 1991) modified to include isotopic homogenization. The model incorporates the effects of chemical diffusion, critical distance of isotopic homogenization, melt velocity, height of the percolating column and grain size. It assumes instantaneous solid-liquid equilibrium at the surface of mineral grains, considered to be spherical, and chemical diffusion within the grains, from surface to core. Isotopic equilibrium between fluid and solid phases is governed by the mass-balance equation of isotopic homogenization at the scale of critical volumes. The critical volume of isotopic homogenization is defined as the volume of percolated peridotite in which melt and matrix have reached isotopic equilibrium during the critical time of percolation (i.e., the times it takes for the melt to reach the top of the column). In addition, a percolation-reaction model (the "plate model" of Vernières et al., 1997) has also been used to evaluate the effects of the refertilization reaction on isotopic reequilibration during melt percolation. The plate model assumes instantaneous solid-liquid equilibrium between the whole mineral matrix and the melt.

Isotopic reequilibration between a rock and a disequilibrium percolating melt involves four distinct processes: (a) advective transport of the elements by interstitial melt; the–chromatographic theory of Navon and Stolper (1987) predicts that incompatible elements in the matrix reequilibrate with the melt at lower melt-rock ratios than more compatible elements, producing extreme chemical fractionations when mineral-melt diffusional exchange is rapid; (b) chemical diffusion within the minerals and the melt; diffusion rates vary according to elements and pressure-temperature conditions; (c) isotopic homogenization of rock volumes by self-diffusion, which is effective even in the lack of chemical potential gradient (e.g. when the percolating melt and the peridotite have reached chemical equilibrium); (d) chemical reaction between the rock and the infiltrating melt that changes the mineralogical composition of the rock and/or the melt fraction.

A detailed parameterization was carried out to assess the influence of the main percolation-diffusion model parameters on the covariation of Hf, Nd and Sr isotopic compositions in a harzburgite column percolated by a melt in equilibrium with the

distal lherzolites. The parameters used for modeling are compiled in Table 2. The protolith was very likely heterogeneous; for modeling we took the most extreme composition characterized by the highest $^{176}Hf/^{177}Hf$ and $^{87}Sr/^{86}Sr$ and the lowest $^{143}Nd/^{144}Nd$ values in the studied harzburgites. As isotopic composition for the melt, we took that of the distal, refertilized lherzolite. This sample is comparable to other Pyrenean lherzolites unrelated to harzburgites (Downes et al., 1991) and is therefore considered to be equilibrated with the fertilizing, infiltrated melt. In all experiments the length of the percolation column has been fixed at 100m. This length corresponds to the typical distance in the Lherz massif between the distal harzburgites, which represents the protolith before percolation, and the distal lherzolites, considered to be fully equilibrated with incoming, fertilizing melt. Mineral/melt partition coefficients are from Blundy (1998), Lee (2007) and McDade (2003). The diffusivity of the elements in interstitial melt is the same for the three elements and fixed at 10^{-8} $cm^2.s^{-1}$ (Lesher, 1994).

For simplicity, the chemical diffusivities in solid phases, d, were considered to be identical for all minerals. Extrapolated at 1250°C and 1.5 Gpa from the experimental data of Van Orman et al. (2001), the diffusion rate of Nd was fixed at $3.4*10^{-17}cm^2.s^{-1}$. The diffusivity of Hf was estimated from its ionic radius and charge, yielding a diffusion rate of $1.2*10^{-17}cm^2.s^{-1}$. The chemical diffusivity of Sr is somewhat controversial. While the study of Sneeringer et al. (1984) indicates that this element has a faster diffusivity in clinopyroxene, compared with REE, the recent study of Von der Handt (2008) on orthopyroxene suggests that the diffusion of Sr is actually slower than that of REE, in both clino- and orthopyroxene. For this reason, we fixed the diffusivity of Sr identical to that of Nd. To assess the effect of chemical diffusivities variations, we run experiments involving variations of this parameter in the range 0.1 to 30 times the d values. The observed range of pyroxenes grains sizes in Lherz varies from 1 to 4mm (Le Roux et al. 2008), except in small-scale mylonitic zones (<1mm). In the models, mineral grain size varies from 0.1 mm to 5 mm. This represents the average diameter of the grains, considered to be spherical. For simplicity, olivines and pyroxenes were considered to have the same size for modeling. The Hf, Nd and Sr contents in the protolith (based on the composition of the most depleted sample) are ~ 0.003, 0.015 and 1 ppm, respectively, and the Hf, Nd and Sr contents in the infiltrated melt (based on equilibrium with clinopyroxenes from distal, refertilized lherzolites) are ~ 2.45, 10.7 and 743 ppm, respectively. To evaluate the effect of the compositional contrast between melt

Parameters common to all models

porosity	0.03
height of the column (m)	100
melt velocity (cm.y^{-1})	1
chemical diffusivity in melt (cm^2.s^{-1})	1*10^{-8}

Minelral/melt partition coefficients

	Cpx	Opx	Spl	Ol
Hf	0.37	0.047	0.05	0.013
Nd	0.3	0.012	0.01	0.00003
Sr	0.074	0.003	0.0002	0.00018

modal composition of the harzburgitic protolith

Ol	Cpx	Opx	Spl
0.85	0.02	0.12	0.01

Element abundances in the infiltrated melt (ppm)

	models 4a / 5a	**models 4b / 5b**	**models 4c / 5c**	**models 4d / 5d**
Hf ppm	2.45	2.45	2.45	2.45
Nd ppm	10.7	10.7	10.7	10.7
Sr ppm	743	743	743	743

Other parameters

	models 4a / 5a	**models 4b / 5b**	**models 4c / 5c**	**models 4d / 5d**
grain size (mm)	3	0.1 to 3 / 1 to 5	3	3
Chemical diffusivity in minerals (cm^2.s^{-1})				
Hf	1.2*10^{-17} to 3.4*10^{-16}	1.2*10^{-17}	1.2*10^{-17}	1.2*10^{-17}
Nd	3.4*10^{-17} to 3.4*10^{-16} / 3.4*10^{-18} to 3.4*10^{-16}	3.4*10^{-17}	3.4*10^{-17}	3.4*10^{-17}
Sr	3.4*10^{-18} to 3.4*10^{-16}	3.4*10^{-17}	3.4*10^{-17}	3.4*10^{-17}
CDIH (m)	0.1	0.1	0.1	0.1 to 10 / 0. to 1
Element abundances in the harzburgitic protolith (ppm)				
Hf ppm	0.003		0.003 to 0.008	
Nd ppm	0.015	0.015	0.007 to 0.022	0.015
Sr ppm	1	1	1	1

Table 2: Fixed and variable modeling parameters used in the one-dimensional model of Vasseur et al. (1991). Ol = olivine; Opx = orthopyroxene; Cpx = clinopyroxene; Spl = spinel. CDIH is the critical distance of isotopic homogenization.

and matrix, we run a series of experiments with a realistic range of daughter element variations in the harzburgites. Hf_{melt}/Hf_{matrix} ratios vary from 817 to 305, assuming constant Hf_{melt} and Nd_{melt}/Nd_{matrix}, and Nd_{melt}/Nd_{matrix} ratios vary from 475 to 1420, assuming constant Nd_{melt} and Sr_{melt}/Sr_{matrix}. The critical distance of isotopic homogenization along the column ranges between 0.1 and 10m.

The parameters used in the percolation-reaction model of Vernières et al. (1997), such as porosity, isotopic ratios and elements concentrations, are the same as for the one-dimensional model. The melt-rock reaction was taken from Le Roux et al. (2007). It is a pyroxene-forming reaction at decreasing melt mass also involving some degree of olivine dissolution.

5.3. Results of the modeling

Representative results of the percolation-diffusion modeling are illustrated on figures 4 and 5. These figures show the isotopic covariations of Hf-Nd (Fig. 4) and Nd-Sr (Fig. 5) along the percolation column, from the composition of the harzburgite protolith (atop the column) to that of the melt (at base of the column). Both Hf-Nd and Nd-Sr covariations define curved trajectories that may be either convex upward, lying above the mixing lines, or convex downward, lying below the mixing lines. These variations imply significant inter-isotopic decoupling, notably for the Hf-Nd pair.

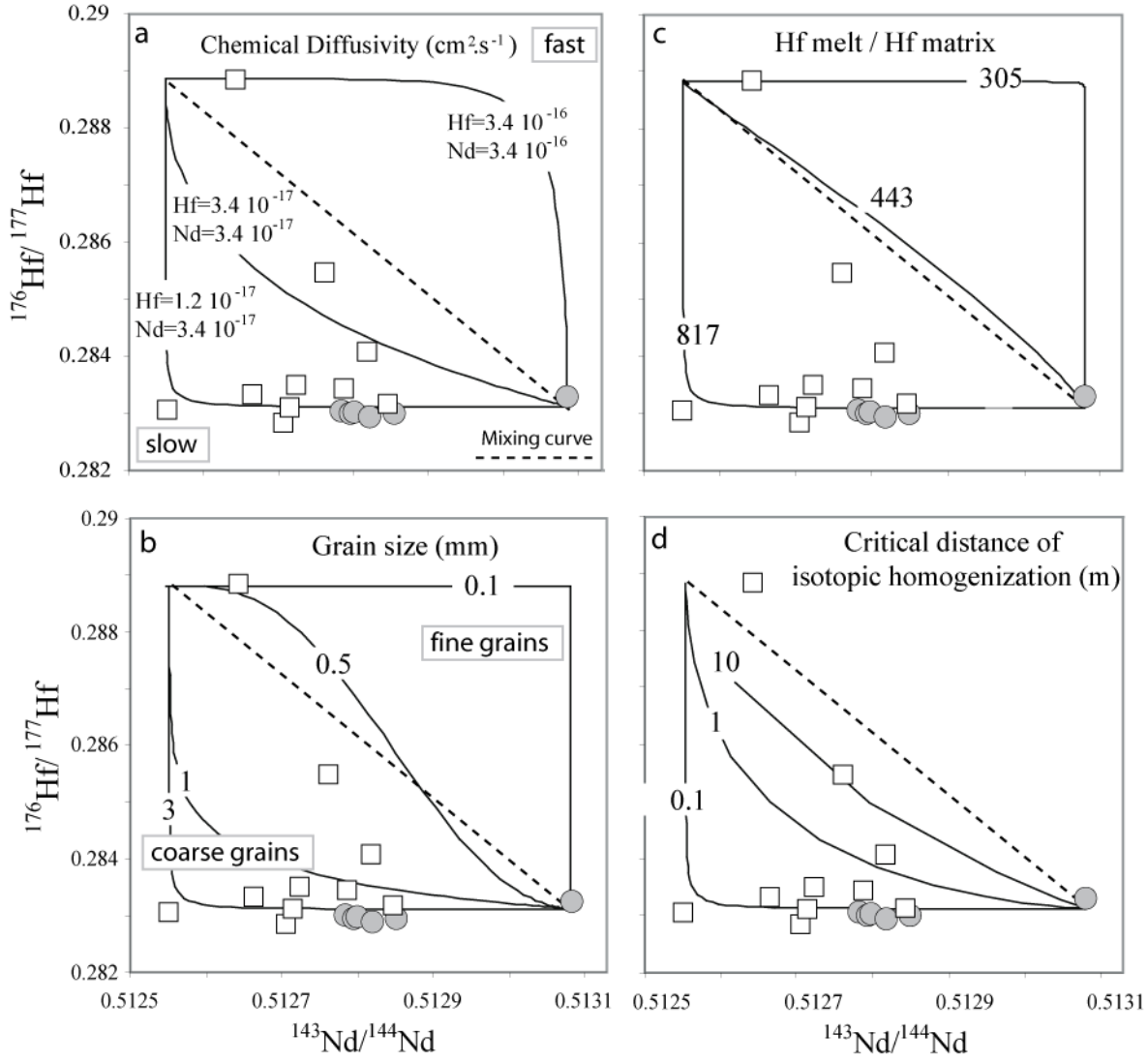

Fig. 4: $^{176}Hf/^{177}Hf$ versus $^{143}Nd/^{144}Nd$ in clinopyroxene separates from Lherz harzburgites (open squares) and lherzolites (solid circles), compared with the mixing curve (dotted line) between a harzburgite protolith and a MORB-type melt, and with the results of the one-dimensional percolation-diffusion modeling (solid lines). The diagrams (a) to (d) illustrate the effects of varying parameters in the model: (a) diffusivity, d, of the elements in minerals; (b) the mineral grain size; (c) the Hf_{melt}/Hf_{matrix} ratio; (d) the critical distance of isotopic homogenization along the column. Heavy lines represent a 'best fit' of the Lherz data.

Drastic variations in the shape of the Hf-Nd isotopic covariation curves may indeed occur for relatively small variations of several critical parameters, namely: (1) element diffusivity in minerals (Fig. 4a), (2) average grain size of minerals (Fig. 4b), (3) compositional contrast between protolith and melt for the daughter elements Hf and Nd (Fig. 4c), and (4) critical distance of isotopic homogenization along the percolation column (Fig. 4d).

The convex-upward Hf-Nd isotopic covariation trend observed for high element diffusivities in minerals (Fig. 4a) and/or small grain sizes (Fig. 4b) is consistent with the chromatography theory of trace-element reequilibration in porous flow systems (Navon and Stolper, 1987). The latter predicts that if the critical time of mineral/melt reequilibration by diffusion is short enough compared to the critical time of percolation (Vasseur et al., 1991) then Nd reequilibrates at lower melt/rock ratio than Hf due to its higher incompatibility degree, e.g. $Kd_{Cpx/melt}$ = 0.30 for Nd compared with 0.37 for Hf (Blundy et al., 1998). This type of Hf-Nd decoupling is also in agreement with the classical assumption that Hf is more robust to mantle metasomatism than Nd (e.g. Bedini, 2004).

However, our experiments also show convex-downward Hf-Nd covariation trends that are opposite to the variation predicted by the chromatographic theory. At a given Hf_{melt}/Hf_{matrix} value, they are systematically observed in experiments involving relatively slow element diffusivities in minerals (Fig. 4a) and/or coarse grain sizes (Fig. 4b), i.e., when the critical time of solid-liquid equilibrium tends to be significant compared to the critical time of percolation (10^4 years in all our experiments). This type of Hf-Nd decoupling does not result from the difference in diffusivity between Hf and Nd as Hf diffuses at a slower rate than Nd. The convex-downward Hf-Nd trends reflect the persistence of solid-liquid chemical disequilibrium in significant parts of the percolation column – notably the uppermost part - where the percolating melt and the matrix partly preserve their original compositions. In these conditions, the chromatographic fractionation process is overwhelmed by the compositional effect of Hf and Nd concentrations in the protolith and disequilibrium melt. This effect results from the dependence of the bulk (solid + melt) isotopic values calculated with the isotopic mixing equation at the scale of critical homogenization volumes on daughter element concentrations in minerals and melt.

For a given set of parameters consistent with the chromatography theory, the convex-upward Hf-Nd isotopic trends are observed in experiments involving relatively low concentration of Hf in melt relative to the matrix (Hf_{melt}/Hf_{matrix} < 443 for the experiments shown on figure 4c). However,

a subtle increase of the Hf concentration in the melt relative to the matrix (Hf_{melt}/Hf_{matrix} = 443 to 817, i.e. Hf matrix = 0.008 to 0.003 on figure 4c) is sufficient to generate a change from convex-upward to convex-downward Hf-Nd isotopic covariation trends.

Finally, the amplitude of the transient Hf-Nd isotopic decoupling along the percolation column is negatively correlated with the efficiency of the isotopic homogenization process. Spatially limited homogenization (i.e., short critical distance of isotopic homogenization along the column) yields strongly convex Hf-Nd covariation curves, either upwards or downwards depending on the other model parameters (e.g., Fig. 4d). Conversely, in the limiting case where the critical distance of isotopic homogenization is of the same length as the percolating column, the result of the percolation-diffusion experiment is similar to that of a mixing between the protolith and the melt (Fig. 4d).

The Lherz data are best explained by a strongly convex-downward Hf-Nd trend (heavy line on figure 4). Within the range of parameters fixed from our petrographical observations (mineralogy and grain size), geochemical data (protolith and inferred melt composition) and published experimental works (partition and diffusion coefficients), this Hf-Nd variation implies that the critical size of the isotopic homogenization volumes was ≤ 1m during the melt percolation event. The dispersion observed for a few samples may be accounted for by subtle variations of critical parameters such as the mineral grain size, or the Hf-Nd content in peridotite or percolating melt.

In contrast with the Hf-Nd isotopic covariations, the modeled Nd-Sr trends are generally hardly distinguishable from the mixing curves in the range of the parameter values constrained by the Lherz data and experimental works (Fig. 5). Within this range of parameters, most experiments yield moderately convex-downward trajectories consistent with the chromatographic theory which predicts that Sr reequilibrates at lower melt/rock ratio than Nd due to its higher incompatibility degree, e.g. $Kd_{Cpx/melt}$ = 0.074 for Sr compared with 0.30 for Nd (Blundy et al., 1998). Noticeable exceptions are the experiments involving relatively high Nd_{melt}/Nd_{matrix} ratios (Fig. 5c). As previously noted by Ionov et al. (2002), the relative concentration of Nd and Sr in the protolith and disequilibrium melt are indeed critical parameters for the relative velocities of the Nd and Sr isotopic reequilibration fronts in a porous flow column. For Nd_{melt}/Nd_{matrix} values in the range defined by the theoretical melt in equilibrium with the Cpx of the distal lherzolite and the distal harzburgites, the modeled Nd-Sr isotopic curves vary from moderately convex upward to moderately convex downward, on either side of the mixing curve. These variations encompass

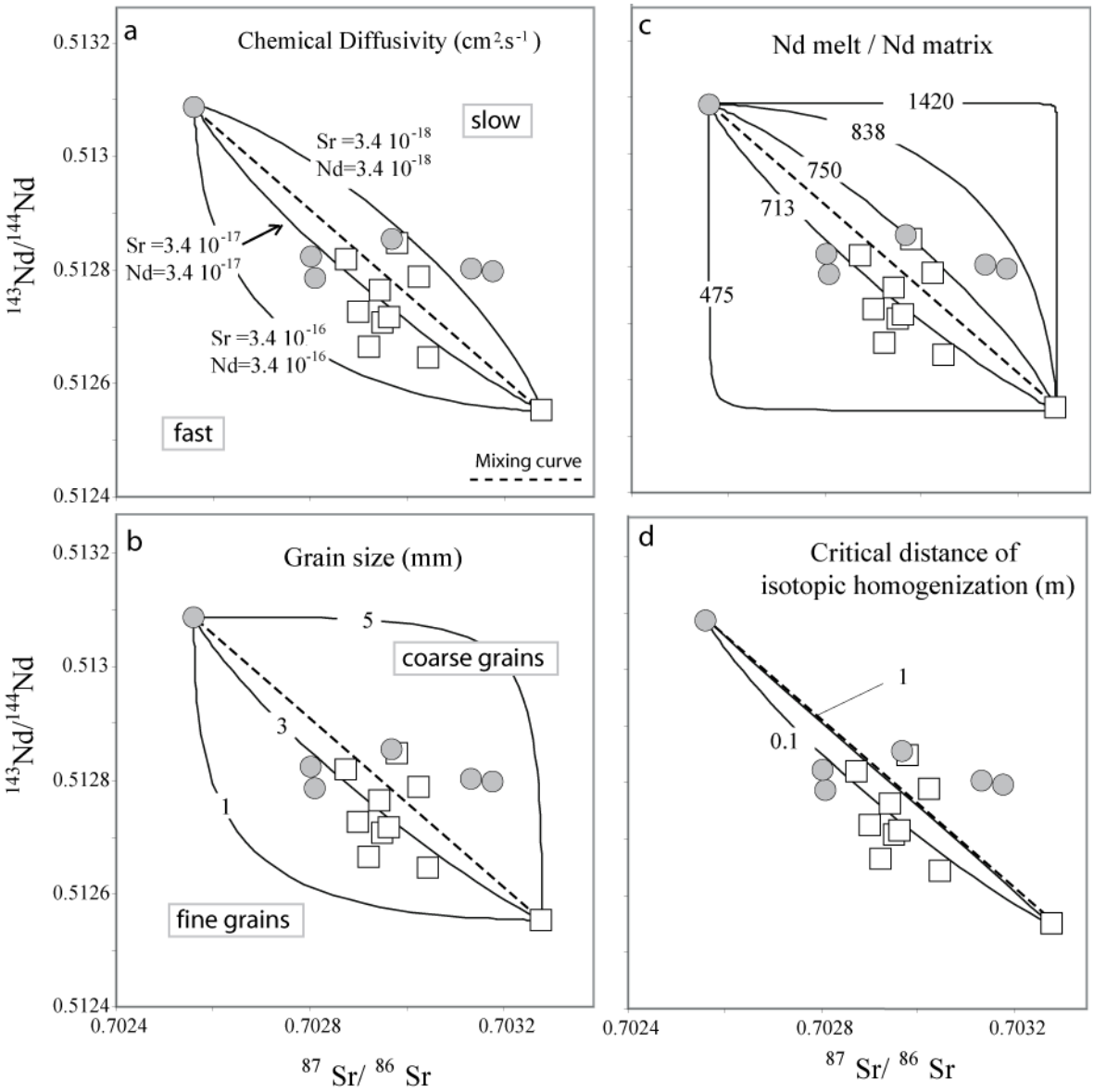

Fig. 5: $^{143}Nd/^{144}Nd$ versus $^{87}Sr/^{86}Sr$ in clinopyroxene separates from Lherz harzburgites (open squares) and lherzolites (solid circles), compared with the mixing curve (dotted line) between a harzburgite protolith and a MORB-type melt, and with the results of the one-dimensional percolation-diffusion modeling (solid lines). The diagrams (a) to (d) illustrate the effects of varying parameters in the model: (a) diffusivities, d, of the elements in minerals; (b) the mineral grain size; (c) the Nd_{melt}/Nd_{matrix} ratio; (d) the critical distance of isotopic homogenization along the column.

the whole range observed in the samples from the transition zone. In contrast with Hf-Nd, no inference on the size of the isotopic homogenization volumes can be drawn from the Nd-Sr covariation (Fig. 5d).

Representative results of the percolation-reaction modeling are illustrated on figure 6, showing the influence of the refertilization, melt-rock reaction on isotopic reequilibration. In order to compare with the percolation-diffusion model, we first run experiments using the plate model without reaction. This yielded convex-upward Hf-Nd isotopic reequilibration trends consistent

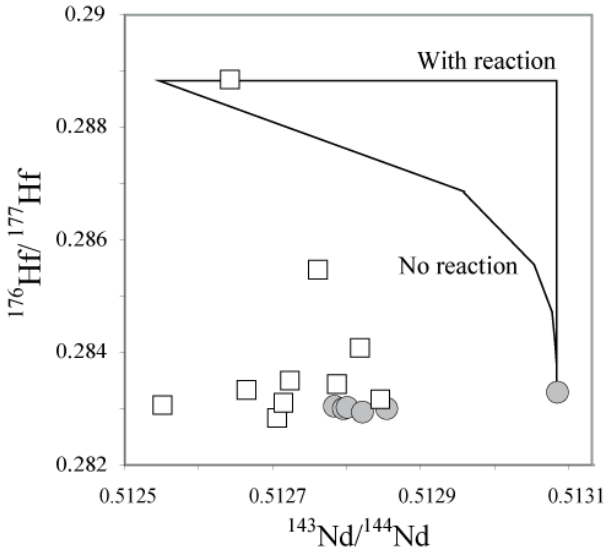

Fig. 6: Results of percolation-reaction modeling (Vernières et al., 1997) for the Hf-Nd isotopes in the Lherz peridotites. Symbols are the same than in previous figures.

with the chromatography theory. Moreover, we show that melt-rock reactions at decreasing melt-mass enhance chromatographic effects by decreasing the porosity. This reflects the key role of porosity on chromatographic fractionation (Bodinier et al, 1990). Besides, isotopic signatures of the lherzolites close to the contact are not consistent with isotopic signatures predicted by a mineralogical reaction, although they result from a refertilization reaction. Therefore, the percolation-reaction model strengthens previous results obtained with the one-dimensional percolation-diffusion model, where chemical diffusion is a required, critical parameter to explain isotopic reequilibration during melt percolation.

6. Conclusions

The isotopic heterogeneity observed in the transition zone between harzburgites and lherzolites in the Lherz massif can be reproduced with a realistic range of physical parameters: a melt fraction of a few percent, a percolation rate of several $cm.y^{-1}$, a distance of percolation from tens to several hundreds of meters associated with a volume of homogenization on the scale of the sample (some tens of cm). The Lherz example suggests that a large range of isotopic signatures may be generated at a melt percolation front, depending on chemical diffusion, isotopic homogenization and peridotite-melt compositions. We also show that mineralogical reactions at decreasing melt-mass enhance chromatographic effects by decreasing the porosity. The variations observed in the Lherz peridotites are more readily governed by diffusional peridotite-melt disequilibrium than by the chromatographic effect of melt transport and the refertilization reaction. The development of these signatures is a transient phenomenon associated with the passage of a percolation front which has been “frozen in” in the Lherz massif. Moreover, we observe that the microstructural characteristics (e.g. the grain size) of the percolated protolith strongly influence the resulting isotopic signature within the percolation front. Thus deformation and recrystallization of mantle

rocks may induce local variations in isotopic signatures, as observed in the Ronda massif (Reisberg and Zindler, 1986) or in xenoliths from the French Massif Central (Downes and Dupuy, 1987). The world-wide association of LREE-enriched harzburgites with LREE-depleted lherzolites, as observed in Lherz, suggests that the interaction of percolating melts with the lithospheric mantle is a widespread process. We observe that, under certain circumstances, these interactions can generate enriched, "intraplate-like" isotopic signatures in the transition zone between the two contrasting components. These results suggest that a part of isotopic signatures of mantle-related rocks could be generated by diffusional processes associated with melt transport.

Acknowledgements

Trace element and isotope data were obtained at GEMOC using instrumentation funded by ARC LIEF, DEST Systemic Infrastructure Grants, Macquarie University and industry, and the work was supported by ARC Discovery project grants (OA, SYO'R and WLG) and INSU DYETI Program. VLR also got funding from the French Ministry of Research and from 'Bourses Lavoisier' for the collaboration with Australia. Peter Wieland and Norman Pearson are deeply thanked for assistance and advice during the isotopic work. We thank James Van Orman and Anette von der Handt for their help in the estimation of elements diffusivities, and Nadine Wittig and an anonymous reviewer for their constructive reviews. This is contribution no. XX from the GEMOC ARC National Key Centre.

References: end of thesis manuscript.

Chapter V: Conclusion and outlook

The present work provides structural evidence that the lherzolites from the Lherz massif, considered as pristine, are actually secondary and formed at the expense of a depleted harzburgitic protolith. Variations of major, minor and trace elements in minerals and whole-rocks peridotites show that the lherzolites result from igneous refertilization reaction between depleted lithospheric mantle and percolating MORB-type partial melts. Local evidence of igneous refertilization has been previously reported in orogenic peridotites. At Lherz, structural arguments show that the whole lherzolite body is secondary and refertilized. As a result, the Lherz massif, type-locality of lherzolites, now represents a case study for the refertilization process in the mantle (Le Roux et al., 2007). Therefore the Lherz massif represents a “frozen” photograph of transient percolation stages in an old refractory lithosphere.

Implications of this result are wide. Not only for the composition of the primitive mantle itself, a major problem in the mantle community, but also for the evolution of the mantle lithosphere and the role of refertilisation in the structural and chemical evolution of the lithospheric mantle. These implications are detailed below.

Together with mantle xenoliths and chondrites, the Lherz massif has been used to infer the composition of the primitive upper mantle, in particular for the highly siderophile elements. However, the formation of the Lherz lherzolites by igneous refertilization raises the question of the validity and significance of the primitive mantle values based on fertile mantle rocks compositions. In this context, primitive mantle values needs to be re-assessed. In particular, the Os-isotope primitive upper mantle composition has major implications for the debate on the “late veneer” composition, the late meteorite bombardment that occurred on Earth after core segregation (Alard et al., 2008; supplementary material).

Evidence of melt percolation observed in previous studies of orogenic peridotites world-wide and in the Lherz massif suggests that a fundamental characteristic of most orogenic lherzolites is their refertilized nature. This suggests that magmatic percolation plays a

significant role in the structural, chemical and isotopic evolution of the lithospheric mantle, contributing to its rejuvenation and thermo-mechanical erosion through time.

This work has revealed that the Lherz massif represents a natural example for feedback between melt percolation and deformation of mantle rocks (Le Roux et al., 2008b), providing natural observations consistent with experimental results (Holtzman et al., 2003). Multiple deformation episodes have been observed via a detailed microstructural study combined with analyses of crystallographic fabrics of minerals in harzburgites, lherzolites and websterites. Depleted harzburgites, percolated lherzolites and related websterites show a continuum of deformation suggesting that larger melt fractions favor strain localization and, in turn, larger strain favor melt percolation through a higher dynamic viscosity. This feedback effect may constitute a major process in the structural evolution of the lithosphere. Indeed it has been suggested for instance that the presence of melt in the lithosphere may reduce its viscosity, favoring the development of rift systems. Therefore, the refertilization process could also play a major role during orogenic stages, favoring the restructuration of the lithosphere.

The progressive deformation observed in the percolated lherzolites with increasing distance to the harzburgitic protolith shows that, in presence of melts, an increase in strain intensity may be associated with a decrease in crystallographic fabrics of minerals. This can be explained by a progressive increase of diffusion-creep accommodated deformation at the expense of dislocation-creep accommodated deformation. Moreover, the development of either [100]-fiber or [010]-fiber in olivines observed in peridotites worldwide may depend on a subtle balance between the strain intensity and the volume of percolating melts. Synchronous to the refertilization episode, the development of a pervasive websteritic banding in lherzolites is also commonly observed in mantle rocks. In the Pyrenean massifs, the websteritic layers probably formed through melt segregation favored by the refertilization reaction which plugged the melt network, and represent multiple “frozen” timesteps of a dynamic melt transport system. However, considering that the websterites does not represent simple crystallized trapped melts, the quantification of the volume of melts which has percolated through the Lherz mantle rocks remains an open question.

The third part of this work has shown that melt percolation by diffuse porous flow is likely to produce a large range of isotopic signatures. The models show that melt percolation may be an alternative way to produce isotopic signatures previously restricted to mantle reservoirs signatures. Indeed, a large range of Hf, Nd and Sr isotopic variations is observed at the transition zone between depleted harzburgites and fertile lherzolites of the Lherz massif, suggesting that significant isotopic decoupling can be produced at a melt percolation front.

The decoupled signatures cannot be explained by a mixing line between the percolated rock and the percolating melt. Modelling of isotopic variations associated with melt infiltration shows that the nature and extent of isotopic decoupling strongly depends on (1) the compositional contrast between protolith and melt with respect to daughter elements (2) the chemical diffusion rates of the elements and (3) the critical times of solid-liquid chemical reequilibration and isotopic homogenization.

Mantle rocks worldwide show a large isotopic variability and interactions between partial melts and lithospheric mantle have often been observed both in xenoliths and orogenic peridotites. Thus, a part of the mantle isotopic variability observed in mantle rocks may not be necessarily representative of the global earth mantle but rather related to percolation processes that affect the lithosphere-asthenosphere boundary. To some extent, the percolation-diffusion process could be responsible for some of the isotopic signatures observed in intraplate lavas, that may originate from melt-rock interactions at the lithosphere-asthenosphere boundary. However, the importance of the isotopic variability originated by this process needs to be further evaluated.

References

Alard, O., Le Roux, V., Lorand, J.P., Bodinier, J.-L., Griffin, W.L., O'Reilly, S.Y., 2008. Mantle refertilisation, Osmium isotopes and the "Primitive Upper Mantle" fallacy, consequences for the nature of the late veneer. In prep.

Albarède, F., Michard-Vitrac, A., 1978. Age and significance of the North Pyrenean metamorphism. Earth and Planetary Science Letters. 40, 327-332.

Allègre, C.J., Turcotte, D.L., 1986. Implications of a two-component marble-cake mantle. Nature. 323, 123-127.

Avé Lallemant, H.G., 1967. Structural and petrographic analysis of an "alpine-type" peridotite. The lherzolite of French Pyrenees. Leidse Geologische Mededelingen. 42, 1-57.

Azambre, B., Ravier, J., 1978. Les écailles de gneiss du faciès granulite du Port de Saleix et de la région de Lherz (Ariège). Nouveaux témoins du socle profond des Pyrénées. Bulletin de la Société Géologique de France. XX, 221-228.

Barrat, J.A., Nesbitt, R.W., 1996. Geochemistry of the Tertiary volcanism of Northern Ireland. Chemical Geology 129, 15– 38.

Barruol, G., Souriau, A., Vauchez, A., Diaz, J., Gallart, J., Tubia, J., Cuevas, J., 1998. Lithospheric anisotropy beneath the Pyrenees from shear wave splitting. Journal of Geophysical Research. 103, 30039-30053.

Barth, M.G., Mason, P.R.D., Davies, G.R., Dijkstra, A.H., Drury, M.R., 2003. Geochemitry of the Othris ophiolite, Greece: evidence for refertilization? Journal of Petrology. 44, 1759-1785.

Bascou, J., Delpech, G., Vauchez, A., Moine, B.N., Cottin, J.-Y., Barruol, G., 2008. An integrated study of microstructural, geochemical and seismic properties of lithospheric mantle above the Kerguelen plume (Indian Ocean). Geochem. Geophys. Geosyst. 9, Q04036, doi:04010.01029/02007GC001879.

Bastow, I.D., Stuart, G.W., Kendall, J.-M., Ebinger, C.J., 2005. Upper-mantle seismic structure in a region of incipient continental breakup: northern Ethiopian rift. Geophysical Journal International. 162, 479-493, doi:410.1111/j.1365-1246X.2005/02666.x.

Becker, H., 1996. Geochemistry of garnet peridotite massifs from lower Austria and the composition of deep lithosphere beneath a Paleozoic convergent plate margin. Chemical Geology. 134, 49-65.

Bedini, R.M., Blichert-Toft, J., Boyet, M., Albarède, F., 2004. Isotopic constraints on the cooling of the continental lithosphere. Earth and Planetary Science Letters. 223, 99-111.

Bedini, R.M., Bodinier, J.-L., Dautria, J.-M., Morten, L., 1997. Evolution of LILE-enriched small melt fractions in the lithospheric mantle: a case study from the East African Rift. Earth and Planetary Science Letters. 153, 67-83.

Ben Ismaïl, W., Mainprice, D., 1998. An olivine fabric database: an overview of upper mantle fabrics and seismic anisotropy. Tectonophysics. 296, 145-157.

Ben Ismaïl, W., Mainprice, D., 2001. The Kaapvaal craton seismic anisotropy: petrophysical analyses of upper mantle kimberlite nodules. Geophysical Research Letters. 28, 2497-2500.

Beyer, E., Brueckner, H.K., Griffin, W.L., O'Reilly, S.Y., Graham, S., 2004. Archean mantle fragments in Proterozoic crust, Western Gneiss Region, Norway. Geology. 32, 609-612.

Beyer, E., Griffin, W.L., O'Reilly, S.Y., 2006. Transformation of Archaean lithospheric mantle by refertilization: evidence from exposed peridotites in the Western Gneiss Region, Norway. Journal of Petrology. 47, 1611-1636.

Bizimis, M., Sen, G., Salters, V.J.M., 2003. Hf-Nd isotope decoupling in the oceanic lithosphere: constraints from spinel peridotites from Oahu, Hawaii. Earth and Planetary Science Letters. 217, 43-58.

Blichert-Toft J., Albarede F., 1997. The Lu-Hf isotope geochemistry of chondrites and the evolution of the mantle-crust system. Earth and Planetary Science Letters. 148, 243-258.

Blichert-Toft, J., 2001. On the Lu-Hf isotope geochemistry of silicate rocks. Geostandards Newsletter. 25, 41-56.

Blundy, J.D., Robinson, J.A.C., Wood, B.J., 1998. Heavy REE are compatible in clinopyroxene on the spinel-lherzolite solidus. Earth and Planetary Science Letters. 160, 493-504.

Bodinier, J.-L., 1988. Geochemistry and petrogenesis of the Lanzo peridotite body, Western Alps. Tectonophysics. 149, 67-88.

Bodinier, J.-L., Dupuy, C., Dostal, J., 1988. Geochemistry and petrogenesis of Eastern Pyrenean peridotites. Geochimica et Cosmochimica Acta. 52, 2893-2907.

Bodinier, J.-L., Fabriès, J., Lorand, J.-P., Dostal, J., Dupuy, C., 1987a. Geochemistry of amphibole pyroxenite veins from the Lherz and Freychinède ultramafic bodies (Ariège, French Pyrenees). Bulletin Minéralogique. 110, 345-358.

Bodinier, J.-L., Godard, M., 2003. Orogenic ophiolitic, and abyssal peridotites. in: R.W. Carlson (Eds), Treatise on Geochemistry - The Mantle and Core. Elsevier, 103-170.

Bodinier, J.-L., Guiraud, M., Fabriès, J., Dostal, J., Dupuy, C., 1987b. Petrogenesis of layered pyroxenites from the Lherz, Freychinède and Prades ultramafic bodies (Ariège, French Pyrenees). Geochimica et Cosmochimica Acta. 51, 279-290.

Bodinier, J.-L., Menzies, M.A., Shimizu, N., Frey, F.A., McPherson, E., 2004. Silicate, hydrous and carbonate metasomatism at Lherz, France: contemporaneous derivatives of silicate melt-harzburgite reaction. Journal of Petrology. 45, 299-320.

Bodinier, J.-L., Vasseur, G., Vernières, J., Dupuy, C., Fabriès, J., 1990. Mechanism of mantle metasomatism: Geochemical evidence from the Lherz orogenic peridotite. Journal of Petrology. 31, 597-628.

Boudier, F., Nicolas, A., Structural control on the partial melting of the Lanzo peridotite, AGU Chapman Conf. Proc. Bull. 96, Geol. Min. Industries, Oregon Dep, 1977.

Brown, M., Solar, G.S., 1998. Shear-zone systems and melts: feedback relations and self-organization in orogenic belts. Journal of Structural Geology. 20, 211-227.

Buck, W.R., 2006. The role of magma in the development of the Afro-Arabian rift system. Geological Society of London, Special Publications. 259, 43-54.

Bunge, H.J., 1982. Texture analysis in material sciences, Butterworths, London.

Burnham, O.M., Rogers, N.W., Pearson, D.G., Van Calsteren, P.W., Hawkesworth, C.J., 1998. The petrogenesis of eastern Pyrenean peridotites: an integrated study of their whole-rock geochemistry and Re-Os isotopic composition. Geochimica et Cosmochimica Acta. 62, 2293-2310.

Canil, D., 2004. Midly incompatible elements in peridotites and the origins of mantle lithosphere. Lithos. 77, 375-393.

Carlson, R.W., Irving, A.J., Schulze, D.J., Carter Hearn Jr, B., 2004. Timing of Precambrian melt depletion and Phanerozoic refertilization events in the lithospheric mantle of the Wyoming Craton and adjacent Central Plains Orogen. Lithos. 77, 453-472.

Carswell, D.A., 1968. Picritic magma — residual dunite relationships in garnet peridotite at Kalskaret near Tafjord, South Norway. Contributions to Mineralogy and Petrology. 19, 97-124.

Chaussidon, M., Lorand, J.-P., 1990. Sulphur isotope composition of orogenic spinel lherzolite massifs from Ariege (north-eastern Pyrenees, France): an ion microprobe study. Geochimica et Cosmochimica Acta. 54, 2835-2846.

Choukroune, P., 1973. La brèche de Lherz dite "d'explosion liée à la mise en place des lherzolites" est une brèche sédimentaire d'âge cénozoïque. Comptes Rendus de l'Académie des Sciences. 277, 2621-2624.

Choukroune, P., 1988. The ECORS deep reflection seismic survey across the Pyrenees. Nature. 331, 508-510.

Choukroune, P., Mattauer, M., 1978. Tectonique des plaques et Pyrénées: sur le fonctionnement de la faille transformante nord-pyrénéenne; comparaison avec des modèles actuels. Bulletin de la Société Géologique de France. 20, 689-700.

Colchen, M., Ternet, Y., Debroas, E.J., Carte géologique de la France au 1/50000, feuille 1086, Aulus-les-Bains, in: é. BRGM, (Ed), 1997.

Conquéré, F., 1971. Les pyroxénites à amphibole et les amphibolites associées aux lherzolites du gisement de Lherz (Ariège, France): un exemple du rôle de l'eau au cours de la cristallisation fractionnée des liquides issus de la fusion partielle des lherzolites. Contributions to Mineralogy and Petrology. 33, 32-61.

Conquéré, F., 1978. Pétrologie des complexes ultramafiques de lherzolite à spinelle de l'Ariège (France). Ph.D. thesis, Univ. Paris.

Conquéré, F., Fabriès, J., 1984. Chemical disequilibrium and its thermal significance in spinel peridotites from the Lherz and Freychinède ultramafic bodies (Ariège, French Pyrenees). in: J. Kornprobst (Eds), Kimberlites II. The mantle and Crust-Mantle Relationships. Elsevier, Amsterdam, 319-331.

Costa, S., Maluski, H., 1988. Use of ^{40}Ar-^{39}Ar stepwise heating method for dating mylonitic zones: an example from the St. Barthelemy Massif (Northern Pyrenees, France). Chemical Geology. 72, 127-144.

Couvy, H., Frost, D.J., Heidelbach, F., Nyilas, K., Ungar, T., Mackwell, S., Cordier, P., 2004. Shear deformation experiments of forsterite at 11 GPa - 1400°C in the multianvil apparatus. European Journal of Mineralogy. 16, 877-889.

Dawson, J.B., 1984. Contrasting types of upper-mantle metasomatism. in: J. Kornprobst (Eds), Kimberlites II. The mantle and Crust-Mantle Relationships. Elsevier, Amsterdam, 289-294.

Debroas, E.J., 1987. Modèle de bassin triangulaire à l'intersection de décrochements divergents pour le fossé albo-cénomanien de la Ballongue (zone nord-pyrénéenne, France). Bulletin de la Société Géologique de France. 8, 887-898.

Deloule, E., Albarède, F., Sheppard, M.F., 1991. Hydrogen isotope heterogeneities in the mantle from ion probe analysis of amphiboles from ultramafic rocks. Earth and Planetary Science Letters. 105, 543-553.

Deng, F. L. and McDougall, J. D., 1992. Proterozoic depletion of the lithosphere recorded in mantle xenoliths from Inner Mongolia. Nature. 360, 333-336.

Dickey Jr, J.S., 1970. Partial fusion products in Alpine-type peridotites: Serrania de La Ronda and other examples. Mineral Soc. Amer. Spec. Pap. 3, 33-49.

Dijkstra, A., Drury, M.R., Vissers, R.L.M., 2001. Structural Petrology of Plagioclase Peridotites in the West Othris Mountains (Greece): Melt Impregnation in Mantle Lithosphere. Journal of Petrology. 42, 5-24.

Downes, H., 2001. Formation and modification of the shallow subcontinental lithospheric mantle: a review of geochemical evidence from ultramafic xenolith suites and

tectonically emplaced ultramafic massifs of western and central Europe. Journal of Petrology. 42, 233-250.

Downes, H., Bodinier, J.-L., Thirlwall, M.F., Lorand, J.-P., Fabriès, J., 1991. REE and Sr-Nd isotopic geochemistry of Eastern Pyrenean peridotite massifs: Sub-continental lithospheric mantle modified by continental magmatism. Journal of Petrology. 97-115.

Downes, H., Cvetkovic, V., Hock, V., Prelevic, D., Lazarov, M., Refertilization of highly depleted lithospheric mantle (Balkan peninsula, SE Europe): evidence from peridotite xenoliths, Goldschmidt Conference Abstracts, 2006.

Downes, H., Dupuy, C., 1987. Textural, isotopic and REE variations in spinel peridotite xenoliths, Massif Central, France. Earth and Planetary Science Letters. 82, 121-135.

Elthon, D., 1992. Chemical trends in abyssal peridotites: refertilization of depleted suboceanic mantle. Journal of Geophysical Research. 97, 9015-9025.

Fabriès, J., Lorand, J.-P., Bodinier, J.-L., 1998. Petrogenetic evolution of orogenic lherzolite massifs in the central and western Pyrenees. Tectonophysics. 292, 145-167.

Fabriès, J., Lorand, J.-P., Bodinier, J.-L., Dupuy, C., 1991. Evolution of the upper mantle beneath the Pyrenees: evidence from orogenic spinel lherzolite massifs. Journal of Petrology. 55-76.

Fortané, A., Duée, G., Lagabrielle, Y., Coutelle, A., 1986. Lherzolites and the Western "Chaînons Béarnais" (French Pyrenees): structural and paleogeographical pattern. Tectonophysics. 129, 81-98.

Frey, F., Shimizu, N., Leinbach, A., Obata, M., Takazawa, E., 1991. Compositional variations within the lower layered zone of the Horoman peridotites, Hokkaido, Japan: constraints on models for melt-solid segregation. in: M.A. Menzies, C. Dupuy, A. Nicolas (Eds), Orogenic lherzolites and mantle processes. Oxford University Press, Oxford,

Frey, F.A., Suen, C.J., Stockman, H.W., 1985. The Ronda high temperature peridotite: geochemistry and petrogenesis. Geochimica et Cosmochimica Acta. 49, 2469-2491.

Garrido, C., Bodinier, J.-L., 1999. Diversity of mafic rocks in the Ronda peridotite: evidence for pervasive melt/rock reaction during heating of subcontinental lithosphere by upwelling asthenosphere. J. Petrol. 40, 729-754.

Gleizes, G., Leblanc, D., Bouchez, J.-L., 1997. Variscan granites of the Pyrenees revisited: their role as syntectonic markers of the orogen. Terra Nova. 9, 38-41.

Godard, M., Jousselin, D., Bodinier, J.-L., 2000. Relationships between geochemistry and structure beneath a paleo-spreading centre: a study of the mantle section in the Oman Ophiolite. Earth and Planetary Science Letters. 180, 133-148.

Golberg, J.-M., Maluski, H., 1988. Données nouvelles et mise au point sur l'âge du métamorphisme pyrénéen. Comptes Rendus de l'Académie des Sciences. 306, 429-435.

Golberg, J.M., Leyreloup, A.F., 1990. High temperature - low pressure Cretaceous metamorphism related to crustal thinning (Eastern North Pyrenean Zone, France. Contributions to Mineralogy and Petrology. 104, 194-207.

Golberg, J.M., Maluski, H., Leyreloup, A.F., 1986. Petrological and age relationship between emplacement of magmatic breccia, alkaline magmatism and static metamorphism in the North Pyrenean Zone. Tectonophysics. 129, 275-290.

Goldschmidt, V.M., 1929. The distribution of chemical elements. Proc. Roy. Inst. Great Britain. 26, 73-86.

Griffin, W.L., O'Reilly, S.Y., Natapov, L.M., Ryan, C.G., 2003. The evolution of lithospheric mantle beneath the Kalahari Craton and its margins. Lithos. 71, 215-242.

Hamelin, B., Allègre, C.J., 1988. Lead isotope study of orogenic lherzolite massifs. Earth and Planetary Science Letters. 91, 117-131.

Hart, S.R., Dunn, T., 1993. Experimental cpx/melt partitioning of 24 trace elements. Contributions to Mineralogy and Petrology. 113, 1-8.

Harte, B., 1983. Mantle peridotites and processes-the kimberlite sample. in: C.J. Hawkesworth, M.J. Norry (Eds), Continental Basalts and Mantle Xenoliths. Shiva Publishing, Cheshire, U.K.,

Harte, B., Hunter, R.H., Kinny, P.D., 1993. Melt geometry, movement and crystallization, in relation to mantle dykes, veins and metasomatism. in: (Eds), Philosophical Transactions of the Royal Society of London. 1-21.

Hartmann, G., Wedephol, K.H., 1993. The composition of peridotites tectonites from the Ivrea complex (N-Italy) representing material at different stages of depletion. Geochimica et Cosmochimica Acta. 57, 1761-1782.

Henry, P., Azambre, B., Montigny, R., Rossy, M., Stevenson, R.K., 1998. Late mantle evolution of the Pyrenean sub-continental lithospheric mantle in the light of new ^{40}Ar-^{39}Ar and Sm-Nd ages on pyroxenites and peridotites (Pyrenees, France). Tectonophysics. 296, 103-123.

Hirth, G., Kohlstedt, D.L., 1995. Experimental constraints on the dynamics of the partially molten upper mantle: deformation in the dislocation creep regime. Journal of Geophysical Research. 100, 15.441-415.449.

Hofmann, A.W., 1997. Mantle geochemistry: the message from oceanic volcanism. Nature. 385, 219-229.

Hofmann, A.W., 2003. Sampling mantle heterogeneity through oceanic basalts: isotopes and trace elements. in: R.W. Carlson (Eds), Treatise on Geochemistry - The Mantle and Core.

Holtzman, B.K., Kohlstedt, D.L., Zimmerman, M.E., Heidelbach, F., Hiraga, T., Hustoft, J., 2003. Melt segregation and strain partitioning: implications for seismic anisotropy and mantle flow. Science. 301, 1227-1230.

Ionov, D., Mukasa, S.B., Bodinier, J.-L., 2002. Sr-Nd-Pb isotopic compositions of peridotite xenoliths from Spitsbergen: numerical modelling indicates Sr-Nd decoupling in the mantle by melt percolation metasomatism. Journal of Petrology. 43, 2261-2278.

Jagoutz, E., Palme, H., Baddenhausen, H., Blum, K., Cendales, M., Dreibus, G., Spettel, B., Lorenz, V., Wänke, H., The abundances of major, minor and trace elements in the Earth's mantle as derived from primitive ultramafic nodules, Proc. 10th Lunar Planetary Science Conference 2031-2050, 1979.

Jung, H., Karato, S., 2001. Water-induced fabric transition in olivine. Science. 293, 1460-1463.

Kelemen, P.B., Dick, H.J.B., 1995. Focused melt flow and localized deformation in the upper mantle: juxtaposition of replacive dunite and ductile shear zones in the Josephine peridotite, SW Oregon. Journal of Geophysical Research. 100, 423-438.

Kendall, J.-M., Pilidou, S., Keir, D., Bastow, I.D., Stuart, G.W., Ayele, A., 2006. Mantle upwellings, melt migration and the rifting of Africa: insights from seismic anisotropy. Geological Society of London, Special Publications. 259, 55-72.

Kisters, A.F.M., Gibson, R.L., Charlesworth, E.G., Anhaeusser, C.R., 1998. The role of strain localization in the segregation and ascent of anatectic melts, Namaqualand, South Africa. Journal of Structural Geology. 20, 229-242.

Kopylova, M.G., Russell, J.K., 2000. Chemical stratification of cratonic lithosphere; constraints from the northern Slave Craton, Canada. Earth and Planetary Science Letters. 181, 71-87.

Kornprobst, J., Vielzeuf, D., 1984. Transcurrent crustal thinning: a mechanism for the uplift of deep continental crust/upper mantle associations. in: J. Kornprobst (Eds),

Kimberlites II. The mantle and Crust-Mantle Relationships. Elsevier, Amsterdam, 347-359.

Lacroix, A., Les péridotites des Pyrénées et les autres roches intrusives non feldspathiques qui les accompagnent, C.R. Académie des Sciences, Paris, 1917.

Lagabrielle, Y., Bodinier, J.-L., 2008. Submarine reworking of exhumed subcontinental mantle rocks: field evidence from the Lherz peridotites, French Pyrenees. Terra Nova. 20, 11-21.

Le Roux, V., Bodinier, J.-L., Alard, O., O'Reilly, S.Y., Griffin, W.L., 2008a. Isotopic decoupling between Hf, Nd and Sr during porous melt flow: case study in the Lherz peridotites (Pyrenees). Earth and Planetary Science Letters. Submitted.

Le Roux, V., Bodinier, J.-L., Tommasi, A., Alard, O., Dautria, J.-M., Vauchez, A., Riches, A.J.V., 2007. The Lherz spinel lherzolite: refertilized rather than pristine mantle. Earth and Planetary Science Letters. 259, 599-612.

Le Roux, V., Tommasi, A., Vauchez, A., 2008. Feedback between melt percolation and deformation in an exhumed lithosphere-asthenosphere boundary. Earth and Planetary Science Letters. 274, 401-413.

Lee, C.-T., Rudnick, R.L., Compositionally stratified cratonic lithosphere: petrology and geochemistry of peridotite xenoliths from the Labait Volcano, Tanzania, in: B.J.v. Dawson, J.J. Gurney, J.L. Gurney, M.D. Pascoe, S.R. Richardson, (Eds), Proc. VIIth International Kimberlite Conference, 1999, pp. 503-521.

Lee, C.-T.A., Harbert, A., Leeman, W.P., 2007. Extension of lattice strain theory to mineral/mineral rare-earth element partitioning: an approach for assessing disequilibrium and developing internally consistent partition coefficients between olivine, orthorpyroxene, clinopyroxene and basaltic melt. Geochimica et Cosmochimica Acta. 71, 481-496.

Lenoir, X., Garrido, C., Bodinier, J.-L., Dautria, J.-M., Gervilla, F., 2001. The recrystallization front of the Ronda peridotite: evidence for melting and thermal erosion of subcontinental lithospheric mantle beneath the Alboran Basin. Journal of Petrology. 42, 141-158.

Lesher, C.E., 1994. Kinetics of Sr and Nd exchange in silicate liquids: theory, experiments, and applications to uphill diffusion, isotopic equilibration, and irreversible mixing of magmas. Journal of Geophysical Research. 99, 9585-9604.

Li, Y., Kind, R., Yuan, X., Wolbern, I., Hanka, W., 2004. Rejuvenation of the lithosphere by the Hawaiian plume. Nature. 427, 827-829.

Liu, X., O'Neill, H.S.C., 2004. The effect of Cr_2O_3 on the partial melting of spinel lherzolite in the system CaO-MgO-Al_2O_3-SiO_2-Cr_2O_3 at 1.1 GPa. Journal of Petrology. 45, 2261-2286.

Lorand, J.-P., 1989. Abundance and distribution of Cu-Fe-Ni sulfides, sulfur, copper and platinium-group elements in orogenic-type spinel lherzolite massifs of Ariège. Earth and Planetary Science Letters. 93, 50-64.

Lorand, J.P., 1991. Sulphide petrology and sulphur geochemistry of orogenic lherzolites: a comparative study of the Pyrenean bodies (France) and the Lanzo massif (Otaly). in: M.A. Menzies, C. Dupuy, A. Nicolas (Eds), Orogenic lherzolites and Mantle Processes. 77-95.

Loubet, M., Allègre, C.J., 1982. Trace elements in orogenic lherzolites reveal the complex history of the upper mantle. Nature. 298, 809-814.

Luguet, A., Alard, O., Lorand, J.P., Pearson, N.J., Ryan, C., O'Reilly, S.Y., 2001. Laser-ablation microprobe (LAM)-ICPMS unravels the highly siderophile element geochemistry of the oceanic mantle. Earth and Planetary Science Letters. 189, 285-294.

Mainprice, D., Tommasi, A., Couvy, A., Cordier, P., Frost, D.J., 2005. Pressure sensitivity of olivine slip systems and seismic anisotropy of the Earth's upper mantle. Nature. 233, 731-733.

McDade, P., Blundy, J.D., Wood, B.J., 2003. Trace element partitioning on the Tinaquillo Lherzolite solidus at 1.5 GPa. Physics of The Earth and Planetary Interiors. 139, 129-147.

McDonough, W.F., Frey, F.A., 1989. Rare earth elements in upper mantle rocks. in: B.R. Lipin, G.A. McKay (Eds), Geochemistry and Mineralogy of Rare Earth Elements. Mineralogical Society of America, Washington DC, 99-139.

McDonough, W.F., Sun, S.-S., 1995. The composition of the Earth. Chemical Geology. 120, 223-253.

McPherson, E., Thirlwall, M.F., Parkinson, I.J., Menzies, M.A., Bodinier, J.-L., Woodland, A., Bussod, G., 1996. Geochemistry of metasomatism adjacent to amphibole-bearing veins in the Lherz peridotite massif. in: M.A. Menzies, J.-L. Bodinier, F.A. Frey, F. Gervilla, P. kelemen (Eds), Melt Processes and Exhumation of Garnet, Spinel and Plagioclase Facies Mantle. Elsevier, Amsterdam, 135-157.

Menzies, M.A., 1983. Mantle ultramafic xenoliths in alkaline magmas: Evidence for mantle heterogeneity modified by magmatic activity. in: C.J. Hawkesworth, M.J. Norry (Eds), Continental Basalts and Mantle Xenoliths. Shiva Publishing, Cheshire, U.K., 92-110.

Menzies, M.A., Allen, C., 1974. Plagioclase lherzolite-residual mantle relationships within two eastern mediterranean ophiolites. Contributions to Mineralogy and Petrology. 45, 197-213.

Menzies, M.A., Rogers, N., Tindle, A., Hawkesworth, C.J., 1987. Metasomatic and enrichment processes in lithospheric peridotites, an effect of asthenosphere-lithosphere interaction. in: M.A. Menzies, C.J. Hawkesworth (Eds), Mantle Metasomatism. Academic Press, London, 313-361.

Minnigh, L.D., Van Calsteren, P.W.C., den Tex, E., 1980. Quenching: an additional model for emplacement of the lherzolite at Lers (French Pyrenees). Geology. 8, 18-21.

Monchoux, P., Les lherzolites pyrénéennes: contribution à l'étude de leur minéralogie, de leur genèse et de leurs transformations., 1970.

Monchoux, P., 1971. Comparaison et classement des massifs de lherzolite de la zone mésozoïque Nord-Pyrénéenne. Bulletin de la Société d'Histoire Naturelle de Toulouse. 107, 393-407.

Monchoux, P., 1972. Roches à saphirine au contact des lherzolites pyrénéennes. Contributions to Mineralogy and Petrology. 37, 47-64.

Montigny, R., Azambre, B., Rossy, M., Thuizat, R., 1986. K-Ar study of Cretaceaous magmatism and metamorphism of the Pyrenees: age and length of rotation of the Iberian Peninsula. Tectonophysics. 129, 257-273.

Mukasa, S.B., Shervais, J.W., Wilshire, H.G., Nielson, J.E., 1991. Intrinsic Nd, Pb and Sr isotopic heterogeneities exhibited by the Lherz alpine peridotite massifs, French Pyrenees. Journal of Petrology. 117-134.

Müntener, O., Pettke, T., Desmurs, L., Meier, M., Schaltegger, U., 2004. Refertilization of mantle peridotite in embryonic ocean basins: trace element and Nd isotopic evidence and implications for crust-mantle relationships. Earth and Planetary Science Letters. 221, 293-308.

Navon, O., Stolper, E., 1987. Geochemical consequence of melt percolation: the upper mantle as a chromatographic column. Journal of Geology. 95, 285-307.

Nicolas, A., Dupuy, C., 1984. Origin of ophiolitic and oceanic lherzolites. Tectonophysics. 110, 177-187.

O'Hara, M.J., 1967. Mineral parageneses in ultramafic rocks. in: P.J. Wyllie (Eds), Ultramafic and related rocks. Wiley, New York, 393-403.

Obata, M., Suen, C.J., Dickey, J.S., The origin of mafic layers in the Ronda high-temperature peridotite intrusion, S. Spain: an evidence of partial fusion and fractional crystallisation in the upper mantle, Orogenic mafic and ultramafic association 272, Colloques Inter. C.N.R.S., 1980, pp. 257-268.

Palme, H., O'Neill, H.S.C., 2003. Cosmochemical estimates of mantle composition. in: R.W. Carlson (Eds), Treatise on Geochemistry - The Mantle and Core. Elsevier, 1-38.

Pattou, L., Lorand, J.-P., Gros, M., 1996. Non-chondritic platinum-group element ratios in the Earth's mantle. Nature. 379, 712-715.

Paulick, H., Bach, W., Godard, M., De Hoog, J.C.M., Suhr, G., Harvey, J., 2006. Geochemistry of abyssal peridotites (Mid-Atlantic Ridge, 15°20′N, ODP Leg 209): Implications for fluid/rock interaction in slow spreading environments. Chemical Geology. 234, 179-210.

Pearson, D.G., Nowell, G.M., 2004. Re-Os and Lu-Hf isotope constraints on the origin and age of pyroxenites from the Beni Bousera peridotite massif: implications for mixed peridotite-pyroxenite mantle sources. Journal of Petrology. 45, 439-455.

Piccardo, G.B., Müntener, O., Zanetti, A., 2004. Alpine-Apennine ophiolitic peridotites: new concepts on their composition and evolution. Ofioliti. 29, 63-74.

Pin, C., Vielzeuf, D., 1983. Granulites and related rocks in Variscan median Europe: a dualistic interpretation. Tectonophysics. 93, 47-74.

Pin, C., Zalduegui, J.F.S., 1997. Sequential separation of light rare-earth elements, thorium and uranium by miniaturized extraction chromatography: application to isotopic analyses of silicate rocks. Analytica Chimica Acta. 339, 79-89.

Polvé, M., Allègre, C.J., 1980. Orogenic lherzolites complexes studied by ^{87}Rb-^{87}Sr: A clue to understanding the mantle convection processes? Earth and Planetary Science Letters. 51, 71-93.

Rabinowicz, M., Ceuleneer, G., 2005. The effect of sloped isotherms on melt migration in the shallow mantle: a physical and numerical model based on observations in the Oman ophiolite. Earth and Planetary Science Letters. 229, 231-246.

Rampone, E., Piccardo, G.B., Hofmann, A.W., 2008. Multi-stage melt–rock interaction in the Mt. Maggiore (Corsica, France) ophiolitic peridotites: microstructural and geochemical evidence. Contributions to Mineralogy and Petrology. DOI 10.1007/s00410-00008-00296-y.

Rampone, E., Piccardo, G.B., Vannucci, R., Bottazzi, P., 1997. Chemistry and origin of trapped melts in ophiolitic peridotites. Geochimica et Cosmochimica Acta. 61, 4557-4569.

Rampone, E., Piccardo, G.B., Vannucci, R., Bottazzi, P., Zanetti, A., 1994. Melt impregnation in ophiolitic peridotite: an ion microprobe study of clinopyroxene and plagioclase. Mineralogical Magazine. 58A, 756-757.

Reisberg, L., Lorand, J.-P., 1995. Longevity of subcontinental mantle lithosphere from osmium isotope systematics in orogenic peridotite massifs. Nature. 376, 159-162.

Reisberg, L., Zindler, A., 1986. Extreme isotopic variations in the upper mantle: Evidence from Ronda. Earth and Planetary Science Letters. 81, 29-45.

Ringwood, A.E., 1975. Composition and Petrology of the Earth's Mantle, McGraw Hill, New York.

Rosenberg, C.L., Handy, M.R., 2000. Syntectonic melt pathways during simple shearing of a partially molten rock analogue (Norcampher-Benzamide). Journal of Geophysical Research. 105, 3135-3149.

Rosenberg, C.L., Handy, M.R., 2001. Mechanisms and orientation of melt segregation paths during pure shearing of a partially molten rock analog (norcamphor-benzamide). Journal of Structural Geology. 23, 19717-11932.

Rosenberg, C.L., Handy, M.R., 2005. Experimental deformation of partially melted granite revisited: implications for the continental crust. Journal of Metamorphic Geology. 23, 19-28.

Rossy, M., Azambre, B., Albarède, F., 1992. REE and Sr-Nd isotope geochemistry of the alkaline magmatism from the Cretaceous North Pyrenean Rift Zone (France-Spain). Chemical Geology. 97, 33-46.

Saal, A.E., Takazawa, E., Frey, F.A., Shimizu, N., Hart, S.R., 2001. Re-Os Isotopes in the Horoman peridotite: evidence for refertilization? Journal of Petrology. 42, 25-37.

Salters, V.J.M., White, W.M., 1998. Hf isotope constraints on mantle evolution. Chemical Geology. 145, 447-460.

Sautter, V., Fabriès, J., 1990. Cooling kinetics of garnet websterites from the Freychinède orogenic lherzolite massif, French Pyrenees. Contributions to Mineralogy and Petrology. 105, 533-549.

Schärer, U., Kornprobst, J., Beslier, M.O., Boillot, G., Girardeau, J., 1995. Gabbro and related rock emplacement beneath rifting continental crust: U-Pb geochronological and geochemical constraints for the Galicia passive margin (Spain). Earth and Planetary Science Letters. 130, 187-200.

Scott, T., Kohlstedt, D.L., 2006. The effect of large melt fraction on the deformation behavior of peridotite. Earth and Planetary Science Letters. 246, 177-187.

Seyler, M., Toplis, M., Lorand, J.P., Luguet, A., Cannat, M., 2001. Clinopyroxene microtextures reveal incompletely extracted melts in abyssal peridotites. Geology. 29, 155-158.

Shervais, J.W., Mukasa, S.B., 1991. The Balmuccia orogenic lherzolite massif, Italy. in: M.A. Menzies, C. Dupuy, A. Nicolas (Eds), Orogenic lherzolites and mantle processes. Oxford University Press, Oxford (U.K.), 155-174.

Sneeringer, M., Stanley, H., Shimizu, N., 1984. Strontium and samarium diffusion in diopside. Geochimica et Cosmochimica Acta. 48, 1589-1608.

Sparks, D.W., Parmentier, E.M., 1991. Melt extraction from the mantle beneath spreading centres. Earth and Planetary Science Letters. 105, 368-377.

Spiegelman, M., 1993. Physics of melt extraction: theory, implications and applications. Philosophical Transactions: Physical Sciences and Engineering. 342, 23-41.

Sun, S.-S., McDonough, W.F., 1989. Chemical and isotopic systematics of oceanic basalts: Implications for mantle composition and processes. in: A.D. Saunders, M.J. Norry (Eds), Magmatism in the Ocean Basins. Geol. Soc. London, 313-345.

Takazawa, E., Okayasu, T., Satoh, Keiichi, 2003. Geochemistry and origin of the basal lherzolites from the northern Oman ophiolite (northern Fizh block). Geochemistry, Geophysics and Geosystems (G3). 4, 2000GC000080.

Takei, Y., 2005. Deformation-induced grain boundary wetting and its effects on the acoustic and rheological properties of partially molten rock analogue. Journal of Geophysical Research. 110, doi:10.1029/2005JB003801.

Tang, Y.-J., Zhang, H.-F., Ying, J.-F., Zhang, J., Liu, X.-M., 2008. Refertilization of ancient lithospheric mantle beneath the central North China Craton: evidence from petrology and geochemistry of peridotite xenoliths. Lithos. 101, 435-452.

Thoraval, C., Tommasi, A., Doin, M.-P., 2006. Plume-lithosphere interactions beneath a fast-moving plate. Geophysical Research Letters. 33, L01301, doi:01310.01029/02005GL024047.

Tommasi, A., Godard, M., Coromina, G., Dautria, J.-M., Barsczus, H., 2004. Seismic anisotropy and compositionally induced velocity anomalies in the lithosphere above mantle plumes: a petrological and microstructural study of mantle xenoliths from French Polynesia. Earth and Planetary Science Letters. 227, 539-556.

Tommasi, A., Mainprice, D., Canova, G., Chastel, Y., 2000. Viscoplastic self-consistent and equilibrium-based modeling of olivine lattice preferred orientations. Implications for upper mantle seismic anisotropy. Journal of Geophysical Research. 105, 7893-7908.

Tommasi, A., Tikoff, B., Vauchez, A., 1999. Upper mantle tectonics: three-dimensional deformation, olivine crystallographic fabrics and seismic properties. Earth and Planetary Science Letters. 168, 173-186.

Tommasi, A., Vauchez, A., 2001. Continental rifting parallel to ancient collisional belts: an effect of the mechanical anisotropy of the lithospheric mantle. Earth and Planetary Science Letters. 185, 199-210.

Tommasi, A., Vauchez, A., Fernandes, L.A.D., Porcher, C.C., 1994. Magma-assisted strain localization in an orogen-parallel transcurrent shear zone of southern Brazil. Tectonics. 13, 421-437.

Tommasi, A., Vauchez, A., Ionov, D., 2008. Deformation, static recrystallization, and reactive melt transport in shallow subcontinental mantle xenoliths (Tok Cenozoic volcanic field, SE Siberia). Earth and Planetary Science Letters. doi: 10.1016/j.epsl.2008.1004.1020.

Van Achtebergh, E., Ryan, C.G., Jackson, S.E., Griffin, W.L., 2001. Data reduction software for LA-ICP-MS. in: P.J. Sylvester (Eds), Laser-Ablation-ICPMS in the Earth Sciences: Principles and Applications. Mineral. Assoc. of Can., Ottawa, Ontario, Canada,

Van der Wal, D., Bodinier, J.-L., 1996. Origin of the recrystallisation front in the Ronda peridotite by km-scale pervasive porous melt flow. Contributions to Mineralogy and Petrology. 122, 387-405.

Van Orman, J.A., Grove, T.L., Shimizu, N., 2001. Rare earth element diffusion in diopside: influence of temperature, pressure, and ionic radius, and an elastic model for diffusion in silicates. Contributions to Mineralogy and Petrology. 141, 687-703.

Vasseur, G., Vernières, J., Bodinier, J.-L., 1991. Modelling of trace element transfer between mantle melt and heterogranular peridotite matrix. Journal of Petrology. 41-54.

Vauchez, A., Barruol, G., 1996. Shear-wave splitting in the Appalachians and the Pyrenees: importance of the inherited tectonic fabric of the lithosphere. Physics of The Earth and Planetary Interiors. 95, 127-138.

Vauchez, A., Dineur, F., Rudnick, R., 2005. Microstructure, texture and seismic anisotropy of the lithospheric mantle above a mantle plume: insights from the Labait volcano xenoliths (Tanzania). Earth and Planetary Science Letters. 232, 295-314.

Vauchez, A., Garrido, C., 2001. Seismic properties of an asthenopherized lithospheric mantle: constraints from lattice preferred orientations in peridotite from the Ronda massif. Earth and Planetary Science Letters. 192, 235-249.

Vauchez, A., Tommasi, A., 2003. Wrench faults down to the asthenosphere: Geological and geophysical evidence and thermo-mechanical effects. in: F. Storti, R.E. Holdsworth, F. Salvini (Eds), Intraplate strike-slip deformation belts. Geol. Soc. London Spec. Publ., London, 15-24.

Vernières, J., Godard, M., Bodinier, J.-L., 1997. A plate model for the simulation of trace element fractionation during partial melting and magma transport in the earth's upper mantle. Journal of Geophysical Research. 102, 24771-24784.

Vervoort, J.D., Patchett, P.J., Blichert-Toft, J., Albarède, F., 1999. Relationships between Lu-Hf and Sm-Nd isotopic systems in the global sedimentary system. Earth and Planetary Science Letters. 168, 79-99.

Vétil, J.Y., Lorand, J.P., Fabriès, J., 1988. Conditions de mise en place des filons des pyroxénites à amphibole du massif ultramafique de Lherz (Ariège, France). C. R. Acad. Sci. Paris 307, 587-593.

Vielzeuf, D., Pétrologie des écailles granulitiques de la région de Lherz (Ariège-Zone Nord Pyrénéenne). Introduction à l'étude expérimentale de l'association grenat(alm-py)-feldspath potassique. Thesis, University of Clermont-Ferrand, 1980.

Vielzeuf, D., Kornprobst, J., 1984. Crustal splitting and the emplacement of Pyrenean lherzolites and granulites. Earth and Planetary Science Letters. 67, 87-96.

Von der Handt, A. 2008. Deciphering petrological signatures of reactive melt stagnation and cooling in the oceanic mantle underneath ultraslow spreading ridges. PhD Thesis. Geochemistry Department. Max-Planck Institute for Chemistry, Mainz. pp 311.

Waff, H.S., Faul, U.H., 1992. Effects of crystalline anisotropy on fluid distribution in ultramafic partial melts. Journal of Geophysical Research. 97, 9003-9014.

Walter, M.J., Sisson, T.W., Presnall, D.C., 1995. A mass proportion method for calculating melting reactions and application to melting of model upper mantle lherzolite. Earth and Planetary Science Letters. 135, 77-90.

Wark, D.A., Watson, B.E., 2000. Effect of grain size on the distribution and transport of deep-seated fluids and melts. Geophysical Research Letters. 27, 2029-2032.

Weis, D., Kieffer, B., Maerschalk, C., Pretorius, W., Barling, J., 2005. High-precision Pb-Sr-Nd-Hf isotopic characterization of USGS BHVO-1 and BHVO-2 reference materials. Geochem. Geophys. Geosyst. 6, Q02002, doi:02010.01029/02004GC000852.

Wilshire, H.G., Pike, J.E.N., Meyer, C.E., Schwarzman, E.C., 1980. Amphibole-rich veins in lherzolite xenoliths, Dish Hill and Dead-man Lake, California. American Journal of Science. 280-A, 576-593.

Wittig, N., Baker, J.A., Downes, H., 2007. U-Th-Pb and Lu-Hf isotopic constraints on teh evolution of the sub-continental lithospheric mantle, French Massif Central. Geochimica et Cosmochimica Acta. 71, 1290-1311.

Wood, B.J., Blundy, J.D., 2003. Trace element partitioning under crustal and uppermost mantle conditions: the influences of ionic radius, cation charge, pressure, and temperature. in: R.W. Carlson (Eds), Treatise on Geochemistry - The Mantle and Core. Elsevier, 395-425.

Woodland, A., Kornprobst, J., McPherson, E., Bodinier, J.-L., Menzies, M.A., 1996. Metasomatic interactions in the lithospheric mantle: petrologic evidence from the Lherz Massif, French Pyrenees. in: M.A. Menzies, J.-L. Bodinier, F.A. Frey, F. Gervilla, P. Kelemen (Eds), Melt Processes and Exhumation of Garnet, Spinel and Plagioclase Facies Mantle. Elsevier, Amsterdam, 83-112.

Zanetti, A., Vannucci, R., Bottazzi, P., Oberti, R., Ottolini, L., 1996. Infiltration metasomatism at Lherz as monitored by systematic ion-microprobe investigations close to a hornblendite vein. in: M.A. Menzies, J.-L. Bodinier, F.A. Frey, F. Gervilla, P. Kelemen (Eds), Melt Processes and Exhumation of Garnet, Spinel and Plagioclase Facies Mantle. Elsevier, Amsterdam, 113-133.

Zindler, A., Hart, S., 1986. Chemical geodynamics. Annual Review of Earth and Planetary Sciences. 14, 493-571.

Supplementary material

TABLE OF CONTENTS

Technical work

After I realized the detailed structural map of the Lherz massif, I have sampled, cut with diamond saw and prepared in proper dimensions for thin sections all the Lherz peridotites studied during this work (~ 160 samples). The thin sections have been realized by Christophe Nevado and Doriane Delmas (Géosciences Montpellier).

The thin sections were used for optical observations (~ 160 thin sections), EPMA and LASER-ICPMS (~ 55 thin sections each) analyses, and manual and automatic EBSD measurements that I have performed (~ 50 thin sections).

I have crushed the whole-rocks into powders (~ 60 samples). I performed a chemical digestion of some of them in the clean lab of Geosciences Montpellier and some others in the clean lab of GEMOC ARC National Key Centre. I made the ICPMS measurements with the help of Olivier Bruguier (Montpellier) and Suzy Elhlou (Sydney).

I have crushed, sieved and passed rocks fractions through magnetic separator. I have made a careful handpicking to get the clinopyroxene separates I used for isotopic data (16 samples of >100mg pure clinopyroxene fractions). I have performed the chemical separation of Hf, Nd and Sr (clinopyroxene separates and corresponding whole-rocks) in the clean lab of GEMOC ARC National Key Centre with the help of Peter Wieland and I have performed the TIMS and MC-ICPMS measurements.

This work was supported by INSU DYETI Program and ARC LIEF, DEST Systemic Infrastructure Grants, Macquarie University and industry, and by ARC Discovery project grants. I have obtained financial help from the French Ministry of Research and a 6 months ‘Bourse Lavoisier Co-tutelle’ scholarship for the collaboration with Australia.

Mantle refertilisation, osmium isotopes and the “Primitive Upper Mantle” fallacy, Consequences for the nature of the late veneer

Article in preparation.

O. Alard[1,2], V. Le Roux[1,2], J.-P. Lorand[3], J.-L. Bodinier[1], W. L. Griffin[2], , S. Y. O’Reilly[2]

[1] Géosciences Montpellier, Université de Montpellier 2 and CNRS, Cc 060, Place E. Bataillon, 34095 Montpellier cedex 5 France

[2] GEMOC, Department of Earth & Planetary Sciences, Macquarie University NSW 2109 AUSTRALIA

[3] Unité de Recherche “Minéralogie”, Muséum National d’Histoire Naturelle de Paris, UMR7160 CNRS, Paris 75005, France.

VLR’s contribution in this paper: data and writing.

Abstract

The abundances of highly siderophile elements in the Earth's mantle are best explained by the addition of chondritic material after core segregation, during a late phase of heavy meteorite bombardment; this "late veneer" may also have delivered water and the seeds of life. However, the Os-isotope composition of the Primitive Upper Mantle, as estimated from supposedly "pristine" mantle rocks, rules out the only wet chondrite group: the carbonaceous chondrites. New data show that the type Lherzolite, a keystone of "primitive mantle" models, consists largely of non-pristine material. This sampling bias and misconceptions about the geochemical behaviour of the highly siderophile elements, mean that the Os-isotope constraint, which has bogged down the debate on the nature of the late veneer, is not robust. The Os-isotope composition of Earth's mantle can only be defined as broadly chondritic, and thus does not rule out carbonaceous chondrites as a major component of the late veneer.

A recurrent question in planetary sciences is: what were the "building blocks" of our planet? Of foremost interest is the nature of the `late veneer'; this late accretion (0.2-0.8% of Earth's *mass)* is seen by many as the carrier of water and possibly the seeds of life for Earth[1]. However, the nature of this late component remains elusive and constraints from various geochemical systems seem at first glance contradictory[2]. The highly siderophile elements (HSE: Os, Ir, Ru, Rh, Pt, Pd, Au and Re) have been seen as one of the most promising first-order constraints on the nature of the late component. The broadly chondritic relative abundances of HSEs in Earth's mantle are assumed to reflect the addition of chondritic material to the mantle after core formation via an intense meteorite bombardment[3,4]. Re and Os are both HSEs, ^{187}Re decays by beta emission to ^{187}Os, with a half-life of 41.6 Ga[5], and the ^{187}Os/^{188}Os of Earth's Primitive Upper Mantle (PUM) reflects its time-integrated Re/Os. The currently accepted ^{187}Os/^{188}Os value for the PUM, derived from peridotites stored in post-Archean continental lithosphere from five continents[6,7] is 0.1296 ± 0.0008. . Taken at face value, the PUM composition rules out carbonaceous chondrites[8] (^{187}Os/^{188}Os$_{CC}$= 0.1262±0.0006) as the source of the "late veneer" and would suggest that ordinary chondrites[8] (^{187}Os/^{188}Os$_{OC}$= 0.1283 ± 0.0017) formed the bulk of this veneer. However, carbonaceous chondrites are the only known water-bearing chondrites and have a Deuterium/Hydrogen ratio (D/H≈150•10^{-6}) similar to Earth's seawater[9]. These inconsistencies led Drake and Righter[2] to propose that the Earth was made of an unsampled type of material, the "Earth-chondrite" or "Earth achondrite". Recently, the Pd/Ir of the PUM has been estimated[10] at ca 2.02 ± 0.30, but no chondrite group shows such fractionated HSE abundances[11].

However, a key question is the robustness and significance of the estimated PUM composition. We show here that the estimate of the Os-isotope composition of the PUM is erroneous, because it is based on sample suites in which the HSE abundances and Os-isotope composition have been altered by metasomatic processes. In the light of these new data the Os-isotope composition of the silicate Earth can currently only be constrained at best to be broadly chondritic.

Behind the PUM

The PUM is the composition of a hypothetical upper mantle reservoir that has never experienced melt depletion or metasomatic enrichment (i.e. the silicate earth prior to crustal differentiation). True PUM almost certainly does not exist anywhere on Earth today. Thus, the PUM

composition has been estimated using correlations between potential indicators of melt depletion such as Al_2O_3 and $^{187}Os/^{188}Os$ (Figure 1) in samples of the sub-continental lithospheric mantle, including xenoliths (scavenged by alkali-basalt volcanoes) and orogenic peridotites (tectonically emplaced into the crust). The PUM estimate relies mainly on two key assumptions: (i) due to the highly refractory nature of Os, the $^{187}Os/^{188}Os$ of a mantle section is "frozen in" during major melt extraction events and is not modified by percolation-reaction with ascending magmas; (ii) the least depleted (high-Al_2O_3) peridotites represent samples from which no (or little) melt has been extracted. However, the validity and robustness of these two assumptions are highly questionable.

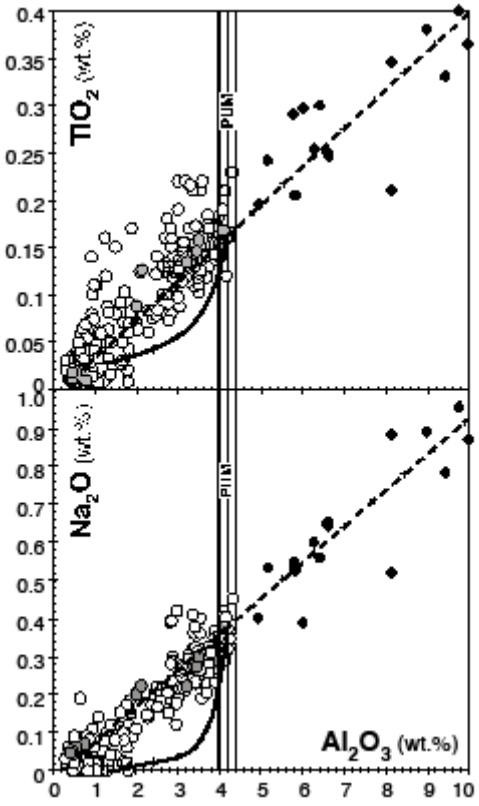

Fig. 1: Whole-rock major-element systematics (TiO_2, Na_2O *vs* Al_2O_3) for the Pyrenées massifs. Open circles, Pyrenées peridotites[12]; grey circles, Lherz samples (this study); black diamonds, interlayered spinel-websterites from all Pyrenées massifs. Solid bold curves show theoretical evolution of Al_2O_3, TiO2 and Na_2O during partial melting[13] (tick marks every 10%). Dashed line denotes mixing between a refractory protolith (Al_2O_3 = 0.45 ; TiO_2=0.01 ; Na_2O= 0.02 wt.%) and a basaltic melt (Al_2O_3 = 15; TiO_2= 0.6 ; Na_2O= 1.45 wt.%); crosses show 5% mixing increments. Vertical lines denote the estimated Al_2O_3 composition of a hypothetical Primitve Upper Mantle[6,7,10] (4.2±0.2 wt.%)

The type Lherzolite under scrutiny

The Lherz massif is the largest and best-exposed peridotite massif in the Pyrenées (France) and is the type locality of fertile mantle rock (i.e. Lherzolite). As such (and for historical reasons) Lherz has played a key role in the PUM estimate; it thus represents an ideal (and emblematic) place to investigate the true nature of the correlation between Al_2O_3 and $^{187}Os/^{188}Os$ and to test the robustness of the PUM estimate.

The Lherz massif shows several features inconsistent with the conventional melt-extraction hypothesis, which regards depleted harzburgites (low Al_2O_3) as derived through partial meting of the fertile lherzolites (high Al_2O_3)[12]. Recent detailed field work[14] has defined a unique set of convergent structural and geochemical evidence demonstrating that the Lherz harzburgites were not derived through partial melting of the fertile lherzolite: (i) harzburgite bodies (1-10m) show a well-

defined foliation (N40-60º) throughout the massif, while the surrounding lherzolites have a weak and variable (N10-N80º) foliation oblique to the harzbugite foliation; (ii) the coarse-grained lherzolites contrast with the deformed (pophyroclastic to mylonitic), fine-grained harzbugites, suggesting coarsening and addition of Opx+Cpx via melt/rock reaction; (iii) harzburgites are LREE-enriched while lherzolites are LREE-depleted; this relationship, although common in both peridotite xenoliths and massifs, is inconsistent with partial melting but can be explained through melt/rock reaction[12]. The Lherz peridotites show strong linear relationships of TiO_2 and NaO *vs* Al_2O_3 (Figure 1), inconsistent with partial melting [13,15,16]. Elements such as Na and Ti, which have relatively low bulk partition coefficients ($D \leq 0.1$), will be more quickly depleted than less incompatible elements such as Al ($D \approx 0.35 \pm 0.05$) during partial melting, thus producing an upward-concave trend. In contrast, linear trends, such as those observed for the Lherz and the Pyrenées peridotites, are typical of mixing processes (Figure 1). Thus, while Al_2O_3 (or CaO, MgO, Lu…) are indices of fertility, they are not necessarily melt depletion indicators[16,17], as has been assumed for the calculations that led to the PUM [6,7,10] estimate. While the positive correlation Al_2O_3-$^{187}Os/^{188}Os$ has been ascribed to an old (Proterozoic) depletion event involving partial melting and stabilization of the lithospheric mantle [18,19], such a scenario cannot explain the negative and positive correlations of Al_2O_3 with $^{87}Sr/^{86}Sr$ and $^{143}Nd/^{144}Nd$, respectively [12,20].

Thus, the (micro- and macro-) structural features suggest that all of the harzburgite bodies once formed a single continuous unit and that the deformation of the harzburgites predates the formation of the lherzolites and websterites. The petrographic and geochemical observations (e.g. Figure 1) are not consistent with a model in which the harzbugite represents the residue left after the extraction of partial melts from the fertile lherzolite. Instead, these features indicate that the lherzolite formed during refertilisation via a near-solidus reaction at the expense of the harzburgite protolith. This reaction caused the precipitation of pyroxenes ± spinel ± amphibole and sulphide. The pervasive websteritic layering in the refertilised lherzolites probably reflects melt segregation, or porosity waves in a matrix in which permeability was decreasing due to the pyroxene-producing refertilisation reaction[21]. Thus, ironically and in contrast to the canonical interpretation, the eponymous lherzolites of the Lherz massif are in fact re-fertilised harzburgites.

The Os-sulphide paradox

Despite the compatible nature of Os, which should give the Re-Os isotopic system

a degree of immunity to metasomatic processes, the isotopic composition of Os commonly is modified during melt-rock percolation-reaction processes[22-26]. This paradox stems from the highly mobile and reactive nature of, the base-metal sulphides[27], which are the main host phase for Os in mantle rocks. Due to their low melting temperature and low viscosity, and their affinity for volatile-rich fluids[28,29] sulphides are extremely mobile and reactive in the mantle[23,24,30,31]. As predicted by modeling and whole-rock observations[32-34] and demonstrated by in-situ analyses[27] and experimental studies[35,36] this mobility is accompanied by severe fractionation of the HSE. For instance, Pd/Ir may vary by several orders of magnitude between sulphide grains a few 10-100s of micrometers apart[24,27,30,31,37,38], and sulphides from the same sample may show extreme isotopic heterogeneity[23,24,26,39,40] reflecting their contrasting petrogenetic history, i.e. residual after melting or metasomatically introduced. Thus the HSE abundances and the isotopic composition of Os in whole-rock samples reflect the proportions of different sulphide populations with contrasting elemental and isotopic compositions.

Sulphides and the Re-Os systematics of the Lherz peridotites

Within this new framework, the relationships between refertilisation and the Os-isotope systematics of the Pyrenées massifs were investigated through the in-situ determination of the Re-Os composition of individual sulphide grains [25]. First, we sampled at the meter scale in the Lherz massif (Figure 1 RM, 10 samples, 103 sulphides, Table RM1). Then we extended our study to the regional scale by investigating "historical" samples - used to estimate the HSE and Os-isotope composition of the PUM[6,7,10]- from Lherz and other peridotite massifs in the Pyrenées (188 sulphides from 12 samples, Table RM1).

Whole-rock data show that these samples also display the Al_2O_3 - Pd/Ir -$^{187}Os/^{188}Os$ correlation, which is the backbone of the PUM estimate (Figure 2). The likelihood of metasomatic enrichment is indicated in the Pyrenées massifs by (1) the fact that the Pd/Ir *vs* Al_2O_3 correlation yields an extremely fractionated fertile mantle (Figure 2a) that is incompatible with the composition of the three main groups of chondrite[11]; (2) although partition coefficients for Pd and Ir are loosely constrained[35] a linear correlation between Pd/Ir and Al_2O_3 is not predicted by melt modeling [25,32]; (3) pyroxenites (probable melts) fall on the correlation lines defined by the peridotites (Figure 2b).

Harzburgites have low sulfur contents (S $\leq$50 ppm); each thin section contains 0 to 2 small sulphide grains ($\leq$50µm). In contrast,

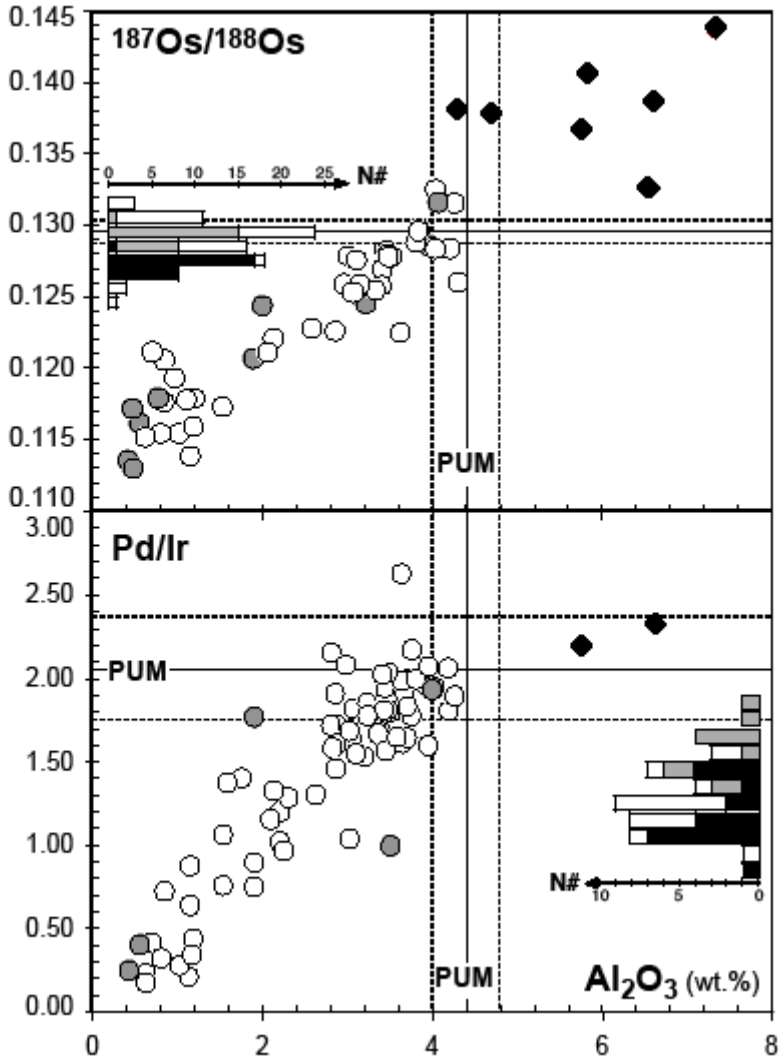

Fig. 2: Symbols as in figure 1; Histogram: black, carbonaceous chondrites; grey, ordinary chondrites; stippled, enstatite chondrites. Chondrite compositions after ref. [8,11]; PUM composition after ref. [6,7,10].

lherzolites have S contents up to ≈300 ppm and show ≥20 large (50-600 µm) sulphide grains per section. All sulphides are interstitial and show polyhedral shapes with inward-convex grain boundaries and low dihedral angles (≤60º). In contrast to the peridotite xenoliths hosted by alkali basalts and kimberlites, no primitive sulphide inclusions (spherical shapes, mono-sulphide solid solution composition[27,35]) in olivine have been found. All sulphides, irrespective of the peridotite type, consist of pentlandite (Pn: $(Fe,Ni)_8S_9$) and minor chalcopyrite (Cp: $CuFeS_2$). The abundance of Cu-rich phases (Cp ± bornite) is higher (up to 20%) in sulphide-rich samples. Thus the sulphides of the Pyrenées lherzolites are not typical of residual mantle; instead, they have a metal (Ni,Cu)-rich composition typical of sulphide melts produced by partial melting of mantle sulphides[35,36]. The abundance of sulphide (up to 415 ppm of S) and the proportion of pyrrhotite (Po: $Fe_{(1-x)}S$) increase in peridotite samples interlayed with websterite. Spinel-

websterites show abundant sulphides (300 <S ≤700 ppm) consisting of Pn, Po, Cp and Pyrite [41] . This spatial variation suggests a cogenetic relationship between sulphides in the lherzolites and websterites.

In-situ data show that the rare small sulphides in the harzburgites have unradiogenic Os-isotope compositions ($^{187}Os/^{188}Os$=0.1137±0.0012, weighed mean, n=21), usually low $^{187}Re/^{188}Os$ (<0.1) and high Os contents (≈30-250 ppm), in broad agreement with whole-rock data[42]. Such low $^{187}Os/^{188}Os$ indicates a long-term evolution in a low Re/Os (depleted) environment and yields some Re-depletion ages (T_{RD}) in excess of 2.5 Ga. In contrast the sulphides of the lherzolites have Os-isotope compositions that vary widely (0.109-0.173). There is also a large spread in $^{187}Re/^{188}Os$ from 0.001 up to values ≥1. Clearly Figure 3 shows that the whole-rock composition represents only an average of the compositional range observed in the sulphides. In fact, the sulphides from a single sample encompass the whole range of Re-Os composition reported for whole-rock samples from Lherz and the other Pyrennées massif peridotites (Figure 3). Several sulphide grains define a trend toward high Re/Os at ≈ constant $^{187}Os/^{188}Os$ (Figure 3). This indicates a recent Re contamination and agrees with previous observations about the mobility of Re and its effects on the whole-rock Re-Os systematics of the Pyrenées peridotite massifs[19]. The upper value of $^{187}Os/^{188}Os$ in sulphide is much more radiogenic than any realistic estimate for the primitive mantle. This simple observation precludes the possibility that the Os-sulphide systematics can reflect partial melting of a PUM-like protolith. On the contrary, the inverse correlation between Os and $^{187}Os/^{188}Os$ (Figure 3) indicates mixing between two end-members.

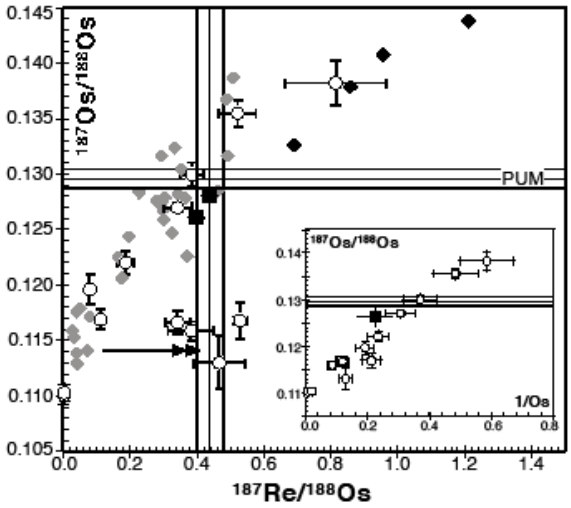

Fig. 3: $^{187}Os/^{188}Os$ *vs* $^{187}Re/^{188}Os$ in sulphides from a single sample and whole-rock samples of Pyrenées peridotites. Open circles: sulphides in a single sample (04LH06), error bars are 2SE; black diamonds, 04LH6 whole-rock composition; grey diamond, Pyrenées peridotites whole-rock compositions[10,18,19,42]. Grey squares are whole-rock spinel-websterites (unpublished data). Solid and dashed lines denote the PUM composition[6,7,10]. The Insert shows the same sulphides plotted in $^{187}Os/^{188}Os$-1/Os space. Such a linear correlation is symptomatic of a mixing trend. Note the agreement with the bulk-rock composition (estimated after Os and corrected S whole-rock content and using a pentlandite composition S=33 wt.%)

One end-member corresponds to a "relict" depleted component found in all peridotite samples irrespective of their

degree of fertility. Most lherzolite samples contain some sulphides with unradiogenic $^{187}Os/^{188}Os$ (< 0.115), low Re/Os and high Os contents, like those found in the harzburgites (Figure 4, RM table). This clearly indicates that all samples have undergone a major melting event during lower Proterozoic time (mean T_{RD}= 2.2±0.2 Ga). This observation strongly supports the hypothesis that the protolith of the Lherz massif consisted of deformed old harzburgites[14]. The second sulphide end-member shows extremely radiogenic Os ($^{187}Os/^{188}Os$>>0.15), high Re/Os and low Os contents (<5 ppm). The increase in sulphide abundance in the lherzolite at the contact with pyroxenite and the continuous trend in whole-rock composition between peridotites and pyroxenites (Figure 2) support a genetic link between the refertilising agent (i.e. the radiogenic end-member) and the interlayered spinel-websterites. Spinel websterites (unpublished data) yield a poorly constrained (MSWD 6.6) Re-Os isochron age of 1.35±0.12 Ga and an initial Os-isotope composition of 0.118±0.004. This age is similar to that of the spinel-websterites in the Beni Bousera massif (Morocco)[43] and for some pyroxenites in the Ronda massif (Spain)[44]. The initial Os-isotope composition of the spinel-websterites is within error of a MORB composition at that time, consistent with lithophile element abundances[14] and isotopic data[45].

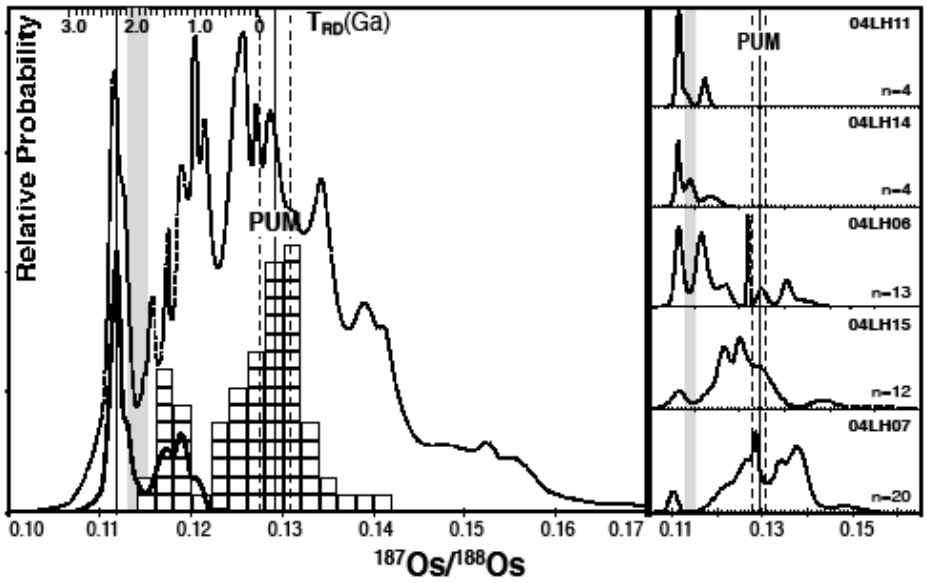

Fig. 4: Relative probability plot of $^{187}Os/^{188}Os$ in Pyrenées sulphides. Solid curve, sulphide $^{187}Os/^{188}Os$ composition in residual harzburgites (n=22, Table 1 repository material); dashed curve, sulphide $^{187}Os/^{188}Os$ for all Pyrenées lherzolites studied here (n=268; Table 1). Histogram of whole-rock compositions[10,18,19,42]. Right column shows the $^{187}Os/^{188}Os$ distribution in single whole-rock samples from the same outcrop, a few meters wide (Figure 1, repository material). Technical limitations inherent to the in-situ technique[25] mean that samples with high Re/Os ($^{187}Re/^{188}Os$>0.7) and/or low Os sulphides (<1ppm) suffer large errors, and the $^{187}Os/^{188}Os$ of sulphide having $^{187}Re/^{188}Os$ >1 cannot be determined. Consequently the sulphide population presented here is slightly biased toward sulphides with high Os contents and low Re/Os. Vertical solid and dashed lines denote the estimated $^{187}Os/^{188}Os$ composition and uncertainty (respectively) of a hypothetical Primitve Upper Mantle[6,7,10]; Shaded region indicates minimum $^{187}Os/^{188}Os$ deduced from whole-rock alumino-isochron [18,19].

Thus the whole-rock $^{187}Os/^{188}Os$ and Re/Os composition of the Pyrenées lherzolites do not reflect partial melting but simply the precipitation of sulphides having the high metal/sulphide ratio and fractionated HSE patterns [27,37] predicted by experimental work [35,36,46]. The only primitive feature preserved in these rocks is probably the relict melt-depletion age carried by the residual sulphide population both the harzburgites and the lherzolites.

Consequences for the "late veneer" and the composition of the upper mantle

The fertile nature of the lherzolites from the Lherz massif - the type locality - is thus not related to small degrees of melting but rather to the referilisation of a refractory ancient mantle lithosphere through the reactive percolation of a MORB-like melt. This event was accompanied by the precipitation of sulphide, which has profoundly modified the Os-isotope composition and HSE abundances of the Lherz mantle. Thus, the commonly-used indices of fertility (e.g. Al_2O_3), the HSE abundances (e.g. Pd/Ir, Re/Os) and the $^{187}Os/^{188}Os$ of the Pyrenées lherzolites are not pristine characteristics. The linear correlation between $^{187}Os/^{188}Os$ and Al_2O_3 must be considered as a mixing line between an injected mafic component ("mantle botox") and an old (Archean-Proterozoic) refractory mantle. The intersections of these trends with a "primitive" Al_2O_3 content therefore have no meaning in terms of the composition of the PUM.

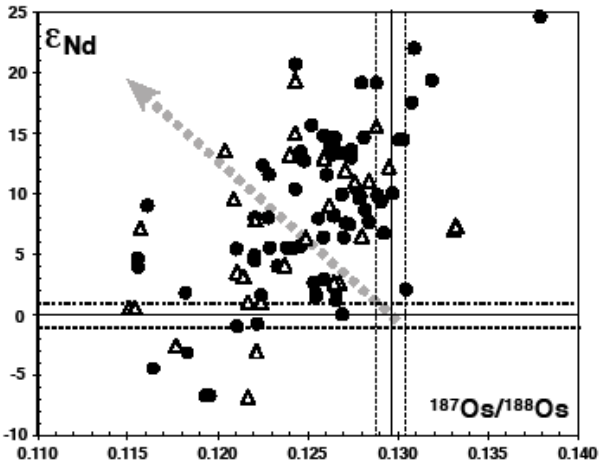

Fig. 5: Nd and Os isotopic composition for the non-Archean lithospheric mantle. Black circles, alkali-basalt hosted peridotite xenoliths; empty triangles, orogenic peridotite massifs, for data source see repository material; dashed grey line shows the expected composition of variably depleted mantle, i.e. old and depleted mantle should have $\varepsilon Nd >> 0$ and $^{187}Os/^{188}Os << 0.13$ depending on the age and extent of melting; conversely pristine undepleted mantle should have $\varepsilon Nd \approx 0$ and $^{187}Os/^{188}Os$ near the PUM composition[6] (i.e. ≈ 0.1296±0.0008). Solid and dotted thin lines denote PUM estimate [6] ($\varepsilon Nd_{PUM} \approx -0.1 \pm 1$).

However, the existence of linear $^{187}Os/^{188}Os$-Al_2O_3 trends and the intersection foci (0.127-0.131) of these trends on a worldwide basis at a fertile composition (Al_2O_3=4.2±0.2 wt.%) remains an important constraint on the large-scale, long-term evolution of the Proterozoic lithospheric mantle[6]. Data from the literature suggest that re-fertilisation processes described here are extremely common; they have been

described in several localities worldwide and from a variety of geodynamic settings: Orogenic peridotite massifs[26,32,33,47,48]; ophiolites[38,49], abyssal peridotite[24,32,34,42], sub-continental mantle xenoliths[23,31,33,50]. Furthermore, many mantle suites, including those used in estimates of the PUM composition [6,10] show the same “symptoms” as the Lherz and Pyrenées massifs. These include (1) behaviour of major- and minor elements inconsistent with melting models; (2) discrepancies between mineral composition, modes and whole-rock composition; (3) fractionated whole-rock HSE patterns inconsistent with any known chondrite group (e.g. Pd/Ir>2); (4) the co-existence at the thin section scale of several unrelated sulphide populations. However, the most convincing arguments stem from the discrepancies between $^{143}Nd/^{144}Nd$ and $^{187}Os/^{188}Os$. It has been recognised that even the most fertile peridotites that were used to estimate the PUM composition show Nd-isotope compositions indicative of old-melting events[6] (i.e. $\varepsilon Nd>>0$; Figure 5). Further work has shown that this observation is not an aberration, but is rather systematic; a broad inverse correlation between Nd and Os isotopes is found on a worldwide basis, similar to that observed in the Pyrenées peridotite massifs (Figure 5). Therefore, we conclude that a large proportion of the sub-continental lithospheric mantle has been refertilised, as suggested by the ubiquitous radiogenic Os composition of the "fertile" upper mantle. This suggests that a fundamental characteristic of the lithospheric mantle is its refertilised nature.

If the $^{187}Os/^{188}Os$-Al_2O_3 correlation, which is the backbone of the PUM estimate, is not due to partial melting then it cannot be used to calculate a primitive mantle composition for the Earth. Due to the complex history of melt extraction and percolation-reaction, which affect the abundances and isotopic composition of the siderophile elements, lithospheric peridotite samples cannot be used to derive a "primitive upper mantle" value that allows distinction between the various chondrite classes that potentially formed the “late veneer”. At best the $^{187}Os/^{188}Os$ and HSE systematics of the primitive upper mantle can be considered as broadly chondritic. The Os-isotope composition of the PUM thus does not rule out the carbonaceous chondrites as a major constituent of the late veneer, and can be reconciled with the D/H ratio of the Earth’ water. From mass-balance considerations, it is obvious that the late veneer had no effect on the O-isotope, Mg/Si or Al/Si composition of the Earth[2]. Therefore, there is no need for a yet unsampled type of chondrite to account for both the elemental[28] and isotopic composition of the HSE in the Earth mantle systematics and the D/H of seawater.

Acknowledgments

We thank N.J. Pearson, P. Wieland and S. Elhou for assistance with chemistry and mass spectrometry, C. Countenceau (the Gypaete barbue crew) and "Momo" for field assistance and S. Demouchy and A. Luguet for comments. Analytical data were obtained at GEMOC, using instrumentation funded by ARC LIEF, a DEST Systemic Infrastructure Grant, Macquarie University and industry. O.A. thanks the Royal Society and the Australian Research Council for financial support. This is publication XXX from the ARC National Key Centre for Geochemical Evolution and Metallogeny of Continents (GEMOC).

References

[1] Martin, H. *et al.*, *Earth, Moon, and Planets* **98**, 97-151 (2006).
[2] Drake, M. J. and Righter, K., *Nature* **416**, 39-43 (2002).
[3] Chou, C. L., presented at the Proc. Lunar Planet. Sci Conf 9th, 1978 (unpublished).
[4] Wänke, H., *Phil. Trans. R. Soc. Lond. A* **303**, 287-302 (1981).
[5] Smoliar, M. I., Walker, R. J., and Morgan, J. W., *Science* **271**, 1099-1102 (1996).
[6] Meisel, T., Walker, R. J., Irving, A. J., and Lorand, J.-P., *Geochim. Cosmochim. Acta* **65** (8), 1311-1323 (2001).
[7] Meisel, T., Walker, R. J., and Morgan, J. W., *Nature* **383** (10 October), 517-520 (1996).
[8] Walker, R. J. *et al.*, *Geochim. Cosmochim. Acta* **66** (23), 4187-4201 (2002).
[9] Robert, F., *Spc. Sci. Rev.* **106**, 87-101 (2003).
[10] Becker, H. *et al.*, *Geochim. Cosmochim. Acta* **70**, 4528-4550 (2006).
[11] Horan, M. F. *et al.*, *Chem. Geol.* **196** (1-4), 5-20 (2003).
[12] Bodinier, J.-L. and Godard, M., in *The mantle and the core*, edited by R. W. Carlson (Elsevier-Pergamon, Oxford (UK), 2003), Vol. 2, 103-170
[13] Niu, Y., Langmuir, C. H., and Kinzler, R. J., *Earth Planet. Sci. Lett.* **152**, 251-265 (1997).
[14] Le Roux, V. *et al.*, *Earth Planet. Sci. Lett.* **259**, 599-612 (2007).
[15] Ghiorso, M. S. and Sack, R. O., *Contrib. Min. Petrol.* **119**, 197-212. (1995).
[16] Langmuir, C. H., (198X).
[17] Palme, H. and O'Neill, H. S. C., in *The mantle and the core*, edited by R. W. Carlson (Elsevier-Pergamon, Oxford (UK), 2003), Vol. 2, 1-38
[18] Burnham, O. M. *et al.*, *Geochim. Cosmochim. Acta* **62** (13), 2293-2310 (1998).
[19] Reisberg, L. and Lorand, J.-P., *Nature* **376**, 159-162 (1995).
[20] Bodinier, J. L. *et al.*, *J. Petrol.* **45** (2), 299-320 (2004).
[21] Le Roux, V., Tommasi, A., and Vauchez, A., *Earth and Planetary Science Letters*, In press (2008).
[22] Brandon, A. D., Creaser, R. A., Shirey, S. B., and Carlson, R. W., *Science* **272** (10 May), 861-864 (1996).
[23] Alard, O. *et al.*, *Earth Planet. Sci. Lett.* **203** (2), 651-663 (2002).
[24] Alard, O. *et al.*, *Nature* **436**, 1005-1008 (2005).
[25] Pearson, N. J. *et al.*, *Geochim. Cosmochim. Acta* **66** (6), 1037-1050 (2002).
[26] Beyer, E. E., Griffin, W. L., and O'Reilly, S. Y., *J. Petrol.* **47**, 1611-1636 (2006).
[27] Alard, O. *et al.*, *Nature* **407**, 891-894 (2000).
[28] Andersen, T., Griffin, W. L., and O'Reilly, S. Y., *Lithos* **20**, 279-294. (1987).

[29] Gaetani, G. A. and Grove, T. L., *Earth Planet. Sci. Lett.* **169**, 147-163 (1999).
[30] Luguet, A. *et al.*, *Earth Planet. Sci. Lett.* **189** (3-4), 285-294 (2001).
[31] Lorand, J.-P. and Alard, O., *Geochim. Cosmochim. Acta* **65** (16), 2789-2806 (2001).
[32] Rehkämper, M. *et al.*, *Earth Planet. Sci. Lett.* **172**, 65-81 (1999).
[33] Pearson, D. G. *et al.*, *Chem. Geol.* **208** (1-4), 29-59 (2004).
[34] Brandon, A. D. *et al.*, *Earth Planet. Sci. Lett.* **177** (3-4), 319-335 (2000).
[35] Ballhaus, C. *et al.*, *Contrib. Min. Petrol.* **152**, 667-684. (2006).
[36] Bockrath, C., Ballhaus, C. G., and Holzheid, A., *Science* **305**, 1951-1953 (2004).
[37] Lorand, J.-P. *et al.*, *Chem. Geol.* **248**, 174-194. (2008).
[38] Luguet, A., Lorand, J.-P., Alard, O., and Cottin, J.-Y., *Chem. Geol.* **208**, 175-194 (2004).
[39] Burton, K. W., Schiano, P., Birck, J.-L., and Allegre, C. J., *Earth Planet. Sci. Lett.* **172** (3-4), 311 (1999).
[40] Meibom, A. *et al.*, *Nature* **410**, 705-708 (2002).
[41] Lorand, J. P., *J. Petrol.* **30**, 987-1015 (1989).
[42] Luguet, A., Horan, M. F., and Carlson, R. W., *Geochim. Cosmochim. Acta* **71**, 3082-3097 (2007).
[43] Pearson, D. G. and Nowell, G. M., *J. Petrol.* **45**, 439-455. (2004).
[44] Reisberg, L., Allègre, C.-J., and Luck, J.-M., *Earth Planet. Sci. Lett.* **105**, 196-213 (1991).
[45] Downes, H. *et al.*, *J. Petrol.* **Special Lherzolite Issue**, 97-115 (1991).
[46] Li, C. *et al.*, *Geochim. Cosmochim. Acta* **60** (7), 1231-1238 (1996).
[47] Piccardo, G. B., Zanetti, A., and Müntener, O., *Lithos* **94** (181-209), (2007).
[48] Saal, A. *et al.*, *J. Petrol.* **42**, 25-37. (2001).
[49] Rampone, E. *et al.*, *Min. Mag.* **58A**, 756-757 (1994).
[50] Lee, C.-T. A., *Geochim. Cosmochim. Acta* **66** (22), 3987-4005 (2002).

Mantle refertilisation Os isotopes and the “Primitive Upper Mantle” fallacy,…

Alard et *al*., 2008

REPOSITORY MATERIAL

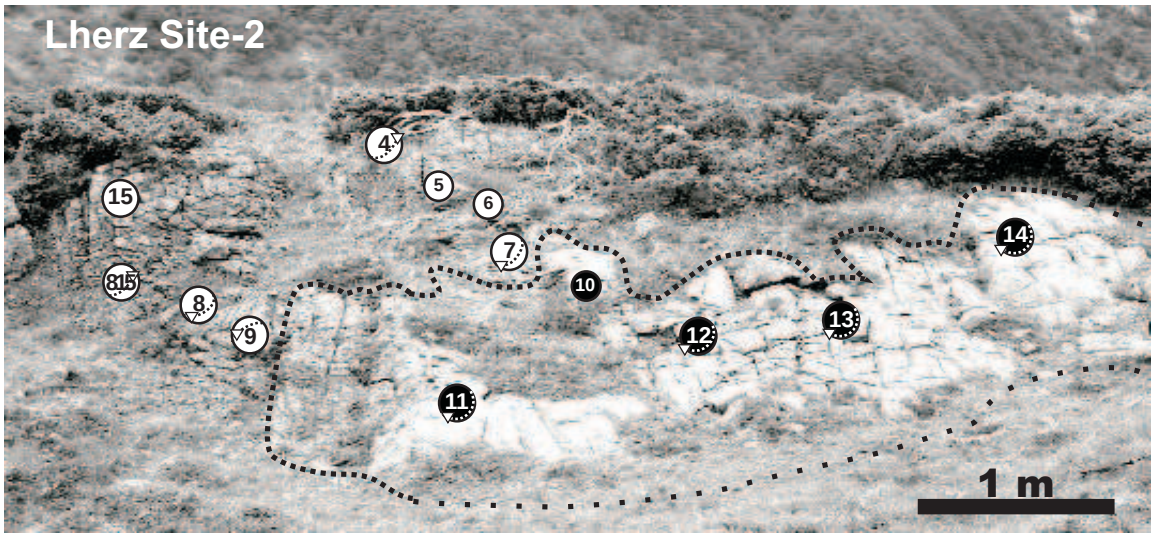

Figure RM1: Photo of the “site 2” outcrop in the Lherz Massif (Pyrennees, France). The dotted line denotes the contact between the harzburgite (black circles) and the lherzolite (white circles). The foliation for each sample is marked by the solid line and the lineation by the small triangle (projections in a geographic reference frame, top to North, lower hemisphere).

Table RM1 : *Alard et al., 2008*

Sample	N#Sulf	Os ppm	$^{187}Re/^{188}Os$	2SE	$^{187}Os/^{188}Os$	2SE	T_{RD} (Ga)	2□	T_{MA} (Ga)	2□
Lherz Site 2										
04LH11	A/s1	187,9	0,00022	0,00010	0,11130	0,00092	2,35	*0,03*	2,35	*0,02*
Al_2O_3=0.57 wt.%	B/s1	124,0	0,00028	0,00012	0,11134	0,00084	2,34	*0,03*	2,34	*0,02*
S=38.5 ppm	B/s2	41,3	0,00275	0,00051	0,1172	0,0013	1,53	*0,03*	1,54	*0,02*
n.Sulf/sectº=1.3	C/s1	131,3	0,0022	0,0011	0,1124	0,0024	2,19	*0,08*	2,21	*0,04*
(Pd/Ir)=0.40										
	WR	$5.14•10^{-3}$	0,0298	0,0015	0,11586	0,00011	1,72	*0,00*	1,85	*0,01*
04LH12	A/s1	34,6	0,2128	0,0024	0,1188	0,0018	1,31	*0,07*	2,61	*0,05*
Al_2O_3=0.48 wt.%	A/s2	74,2	0,00207	0,00015	0,1124	0,0014	2,19	*0,05*	2,20	*0,02*
S=36 ppm	A/s6	188,8	0,00054	0,00013	0,1100	0,0026	2,53	*0,10*	2,53	*0,05*
n.Sulf/sectº=8	**WR**	$4.82•10^{-3}$	0,0437	0,0022	0,11298	0,00008	2,12	*0,00*	2,36	*0,01*
04LH13	A/s1	29,9	0,0297	0,0017	0,1164	0,0015	1,65	*0,04*	1,77	*0,02*
Al_2O_3=0.47 wt.%	A/s5a	57,4	0,0335	0,0045	0,11290	0,00082	2,13	*0,03*	2,31	*0,03*
S=27 ppm	A/s5b	154,6	0,0093	0,0026	0,11208	0,00046	2,24	*0,02*	2,29	*0,02*
n.Sulf/sectº=6										
(Pd/Ir)=0.25										
	WR	$4.00•10^{-3}$	0,0422	0,0021	0,11385	0,00012	2,00	*0,00*	2,22	*0,01*
04LH14	A/s1	144,4	0,0310	0,0028	0,11124	0,00080	2,36	*0,03*	2,54	*0,02*
Al_2O_3=0.47 wt.%	A/s2	39,2	0,0546	0,0049	0,1141	0,0016	1,97	*0,06*	2,26	*0,04*
S=57 ppm	A/s3	29,5	0,3053	0,0041	0,1184	0,0036	1,37	*0,28*	4,83	*0,22*
n.Sulf/sectº=8	A/s8	69,6	0,109	0,010	0,1117	0,0022	2,30	*0,11*	3,07	*0,11*
	WR	$4.58•10^{-3}$	0,0819	0,0041	0,11622	0,00009	1,67	*0,00*	2,07	*0,02*
04LH09	A/s1	5,9	0,9203	0,0019	0,1574	0,0051	-4,33	*0,28*	3,42	*0,14*
Al_2O_3=1.9 wt.%	A/s2	5,8	0,8232	0,0011	0,1428	0,0044	-2,13	*0,15*	2,15	*0,08*
S= ppm	A/s3	9,8	0,433	0,053	0,1290	0,0018	-0,12	*0,12*	4,23	*18,83*
n.Sulf/sectº=10	A/s3[rep]	10,2	0,404	0,071	0,1289	0,0014	-0,11	*0,06*	-2,79	*11,54*
(Pd/Ir)=1.77	A/s4c	21,3	0,00210	0,00013	0,1365	0,0044	-1,20	*0,08*	-1,21	*0,04*
	A/s4a	9,6	0,831	0,002	0,1556	0,0030	-4,05	*0,18*	3,89	*0,09*
	A/s5	89,8	0,0419	0,0057	0,1206	0,0052	1,06	*0,10*	1,17	*0,05*
	A/s8	27,4	0,0035	0,0005	0,11270	0,00096	2,16	*0,03*	2,17	*0,02*
	A/s7	3,9	*1,20*	*0,13*	*0,169*	*0,017*	*-6,09*	*0,89*	*3,05*	*0,67*
	WR	$3.45•10^{-3}$	0,1770	0,0044	0,1207	0,00012	1,05	*0,00*	1,81	*0,03*
O4LH07	A/s1	6,8	0,307	0,074	0,1226	0,0070	0,78	*0,32*	2,84	*1,85*
Al_2O_3=2.00 wt.%	A/s2	8,8	0,0975	0,0060	0,1297	0,0052	-0,23	*0,03*	-0,30	*0,01*
S= 139 ppm	A/s3	10,8	0,0640	0,0058	0,1261	0,0026	0,29	*0,01*	0,34	*0,01*
Se=42.4 ppb	A/s4	4,2	0,89	0,17	0,1395	0,0056	-1,65	*0,13*	1,45	*0,53*
n.Sulf/sectº=	A/s5a	4,5	0,82	0,16	0,1319	0,0042	-0,55	*0,04*	0,57	*0,23*
	A/s5c	9,2	0,358	0,081	0,1285	0,0010	-0,06	*0,01*	-0,39	*0,50*
	A/s7	4,0	0,223	0,017	0,1268	0,0036	0,18	*0,02*	0,39	*0,04*
	A/s10	5,0	0,0542	0,0053	0,1350	0,0074	-0,99	*0,14*	-1,14	*0,07*
	A/s14	7,1	0,0361	0,0039	0,1239	0,0060	0,60	*0,06*	0,65	*0,03*
	A/s14[rep]	9,0	0,059	0,010	0,1222	0,0046	0,84	*0,07*	0,98	*0,04*
	A/s15a	1,5	*1,190*	*0,078*	*0,1488*	*0,0066*	*-3,02*	*0,17*	*1,59*	*0,18*
	A/s15a[rep]	2,0	*0,97*	*0,16*	*0,1397*	*0,0062*	*-1,68*	*0,12*	*1,26*	*0,37*
	A/s15b	3,1	0,295	0,048	0,1294	0,0068	-0,18	*0,07*	-0,60	*0,23*
	A/s17	19,6	0,745	0,095	0,1382	0,0024	-1,46	*0,07*	1,85	*0,54*
	A/s18	2,2	0,376	0,068	0,1375	0,0052	-1,36	*1,15*	-13,9	*20,78*
	A/s19	5,0	0,340	0,057	0,1337	0,0020	-0,81	*0,13*	-4,35	*3,08*
	A/s22a	7,8	0,0232	0,0013	0,1219	0,0058	0,87	*0,09*	0,93	*0,04*
	A/s22b	183,9	0,0112	0,0011	0,1102	0,0018	2,50	*0,07*	2,56	*0,04*
	A/s25	3,3	0,343	0,014	0,1349	0,0030	-0,97	*0,26*	-5,43	*0,98*
	A/s26	4,7	0,151	0,016	0,1368	0,0022	-1,25	*0,07*	-1,96	*0,12*
	A/s27a	26,8	0,700	0,065	0,1281	0,0036	0,00	*0,00*	0,00	*0,00*
	A/s27c	18,1	0,883	0,018	0,1374	0,0032	-1,34	*0,06*	1,19	*0,06*
	WR	$4.57•10^{-3}$	0,1237	0,0036	0,12435	0,00018	0,53	*0,00*	0,75	*0,01*
04LH15	A/s1	6,2	0,191	0,036	0,1290	0,0050	-0,12	*0,02*	-0,22	*0,04*
Al_2O_3=3.99 wt.%	A/s2	158,6	0,0023	0,0005	0,1115	0,0027	2,31	*0,10*	2,33	*0,05*
S= 203 ppm	A/s3	34,1	0,753	0,063	0,1109	0,0096	2,41	*0,50*	-3,20	*0,66*

n.Sulf/sect°=28	*A/s5a*	16,3	*0,099*	*0,012*	*0,1215*	*0,0022*	0,93	*0,04*	1,21	*0,05*
(Pd/Ir)=1.93	*A/s5b*	2,5	*1,08*	*0,15*	*0,153*	*0,014*	-3,64	*0,52*	2,20	*0,56*
	A/s6	6,7	0,256	0,030	0,1257	0,0024	0,34	*0,03*	0,87	*0,16*
	A/s7	2,0	0,589	0,072	0,1432	0,0053	-2,19	*0,44*	5,15	*2,21*
	A/s8	4,3	0,0602	0,0083	0,1281	0,0054	0,00	*0,00*	0,00	*0,00*
	A/s10	5,6	0,351	0,056	0,1318	0,0072	-0,53	*0,37*	-3,23	*2,58*
	A/s11	4,6	0,0722	0,0070	0,1250	0,0032	0,44	*0,03*	0,53	*0,02*
	A/s13	44,2	*1,05*	*0,22*	*0,1180*	*0,0032*	1,43	*0,05*	-0,97	*0,34*
	A/s14	5,2	0,0550	0,0013	0,1248	0,0017	0,47	*0,01*	0,54	*0,01*
	A/s15	5,8	0,179	0,027	0,1217	0,0026	0,90	*0,06*	1,57	*0,18*
	A/s16a	7,6	0,224	0,033	0,1210	0,0026	1,01	*0,09*	2,14	*0,36*
	A/s16b	4,3	0,147	0,010	0,1311	0,0044	-0,43	*0,05*	-0,66	*0,03*
	A/s16c	4,9	0,151	0,018	0,1237	0,0058	0,62	*0,09*	0,96	*0,08*
	A/s17a	3,9	0,166	0,015	0,1287	0,0040	-0,08	*0,01*	-0,13	*0,01*
	A/s18a	2,1	0,155	0,020	0,1297	0,0066	-0,23	*0,04*	-0,37	*0,03*
	A/s18b	8,5	0,235	0,022	0,1224	0,0056	0,80	*0,16*	1,80	*0,23*
	WR	$3.90 \cdot 10^{-3}$	0,4590	0,0069	0,12857	0,00014	-0,07	*0,00*	0,74	*0,13*
04LH815	A/s1	20,6	0,265	0,027	0,1227	0,0040	0,76	*0,13*	2,04	*0,36*
Al_2O_3=3.50 wt.%	A/s2a	16,3	0,573	0,084	0,1391	0,0024	-1,59	*0,16*	4,19	*2,31*
S= 188 ppm	A/s2b	9,4	0,386	0,041	0,1203	0,0050	1,10	*0,95*	11,99	*13,99*
n.Sulf/sect°=20	A/s2c	58,3	0,807	0,080	0,1115	0,0082	2,33	*0,35*	-2,64	*0,58*
	A/s3	11,3	0,279	0,037	0,1172	0,0036	1,54	*0,25*	4,44	*1,16*
	A/s4	47,1	0,482	0,061	0,1291	0,0022	-0,15	*0,04*	1,02	*1,01*
	A/s5a	10,4	0,64	0,10	0,1423	0,0028	-2,05	*0,17*	3,77	*1,73*
	A/s5b	4,1	*1,098*	*0,068*	*0,1477*	*0,0064*	*-2,86*	*0,18*	*1,71*	*0,19*
	A/s7	6,7	0,127	0,031	0,1316	0,0048	-0,50	*0,06*	-0,72	*0,08*
	A/s8	33,5	0,893	0,063	0,1117	0,0058	2,29	*0,20*	-2,12	*0,30*
	A/s10	13,9	0,18723	0,00085	0,1313	0,0012	-0,46	*0,02*	-0,83	*0,01*
	A/s12a	3,6	0,925	0,091	0,1426	0,0038	-2,10	*0,10*	1,70	*0,31*
	WR	$4.03 \cdot 10^{-3}$	0,447	0,012	0,12788	0,00012	0,03	*0,00*	-0,51	*0,23*
04LH06	A/s1	122,4	0,00251	0,00011	0,1116	0,0018	2,31	*0,07*	2,32	*0,03*
Al_2O_3=3.46 wt.%	A/s2	2,7	0,385	0,034	0,1300	0,0022	-0,27	*0,11*	-3,20	*3,04*
S= 185 ppm	A/s3	11,4	0,383	0,069	0,1159	0,0016	1,72	*0,43*	16,62	*29,92*
Se=63.5 ppb	A/s4	8,5	0,112	0,010	0,1169	0,0018	1,58	*0,06*	2,14	*0,07*
n.Sulf/sect°=18	A/s5	3,2	0,343	0,043	0,1270	0,0004	0,16	*0,01*	0,84	*0,46*
	A/s6	5,1	0,081	0,010	0,1196	0,0028	1,20	*0,07*	1,49	*0,05*
	A/s7	49,6	0,00469	0,00014	0,1113	0,0012	2,35	*0,05*	2,38	*0,02*
	A/s7[rep]	44,3	0,00362	0,00031	0,1116	0,0018	2,31	*0,07*	2,33	*0,03*
	A/s8a	4,2	0,188	0,025	0,1220	0,0022	0,86	*0,05*	1,54	*0,17*
	A/s8b	2,0	0,522	0,055	0,1355	0,0018	-1,06	*0,12*	4,24	*2,31*
	A/s9	7,6	0,468	0,075	0,1130	0,0048	2,12	*1,79*	-23,5	*37,73*
	A/s12	8,1	0,343	0,037	0,1166	0,0020	1,61	*0,26*	8,22	*3,89*
	A/s13	4,6	0,528	0,020	0,1168	0,0032	1,59	*0,34*	-6,70	*1,26*
	A/s16	1,7	*0,81*	*0,15*	*0,1382*	*0,0062*	-1,46	*0,15*	1,52	*0,59*
	WR	$3.28 \cdot 10^{-3}$	0,442	0,013	0,12830	0,00007	-0,03	*0,00*	0,55	*0,33*
	WR[rep]	$3.51 \cdot 10^{-3}$	0,398	0,012	0,12583	0,00011	0,32	*0,01*	5,70	*3,09*
		3,8					15,95			
O4LH04	*A/s2*	3,7	*1,063*	*0,220*	*0,166*	*0,026*	*-5,65*	*1,55*	*3,43*	*1,41*
Al_2O_3=3.22 wt.%	A/s3b	4,5	0,784	0,088	0,1482	0,0082	-2,94	*0,43*	3,23	*0,81*
S= 165 ppm	A/s4	9,7	0,38	0,11	0,1239	0,0028	0,59	*0,27*	6,02	*16,71*
n.Sulf/sect°=17	A/s5	16,3	0,186	0,018	0,1252	0,0032	0,41	*0,04*	0,73	*0,06*
	A/s5b	11,1	0,225	0,029	0,1301	0,0046	-0,28	*0,04*	-0,61	*0,09*
	A/s6	16,3	0,3884	0,0057	0,1344	0,0013	-0,91	*0,26*	-12,9	*2,25*
	A/s7	13,4	0,222	0,052	0,1319	0,0034	-0,54	*0,06*	-1,15	*0,30*
	A/s9	1,9	*1,29*	*0,21*	*0,167*	*0,030*	*-5,78*	*1,38*	*2,61*	*0,93*
	A/s10	6,6	0,611	0,023	0,1477	0,0032	-2,86	*0,30*	5,89	*0,73*
	A/s11	5,6	1,04	0,21	0,119	0,011	1,29	*0,16*	-0,89	*0,31*
	A/s12	13,3	0,264	0,020	0,1256	0,0056	0,36	*0,09*	0,96	*0,13*
	A/s15	107,1	0,1129	0,0011	0,1129	0,0011	2,13	*0,05*	2,90	*0,03*
	A/s17	24,8	0,398	0,079	0,1298	0,0014	-0,24	*0,10*	-4,57	*15,59*
	WR	$3.71 \cdot 10^{-3}$	0,3637	0,0055	0,12471	0,00020	0,48	*0,01*	3,45	*0,33*
Lherz 'Historic'										
71-323	A/s1	39,2	0,00233	0,00018	0,1207	0,0013	1,05	*0,02*	1,05	*0,01*
Al_2O_3=0.76 wt.%	A/s1[rep]	33,9	0,00136	0,00037	0,1183	0,0024	1,38	*0,05*	1,39	*0,03*
S= 22 ppm	A/s2	102,9	0,00036	0,00005	0,1117	0,0012	2,30	*0,04*	2,30	*0,02*
n.Sulf/sect°=3.5	A/s3	39,8	0,00039	0,00002	0,11898	0,00090	1,29	*0,02*	1,29	*0,01*

(Pd/Ir)=0,3 ‡	B/s2	251,2	0,041	0,010	0,11165	0,00078	2,30	*0,03*	2,54	*0,07*
	B/s2[rep]	208,8	0,0277	0,0093	0,11099	0,00090	2,39	*0,04*	2,56	*0,06*
	B/s3	32,1	0,12666	0,00086	0,1174	0,0030	1,51	*0,10*	2,15	*0,05*
	B/s4	131,6	0,0326	0,0068	0,11177	0,00054	2,28	*0,02*	2,47	*0,04*
	WR‡	2.8•10-3	0,03405	0,00085	0,11530	0,00080	1,80	*0,02*	1,95	*0,01*
82-4	A/sX	10,4	0,456	0,018	0,1200	0,0019	1,15	*0,48*	-16	*8*
Al_2O_3=1.14 wt.%	A/s1	3,7	0,201	0,044	0,1489	0,0046	-3,04	*0,44*	-5,98	*1,22*
S= 80 ppm	A/s2	3,1	0,600	0,026	0,1518	0,0080	-3,47	*0,96*	7,46	*1,19*
n.Sulf/sectº=10.3	A/s3	4,2	0,373	0,027	0,1385	0,0082	-1,50	*1,93*	-15	*8*
(Pd/Ir)=0,64 †	A/s4	10,5	0,0210	0,0007	0,1243	0,0013	0,54	*0,01*	0,57	*0,01*
(Pd/Ir)=0,87 ©	A/s4[rep]	9,5	0,558	0,033	0,1239	0,0062	0,60	*0,19*	-1,87	*0,46*
	A/s5	9,7	0,455	0,018	0,1202	0,0014	1,11	*0,36*	-15,95	*8,53*
	A/s7a	18,6	0,0969	0,0077	0,1182	0,0014	1,39	*0,04*	1,80	*0,05*
	A/s7b	69,7	0,1860	0,0044	0,1116	0,0012	2,31	*0,08*	4,08	*0,09*
	A/s7b[rep]	103,2	0,0085	0,0009	0,1088	0,0018	2,69	*0,08*	2,74	*0,04*
	A/s8a	36,5	0,0279	0,0050	0,1110	0,0026	2,39	*0,10*	2,56	*0,06*
	A/s8b	16,5	0,0448	0,0040	0,11513	0,00096	1,82	*0,03*	2,03	*0,03*
	A/s9	4,5	0,190	0,032	0,1277	0,0056	0,06	*0,01*	0,12	*0,02*
	A/s11a	9,6	0,125	0,020	0,1219	0,0020	0,88	*0,04*	1,25	*0,09*
	A/s11b	25,4	0,461	0,030	0,1159	0,0024	1,72	*0,83*	-22	*17*
	B/s1a	4,5	0,1169	0,0057	0,1382	0,0028	-1,46	*0,09*	-2,03	*0,06*
	B/s1b	37,5	0,0203	0,0027	0,1249	0,0014	0,45	*0,01*	0,47	*0,01*
	B/s5	31,9	0,2988	0,0045	0,1132	0,0017	2,09	*0,18*	6,92	*0,27*
	B/s6	27,4	0,0260	0,0002	0,11723	0,00074	1,53	*0,02*	1,63	*0,01*
	B/s7a	37,5	0,555	0,054	0,12686	0,00090	0,18	*0,01*	-0,56	*0,23*
	B/s7b	2,6	0,4040	0,0031	0,1483	0,0098	-2,95	*0,19*		
	B/s7c	4,9	0,184	0,012	0,1329	0,0044	-0,69	*0,09*	-1,23	*0,08*
	B/s8	4,1	0,0133	0,0013	0,1354	0,0076	-1,05	*0,13*	-1,09	*0,07*
	B/s8[rep]	5,9	0,1545	0,0039	0,1332	0,0024	-0,73	*0,04*	-1,16	*0,03*
	C/s1	17,8	0,1494	0,0069	0,12566	0,00082	0,35	*0,01*	0,54	*0,01*
	C/s2	4,9	0,1454	0,0087	0,1252	0,0022	0,41	*0,02*	0,62	*0,02*
	C/s3	6,6	0,1447	0,0022	0,1299	0,0020	-0,25	*0,01*	-0,39	*0,01*
	WR†	$4.72•10^{-3}$	0,075	0,0015	0,11410	0,00023	1,96	*0,01*	2,38	*0,01*
71-322	A/s1	8,2	0,0153	0,0012	0,1332	0,0046	-0,74	*0,06*	-0,76	*0,03*
Al_2O_3=1.5 wt.%	A/s2	14,4	0,627	0,026	0,1155	0,0058	1,77	*0,35*	-3,79	*0,51*
S= 56 ppm	A/s6	144,2	0,0019	0,0005	0,1124	0,0010	2,19	*0,04*	2,20	*0,02*
n.Sulf/sectº=8	A/s8	4,1	0,088	0,021	0,1550	0,0060	-3,96	*0,49*	-5,06	*0,40*
(Pd/Ir)=1,09 ©	A/s10	12,9	0,0519	0,0070	0,1274	0,0028	0,09	*0,00*	0,11	*0,00*
(Pd/Ir)=0,76 †	B/s2	145,4	0,0001	0,0000	0,11188	0,00044	2,27	*0,02*	2,27	*0,01*
	B/s3	3,1	0,70	0,22	0,173	0,013	-6,71	*1,96*	8,87	*7,05*
	B/s4	6,1	0,078	0,010	0,1435	0,0056	-2,23	*0,25*	-2,75	*0,15*
	B/s6	17,3	0,0095	0,0003	0,1246	0,0012	0,50	*0,01*	0,51	*0,00*
	WR*	$3.91•10^{-3}$	0,0671	0,0013	0,1173	0,00023	1,52	*0,01*	1,80	*0,01*
	WR†	$4.03•10^{-3}$	0,0544	0,0011	0,1235	0,00025	0,65	*0,00*	0,75	*0,00*
71-324	A/s1a	412,2	0,0098	0,0006	0,11109	0,00058	2,38	*0,02*	2,43	*0,01*
Al_2O_3=2.96 wt.%	A/s1b	291,0	0,0007	0,0000	0,11136	0,00078	2,34	*0,03*	2,34	*0,01*
S= 170 ppm	A/s3	184,9	0,0070	0,0011	0,1147	0,0011	1,88	*0,03*	1,91	*0,02*
n.Sulf/sectº= 24	A/s2	106,1	0,0117	0,0003	0,11901	0,00078	1,28	*0,02*	1,32	*0,01*
(Pd/Ir)=2,05 ®	A/s2[rep]	93,3	0,0155	0,0005	0,11853	0,00056	1,35	*0,01*	1,40	*0,01*
	A/s5	12,4	0,085	0,018	0,1360	0,0022	-1,14	*0,05*	-1,44	*0,08*
	A/s6a	16,6	0,0458	0,0014	0,12847	0,00098	-0,05	*0,00*	-0,06	*0,00*
	A/s6b	19,8	0,425	0,047	0,1275	0,0022	0,08	*0,28*	-8,16	*85,61*
	A/s8	12,8	0,524	0,022	0,1312	0,0012	-0,44	*0,03*	1,75	*0,38*
	A/s10	9,6	0,0812	0,0028	0,1413	0,0010	-1,91	*0,04*	-2,38	*0,03*
	A/s11	6,5	0,1856	0,0012	0,1526	0,0016	-3,60	*0,17*	-6,60	*0,09*
	A/s14	127,0	0,0110	0,0013	0,11895	0,00056	1,29	*0,01*	1,33	*0,01*
	WR*	$3.92•10^{-3}$	0,302	0,0060	0,12590	0,00025	0,31	*0,00*	1,10	*0,06*
71-326	A/s3	29,3	0,0878	0,0089	0,12575	0,00044	0,33	*0,00*	0,42	*0,01*
Al_2O_3=3.58 wt.%	A/s4	14,0	0,108	0,012	0,1346	0,0016	-0,94	*0,03*	-1,26	*0,05*
S= 170 ppm	A/s5	37,5	0,362	0,042	0,1273	0,0017	0,12	*0,02*	0,85	*0,60*
n.Sulf/sectº= 28	A/s6a	23,8	0,217	0,031	0,1294	0,0020	-0,19	*0,01*	-0,39	*0,06*
	A/s6b	5,9	0,0820	0,0066	0,1510	0,0034	-3,35	*0,23*	-4,19	*0,14*
	A/s7	14,7	0,00539	0,00032	0,1323	0,0020	-0,60	*0,02*	-0,60	*0,01*
	A/s10	8,3	0,354	0,065	0,1393	0,0032	-1,62	*0,56*	-11,0	*10,7*
	A/s11	5,5	0,1688	0,0071	0,1416	0,0048	-1,95	*0,25*	-3,29	*0,16*
	A/s12	21,2	0,254	0,026	0,12752	0,00090	0,08	*0,00*	0,21	*0,03*
	A/s13a	154,9	0,0121	0,0026	0,11146	0,00032	2,33	*0,01*	2,39	*0,02*
	A/s13b	7,5	0,4215	0,0026	0,1559	0,0036	-4,10	*13,85*	243	*1269*
	A/s13c	6,1	0,429	0,088	0,1313	0,0062	-0,46	*2,00*	20	*218*

	A/s14a	11,9	0,511	0,079	0,1251	0,0068	0,43	*0,22*	-2,05	*1,80*
	A/s14b	5,7	0,515	0,048	0,1349	0,0048	-0,98	*0,32*	4,23	*2,17*
	A/s15	6,5	0,0561	0,0031	0,1411	0,0030	-1,88	*0,10*	-2,17	*0,05*
	A/s16	5,7	0,0481	0,0047	0,1390	0,0022	-1,57	*0,06*	-1,77	*0,04*
	A/s17	7,3	0,438	0,027	0,1342	0,0026	-0,88	*0,76*	19	*30*
	A/s18	5,1	0,0286	0,0033	0,1382	0,0030	-1,46	*0,07*	-1,57	*0,04*
	A/s19	10,0	0,0727	0,0050	0,1288	0,0020	-0,10	*0,00*	-0,12	*0,00*
	A/s20	7,0	0,509	0,042	0,1327	0,0014	-0,66	*0,07*	3,05	*1,46*
72-442	A/s1	108,2	0,0364	0,0061	0,1190	0,0013	1,28	*0,03*	1,41	*0,03*
Al_2O_3=1.21 wt.%	A/s2	160,4	0,00441	0,00048	0,11756	0,00013	1,48	*0,00*	1,50	*0,00*
S= 23 ppm	A/s2[rep]	142,0	0,00396	0,00007	0,11729	0,00076	1,52	*0,02*	1,54	*0,01*
n.Sulf/sectº=2.5	A/s3	57,3	0,177	0,018	0,1270	0,0034	0,16	*0,01*	0,28	*0,02*
(Pd/Ir)=0.30 ‡	B/s1	397,9	0,0001	0,0000	0,11109	0,00030	2,38	*0,01*	2,38	*0,01*
(Pd/Ir)=0.29 ǂ	B/s2	125,1	0,0120	0,0032	0,1195	0,0014	1,21	*0,03*	1,25	*0,02*
(Pd/Ir)=0,44 ©	**WR***	$2.89 \cdot 10^{-3}$	0,058	0,0012	0,11780	0,00024	1,45	*0,01*	1,68	*0,01*
	WR‡	$2.79 \cdot 10^{-3}$	0,051	0,0010	0,11775	0,00004	1,46	*0,00*	1,66	*0,00*
	WR‡	$3.17 \cdot 10^{-3}$	0,045	0,0009	0,11810	0,00040	1,41	*0,01*	1,58	*0,01*
72-273	A/s1	10,4	0,0783	0,0034	0,1252	0,0016	0,41	*0,01*	0,50	*0,01*
Al_2O_3=3.11 wt.%	A/s2	14,2	0,498	0,097	0,1103	0,0072	2,49	*1,81*	-16	*20*
S= 185 ppm	A/s3	8,1	0,0617	0,0057	0,1261	0,0034	0,28	*0,02*	0,33	*0,01*
n.Sulf/sectº=14	A/s4	6,6	0,629	0,078	0,135	0,010	-0,99	*0,33*	1,95	*0,75*
	A/s5	154,5	0,0130	0,0025	0,1103	0,0022	2,49	*0,09*	2,57	*0,05*
	A/s6a	41,0	0,147	0,042	0,1150	0,0048	1,84	*0,21*	2,80	*0,44*
	A/s6b	23,8	0,0109	0,0017	0,1197	0,0050	1,18	*0,10*	1,21	*0,05*
Frechynede 'Historic'										
71-339	A/s1	7,9	0,080	0,015	0,1207	0,0019	1,05	*0,04*	1,30	*0,06*
Al_2O_3=3.41wt.%	A/s1[rep]	8,2	0,070	0,013	0,1213	0,0016	0,96	*0,03*	1,15	*0,04*
S= 244 ppm	A/s2	9,0	0,288	0,074	0,1251	0,0017	0,43	*0,04*	1,35	*0,75*
n.Sulf/sectº=36	A/s3	2,8	0,0143	0,0006	0,1211	0,0046	0,99	*0,07*	1,02	*0,04*
(Pd/Ir)=2,02 ©	A/s4	5,3	0,417	0,073	0,1274	0,0044	0,10	*0,68*	10	*181*
	A/s5	42,6	0,0683	0,0018	0,12028	0,00044	1,10	*0,01*	1,32	*0,01*
	A/s6	13,4	0,668	0,022	0,1193	0,0024	1,24	*0,08*	-2,17	*0,20*
	A/s18[nug]	90,8	0,0305	0,0066	0,12137	0,00048	0,95	*0,01*	1,03	*0,02*
	A/s18[all]	22,2	0,246	0,037	0,1214	0,0011	0,95	*0,04*	2,26	*0,48*
	A/s19	21,4	0,0368	0,0038	0,1215	0,0013	0,93	*0,02*	1,02	*0,01*
	A/s20	8,6	0,0680	0,0014	0,1204	0,0020	1,08	*0,04*	1,29	*0,02*
	A/s21a	4,3	0,591	0,098	0,1256	0,0064	0,36	*0,09*	-0,91	*0,53*
	A/s21b	4,1	0,44	0,11	0,1317	0,0060	-0,52	*0,99*	10	*59*
	A/s22a	11,1	0,1171	0,0019	0,1257	0,0016	0,34	*0,01*	0,46	*0,01*
	A/s22b	18,7	0,757	0,042	0,1197	0,0022	1,18	*0,05*	-1,52	*0,19*
	A/s22c	3,9	0,553	0,024	0,1286	0,0060	-0,07	*0,02*	0,22	*0,04*
	A/s23	2,0	0,177	0,039	0,132	0,010	-0,61	*0,17*	-1,05	*0,19*
	A/s24a	10,6	0,0466	0,0092	0,1267	0,0018	0,19	*0,01*	0,22	*0,01*
	A/s24b	120,2	0,0217	0,0068	0,1115	0,0020	2,32	*0,08*	2,44	*0,06*
	A/s24c	12,0	0,671	0,068	0,1154	0,0034	1,79	*0,17*	-3,13	*0,85*
	A/s25a	12,5	0,0488	0,0082	0,1255	0,0017	0,37	*0,01*	0,42	*0,01*
	A/s25b	4,3	0,539	0,061	0,1247	0,0072	0,49	*0,21*	-1,78	*0,93*
	A/s26	5,9	0,339	0,034	0,1137	0,0066	2,02	*1,02*	9,67	*4,02*
	A/s27	12,1	0,572	0,088	0,1130	0,0074	2,12	*0,75*	-6,31	*3,69*
	A/s28	4,8	0,152	0,012	0,1262	0,0056	0,27	*0,04*	0,42	*0,03*
	A/s30	2,7	0,852	0,090	0,1372	0,0112	-1,31	*0,23*	1,25	*0,29*
	WR*	$3.47 \cdot 10^{-3}$	0,2995	0,0060	0,12680	0,00025	0,19	*0,00*	0,64	*0,03*
71-336	A/s2	2,8	0,436	0,061	0,1329	0,0044	-0,69	*1,19*	17,02	*70,78*
Al_2O_3=3.45wt.%	A/s4	117,1	0,0046	0,0017	0,11269	0,00072	2,16	*0,02*	2,18	*0,02*
S= 179 ppm	A/s5a	1,9	0,566	0,080	0,1426	0,0065	-2,10	*0,59*	5,71	*3,17*
n.Sulf/sectº=24	A/s5a[rep]	1,7	0,512	0,028	0,1412	0,0031	-1,90	*0,39*	8,11	*2,51*
(Pd/Ir)=1,81 ®	A/s6	3,4	0,0123	0,0009	0,1207	0,0066	1,05	*0,11*	1,08	*0,06*
	A/s8	5,9	0,0374	0,0008	0,1230	0,0028	0,72	*0,04*	0,79	*0,02*
	A/s10	18,1	0,0200	0,0009	0,1242	0,0012	0,55	*0,01*	0,58	*0,01*
	A/s13	13,3	0,093	0,010	0,1252	0,0010	0,41	*0,01*	0,52	*0,02*
	A/s15	2,2	0,0297	0,0030	0,130	0,014	-0,33	*0,08*	-0,35	*0,04*
	A/s16	2,8	0,0997	0,0040	0,1241	0,0086	0,57	*0,10*	0,75	*0,05*
	A/s18	2,4	0,0734	0,0051	0,1218	0,0068	0,89	*0,12*	1,08	*0,06*
	A/s19	1,2	0,83	0,20	0,148	0,017	-2,96	*0,84*	2,89	*1,47*
	A/s23	1,4	1,59	0,25	0,1264	0,0260	0,24	*0,04*	-0,09	*0,03*
	A/s20	40,0	0,049	0,010	0,12032	0,00080	1,10	*0,02*	1,24	*0,03*
	A/s21	8,9	0,187	0,014	0,1249	0,0011	0,45	*0,01*	0,80	*0,05*

	WR*	$3.47 \cdot 10^{-3}$	0,228	0,005	0,1284	0,0003	-0,04	*0,00*	-0,09	*0,00*
71-335										
Al_2O_3=2.86 wt.%	A/s1	7,3	0,0410	0,0066	0,1270	0,0066	0,16	*0,02*	0,18	*0,01*
S= 312 ppm	A/s2	6,8	0,143	0,058	0,1271	0,0040	0,14	*0,01*	0,21	*0,04*
n.Sulf/sectº= 22	A/s3	5,2	0,550	0,091	0,1330	0,0070	-0,71	*0,25*	2,24	*1,58*
(Pd/Ir)=1,46 ©	A/s4	117,1	0,0046	0,0017	0,11147	0,00072	2,33	*0,03*	2,35	*0,02*
	A/s4[rep]	128,7	0,059	0,010	0,1113	0,0011	2,34	*0,05*	2,72	*0,08*
	A/s5	119,6	0,142	0,065	0,11565	0,00040	1,75	*0,02*	2,62	*0,61*
	A/s6	1,9	0,813	0,092	0,1459	0,0050	-2,60	*0,21*	2,67	*0,64*
	A/s7	21,9	0,355	0,015	0,1207	0,0030	1,04	*0,30*	6,39	*1,47*
	A/s8	3,2	0,726	0,078	0,1426	0,0042	-2,11	*0,19*	2,80	*0,72*
	A/s9a	.	0,383	0,056	0,1303	0,0026	-0,31	*0,14*	-3,49	*5,12*
	A/s9b	5,9	0,118	0,060	0,1241	0,0040	0,57	*0,05*	0,79	*0,16*
	A/s9c	9,1	0,004	0,000	0,1212	0,0024	0,98	*0,04*	0,99	*0,02*
	A/s10a	52,9	0,0093	0,0007	0,1124	0,0012	2,19	*0,04*	2,24	*0,02*
	A/s10b	35,6	0,040	0,006	0,1191	0,0024	1,27	*0,05*	1,40	*0,03*
	A/s11	29,7	0,0088	0,0034	0,12001	0,00098	1,14	*0,02*	1,17	*0,01*
	A/s15	49,9	0,517	0,030	0,1184	0,0024	1,37	*0,24*	-6,42	*2,01*
	WR*	$4.12 \cdot 10^{-3}$	0,270	0,005	0,1226	0,0002	0,78	*0,01*	2,15	*0,08*
72-425	A/ s0	8,4	0,0097	0,0008	0,1316	0,0042	-0,50	*0,03*	-0,51	*0,02*
Al_2O_3=3.63 wt.%	A/ s1	7,0	0,0857	0,0047	0,1356	0,0056	-1,08	*0,12*	-1,35	*0,06*
S= 389 ppm	A/ s2	7,1	0,140	0,014	0,1332	0,0024	-0,74	*0,04*	-1,11	*0,06*
n.Sulf/sectº= 39	A/ s3	4,9	0,342	0,018	0,1386	0,0042	-1,52	*0,57*	-8,52	*1,95*
	A/ s4	4,4	0,184	0,011	0,1410	0,0060	-1,86	*0,32*	-3,35	*0,22*
	A/ s5	413,4	0,0051	0,0012	0,11225	0,00072	2,22	*0,03*	2,25	*0,01*
	A/ s6	1,6	*1,235*	*0,094*	*0,1698*	*0,0240*	*-6,25*	*1,24*	*3,00*	*0,71*
	A/ s7	16,6	0,244	0,033	0,1288	0,0012	-0,10	*0,00*	-0,24	*0,04*
	A/ s8	3,0	0,0583	0,0010	0,147	0,011	-2,74	*0,58*	-3,19	*0,29*
	A/ s9	2,5	*1,56*	*0,14*	*0,137*	*0,017*	*-1,33*	*0,14*	*0,48*	*0,09*
	A/s10	1,9	0,768	0,083	0,1593	0,0086	-4,62	*0,72*	5,16	*1,28*
	A/s11	6,9	*1,44*	*0,23*	*0,1392*	*0,0026*	*-1,60*	*0,03*	*0,65*	*0,15*
	A/s14b	2,7	0,153	0,013	0,1545	0,0056	-3,88	*0,56*	-6,21	*0,41*
	A/s15	4,6	0,245	0,023	0,1488	0,0060	-3,03	*0,72*	-7,54	*1,05*
	A/s16	7,7	0,0309	0,0018	0,1336	0,0022	-0,79	*0,03*	-0,85	*0,02*
	A/s20	5,9	0,0883	0,0062	0,1407	0,0030	-1,83	*0,11*	-2,32	*0,07*
	A/s22	17,3	*1,09*	*0,13*	*0,1328*	*0,0042*	*-0,67*	*0,03*	*0,42*	*0,08*
	A/s24a	8,5	0,0435	0,0020	0,1312	0,0030	-0,44	*0,02*	-0,50	*0,01*
	A/s24b	27,7	0,0201	0,0038	0,1234	0,0019	0,67	*0,02*	0,70	*0,01*
	A/s25a	12,9	0,0998	0,0022	0,1284	0,0022	-0,05	*0,00*	-0,06	*0,00*
	A/s25b	6,9	0,1073	0,0070	0,1341	0,0030	-0,86	*0,05*	-1,15	*0,04*
	A/s26a	90,6	0,013	0,020	0,1131	0,0022	2,11	*0,08*	2,18	*0,11*
	A/s26b	10,2	0,577	0,018	0,1304	0,0020	-0,33	*0,03*	0,90	*0,10*
	A/s26c	14,4	0,677	0,020	0,1244	0,0024	0,53	*0,03*	-0,88	*0,07*
	A/s28	6,6	0,0532	0,0018	0,1345	0,0048	-0,92	*0,08*	-1,06	*0,04*
	WR*	$4.15 \cdot 10^{-3}$	0,168	0,003	0,1225	0,0002	0,79	*0,01*	1,31	*0,02*
Fontete Rouge *'historic'*										
FON-B-93	A/s1a	6,6	0,518	0,095	0,13703	0,00340	-1,29	*0,28*	5,27	*5,14*
Al_2O_3=3.23 wt.%	A/s1b	5,9	0,409	0,028	0,13921	0,00200	-1,60	*5,14*	-163	*385*
S= 277 ppm	A/s1c	10,7	0,349	0,019	0,13440	0,00164	-0,90	*0,14*	-5,53	*1,47*
n.Sulf/sectº= 16	A/s2a	15,2	0,677	0,028	0,13278	0,00280	-0,67	*0,05*	1,09	*0,12*
(Pd/Ir)=1,85 ®	A/s2b	8,1	0,211	0,013	0,13011	0,00280	-0,29	*0,03*	-0,58	*0,04*
(Pd/Ir)=1,78 @	A/s3a	3,3	0,814	0,028	0,15001	0,00640	-3,21	*0,33*	3,26	*0,29*
	A/s3a[rep]	4,5	0,876	0,017	0,15194	0,00780	-3,50	*0,39*	3,07	*0,22*
	A/s3c	7,1	0,397	0,023	0,13490	0,00194	-0,98	*0,61*	-20	*19*
	A/s4	7,3	0,429	0,023	0,13441	0,00142	-0,91	*0,75*	34	*92*
	A/s5	7,9	0,223	0,011	0,13413	0,00320	-0,87	*0,09*	-1,85	*0,11*
	A/s6	5,0	0,585	0,015	0,14149	0,00200	-1,94	*0,15*	4,71	*0,44*
	A/s8	20,1	0,125	0,029	0,12613	0,00220	0,28	*0,01*	0,40	*0,04*
	A/s9	68,1	0,013	0,004	0,12016	0,00054	1,12	*0,01*	1,16	*0,01*
	A/s10	38,9	0,684	0,041	0,12268	0,00220	0,77	*0,04*	-1,25	*0,20*
	A/s11	5,3	0,202	0,017	0,13493	0,00420	-0,98	*0,13*	-1,90	*0,16*
	A/s12	25,0	0,780	0,045	0,12773	0,00660	0,05	*0,01*	-0,06	*0,01*
	$WR^{(AL)}$	$4.4 \cdot 10^{-3}$	0,658	0,013	0,12841	0,0003	-0,04	*0,00*	0,08	*0,00*

Table RM1(caption):

Sample information: Al_2O_3 content (in W.t. %) and S content (in ppm) are from Bodinier (1989), Pattou et *al*., 1995, Lorand et al., 1999 Le Roux et al., 2007 (Ref-13); Pd/Ir from ®, Pattou et *al*., 1995; ©, Lorand et al., 1999; †, Becker et *al*., 2006 (Ref-10); ‡, Luguet et *al*., 2007 (Ref-42), @, Lorand et *al*., 2008 (Ref-37).

Whole rock (**WR**) Re-Os Composition; *, Reisberg & Lorand, 1995 (Ref-19); ‡, Luguet et al., 2007 (Ref-42); †, Becker et al., 2006 (Ref-10) and unpublished data from A. Luguet (^{AL}). Unless reported by the authors, 2SE (standard error) was set at 0.2% and 2% for $^{187}Os/^{188}Os$ and $^{187}Re/^{188}Os$ respectively.

Sulfide: N# Denotes the sulphide number in a given section; A,B, C are the thin section numbers; [rep] denotes replicate i.e. a second analysis of the same large sulphide grain (Ø>120 µm).

Os sulphide content*:* Note, that the method used, laser ablation MC-ICP-MS [25], only allows determination of mass ratio, and not Re and Os concentrations, as internal normalisation is not possible. Thus, Os concentrations (given in ppm) are estimates computed from Os voltage measured on sulphide and on the PGE-A standard bracketing the analyses. Average uncertainties using this method are at least about 20% when internal error on voltage measurements and external reproducibility for PGE-A are propagated through; other sources of uncertainties are: between-run variation of laser output energy, gas flow fluctuation, ...

Re-Os isotopic composition: SE, standard error of means, Data are processed in time-resolved mode as described in Pearson et *al*., (2002; Ref-25). We emphasize here that the correction for ^{187}Re overlap on ^{187}Os has been demonstrated to be reliable only for sulphide having $^{187}Re/^{188}Os \leq 1$ (Pearson et al., 2002; Ref-25), Therefore, ***data in italics*** (high Re/Os sulphides) are for information only. They are reported in order to show the reader that sulphide with high $^{187}Re/^{188}Os$ (>1) occur and because they show values broadly consistent with sulphides from the same sample having lower Re/Os ratio. Consequently the reader must be aware that our sampling is biased toward sulphides having Os content >1 ppm and low Re/Os.

Model ages: $\mathbf{T_{MA}}$ is the Re-Os model age and is defined as:

$$T_{MA} = \frac{1}{\lambda_{\mathrm{Re}}} \bullet \ln\left(1 + \frac{(^{187}Os/^{188}Os)_{Sulf} - (^{187}Os/^{188}Os)_{\mathrm{REF}}}{(^{187}Re/^{188}Os)_{Sulf} - (^{187}Re/^{188}Os)_{\mathrm{REF}}}\right) \quad (Eq.1),$$

where λ_{Re} is the ^{187}Re decay constant ($1.666 \bullet 10^{-11}$ a^{-1}; [5]; *Sulf*, Sulphide; REF denotes the reference model chosen (see below). T_{MA} relies on the assumption that there has been no disturbance of the Re/Os ratio. That is obviously not the case here (Re-addition; see text), since T_{MA} model ages for some sulphides are unrealistic, giving future ages or ages older than 4.5 Ga.

$\mathbf{T_{RD}}$, the Re depletion age, assumes that all Re has been removed from the residue ($(^{187}Re/^{188}Os)_{Sulf}=0$ in *Eq. 1*) and thus yields a minimum depletion age, but one that is more 'robust' to addition or removal of Re by recent secondary processes. Model ages are here calculated relative to the Enstatite (EC) Chondrite reference model, i.e. $(^{187}Os/^{188}Os)_{REF} = (^{187}Os/^{188}Os)_{EC}$ and $(^{187}Re/^{188}Os)_{REF} = (^{187}Re/^{188}Os)_{EC}$, with $(^{187}Os/^{188}Os)_{EC}=0.1281\pm0.0004$ and $(^{187}Re/^{188}Os)_{EC}=0.421\pm0.013$ [8]. An EC type composition for the primitive Earth' mantle has been arbitrarily chosen because its value is intermediate between the carbonaceous chondrite (CC) model [8] and the PUM model (Meisel et *al*., 2001; Ref-6) Uncertainties for T_{RD} and T_{MA} were calculated following Albarède's formulation [51], model uncertainties are not propagated through. Note that T_{RD} will be roughly younger or older by ~0.15 Ga if computed relative to CC (0.1275) or PUM (0.1296) Os isotopic composition, respectively.

RM-References

Bodinier J.L., 1989, Distribution des terres rares dans les massifs lherzolitiques de Lanzo et de l'Ariège, State Thesis, Université de Montpellier 2, Document et travaux du Centre Géologique et Géophysique de Montpellier, 22: 177 pp.

Albaréde, F., 1995. Introduction to Geochemical Modelling. Cambridge University Press, Cambridge, 543 pp.

Lorand, J.P., Pattou, L., Gros, M., 1999. Fractionation of platinum-group elements and gold in the upper mantle: a detailled study in the Pyrenean orogenic lherzolites, J.Petrol., 40:957-981.

Pattou, L., Lorand, J.P., Gros, M., 1996. Non-chondritic PGE ratios in the terrestrial upper mantle, Nature, 379: 712-715.

Table 1 - Crystallographic fabrics strengths of minerals

Sample	sample number in Le Roux et al. 2008a	distance to the contact (m)	Olivine [100]	Olivine [010]	Olivine [001]	number of measurements	Jindex olivine	Enstatite [100]	Enstatite [010]	Enstatite [001]	Jindex Opx	Diopside [100]	Diopside [010]	Diopside [001]
Harzburgites														
05LA16		1	**6,3**	5,2	3,1	183	5,6	-	-	-	-	-	-	-
04LH9	section 2	0,05	4,4	**5,1**	2,7	230	4	-	-	-	-	-	-	-
05LA4	section 1	0,05	**9**	5	3,5	233	8,6	-	-	-	-	-	-	-
05LA3	section 1	0,1	**6**	4	2,8	246	6,6	-	-	-	-	-	-	-
04LH11	section 2	1	**5,9**	4,3	2,4	208	4	-	-	-	-	-	-	-
04LH14	section 2	1,2	**8,5**	6,2	4,1	230	7,9	-	-	-	-	-	-	-
04LH12	section 2	1,5	**11,2**	5,8	3,7	207	8,7	-	-	-	-	-	-	-
04LH13	section 2	2	**10**	6,6	4,7	284	9,7	-	-	-	-	-	-	-
05LA2	section 1	4,5	**12**	4,5	4,1	262	10	-	-	-	-	-	-	-
05LA1	section 1	3,5	**10,7**	4,6	3,7	284	9,2	-	-	-	-	-	-	-
06LD6	5	20	**11,5**	5	4	637	9,2	5	5	5,5	3	10	24	10
06LD8	6	20,5	**14,5**	5	5	417	10,1	5,5	5,5	6,5	4,3	6	11	6
05LD1	3	21	**9,3**	5,1	5,1	276	8,7	-	-	-	-	-	-	-
05LD4	4	21,5	**8,8**	5,1	3,7	280	10	-	-	-	-	-	-	-
05LA9	section 1	1	**11**	4	3,8	263	8,5	-	-	-	-	-	-	-
06LE6		2	**11**	4	4	788	6,1	4,5	5	6	2,8	2	5,5	2,5
06LF27		4	**9,5**	4	4	671	5,5	3,7	3,5	4,9	3,2	5	9,3	7
06LF4		3	**10,5**	7	5	480	7	6	7	10	3,9	5	7,2	4,5
05LA12		0,1	**9,3**	4,3	4,4	98	9,2	-	-	-	-	-	-	-
average							7,8				3,44			
Lherzolites														
04LH8	section 2	0,1	3,2	**4,6**	3,3	200	3,6	-	-	-	-	-	-	-
04LH7	section 2	0,8	**5,3**	4,7	3	206	4,1	-	-	-	-	-	-	-
04LH815	section 2	0,5	3,4	**4,9**	3,4	240	4,6	-	-	-	-	-	-	-
05LA5	section 1	1,5	**4,4**	3,6	3,6	234	3,8	-	-	-	-	-	-	-
04LH4	section 2	1,5	2,8	**3,67**	3,24	227	4	-	-	-	-	-	-	-
05LA6	section 1	3	4,4	**7,6**	3,1	264	6	-	-	-	-	-	-	-
05LA8	section 1	5	5,7	**8,1**	3,5	268	7	-	-	-	-	-	-	-
05LA15		5	4,3	**5,4**	4	137	5,9	-	-	-	-	-	-	-
06LF3L		4	6	**8**	4,2	607	5,3	3,5	4,5	4,7	4	4,5	7,6	3
average							4,9							

Table 1 - continued

Sample	sample number in Le Roux et al. 2008a	distance to the contact (m)	Olivine [100]	Olivine [010]	Olivine [001]	number of measurements	Jindex olivine	Enstatite [100]	Enstatite [010]	Enstatite [001]	Jindex Opx	Diopside [100]	Diopside [010]	Diopside [001]
Distal lherzolites														
06LF26L	7	30	**6,3**	4	3	735	4,3	3,5	5,8	4,2	3,5	3	7,3	5,5
06LF9	8	50	3,5	**6**	3	762	3,4	6,5	8	7,5	3,8	2	6,5	4
06LF11	14	80	**4,3**	3,5	3	776	2,9	5,3	5,3	4	2,8	3	4,4	2,5
06LE5	11	150	5	**6,8**	2	587	4,4	4,9	3	4	3,4	2	5	4
06LF15	15	80	**4,2**	2,5	3	1010	3,2	3,5	4	5,8	2,8	2,2	4	2,5
06LF23	10	70	**4,5**	3,5	2,5	407	2,6	7,7	6	6,5	3,7	2,5	3,5	2,2
06LF16		80	**4,6**	3	4,6	668	2,4	8	10,8	8	4,7	2,8	4,8	2,8
06LF21W	9	60	2,8	**3,3**	2,2	716	1,75	5	6	5,2	2,3	2,8	3,9	2,8
06LF25		20	**4,3**	4	3	690	3	4,2	3	4,2	3,4	3	4,6	4
05LE1	13	150	**4**	3,6	4	226	4	-	-	-	-	-	-	-
05LE2		150	**4,3**	4,2	4	129	3,5	-	-	-	-	-	-	-
05L3	12	150	**7,8**	5,8	4,6	249	6,8	-	-	-	-	-	-	-
average							3,5				3,4			
Websterites														
06LF3W	16	10	3	8	4,5	143	3,6	11	12	13,5	8	4,5	7	5
06LF8	17	30	3,5	3,5	4,2	85	2,3	6	4	5	4,6	3,5	5,5	3
06LF26W	18	30	4	7	3,5	339	3,5	4,5	4	3,5	3,8	2,5	4,7	3,5
06LF17		100	3	3,5	3,5	64	2	8	9	10	8	3,5	5	4
06LF20		100	7	9,7	7	63	1,7	4	6	4	3,4	2,5	5	3,5
average							2,6				5,56			

Table 1: Crystallographic fabric strengths and J_{index} (in grey) of olivine and pyroxenes in harzburgites, lherzolites and websterites from the Lherz massif, presented according to their distance with the harzburgite-lherzolite contacts and obtained by EBSD-SEM system (Géosciences Montpellier). The fabric fiber is in bold. Manual indexing usually does not yield enough measurements for pyroxenes (which should be >100 to be representative). Thus, only the fabric strengths obtained by automatic indexing are shown. The sample numbering is the same as in chapter 4 (Le Roux et al., EPSL 2008). Samples with number > 18 are additional samples not shown in publication for space reason and presented in italics.

Figure 1 - Crystal-preferred orientations of minerals (CPO)

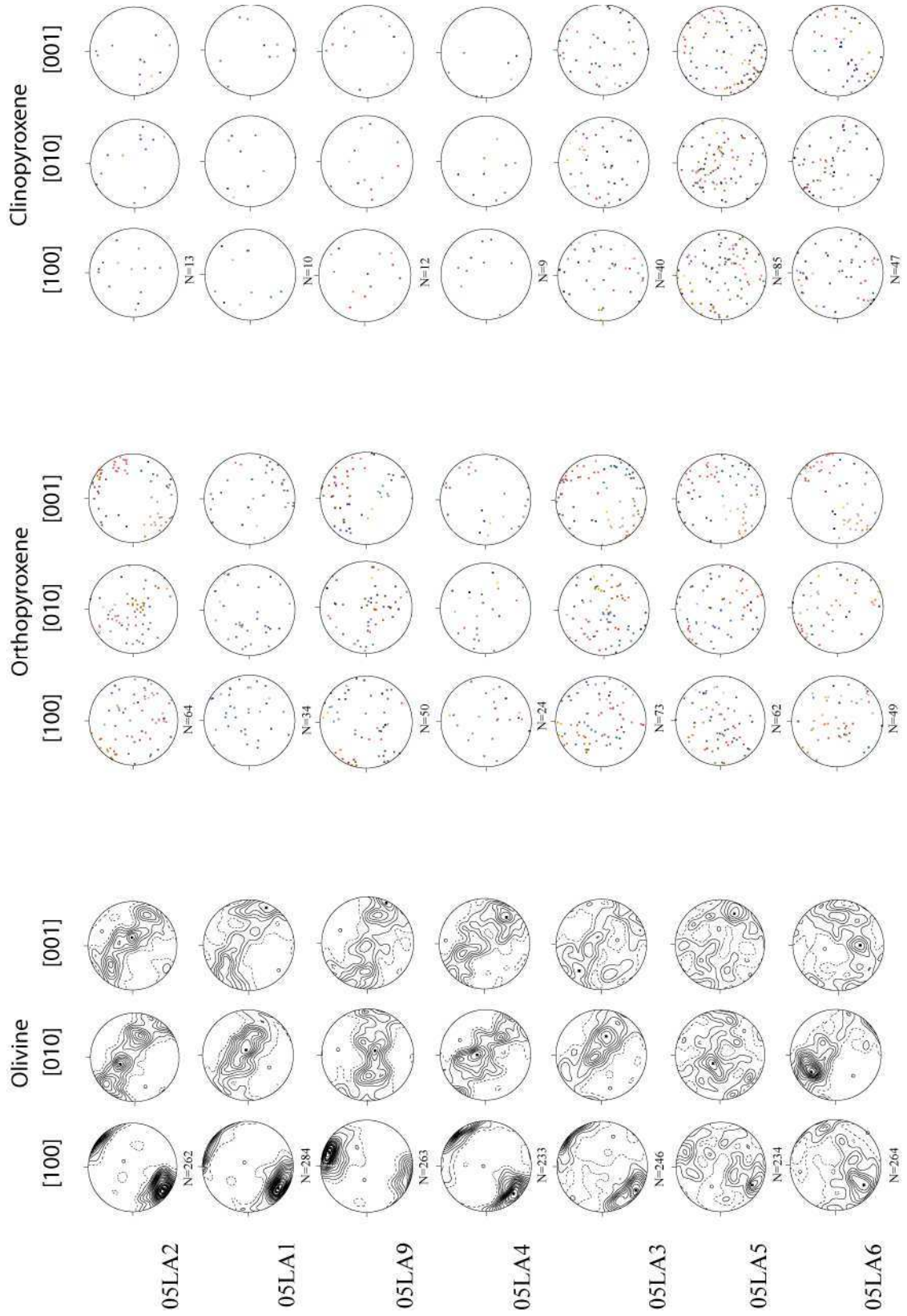

Figure 1 - continued

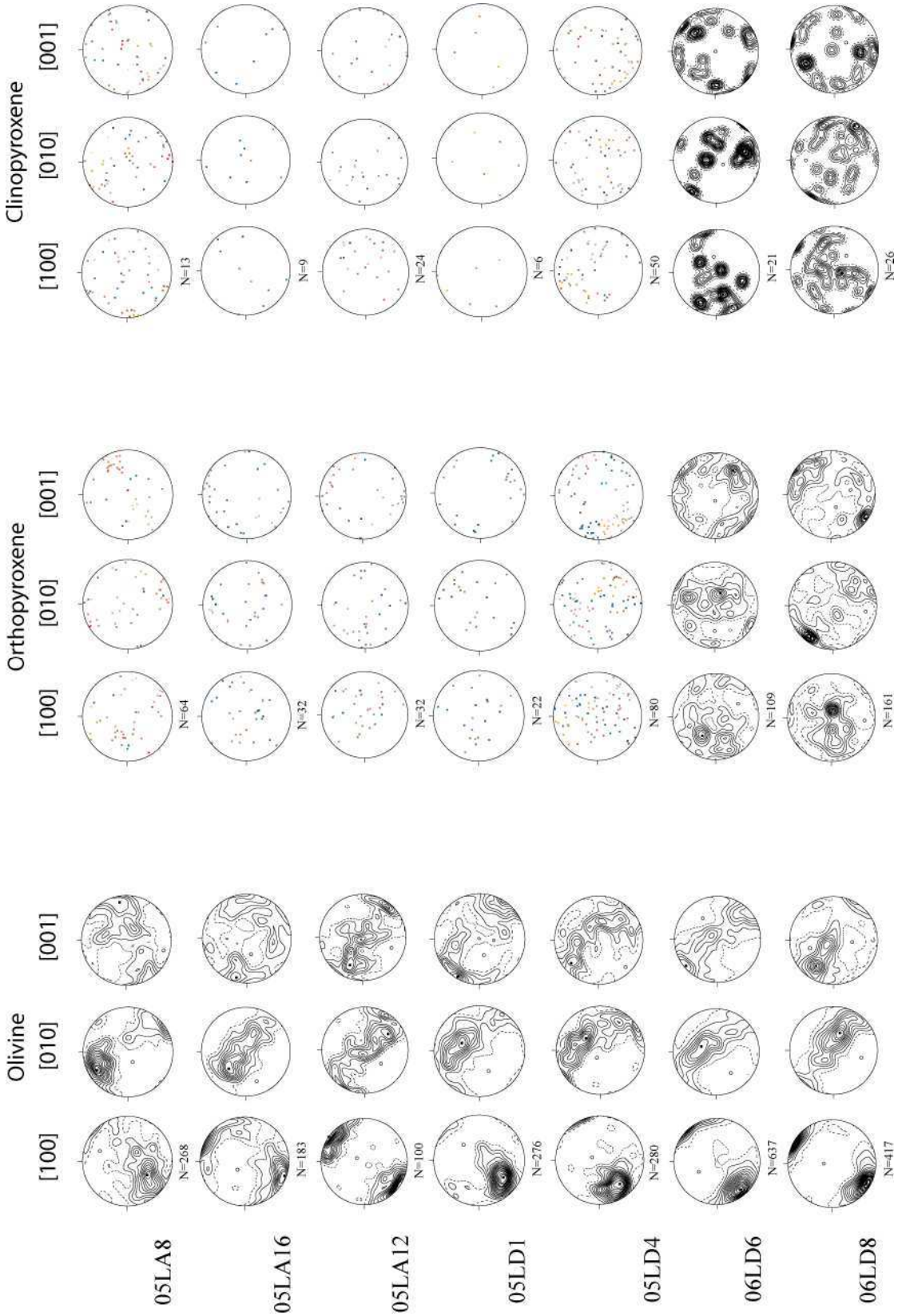

Figure 1 - continued

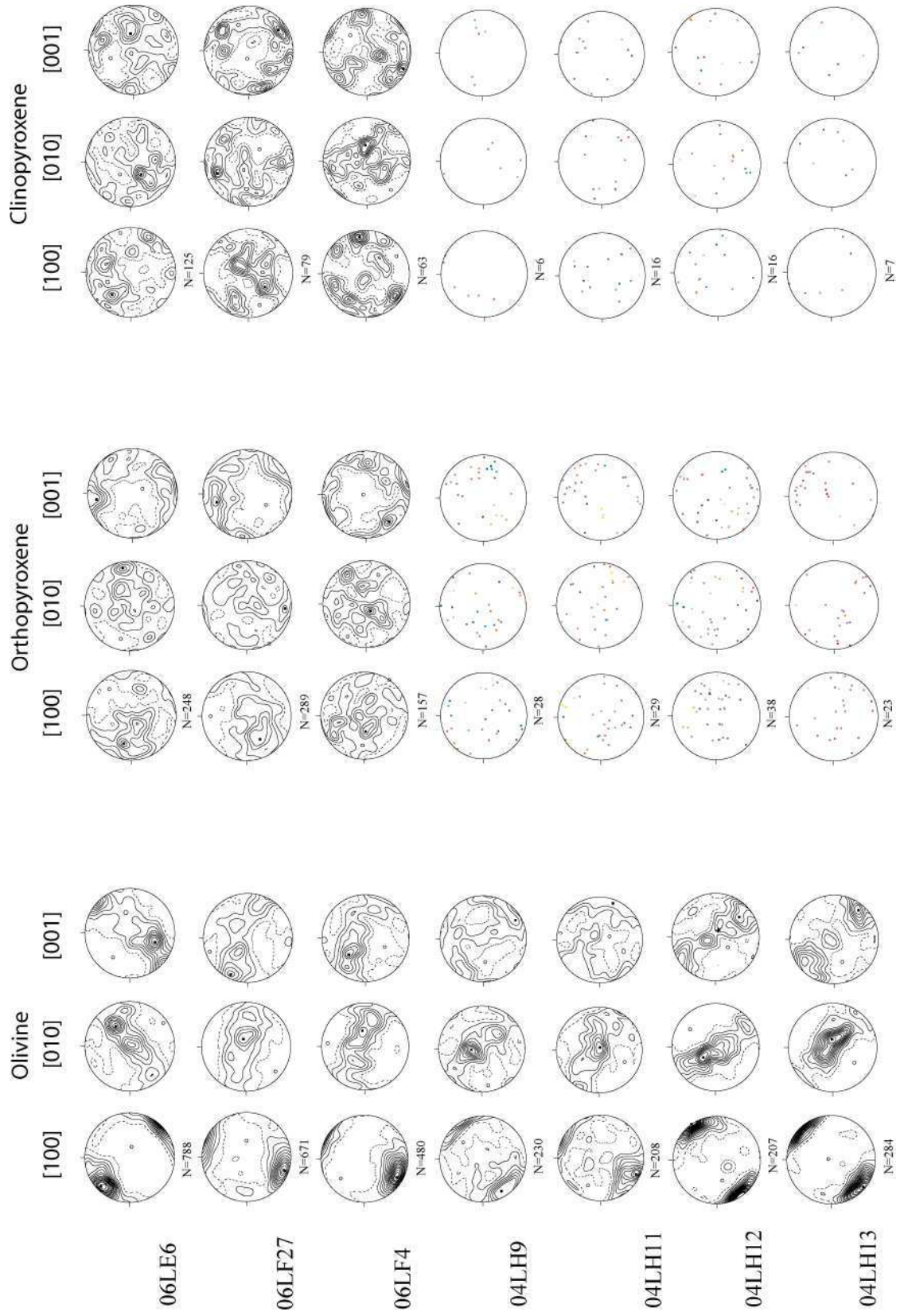

Figure 1 - continued

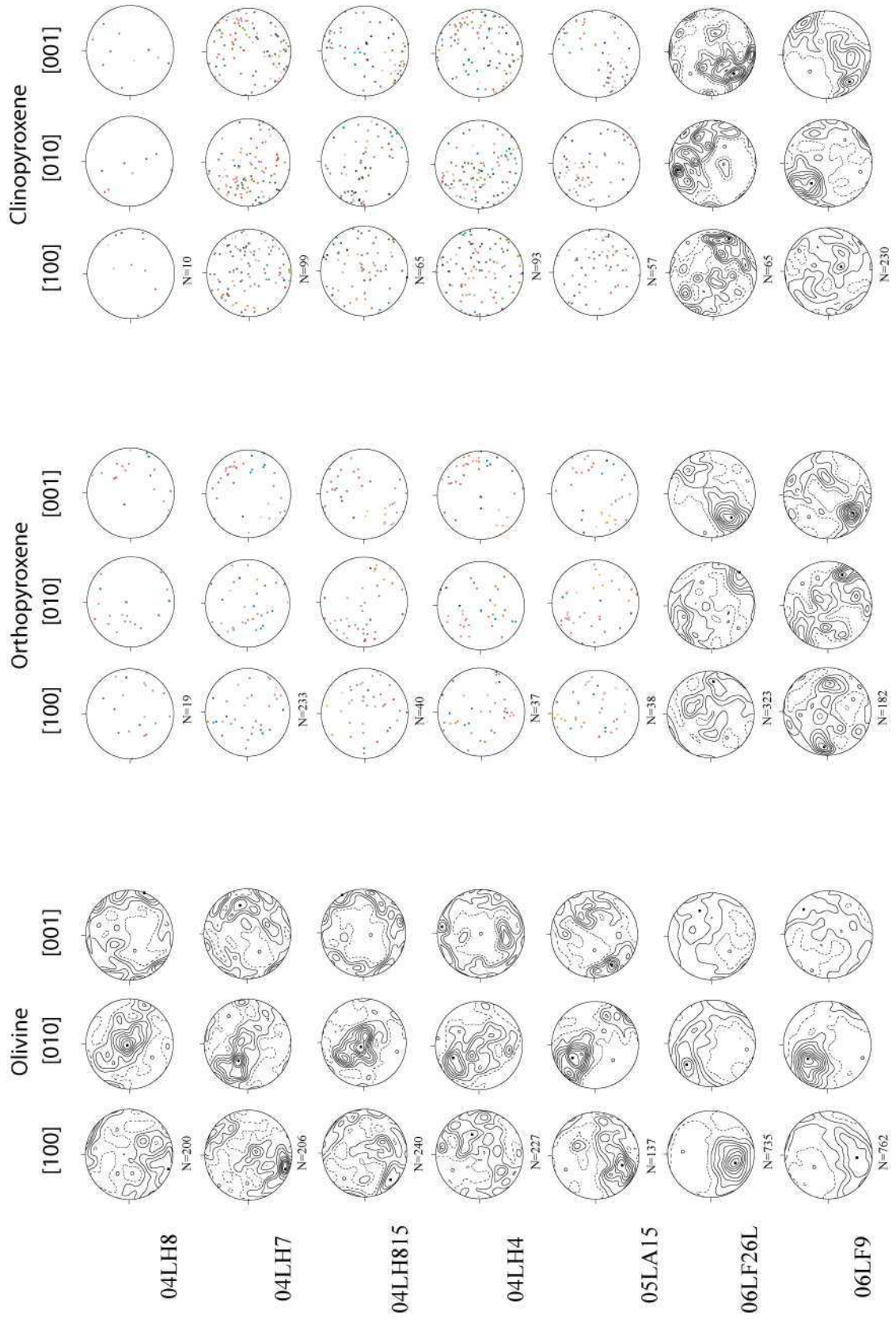

Figure 1 - continued

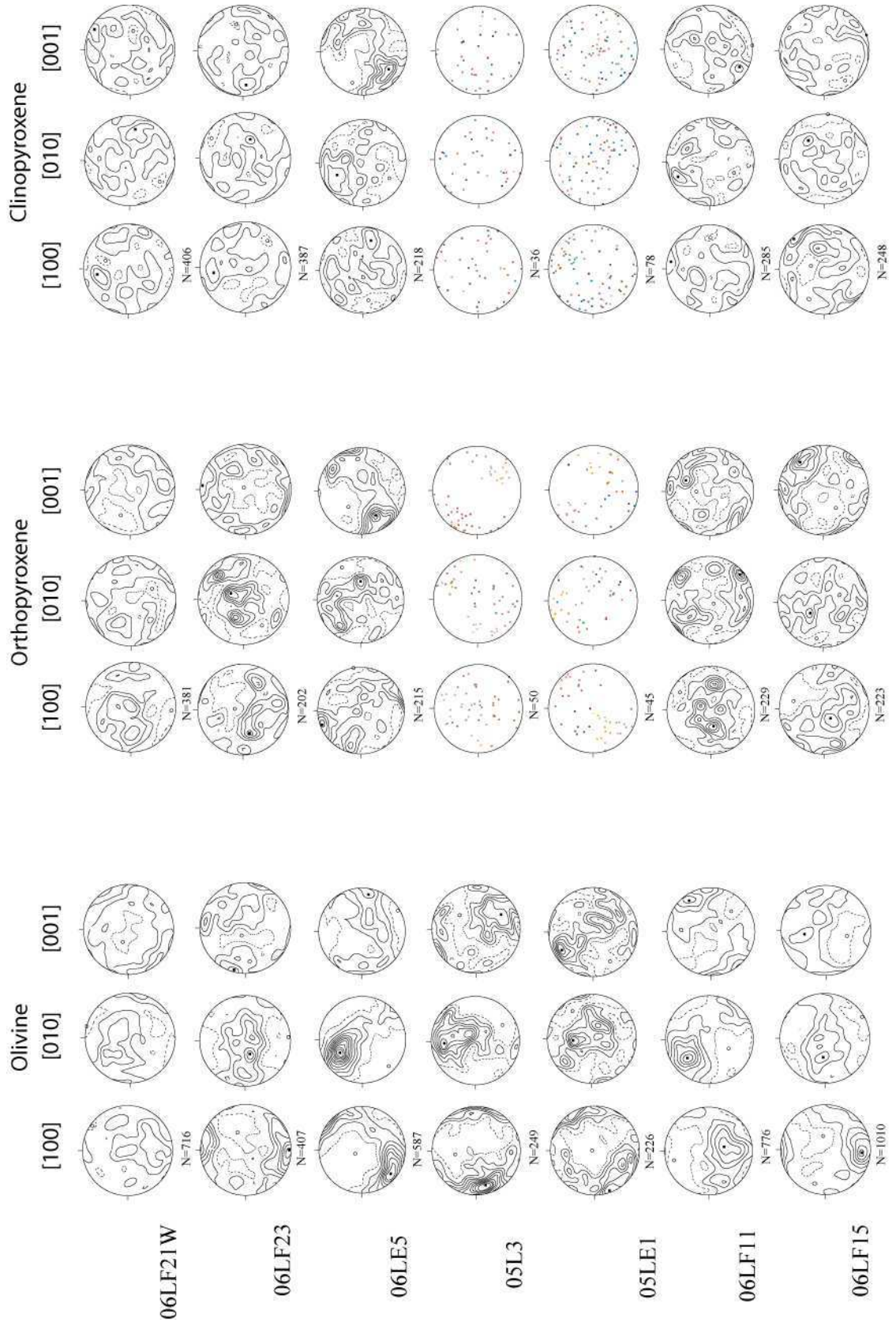

Figure 1 - continued

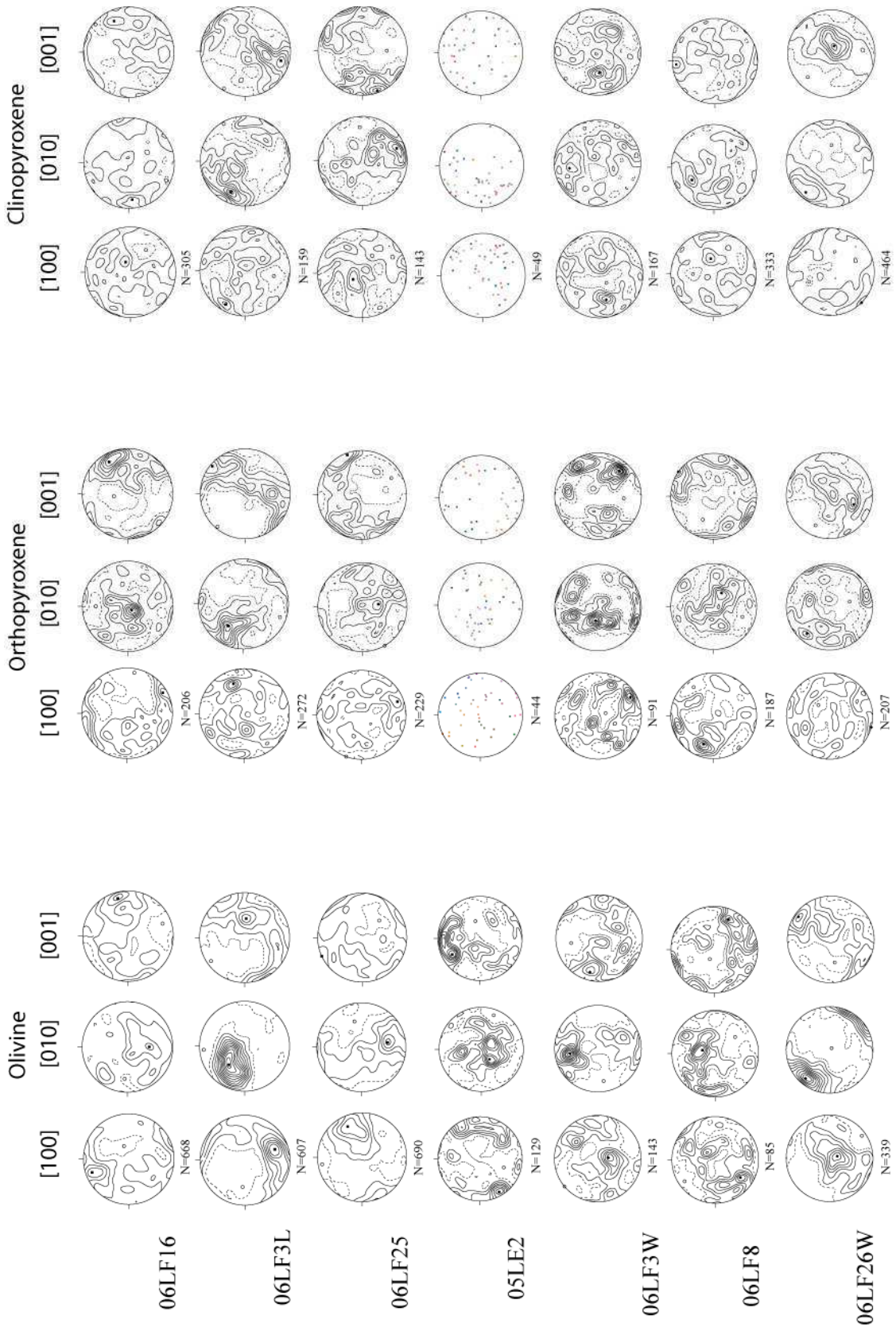

Figure 1 - continued

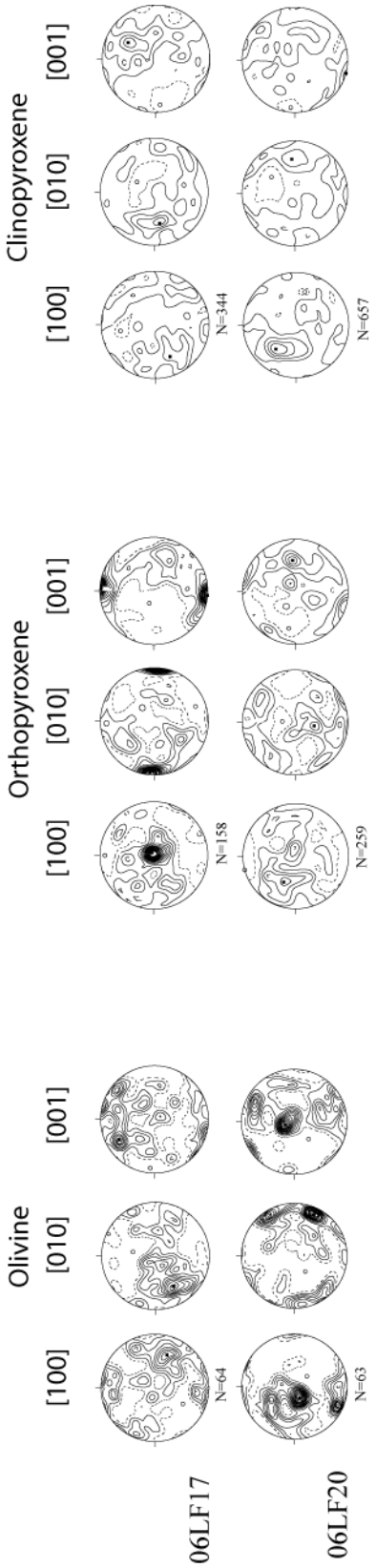

Figure 1 : Crystal-preferred orientations of olivine, orthopyroxene and clinopyroxene in harzburgites, lherzolites and websterites from the Lherz massif. Lower hemisphere equal area projections in the geographic reference frame (N at the top, E on the right). Contours at 0.5 of multiple of an uniform distribution intervals. 1 measurement per grain. N= Number of grains measured.

Table 2 - Major and minor elements compositions of minerals from Lherz peridotites

Sample	05LD1 (harz)				05LD4 (harz)				05LA2 (harz)				05LA1 (harz)				05LA16 (harz)			
distance from contact	>15m				>15m				4.5m				3.5m				1m			
	Ol	**Opx**	**Cpx**	**Spl**	**Ol**	**Opx**	**Cpx**	**Spl**	**Ol**	**Opx**	**Cpx**	**Spl**	**Ol**	**Opx**	**Cpx**	**Spl**	**Ol**	**Opx**	**Cpx**	**Spl**
SiO_2 (wt. %)	41,2	57,5	54,3	0,2	41,2	57,2	54,0	0,2	41,3	57,4	54,2	0,1	41,1	56,8	53,7	0,1	41,1	57,4	54,0	0,2
TiO_2	0,006	0,018	0,051	0,056	0,002	0,028	0,064	0,034	0,007	0,021	0,062	0,024	0,005	0,095	0,264	0,104	0,006	0,068	0,254	0,172
Al_2O_3	0,007	1,91	2,57	33,3	0,001	1,99	2,34	36,0	0,003	2,19	4,14	43,2	0,007	2,41	4,28	40,5	0,008	2,10	4,21	35,2
Cr_2O_3	0,006	0,398	1,01	35,1	0,002	0,366	0,824	31,8	0,000	0,331	1,48	25,7	0,011	0,378	1,43	28,5	0,004	0,416	1,79	33,5
FeO	8,78	5,77	1,95	17,41	8,69	5,75	1,86	17,41	8,77	5,80	1,93	14,63	8,69	5,81	1,94	14,95	9,02	5,94	1,97	17,45
MnO	0,125	0,135	0,084	0,257	0,128	0,140	0,055	0,219	0,126	0,153	0,087	0,194	0,131	0,140	0,073	0,190	0,128	0,153	0,082	0,254
MgO	49,7	33,8	16,3	13,7	49,6	33,7	16,4	13,7	48,7	34,0	15,1	16,2	48,0	33,9	15,2	15,9	49,4	33,9	14,7	13,8
CaO	0,020	0,419	23,0	0,006	0,017	0,446	23,3	0,011	0,012	0,350	21,3	0,002	0,011	0,382	21,0	0,004	0,013	0,415	20,6	0,005
Na_2O	0,004	0,021	0,854	0,000	0,003	0,022	0,685	0,013	0,008	0,032	1,75	0,000	0,006	0,035	1,71	0,000	0,004	0,046	2,14	0,007
NiO	0,425	0,070	0,037	0,104	0,436	0,072	0,042	0,105	0,430	0,082	0,038	0,164	0,431	0,097	0,031	0,158	0,416	0,078	0,038	0,116
Total	100,2	100,0	100,2	100,1	100,0	99,7	99,6	99,5	99,3	100,3	100,0	100,2	98,4	100,1	99,7	100,4	100,1	100,5	99,8	100,7
SiO_2 (wt. %)	*0,321*	*0,169*	*0,258*	*0,009*	*0,253*	*0,128*	*0,094*	*0,015*	*0,389*	*0,336*	*0,139*	*0,018*	*0,284*	*0,298*	*0,297*	*0,008*	*0,405*	*0,148*	*0,127*	*0,004*
TiO_2	*0,005*	*0,015*	*0,019*	*0,014*	*0,003*	*0,014*	*0,007*	*0,015*	*0,009*	*0,012*	*0,013*	*0,017*	*0,005*	*0,022*	*0,015*	*0,014*	*0,004*	*0,008*	*0,029*	*0,016*
Al_2O_3	*0,004*	*0,072*	*0,290*	*1,538*	*0,001*	*0,292*	*0,128*	*4,284*	*0,006*	*0,385*	*0,169*	*4,871*	*0,008*	*0,299*	*0,284*	*1,340*	*0,013*	*0,128*	*0,073*	*1,073*
Cr_2O_3	*0,005*	*0,014*	*0,196*	*1,734*	*0,002*	*0,089*	*0,142*	*4,289*	*0,000*	*0,118*	*0,083*	*5,078*	*0,011*	*0,122*	*0,266*	*1,215*	*0,004*	*0,036*	*0,139*	*0,864*
FeO	*0,083*	*0,004*	*0,038*	*0,444*	*0,086*	*0,062*	*0,021*	*0,984*	*0,091*	*0,029*	*0,037*	*0,935*	*0,099*	*0,080*	*0,088*	*0,647*	*0,108*	*0,070*	*0,087*	*0,325*
MnO	*0,016*	*0,011*	*0,018*	*0,013*	*0,009*	*0,005*	*0,009*	*0,027*	*0,013*	*0,012*	*0,009*	*0,030*	*0,008*	*0,004*	*0,010*	*0,011*	*0,005*	*0,015*	*0,008*	*0,022*
MgO	*0,602*	*0,063*	*0,166*	*0,323*	*0,639*	*0,299*	*0,162*	*0,965*	*0,439*	*0,338*	*0,236*	*1,004*	*1,160*	*0,307*	*0,266*	*0,406*	*0,360*	*0,052*	*0,289*	*0,390*
CaO	*0,005*	*0,027*	*0,207*	*0,004*	*0,004*	*0,059*	*0,143*	*0,000*	*0,003*	*0,054*	*0,169*	*0,001*	*0,006*	*0,050*	*0,293*	*0,005*	*0,005*	*0,014*	*0,086*	*0,002*
Na_2O	*0,005*	*0,001*	*0,047*	*0,000*	*0,003*	*0,012*	*0,059*	*0,001*	*0,004*	*0,028*	*0,076*	*0,000*	*0,006*	*0,008*	*0,102*	*0,000*	*0,003*	*0,007*	*0,134*	*0,010*
NiO	*0,003*	*0,004*	*0,010*	*0,009*	*0,004*	*0,016*	*0,010*	*0,004*	*0,005*	*0,014*	*0,006*	*0,020*	*0,003*	*0,019*	*0,012*	*0,015*	*0,004*	*0,012*	*0,015*	*0,013*
Total	*0,491*	*0,011*	*0,075*	*0,313*	*0,509*	*0,161*	*0,184*	*0,048*	*0,853*	*0,232*	*0,158*	*0,159*	*1,449*	*0,242*	*0,185*	*0,100*	*0,418*	*0,116*	*0,221*	*0,209*

Table 2 - continued

Sample	05LA9 (harz) 1m				05LA12 (harz) 10cm				05LA3 (harz) 10cm				05LA4 (harz) 5cm				05LA5 (lherz) 1.5m			
distance from contact																				
	Ol	**Opx**	**Cpx**	**Spl**	**Ol**	**Opx**	**Cpx**	**Spl**	**Ol**	**Opx**	**Cpx**	**Spl**	**Ol**	**Opx**	**Cpx**	**Spl**	**Ol**	**Opx**	**Cpx**	**Spl**
SiO_2 (wt. %)	41,3	56,7	53,7	0,1	41,1	57,1	53,7	0,2	41,4	57,3	53,8	0,1	41,2	57,3	53,5	0,1	41,0	56,4	52,6	0,1
TiO_2	0,003	0,014	0,050	0,018	0,014	0,080	0,314	0,103	0,004	0,070	0,274	0,129	0,003	0,074	0,298	0,113	0,011	0,132	0,630	0,052
Al_2O_3	0,006	2,81	3,37	42,7	0,005	2,44	4,88	40,8	0,004	2,35	4,83	36,8	0,003	1,99	5,06	42,7	0,010	3,75	7,45	61,3
Cr_2O_3	0,011	0,562	1,17	26,6	0,001	0,358	1,50	27,6	0,006	0,418	1,73	32,5	0,005	0,332	1,60	26,0	0,004	0,225	0,664	6,74
FeO	8,43	5,51	1,86	13,70	9,20	6,13	2,13	16,14	8,73	5,84	1,94	15,54	8,89	5,92	1,96	14,69	10,37	6,84	2,29	11,16
MnO	0,120	0,149	0,070	0,182	0,132	0,149	0,078	0,208	0,126	0,161	0,080	0,228	0,125	0,150	0,080	0,192	0,151	0,153	0,090	0,105
MgO	50,9	33,8	15,9	16,8	49,1	33,6	14,7	15,4	49,0	33,7	14,6	14,9	49,0	33,8	14,4	16,0	48,5	32,7	13,7	19,7
CaO	0,018	0,505	22,3	0,005	0,018	0,416	20,6	0,002	0,013	0,394	20,7	0,022	0,015	0,331	20,6	0,005	0,014	0,379	20,7	0,002
Na_2O	0,005	0,028	1,05	0,000	0,004	0,047	2,00	0,000	0,004	0,049	2,02	0,004	0,003	0,031	2,01	0,003	0,002	0,041	2,11	0,008
NiO	0,433	0,075	0,055	0,198	0,414	0,078	0,024	0,166	0,429	0,080	0,032	0,157	0,421	0,076	0,026	0,168	0,425	0,082	0,028	0,462
Total	101,2	100,1	99,5	100,4	100,0	100,3	100,0	100,5	99,7	100,4	100,1	100,4	99,6	100,0	99,6	100,0	100,4	100,7	100,3	99,6
SiO_2 (wt. %)	*0,248*	*0,073*	*0,196*	*0,012*	*0,227*	*0,579*	*0,151*	*0,004*	*0,457*	*0,178*	*0,145*	*0,017*	*0,337*	*0,417*	*0,255*	*0,015*	*0,329*	*0,270*	*0,300*	*0,005*
TiO_2	*0,003*	*0,010*	*0,014*	*0,008*	*0,010*	*0,009*	*0,031*	*0,019*	*0,006*	*0,018*	*0,018*	*0,006*	*0,007*	*0,012*	*0,024*	*0,016*	*0,009*	*0,013*	*0,019*	*0,024*
Al_2O_3	*0,009*	*0,049*	*0,190*	*3,284*	*0,005*	*0,636*	*0,349*	*0,882*	*0,005*	*0,275*	*0,086*	*1,145*	*0,003*	*0,467*	*0,186*	*1,928*	*0,015*	*0,361*	*0,110*	*0,215*
Cr_2O_3	*0,013*	*0,041*	*0,104*	*3,438*	*0,001*	*0,140*	*0,160*	*0,846*	*0,006*	*0,082*	*0,033*	*0,920*	*0,008*	*0,099*	*0,046*	*2,006*	*0,005*	*0,014*	*0,025*	*0,153*
FeO	*0,070*	*0,024*	*0,079*	*1,022*	*0,073*	*0,019*	*0,075*	*0,258*	*0,198*	*0,097*	*0,042*	*0,513*	*0,149*	*0,094*	*0,046*	*0,597*	*0,121*	*0,048*	*0,047*	*0,119*
MnO	*0,004*	*0,016*	*0,013*	*0,020*	*0,006*	*0,021*	*0,010*	*0,019*	*0,011*	*0,011*	*0,014*	*0,017*	*0,011*	*0,015*	*0,010*	*0,018*	*0,009*	*0,020*	*0,012*	*0,012*
MgO	*1,411*	*0,194*	*0,144*	*0,796*	*0,280*	*0,334*	*0,111*	*0,111*	*0,523*	*0,230*	*0,096*	*0,408*	*0,510*	*0,227*	*0,096*	*0,413*	*0,721*	*0,210*	*0,047*	*0,131*
CaO	*0,005*	*0,089*	*0,138*	*0,004*	*0,004*	*0,059*	*0,351*	*0,003*	*0,004*	*0,084*	*0,093*	*0,033*	*0,004*	*0,054*	*0,103*	*0,003*	*0,004*	*0,062*	*0,100*	*0,002*
Na_2O	*0,004*	*0,001*	*0,072*	*0,000*	*0,005*	*0,011*	*0,062*	*0,000*	*0,005*	*0,021*	*0,069*	*0,006*	*0,004*	*0,015*	*0,071*	*0,005*	*0,003*	*0,018*	*0,061*	*0,011*
NiO	*0,003*	*0,016*	*0,023*	*0,026*	*0,003*	*0,015*	*0,016*	*0,008*	*0,007*	*0,015*	*0,008*	*0,025*	*0,002*	*0,010*	*0,011*	*0,027*	*0,007*	*0,011*	*0,011*	*0,018*
Total	*1,231*	*0,156*	*0,233*	*0,378*	*0,376*	*0,064*	*0,175*	*0,210*	*0,754*	*0,183*	*0,207*	*0,196*	*0,512*	*0,115*	*0,304*	*0,247*	*0,500*	*0,196*	*0,278*	*0,083*

Table 2 - continued

Sample	05LA6 (lherz)					05LA8 (lherz)					05LA15 (lherz)					05L3 (lherz)					05LE3 (lherz)				
distance from contact	3m					5m					5m					150m					150,000				
	Ol	**Opx**	**Cpx**	**Spl**	**Ol**	**Opx**	**Cpx**	**Spl**	**Ol**	**Opx**	**Cpx**	**Spl**	**Ol**	**Opx**	**Cpx**	**Spl**	**Ol**	**Opx**	**Cpx**	**Spl**
SiO_2 (wt. %)	40,9	56,3	52,5	0,1	41,0	55,5	52,4	0,1	41,0	56,6	53,2	0,1	41,3	56,1	52,8	0,1	41,0	56,2	52,6	0,1
TiO_2	0,003	0,107	0,660	0,049	0,006	0,193	0,662	0,071	0,000	0,103	0,550	0,054	0,002	0,124	0,628	0,045	0,002	0,108	0,574	0,025
Al_2O_3	0,004	3,24	7,12	59,0	0,008	4,34	7,14	58,2	0,004	3,38	6,21	59,1	0,005	3,81	6,38	58,3	0,005	3,73	6,51	58,4
Cr_2O_3	0,015	0,215	0,785	8,70	0,007	0,325	0,791	9,45	0,001	0,214	0,602	9,12	0,004	0,293	0,807	9,66	0,003	0,268	0,745	9,58
FeO	10,65	6,86	2,37	12,20	10,70	6,68	2,32	12,45	10,09	6,70	2,25	11,67	10,20	6,65	2,28	11,79	9,85	6,38	2,26	12,00
MnO	0,147	0,153	0,080	0,109	0,150	0,163	0,082	0,121	0,145	0,146	0,070	0,106	0,148	0,156	0,086	0,112	0,141	0,151	0,088	0,116
MgO	48,7	32,6	13,8	19,0	48,7	31,3	13,7	18,7	48,3	33,0	14,4	19,1	47,3	32,2	13,8	18,6	49,0	32,7	14,1	19,0
CaO	0,013	0,318	20,3	0,003	0,016	1,324	20,3	0,006	0,014	0,360	21,0	0,002	0,011	0,311	21,1	0,000	0,016	0,355	21,0	0,003
Na_2O	0,008	0,028	2,12	0,000	0,006	0,217	2,18	0,000	0,004	0,029	1,94	0,012	0,003	0,041	2,06	0,000	0,005	0,051	2,04	0,000
NiO	0,408	0,063	0,040	0,361	0,408	0,086	0,037	0,364	0,420	0,070	0,039	0,379	0,375	0,049	0,035	0,364	0,422	0,085	0,035	0,381
Total	100,8	99,9	99,8	99,6	101,0	100,2	99,6	99,4	100,0	100,6	100,2	99,7	99,4	99,7	99,9	99,0	100,4	100,0	100,0	99,6
SiO_2 (wt. %)	*0,225*	*0,146*	*0,237*	*0,014*	*0,218*	*0,459*	*0,270*	*0,018*	*0,365*	*0,465*	*0,394*	*0,017*	*0,067*	*0,242*	*0,299*	*0,000*	*0,221*	*0,327*	*0,452*	*0,011*
TiO_2	*0,004*	*0,028*	*0,034*	*0,008*	*0,005*	*0,059*	*0,041*	*0,015*	*0,000*	*0,023*	*0,044*	*0,016*	*0,003*	*0,011*	*0,019*	*0,000*	*0,002*	*0,009*	*0,068*	*0,006*
Al_2O_3	*0,006*	*0,445*	*0,265*	*0,284*	*0,007*	*0,465*	*0,130*	*0,676*	*0,006*	*0,561*	*0,732*	*1,855*	*0,006*	*0,423*	*0,321*	*0,000*	*0,005*	*0,421*	*0,778*	*0,127*
Cr_2O_3	*0,009*	*0,048*	*0,026*	*0,389*	*0,009*	*0,058*	*0,030*	*0,747*	*0,002*	*0,039*	*0,118*	*1,934*	*0,007*	*0,020*	*0,078*	*0,000*	*0,003*	*0,085*	*0,141*	*0,112*
FeO	*0,082*	*0,118*	*0,081*	*0,090*	*0,063*	*0,137*	*0,165*	*0,179*	*0,113*	*0,049*	*0,057*	*0,444*	*0,112*	*0,015*	*0,064*	*0,000*	*0,118*	*0,096*	*0,050*	*0,104*
MnO	*0,007*	*0,015*	*0,005*	*0,020*	*0,011*	*0,017*	*0,011*	*0,004*	*0,010*	*0,013*	*0,018*	*0,009*	*0,012*	*0,003*	*0,006*	*0,000*	*0,007*	*0,013*	*0,009*	*0,012*
MgO	*1,032*	*0,110*	*0,236*	*0,101*	*1,136*	*0,685*	*0,151*	*0,193*	*0,454*	*0,357*	*0,365*	*0,370*	*0,304*	*0,295*	*0,197*	*0,000*	*0,772*	*0,189*	*0,385*	*0,060*
CaO	*0,005*	*0,009*	*0,330*	*0,003*	*0,004*	*0,666*	*0,185*	*0,003*	*0,004*	*0,043*	*0,361*	*0,002*	*0,003*	*0,018*	*0,149*	*0,000*	*0,006*	*0,005*	*0,264*	*0,003*
Na_2O	*0,007*	*0,013*	*0,052*	*0,000*	*0,007*	*0,121*	*0,151*	*0,000*	*0,004*	*0,007*	*0,164*	*0,008*	*0,004*	*0,005*	*0,089*	*0,000*	*0,009*	*0,017*	*0,155*	*0,000*
NiO	*0,008*	*0,014*	*0,017*	*0,012*	*0,004*	*0,010*	*0,008*	*0,029*	*0,007*	*0,006*	*0,012*	*0,041*	*0,029*	*0,007*	*0,012*	*0,000*	*0,005*	*0,017*	*0,017*	*0,016*
Total	*0,862*	*0,313*	*0,121*	*0,121*	*0,905*	*0,164*	*0,117*	*0,017*	*0,520*	*0,263*	*0,105*	*0,205*	*0,333*	*0,049*	*0,151*	*0,000*	*0,587*	*0,143*	*0,198*	*0,114*

Table 2 - continued

Sample	04LH13 (harz)					04LH12 (harz)					04LH14 (harz)					04LH11 (harz)					04LH08 (lherz)				
distance from contact	2m					1.5m					1.2m					1m					10cm				
	Ol	**Opx**	**Cpx**	**Spl**	**Ol**	**Opx**	**Cpx**	**Spl**	**Ol**	**Opx**	**Cpx**	**Spl**	**Ol**	**Opx**	**Cpx**	**Spl**	**Ol**	**Opx**	**Cpx**	**Spl**	**Ol**	**Opx**	**Cpx**	**Spl**
SiO_2 (wt. %)	41,0	57,1	54,1	0,1	40,5	57,0	53,9	0,1	40,5	57,2	54,4	0,2	40,6	56,5	54,1	0,1	40,8	56,6	51,7	0,1
TiO_2	0,007	0,021	0,078	0,081	0,004	0,039	0,099	0,107	0,010	0,059	0,154	0,126	0,005	0,044	0,203	0,125	0,008	0,107	0,772	0,083
Al_2O_3	0,002	1,65	3,34	26,1	0,003	2,14	3,87	29,7	0,003	2,17	3,88	30,8	0,006	2,01	4,23	33,4	0,005	1,90	5,99	46,4
Cr_2O_3	0,002	0,338	1,55	41,6	0,006	0,493	1,57	37,7	0,005	0,445	1,77	36,5	0,004	0,393	1,50	33,4	0,004	0,204	1,30	21,4
FeO	8,92	5,87	2,10	19,63	8,93	6,00	2,09	19,17	9,01	5,84	2,06	18,54	8,98	6,00	2,16	18,20	9,28	6,27	2,18	14,61
MnO	0,141	0,133	0,088	0,316	0,131	0,175	0,072	0,279	0,130	0,153	0,079	0,253	0,130	0,143	0,086	0,275	0,149	0,147	0,065	0,190
MgO	49,3	34,3	15,3	11,9	49,6	34,0	14,9	12,7	49,6	34,0	14,9	12,9	49,6	34,1	14,8	13,5	49,0	34,0	14,4	16,5
CaO	0,014	0,352	21,4	0,005	0,012	0,407	21,0	0,004	0,012	0,331	20,9	0,003	0,010	0,374	21,0	0,002	0,022	0,282	21,1	0,002
Na_2O	0,011	0,043	1,90	0,001	0,002	0,047	2,14	0,011	0,008	0,035	2,19	0,008	0,004	0,040	2,08	0,004	0,003	0,023	1,97	0,000
NiO	0,432	0,073	0,033	0,074	0,428	0,069	0,075	0,097	0,425	0,087	0,033	0,098	0,428	0,088	0,039	0,111	0,434	0,074	0,044	0,227
Total	99,8	99,9	99,8	99,8	99.7	100,2	99,9	99,9	99,6	100,3	100,4	99,3	99,7	99,7	100,2	99,1	99,7	99,7	99,6	99,5
SiO_2 (wt. %)	*0,372*	*0,513*	*0,421*	*0,021*	*0,462*	*0,111*	*0,383*	*0,021*	*0,677*	*0,243*	*0,337*	*0,050*	*0,273*	*0,373*	*0,071*	*0,006*	*0,295*	*0,653*	*0,448*	*0,005*
TiO_2	*0,009*	*0,011*	*0,010*	*0,018*	*0,004*	*0,010*	*0,013*	*0,019*	*0,009*	*0,013*	*0,035*	*0,010*	*0,005*	*0,012*	*0,017*	*0,006*	*0,010*	*0,033*	*0,095*	*0,006*
Al_2O_3	*0,002*	*0,147*	*0,167*	*2,223*	*0,005*	*0,077*	*0,035*	*0,898*	*0,005*	*0,115*	*0,066*	*0,614*	*0,008*	*0,329*	*0,320*	*0,421*	*0,011*	*0,499*	*0,081*	*1,136*
Cr_2O_3	*0,002*	*0,049*	*0,205*	*2,027*	*0,005*	*0,025*	*0,016*	*0,892*	*0,009*	*0,041*	*0,156*	*0,380*	*0,006*	*0,094*	*0,390*	*0,235*	*0,006*	*0,097*	*0,118*	*1,302*
FeO	*0,183*	*0,138*	*0,104*	*0,733*	*0,139*	*0,023*	*0,005*	*0,680*	*0,048*	*0,055*	*0,081*	*0,477*	*0,072*	*0,148*	*0,045*	*0,530*	*0,151*	*0,120*	*0,111*	*0,278*
MnO	*0,013*	*0,025*	*0,019*	*0,021*	*0,012*	*0,008*	*0,024*	*0,019*	*0,005*	*0,019*	*0,011*	*0,011*	*0,012*	*0,024*	*0,018*	*0,012*	*0,024*	*0,022*	*0,007*	*0,018*
MgO	*0,267*	*0,164*	*0,175*	*0,512*	*0,380*	*0,079*	*0,097*	*0,272*	*0,506*	*0,113*	*0,220*	*0,240*	*0,377*	*0,361*	*0,127*	*0,344*	*0,177*	*0,302*	*0,416*	*0,078*
CaO	*0,006*	*0,052*	*0,099*	*0,003*	*0,004*	*0,041*	*0,111*	*0,002*	*0,003*	*0,082*	*0,209*	*0,002*	*0,005*	*0,208*	*0,472*	*0,002*	*0,022*	*0,039*	*0,217*	*0,002*
Na_2O	*0,010*	*0,020*	*0,116*	*0,003*	*0,003*	*0,011*	*0,005*	*0,009*	*0,013*	*0,028*	*0,140*	*0,006*	*0,006*	*0,038*	*0,125*	*0,007*	*0,006*	*0,012*	*0,102*	*0,000*
NiO	*0,019*	*0,014*	*0,018*	*0,022*	*0,003*	*0,043*	*0,044*	*0,018*	*0,003*	*0,028*	*0,011*	*0,019*	*0,003*	*0,016*	*0,012*	*0,014*	*0,027*	*0,013*	*0,024*	*0,001*
Total	*0,690*	*0,541*	*0,461*	*0,539*	*0,439*	*0,386*	*0,567*	*0,606*	*0,640*	*0,418*	*0,213*	*0,199*	*0,383*	*0,587*	*0,453*	*0,064*	*0,320*	*0,432*	*0,532*	*0,384*

Table 2 - continued

Sample	04LH815 (lherz)					04LH07 (lherz)					04LH04 (lherz)					06LI16 (harz)					06LI15 (harz)				
distance from contact	50cm					80cm					1.5m					15m					15m				
	Ol	**Opx**	**Cpx**	**Spl**	**Ol**	**Opx**	**Cpx**	**Spl**	**Ol**	**Opx**	**Cpx**	**Spl**	**Ol**	**Opx**	**Cpx**	**Spl**	**Ol**	**Opx**	**Cpx**	**Spl**	**Ol**	**Opx**	**Cpx**	**Spl**
SiO_2 (wt. %)	40,5	55,7	51,8	0,1	40,6	55,6	52,3	0,1	40,6	54,8	51,8	0,1	41,3	57,2	54,0	0,0	41,6	57,6	54,3	0,0
TiO_2	0,010	0,123	0,734	0,042	0,006	0,131	0,693	0,056	0,007	0,123	0,698	0,030	0,010	0,031	0,102	0,095	0,002	0,012	0,022	0,028
Al_2O_3	0,007	3,23	7,14	60,1	0,003	3,74	6,22	52,9	0,003	4,43	6,32	59,0	0,007	2,02	3,27	31,3	0,002	2,09	2,05	33,6
Cr_2O_3	0,003	0,197	0,689	7,96	0,009	0,403	1,06	14,7	0,009	0,315	0,736	8,30	0,002	0,433	1,35	36,5	0,009	0,428	0,655	34,6
FeO	9,79	6,46	2,26	11,15	9,13	6,11	1,99	12,24	9,91	6,53	2,20	11,46	8.83	5,76	2,05	17,59	8,79	5,74	1,85	16,80
MnO	0,145	0,151	0,080	0,107	0,126	0,149	0,074	0,128	0,148	0,164	0,077	0,134	0,131	0,131	0,075	0,243	0,143	0,159	0,065	0,212
MgO	48,7	33,3	13,9	20,0	49,2	33,3	14,2	18,4	48,4	32,9	14,3	19,5	50,2	34,9	16,0	13,9	50,5	34,9	17,2	14,6
CaO	0,012	0,310	21,1	0,006	0,006	0,462	21,2	0,044	0,012	0,336	21,5	0,035	0,012	0,395	22,2	0,002	0,018	0,445	23,6	0,006
Na_2O	0,003	0,025	2,08	0,003	0,006	0,048	2,04	0,000	0,004	0,032	1,85	0,011	0,003	0,027	1,30	0,006	0,002	0,018	0,559	0,005
NiO	0,420	0,088	0,035	0,412	0,450	0,062	0,065	0,293	0,414	0,089	0,046	0,413	0,449	0,084	0,028	0,119	0,415	0,085	0,046	0,105
Total	99,6	99,6	99,8	99,8	99,5	99,9	99,9	98,9	99,5	99,8	99,5	99,0	101,0	101,0	100,3	100,1	101,5	101,5	100,5	100,3
SiO_2 (wt. %)	*0,333*	*0,430*	*0,334*	*0,016*	*0,259*	*0,196*	*0,106*	*0,013*	*0,080*	*0,614*	*0,433*	*0,005*	*0,268*	*0,155*	*0,213*	*0,007*	*0,134*	*0,261*	*0,300*	*0,018*
TiO_2	*0,010*	*0,037*	*0,046*	*0,014*	*0,003*	*0,021*	*0,049*	*0,002*	*0,003*	*0,025*	*0,081*	*0,002*	*0,005*	*0,016*	*0,013*	*0,002*	*0,002*	*0,002*	*0,009*	*0,004*
Al_2O_3	*0,008*	*0,808*	*0,298*	*0,296*	*0,005*	*0,265*	*0,343*	*0,148*	*0,002*	*0,982*	*0,787*	*0,330*	*0,005*	*0,234*	*0,157*	*1,202*	*0,004*	*0,138*	*0,213*	*0,552*
Cr_2O_3	*0,005*	*0,068*	*0,052*	*0,109*	*0,009*	*0,019*	*0,088*	*0,102*	*0,009*	*0,081*	*0,202*	*0,357*	*0,004*	*0,086*	*0,081*	*1,189*	*0,010*	*0,019*	*0,159*	*0,621*
FeO	*0,095*	*0,134*	*0,072*	*0,229*	*0,114*	*0,090*	*0,018*	*0,055*	*0,085*	*0,171*	*0,095*	*0,246*	*0,081*	*0,100*	*0,063*	*0,367*	*0,111*	*0,014*	*0,033*	*0,185*
MnO	*0,017*	*0,018*	*0,016*	*0,028*	*0,007*	*0,023*	*0,007*	*0,008*	*0,023*	*0,031*	*0,027*	*0,004*	*0,021*	*0,022*	*0,010*	*0,007*	*0,018*	*0,022*	*0,017*	*0,026*
MgO	*0,484*	*0,318*	*0,222*	*0,131*	*0,238*	*0,157*	*0,166*	*0,027*	*0,195*	*0,479*	*0,453*	*0,267*	*0,334*	*0,116*	*0,148*	*0,245*	*0,171*	*0,216*	*0,163*	*0,169*
CaO	*0,006*	*0,057*	*0,262*	*0,003*	*0,005*	*0,135*	*0,237*	*0,042*	*0,007*	*0,058*	*0,348*	*0,020*	*0,011*	*0,029*	*0,071*	*0,002*	*0,004*	*0,059*	*0,144*	*0,005*
Na_2O	*0,004*	*0,011*	*0,153*	*0,005*	*0,006*	*0,017*	*0,105*	*0,000*	*0,005*	*0,014*	*0,168*	*0,011*	*0,004*	*0,004*	*0,032*	*0,005*	*0,002*	*0,002*	*0,059*	*0,004*
NiO	*0,006*	*0,018*	*0,018*	*0,027*	*0,021*	*0,017*	*0,040*	*0,028*	*0,024*	*0,023*	*0,022*	*0,009*	*0,035*	*0,027*	*0,017*	*0,004*	*0,028*	*0,025*	*0,024*	*0,011*
Total	*0,514*	*0,447*	*0,453*	*0,398*	*0,356*	*0,358*	*0,429*	*0,053*	*0,156*	*0,685*	*0,274*	*0,026*	*0,501*	*0,388*	*0,086*	*0,173*	*0,313*	*0,065*	*0,297*	*0,314*

Table 2 - continued

Sample	06LI8 (harz)					06LI7 (harz)					06LI6 (harz)					06LI10b (harz)					06LI10a (harz)				
distance from contact	5m					4m					3m					2.2m					2m				
	Ol	**Opx**	**Cpx**	**Spl**	**Ol**	**Opx**	**Cpx**	**Spl**	**Ol**	**Opx**	**Cpx**	**Spl**	**Ol**	**Opx**	**Cpx**	**Spl**	**Ol**	**Opx**	**Cpx**	**Spl**	**Ol**	**Opx**	**Cpx**	**Spl**
SiO_2 (wt. %)	41,4	57,5	54,1	0,0	41,4	57,5	54,4	0,0	41,5	57,7	54,3	0,0	41,4	57,3	54,1	0,0	41,3	57,8	54,5	0,0
TiO_2	0,004	0,012	0,117	0,087	0,006	0,022	0,070	0,083	0,003	0,036	0,159	0,127	0,008	0,026	0,140	0,122	0,005	0,017	0,079	0,094
Al_2O_3	0,001	1,73	3,93	30,6	0,002	1,79	3,38	26,5	0,002	1,49	3,92	31,3	0,005	1,73	4,26	27,9	0,004	1,58	3,37	26,9
Cr_2O_3	0,012	0,352	1,62	37,1	0,006	0,410	1,62	41,1	0,010	0,344	1,78	36,3	0,000	0,379	1,78	40,4	0,011	0,336	1,54	40,9
FeO	9,18	6,05	2,09	18,96	8,98	5,92	2,22	19,89	9,00	6,01	2,14	18,70	8,95	5,89	2,12	18,85	8,98	5,91	2,11	19,67
MnO	0,136	0,154	0,059	0,266	0,135	0,131	0,066	0,259	0,133	0,146	0,045	0,256	0,127	0,144	0,061	0,271	0,127	0,136	0,050	0,262
MgO	49,8	34,7	15,1	13,1	49,9	34,9	15,8	12,1	50,1	35,1	15,2	13,4	49,9	34,6	14,7	12,7	50,3	35,0	15,6	12,2
CaO	0,010	0,363	21,0	0,005	0,020	0,468	20,6	0,002	0,007	0,323	20,9	0,002	0,014	0,528	20,4	0,004	0,010	0,355	21,1	0,004
Na_2O	0,003	0,044	2,12	0,006	0,006	0,058	1,88	0,008	0,002	0,029	2,16	0,007	0,016	0,065	2,39	0,008	0,002	0,039	1,91	0,006
NiO	0,395	0,091	0,024	0,089	0,434	0,083	0,033	0,061	0,422	0,081	0,041	0,092	0,431	0,085	0,039	0,097	0,440	0,075	0,025	0,089
Total	101,0	101,0	100,1	100,5	100,9	101,3	100,1	100,4	101,2	101,3	100,6	100,6	100,8	100,8	100,1	100,7	101,2	101,2	100,3	100,5
SiO_2 (wt. %)	*0,169*	*0,195*	*0,189*	*0,008*	*0,089*	*0,164*	*0,123*	*0,006*	*0,180*	*0,082*	*0,156*	*0,008*	*0,058*	*0,293*	*0,284*	*0,012*	*0,305*	*0,138*	*0,239*	*0,010*
TiO_2	*0,006*	*0,007*	*0,010*	*0,010*	*0,004*	*0,015*	*0,026*	*0,004*	*0,003*	*0,015*	*0,044*	*0,008*	*0,010*	*0,012*	*0,009*	*0,015*	*0,006*	*0,006*	*0,012*	*0,002*
Al_2O_3	*0,002*	*0,075*	*0,083*	*1,366*	*0,002*	*0,062*	*0,065*	*0,556*	*0,003*	*0,063*	*0,189*	*2,858*	*0,004*	*0,385*	*0,144*	*2,277*	*0,004*	*0,102*	*0,056*	*0,831*
Cr_2O_3	*0,008*	*0,027*	*0,207*	*1,437*	*0,008*	*0,076*	*0,096*	*0,560*	*0,005*	*0,023*	*0,133*	*2,587*	*0,000*	*0,137*	*0,142*	*2,191*	*0,008*	*0,073*	*0,148*	*0,627*
FeO	*0,049*	*0,031*	*0,103*	*0,861*	*0,075*	*0,036*	*0,121*	*0,451*	*0,129*	*0,038*	*0,130*	*0,793*	*0,236*	*0,091*	*0,098*	*0,706*	*0,095*	*0,054*	*0,062*	*0,488*
MnO	*0,031*	*0,018*	*0,020*	*0,015*	*0,011*	*0,019*	*0,010*	*0,007*	*0,012*	*0,024*	*0,020*	*0,036*	*0,016*	*0,014*	*0,027*	*0,045*	*0,016*	*0,010*	*0,016*	*0,063*
MgO	*0,208*	*0,075*	*0,186*	*0,574*	*0,205*	*0,137*	*0,668*	*0,250*	*0,124*	*0,161*	*0,071*	*0,673*	*0,160*	*0,332*	*0,086*	*0,646*	*0,085*	*0,103*	*0,303*	*0,237*
CaO	*0,006*	*0,043*	*0,198*	*0,002*	*0,007*	*0,179*	*0,677*	*0,003*	*0,006*	*0,027*	*0,280*	*0,002*	*0,006*	*0,274*	*0,232*	*0,004*	*0,007*	*0,042*	*0,079*	*0,003*
Na_2O	*0,005*	*0,012*	*0,066*	*0,005*	*0,007*	*0,021*	*0,099*	*0,005*	*0,003*	*0,003*	*0,043*	*0,004*	*0,023*	*0,038*	*0,095*	*0,004*	*0,002*	*0,008*	*0,067*	*0,004*
NiO	*0,021*	*0,013*	*0,018*	*0,016*	*0,024*	*0,011*	*0,026*	*0,013*	*0,031*	*0,014*	*0,027*	*0,005*	*0,026*	*0,017*	*0,024*	*0,019*	*0,007*	*0,013*	*0,016*	*0,020*
Total	*0,310*	*0,234*	*0,422*	*0,213*	*0,362*	*0,147*	*0,095*	*0,121*	*0,291*	*0,218*	*0,164*	*0,217*	*0,203*	*0,141*	*0,179*	*0,260*	*0,351*	*0,273*	*0,111*	*0,089*

Table 2 - continued

Sample	06L15b (harz)				06L15a (harz)				06L14 (harz)				06L19 (lherz)				06L13 (lherz)			
distance from contact	1,3m				1m				20cm				20cm				1m			
	Ol	**Opx**	**Cpx**	**Spl**	**Ol**	**Opx**	**Cpx**	**Spl**	**Ol**	**Opx**	**Cpx**	**Spl**	**Ol**	**Opx**	**Cpx**	**Spl**	**Ol**	**Opx**	**Cpx**	**Spl**
SiO_2 (wt. %)	41,5	57,3	54,3	0,0	41,4	57,2	54,2	0,0	41,3	57,3	53,4	0,0	41,4	57,0	53,7	0,0	41,4	57,2	53,2	0,0
TiO_2	0,006	0,031	0,219	0,142	0,009	0,038	0,202	0,123	0,000	0,077	0,419	0,103	0,001	0,090	0,401	0,156	0,003	0,118	0,536	0,132
Al_2O_3	0,003	2,17	4,55	30,6	0,004	2,08	4,55	31,8	0,004	2,47	5,30	43,4	0,003	2,33	5,01	40,8	0,004	2,52	5,45	45,1
Cr_2O_3	0,003	0,403	1,62	37,0	0,004	0,424	1,63	35,9	0,001	0,383	1,57	24,3	0,004	0,357	1,44	27,1	0,003	0,319	1,41	22,7
FeO	9,18	6,10	2,44	18,97	9,18	6,00	2,21	18,82	9,42	6,17	2,18	16,23	9,38	6,21	2,16	16,25	9,44	6,38	2,20	15,04
MnO	0,135	0,153	0,052	0,232	0,146	0,137	0,076	0,270	0,136	0,123	0,061	0,179	0,126	0,153	0,048	0,182	0,138	0,152	0,068	0,168
MgO	50,0	34,4	15,6	13,1	50,0	34,7	15,0	13,0	50,0	34,6	14,5	15,8	49,9	34,5	14,7	15,6	50,0	34,3	14,6	16,6
CaO	0,011	0,320	19,4	0,001	0,013	0,464	20,1	0,006	0,014	0,329	20,8	0,006	0,003	0,429	20,8	0,001	0,015	0,343	20,9	0,000
Na_2O	0,004	0,032	2,29	0,006	0,004	0,049	2,33	0,008	0,003	0,032	2,27	0,015	0,002	0,051	2,15	0,005	0,013	0,031	2,12	0,009
NiO	0,407	0,069	0,040	0,094	0,418	0,074	0,043	0,100	0,416	0,081	0,045	0,156	0,415	0,049	0,034	0,160	0,394	0,049	0,057	0,205
Total	101,2	101,0	100,6	100,5	101,1	101,1	100,4	100,4	101,3	101,5	100,5	100,5	101,2	101,2	100,5	100,6	101,5	101,4	100,5	100,2
SiO_2 (wt. %)	*0,099*	*0,171*	*0,299*	*0,003*	*0,078*	*0,079*	*0,228*	*0,008*	*0,171*	*0,315*	*0,130*	*0,012*	*0,124*	*0,580*	*0,270*	*0,002*	*0,158*	*0,284*	*0,281*	*0,015*
TiO_2	*0,010*	*0,007*	*0,034*	*0,003*	*0,009*	*0,022*	*0,021*	*0,018*	*0,001*	*0,024*	*0,050*	*0,040*	*0,001*	*0,018*	*0,031*	*0,049*	*0,004*	*0,015*	*0,012*	*0,039*
Al_2O_3	*0,003*	*0,207*	*0,279*	*1,641*	*0,004*	*0,124*	*0,098*	*2,649*	*0,004*	*0,366*	*0,165*	*2,997*	*0,002*	*0,727*	*0,233*	*1,187*	*0,007*	*0,379*	*0,337*	*0,697*
Cr_2O_3	*0,004*	*0,046*	*0,283*	*1,881*	*0,003*	*0,009*	*0,218*	*2,424*	*0,001*	*0,059*	*0,080*	*3,013*	*0,005*	*0,152*	*0,227*	*0,788*	*0,004*	*0,096*	*0,250*	*0,738*
FeO	*0,081*	*0,020*	*0,433*	*0,338*	*0,086*	*0,041*	*0,071*	*0,720*	*0,141*	*0,045*	*0,054*	*0,087*	*0,078*	*0,115*	*0,064*	*0,777*	*0,085*	*0,136*	*0,040*	*0,356*
MnO	*0,014*	*0,013*	*0,015*	*0,041*	*0,016*	*0,024*	*0,003*	*0,025*	*0,021*	*0,025*	*0,006*	*0,011*	*0,020*	*0,024*	*0,018*	*0,010*	*0,036*	*0,011*	*0,013*	*0,024*
MgO	*0,054*	*0,109*	*1,715*	*0,337*	*0,195*	*0,123*	*0,592*	*0,574*	*0,127*	*0,198*	*0,066*	*0,193*	*0,106*	*0,484*	*0,135*	*0,590*	*0,031*	*0,221*	*0,239*	*0,253*
CaO	*0,010*	*0,050*	*1,777*	*0,001*	*0,008*	*0,201*	*0,261*	*0,006*	*0,008*	*0,061*	*0,164*	*0,004*	*0,003*	*0,154*	*0,178*	*0,000*	*0,010*	*0,024*	*0,128*	*0,000*
Na_2O	*0,006*	*0,012*	*0,212*	*0,000*	*0,003*	*0,012*	*0,118*	*0,002*	*0,004*	*0,012*	*0,048*	*0,012*	*0,003*	*0,033*	*0,037*	*0,003*	*0,014*	*0,013*	*0,112*	*0,006*
NiO	*0,041*	*0,018*	*0,011*	*0,020*	*0,017*	*0,018*	*0,026*	*0,016*	*0,019*	*0,008*	*0,017*	*0,017*	*0,018*	*0,021*	*0,020*	*0,009*	*0,020*	*0,025*	*0,018*	*0,009*
Total	*0,181*	*0,182*	*0,247*	*0,445*	*0,119*	*0,099*	*0,383*	*0,244*	*0,117*	*0,052*	*0,286*	*0,252*	*0,156*	*0,183*	*0,397*	*0,251*	*0,142*	*0,215*	*0,382*	*0,075*

Table 2 - continued

Sample	06LI2 (lherz)					06LI1 (lherz)					06LI12 (lherz)					06LI17 (lherz)					06LF4 (harz)				
distance from contact	2m					3m					5m					50m					3m				
	Ol	**Opx**	**Cpx**	**Spl**	**Ol**	**Opx**	**Cpx**	**Spl**	**Ol**	**Opx**	**Cpx**	**Spl**	**Ol**	**Opx**	**Cpx**	**Spl**	**Ol**	**Opx**	**Cpx**	**Spl**	**Ol**	**Opx**	**Cpx**	**Spl**
SiO_2 (wt. %)	41,3	56,9	52,7	0,0	41,5	56,3	52,4	0,0	41,4	56,4	52,3	0,0	41,2	56,2	52,5	0,0	40,8	56,3	52,8	0,1
TiO_2	0,002	0,113	0,588	0,080	0,007	0,106	0,760	0,031	0,011	0,123	0,763	0,057	0,000	0,107	0,642	0,044	-0,011	0,071	0,260	0,051
Al_2O_3	0,089	2,47	5,82	47,1	0,001	3,47	7,31	62,0	0,001	3,30	6,88	57,0	0,002	3,50	6,52	57,0	-0,010	2,36	4,03	46,6
Cr_2O_3	0,015	0,294	1,32	20,7	0,004	0,159	0,518	5,33	0,005	0,238	0,833	10,1	0,003	0,265	0,801	10,2	-0,003	0,348	0,984	22,2
FeO	9,43	6,38	2,13	14,20	9,47	6,44	2,16	10,18	10,19	6,82	2,35	12,57	10,05	6,69	2,32	12,28	8,85	5,82	2,03	14,10
MnO	0,147	0,142	0,087	0,175	0,145	0,171	0,081	0,092	0,148	0,165	0,087	0,123	0,152	0,151	0,088	0,143	0,121	0,145	0,082	0,168
MgO	49,6	34,2	14,3	17,2	49,7	34,1	14,1	20,5	49,4	34,0	14,1	19,0	49,3	33,7	14,3	19,1	49,1	33,7	15,6	16,6
CaO	0,006	0,385	21,1	0,005	0,004	0,326	21,2	0,000	0,003	0,312	21,1	0,002	0,012	0,378	21,2	0,002	0,010	0,488	21,9	0,003
Na_2O	0,001	0,038	2,05	0,005	0,003	0,018	1,99	0,011	0,003	0,019	2,07	0,007	0,002	0,043	1,99	0,003	0,010	0,024	1,45	-0,011
NiO	0,409	0,058	0,028	0,224	0,469	0,090	0,039	0,469	0,408	0,090	0,042	0,328	0,425	0,079	0,031	0,339	0,385	0,090	0,043	0,218
Total	101,0	101,0	100,2	99,9	101,3	101,1	100,5	98,7	101,6	101,5	100,4	99,4	101,2	101,1	100,4	99,3	99,3	99,4	99,1	100,0
SiO_2 (wt. %)	*0,156*	*0,670*	*0,052*	*0,005*	*0,162*	*0,546*	*0,474*	*0,004*	*0,069*	*0,186*	*0,168*	*0,013*	*0,104*	*0,674*	*0,287*	*0,008*	*0,135*	*0,464*	*0,430*	*0,010*
TiO_2	*0,003*	*0,042*	*0,041*	*0,029*	*0,006*	*0,020*	*0,059*	*0,001*	*0,010*	*0,007*	*0,039*	*0,012*	*0,000*	*0,019*	*0,024*	*0,016*	*0,013*	*0,015*	*0,037*	*0,025*
Al_2O_3	*0,170*	*0,807*	*0,105*	*1,411*	*0,001*	*0,616*	*0,539*	*0,334*	*0,001*	*0,167*	*0,110*	*0,398*	*0,002*	*0,722*	*0,379*	*0,323*	*0,006*	*0,502*	*0,517*	*2,387*
Cr_2O_3	*0,026*	*0,123*	*0,023*	*1,415*	*0,004*	*0,037*	*0,023*	*0,104*	*0,007*	*0,006*	*0,036*	*0,502*	*0,005*	*0,075*	*0,079*	*0,386*	*0,014*	*0,111*	*0,244*	*2,304*
FeO	*0,189*	*0,211*	*0,048*	*0,591*	*0,111*	*0,060*	*0,097*	*0,368*	*0,138*	*0,093*	*0,102*	*0,328*	*0,185*	*0,024*	*0,056*	*0,477*	*0,049*	*0,085*	*0,062*	*0,631*
MnO	*0,009*	*0,026*	*0,014*	*0,021*	*0,007*	*0,015*	*0,007*	*0,019*	*0,022*	*0,010*	*0,028*	*0,004*	*0,033*	*0,023*	*0,023*	*0,021*	*0,009*	*0,022*	*0,006*	*0,013*
MgO	*0,150*	*0,448*	*0,088*	*0,394*	*0,132*	*0,398*	*0,256*	*0,290*	*0,054*	*0,127*	*0,063*	*0,222*	*0,172*	*0,372*	*0,187*	*0,230*	*0,090*	*0,317*	*0,260*	*0,584*
CaO	*0,006*	*0,098*	*0,087*	*0,002*	*0,001*	*0,098*	*0,277*	*0,000*	*0,005*	*0,003*	*0,085*	*0,003*	*0,010*	*0,035*	*0,170*	*0,002*	*0,003*	*0,271*	*0,493*	*0,005*
Na_2O	*0,001*	*0,019*	*0,033*	*0,002*	*0,003*	*0,013*	*0,181*	*0,004*	*0,002*	*0,003*	*0,017*	*0,003*	*0,001*	*0,008*	*0,046*	*0,001*	*0,007*	*0,019*	*0,110*	*0,007*
NiO	*0,034*	*0,004*	*0,003*	*0,020*	*0,008*	*0,022*	*0,002*	*0,026*	*0,025*	*0,020*	*0,013*	*0,015*	*0,039*	*0,013*	*0,012*	*0,021*	*0,023*	*0,014*	*0,019*	*0,016*
Total	*0,193*	*0,262*	*0,109*	*0,218*	*0,136*	*0,262*	*0,118*	*0,356*	*0,161*	*0,309*	*0,228*	*0,161*	*0,270*	*0,284*	*0,095*	*0,203*	*0,150*	*0,206*	*0,626*	*0,268*

Table 2 - continued

Sample	06LF27 (harz)					06LF3L (lherz)					06LF25 (lherz)					06LF26L (lherz)					06LF26W (websti)				
distance from contact	4m					4m					20m					30m					30m				
	Ol	**Opx**	**Cpx**	**Spl**	**Ol**	**Opx**	**Cpx**	**Spl**	**Ol**	**Opx**	**Cpx**	**Spl**	**Ol**	**Opx**	**Cpx**	**Spl**	**Ol**	**Opx**	**Cpx**	**Spl**	**Ol**	**Opx**	**Cpx**	**Spl**
SiO_2 (wt. %)	41,5	57,1	53,2	0,2	40,8	55,4	51,9	0,1	40,9	55,3	52,5	0,1	41,2	56,1	52,6	0,1	40,9	55,7	52,0	0,2
TiO_2	0,005	0,095	0,346	0,137	-0,001	0,127	0,682	0,032	-0,002	0,134	0,635	0,031	0,004	0,117	0,594	0,051	0,005	0,094	0,575	0,032
Al_2O_3	0,005	2,08	4,10	42,9	-0,004	3,65	7,22	60,5	0,003	3,98	7,13	58,8	-0,003	3,60	6,40	58,0	0,010	4,07	7,36	63,1
Cr_2O_3	-0,006	0,298	1,30	25,8	0,004	0,224	0,683	7,56	0,002	0,307	0,793	9,11	-0,003	0,325	0,929	9,95	-0,005	0,162	0,422	4,49
FeO	8,31	5,53	1,83	13,63	9,97	6,48	2,24	11,13	10,00	6,52	2,34	11,67	10,15	6,74	2,31	12,24	10,43	6,80	2,35	10,66
MnO	0,126	0,145	0,067	0,183	0,142	0,155	0,077	0,107	0,141	0,158	0,082	0,115	0,146	0,156	0,068	0,121	0,158	0,152	0,096	0,093
MgO	49,3	34,0	15,2	16,5	48,0	32,9	13,9	19,3	47,9	32,4	13,7	19,1	48,1	32,9	14,2	18,8	47,8	32,6	13,8	19,9
CaO	0,018	0,391	21,8	0,018	0,017	0,324	20,8	0,007	0,014	0,526	20,9	0,005	0,015	0,397	20,7	0,006	0,014	0,337	20,9	0,003
Na_2O	0,003	0,025	1,59	-0,008	-0,001	0,019	2,15	-0,002	0,005	0,059	2,15	-0,005	-0,003	0,053	2,17	-0,008	-0,009	0,020	2,01	-0,004
NiO	0,421	0,075	0,034	0,211	0,424	0,090	0,025	0,419	0,402	0,086	0,029	0,388	0,390	0,077	0,039	0,381	0,419	0,097	0,035	0,517
Total	99,7	99,8	99,5	99,5	99,4	99,4	99,7	99,1	99,5	99,5	100,3	99,3	100,0	100,5	100,0	99,7	99,7	100,0	99,6	99,0
SiO_2 (wt. %)	*0,175*	*0,128*	*0,172*	*0,009*	*0,218*	*0,266*	*0,415*	*0,013*	*0,272*	*0,522*	*0,234*	*0,016*	*0,205*	*0,416*	*0,145*	*0,021*	*0,135*	*0,228*	*0,105*	*0,011*
TiO_2	*0,010*	*0,016*	*0,022*	*0,036*	*0,012*	*0,019*	*0,020*	*0,014*	*0,012*	*0,023*	*0,019*	*0,005*	*0,008*	*0,015*	*0,036*	*0,016*	*0,021*	*0,014*	*0,046*	*0,011*
Al_2O_3	*0,012*	*0,262*	*0,132*	*2,267*	*0,016*	*0,433*	*0,337*	*0,111*	*0,007*	*0,742*	*0,158*	*0,185*	*0,011*	*0,372*	*0,323*	*2,438*	*0,007*	*0,459*	*0,347*	*1,016*
Cr_2O_3	*0,015*	*0,067*	*0,117*	*2,362*	*0,015*	*0,059*	*0,029*	*0,263*	*0,007*	*0,079*	*0,035*	*0,067*	*0,016*	*0,056*	*0,119*	*2,778*	*0,008*	*0,010*	*0,041*	*1,038*
FeO	*0,130*	*0,088*	*0,023*	*0,469*	*0,170*	*0,053*	*0,153*	*0,128*	*0,154*	*0,159*	*0,038*	*0,133*	*0,118*	*0,033*	*0,087*	*0,529*	*0,184*	*0,119*	*0,048*	*0,273*
MnO	*0,010*	*0,011*	*0,008*	*0,021*	*0,019*	*0,008*	*0,008*	*0,009*	*0,012*	*0,011*	*0,008*	*0,011*	*0,012*	*0,005*	*0,013*	*0,012*	*0,013*	*0,012*	*0,017*	*0,007*
MgO	*0,170*	*0,171*	*0,122*	*0,600*	*0,201*	*0,213*	*0,217*	*0,115*	*0,124*	*0,475*	*0,088*	*0,129*	*0,113*	*0,279*	*0,218*	*0,432*	*0,073*	*0,259*	*0,159*	*0,244*
CaO	*0,005*	*0,037*	*0,134*	*0,022*	*0,002*	*0,034*	*0,271*	*0,004*	*0,003*	*0,387*	*0,223*	*0,004*	*0,002*	*0,024*	*0,294*	*0,002*	*0,005*	*0,048*	*0,179*	*0,002*
Na_2O	*0,011*	*0,005*	*0,086*	*0,017*	*0,009*	*0,016*	*0,115*	*0,008*	*0,006*	*0,045*	*0,019*	*0,004*	*0,002*	*0,004*	*0,094*	*0,004*	*0,010*	*0,010*	*0,091*	*0,003*
NiO	*0,007*	*0,016*	*0,019*	*0,013*	*0,013*	*0,013*	*0,014*	*0,023*	*0,016*	*0,015*	*0,008*	*0,014*	*0,007*	*0,016*	*0,010*	*0,057*	*0,013*	*0,016*	*0,009*	*0,039*
Total	*0,357*	*0,148*	*0,226*	*0,367*	*0,146*	*0,260*	*0,167*	*0,118*	*0,393*	*0,134*	*0,281*	*0,176*	*0,203*	*0,295*	*0,058*	*0,405*	*0,186*	*0,283*	*0,101*	*0,278*

Table 2 - continued

Sample	06LF9 (lherz)					06LF23 (lherz)					06LF11 (lherz)					06LF15 (lherz)					06LF16 (lherz)				
distance from contact	50m					70m					80m					80m					80m				
	Ol	**Opx**	**Cpx**	**Spl**	**Ol**	**Opx**	**Cpx**	**Spl**	**Ol**	**Opx**	**Cpx**	**Spl**	**Ol**	**Opx**	**Cpx**	**Spl**	**Ol**	**Opx**	**Cpx**	**Spl**	**Ol**	**Opx**	**Cpx**	**Spl**
SiO_2 (wt. %)	41,4	55,7	52,5	0,126	40,9	56,2	51,6	0,2	40,9	56,0	51,8	0,1	40,9	55,5	52,4	0,1	41,0	55,3	51,9	0,1
TiO_2	0,002	0,111	0,609	0,045	0,017	0,076	0,623	0,030	-0,003	0,106	0,679	0,029	0,002	0,104	0,519	0,049	0,002	0,116	0,599	0,037
Al_2O_3	-0,007	3,78	6,70	58,9	0,018	2,98	7,17	61,9	0,011	2,85	6,71	59,1	0,001	3,71	6,11	56,3	-0,004	3,78	6,62	57,3
Cr_2O_3	0,006	0,253	0,755	9,05	-0,001	0,155	0,550	5,65	0,009	0,171	0,718	8,62	0,005	0,316	0,830	11,9	-0,008	0,351	0,904	10,9
FeO	10,19	6,64	2,29	11,9	9,93	6,57	2,28	10,71	9,63	6,42	2,20	11,33	9,54	6,31	2,20	12,00	9,16	5,95	2,14	11,18
MnO	0,142	0,156	0,090	0,111	0,144	0,165	0,084	0,096	0,146	0,164	0,078	0,105	0,140	0,151	0,077	0,109	0,136	0,142	0,080	0,111
MgO	48,1	32,7	14,1	19,0	47,1	33,0	13,8	20,0	48,4	33,3	14,1	19,5	48,4	33,0	14,4	18,7	48,8	33,1	14,2	19,3
CaO	0,015	0,380	21,0	-0,003	0,018	0,310	21,0	0,007	0,016	0,333	21,2	0,004	0,012	0,335	21,2	0,004	0,013	0,407	20,9	0,009
Na_2O	0,004	0,041	2,08	0,004	0,002	0,017	1,99	0,002	-0,002	0,032	2,02	0,005	0,000	0,030	1,98	-0,004	-0,006	0,040	2,02	-0,008
NiO	0,428	0,088	0,038	0,399	0,405	0,086	0,043	0,471	0,391	0,086	0,031	0,397	0,390	0,078	0,028	0,342	0,425	0,089	0,045	0,365
Total	100,3	99,9	100,0	99,6	98,5	99,6	99,2	99,0	99,5	99,5	99,4	99,2	99,5	99,6	99,7	99,4	99,5	99,2	99,4	99,3
SiO_2 (wt. %)	*0,158*	*0,464*	*0,220*	*0,018*	*0,193*	*0,657*	*0,347*	*0,017*	*0,206*	*0,440*	*0,126*	*0,011*	*0,140*	*0,219*	*0,358*	*0,013*	*0,080*	*0,284*	*0,172*	*0,012*
TiO_2	*0,006*	*0,019*	*0,033*	*0,007*	*0,015*	*0,030*	*0,035*	*0,020*	*0,012*	*0,024*	*0,028*	*0,009*	*0,006*	*0,008*	*0,033*	*0,015*	*0,003*	*0,014*	*0,027*	*0,009*
Al_2O_3	*0,008*	*0,514*	*0,265*	*0,757*	*0,018*	*0,905*	*0,269*	*0,593*	*0,004*	*0,420*	*0,172*	*0,250*	*0,009*	*0,380*	*0,751*	*0,476*	*0,005*	*0,422*	*0,107*	*0,266*
Cr_2O_3	*0,009*	*0,052*	*0,051*	*0,966*	*0,008*	*0,031*	*0,043*	*0,730*	*0,008*	*0,044*	*0,025*	*0,489*	*0,013*	*0,068*	*0,159*	*0,478*	*0,007*	*0,024*	*0,011*	*0,291*
FeO	*0,083*	*0,067*	*0,042*	*0,204*	*0,195*	*0,120*	*0,028*	*0,447*	*0,140*	*0,120*	*0,058*	*0,116*	*0,128*	*0,055*	*0,035*	*0,124*	*0,071*	*0,062*	*0,084*	*0,204*
MnO	*0,008*	*0,009*	*0,006*	*0,009*	*0,010*	*0,007*	*0,009*	*0,016*	*0,016*	*0,017*	*0,014*	*0,005*	*0,008*	*0,005*	*0,010*	*0,005*	*0,009*	*0,009*	*0,007*	*0,008*
MgO	*0,113*	*0,218*	*0,151*	*0,177*	*1,056*	*0,391*	*0,114*	*0,291*	*0,110*	*0,254*	*0,093*	*0,157*	*0,135*	*0,119*	*0,416*	*0,155*	*0,125*	*0,206*	*0,171*	*0,170*
CaO	*0,004*	*0,038*	*0,162*	*0,002*	*0,007*	*0,037*	*0,213*	*0,003*	*0,006*	*0,022*	*0,127*	*0,004*	*0,004*	*0,034*	*0,271*	*0,003*	*0,004*	*0,128*	*0,154*	*0,002*
Na_2O	*0,004*	*0,008*	*0,099*	*0,008*	*0,014*	*0,009*	*0,083*	*0,017*	*0,008*	*0,014*	*0,065*	*0,009*	*0,007*	*0,006*	*0,123*	*0,005*	*0,008*	*0,022*	*0,087*	*0,007*
NiO	*0,019*	*0,011*	*0,009*	*0,019*	*0,012*	*0,014*	*0,009*	*0,041*	*0,018*	*0,006*	*0,011*	*0,015*	*0,012*	*0,010*	*0,009*	*0,016*	*0,009*	*0,010*	*0,003*	*0,005*
Total	*0,236*	*0,244*	*0,237*	*0,283*	*1,387*	*0,248*	*0,263*	*0,362*	*0,201*	*0,465*	*0,294*	*0,169*	*0,027*	*0,258*	*0,187*	*0,124*	*0,152*	*0,229*	*0,261*	*0,248*

Table 2 - continued

Sample	06LF3W (webst)					06LF8 (webst)					06LF17 (webst)					06LP20 (webst)				
distance from contact	10m					30m					100m					100m				
	Ol	**Opx**	**Cpx**	**Spl**	**Ol**	**Opx**	**Cpx**	**Spl**	**Ol**		**Opx**	**Cpx**	**Spl**	**Ol**		**Opx**	**Cpx**	**Spl**		
SiO_2 (wt. %)	40,8	54,9	51,4	0,2		55,7	51,9	0,2			55,8	52,1	0,2			54,9	51,8	0,2		
TiO_2	0,004	0,122	0,668	0,039		0,119	0,744	0,056			0,102	0,548	0,032			0,096	0,538	0,023		
Al_2O_3	0,007	4,53	7,38	59,4		3,90	7,42	60,6			3,72	7,19	59,7			5,30	8,04	64,0		
Cr_2O_3	0,009	0,291	0,676	8,51		0,225	0,650	7,60			0,235	0,711	8,03			0,157	0,352	3,73		
FeO	9,81	6,51	2,23	10,98		6,49	2,18	10,47			6,45	2,25	10,76			6,97	2,25	10,19		
MnO	0,149	0,149	0,084	0,106		0,156	0,073	0,101			0,160	0,084	0,095			0,173	0,093	0,107		
MgO	48,5	32,5	13,7	19,6		32,7	13,7	20,0			33,0	13,9	19,9			31,8	13,5	20,4		
CaO	0,014	0,393	20,8	0,003		0,354	20,8	0,003			0,313	20,9	0,004			0,352	21,2	0,003		
Na_2O	-0,003	0,052	2,13	-0,005		0,032	2,17	-0,002			0,016	2,03	-0,009			0,026	1,99	0,002		
NiO	0,427	0,096	0,044	0,434		0,086	0,032	0,458			0,089	0,024	0,426			0,072	0,031	0,443		
Total	99,7	99,6	99,1	99,2		99,8	99,7	99,5			99,9	99,8	99,1			99,9	99,8	99,1		
SiO_2 (wt. %)	*0,109*	*0,453*	*0,151*	*0,025*		*0,577*	*0,236*	*0,019*			*0,462*	*0,085*	*0,017*			*0,245*	*0,146*	*0,011*		
TiO_2	*0,008*	*0,021*	*0,018*	*0,009*		*0,018*	*0,053*	*0,011*			*0,024*	*0,013*	*0,013*			*0,024*	*0,050*	*0,010*		
Al_2O_3	*0,004*	*0,535*	*0,143*	*2,046*		*0,766*	*0,392*	*0,837*			*0,548*	*0,247*	*0,379*			*0,535*	*0,088*	*0,240*		
Cr_2O_3	*0,001*	*0,039*	*0,026*	*2,212*		*0,056*	*0,051*	*0,884*			*0,050*	*0,024*	*0,268*			*0,028*	*0,037*	*0,210*		
FeO	*0,114*	*0,107*	*0,077*	*0,478*		*0,090*	*0,046*	*0,321*			*0,079*	*0,089*	*0,292*			*0,115*	*0,049*	*0,158*		
MnO	*0,014*	*0,013*	*0,020*	*0,018*		*0,007*	*0,011*	*0,017*			*0,015*	*0,006*	*0,011*			*0,011*	*0,014*	*0,013*		
MgO	*0,045*	*0,313*	*0,089*	*0,493*		*0,378*	*0,133*	*0,225*			*0,319*	*0,324*	*0,133*			*0,338*	*0,133*	*0,123*		
CaO	*0,000*	*0,155*	*0,077*	*0,006*		*0,069*	*0,243*	*0,006*			*0,028*	*0,193*	*0,004*			*0,075*	*0,181*	*0,004*		
Na_2O	*0,008*	*0,035*	*0,061*	*0,007*		*0,024*	*0,093*	*0,013*			*0,019*	*0,107*	*0,014*			*0,026*	*0,084*	*0,006*		
NiO	*0,029*	*0,014*	*0,005*	*0,046*		*0,010*	*0,014*	*0,054*			*0,013*	*0,010*	*0,019*			*0,010*	*0,014*	*0,028*		
Total	*0,035*	*0,203*	*0,243*	*0,186*		*0,197*	*0,351*	*0,172*			*0,231*	*0,145*	*0,155*			*0,262*	*0,096*	*0,055*		

Table 2: Major and minor elements mineral compositions of harzburgites (harz), lherzolites (lherz) and websterites (webst) from the Lherz massif. Ol= olivine; Opx= orthopyroxene; Cpx= clinopyroxene; Spl= spinel. In each thin section, at least 5 analyses per mineral were performed (minimum of. 20 analyses per section). Analyses have been performed with CAMECA SX 100 (Géosciences Montpellier and GEMOC ARC National Key Centre).

Table 3 - Whole-rock chemical compositions – major and minor elements (ppm)

Sample	05LD1 distal harz.	05LD4 distal harz.	05LA2 harz.	05LA1 harz.	05LA16 harz.	05LA9 harz.	05LA12 harz.	05LA3 harz.	05LA4 harz.	05LA5 lherz.	05LA6 lherz.	05LA8 lherz.	05LA15 lherz.	05LE3 lherz.
SiO2	39,2	42,1	44,7	43,1	42,3	41,9	42,2	41,4	41,5	46,2	44,8	45,4	46,9	44,4
Al2O3	0,170	0,920	1,87	0,88	0,64	0,98	2,46	1,26	0,700	4,97	3,01	3,53	4,03	2,95
Cr2O3	0,094	0,437	0,796	0,293	0,304	0,299	1,06	0,596	0,230	0,463	0,341	0,394	0,386	0,353
FeO	7,82	7,59	7,31	7,43	7,94	6,85	7,80	7,85	7,84	7,43	8,63	8,26	7,29	7,79
MgO	45,5	43,1	41,9	43,9	44,4	40,8	40,5	42,0	43,0	34,9	38,6	37,2	36,4	39,6
CaO	0,280	0,610	0,730	0,500	0,320	0,580	1,90	0,470	0,440	4,70	2,20	3,42	3,31	2,46
MnO	0,120	0,120	0,130	0,120	0,120	0,120	0,120	0,120	0,120	0,130	0,140	0,140	0,130	0,130
NiO	0,370	0,313	0,263	0,296	0,290	0,283	0,267	0,297	0,299	0,232	0,246	0,243	0,209	0,251
Na2O	0,050	0,060	0,090	0,070	0,080	0,060	0,160	0,070	0,070	0,360	0,200	0,290	0,260	0,200
TiO2	0,030	0,020	0,040	0,060	0,050	0,030	0,060	0,050	0,040	0,200	0,100	0,140	0,160	0,120
LOI	6,44	4,46	2,93	3,85	3,48	7,83	3,41	5,95	5,73	0,48	1,33	1,04	0,82	1,43
TOTAL	100,1	99,6	100,8	100,5	99,9	99,8	100,0	100,0	99,9	100,0	99,6	100,1	99,8	99,7
total-LOI	93,6	95,2	97,9	96,6	96,4	91,9	96,6	94,1	94,2	99,5	98,2	99,0	99,0	98,3
recalculated without LOI														
SiO2	41,8	44,2	45,7	44,6	43,9	45,6	43,7	44,0	44,0	46,4	45,6	45,9	47,3	45,2
Al2O3	0,182	0,967	1,91	0,91	0,66	1,07	2,55	1,34	0,743	5,00	3,06	3,56	4,07	3,00
Cr2O3	0,101	0,459	0,814	0,303	0,315	0,325	1,10	0,634	0,245	0,465	0,347	0,398	0,390	0,359
FeO	8,35	7,97	7,47	7,69	8,23	7,45	8,08	8,34	8,33	7,47	8,78	8,34	7,36	7,92
MgO	48,6	45,2	42,9	45,4	46,0	44,4	42,0	44,6	45,6	35,0	39,3	37,5	36,7	40,3
CaO	0,299	0,641	0,746	0,518	0,332	0,631	1,97	0,500	0,467	4,72	2,24	3,45	3,34	2,50
MnO	0,128	0,126	0,133	0,124	0,124	0,131	0,124	0,128	0,127	0,131	0,142	0,141	0,131	0,132
NiO	0,395	0,329	0,268	0,307	0,301	0,308	0,276	0,316	0,317	0,233	0,250	0,246	0,211	0,255
Na2O	0,053	0,063	0,092	0,072	0,083	0,065	0,166	0,074	0,074	0,362	0,204	0,293	0,263	0,203
TiO2	0,032	0,021	0,041	0,062	0,052	0,033	0,062	0,053	0,042	0,201	0,102	0,141	0,162	0,122
total	100,0	100,0	100,0	100,0	100,0	100,0	100,0	100,0	100,0	100,0	100,0	100,0	100,0	100,0

Table 3 - continued

Sample	04LH13 harz.	04LH12 harz.	04LH14 harz.	04LH11 harz.	04LH08 lherz.	04LH815 lherz.	04LH07 lherz.	04LH04 lherz.	05L3 lherz.
SiO2	41,3	41,5	41,5	41,9	43,9	43,8	40,9	44,3	44,1
Al2O3	0,439	0,450	0,444	0,539	2,10	3,40	1,87	3,15	2,99
Cr2O3	0,287	0,252	0,223	0,274	0,461	0,356	0,547	0,377	0,342
FeO	7,70	7,71	7,88	7,87	7,65	7,57	7,72	7,87	7,91
MgO	43,8	43,4	43,8	44,2	41,9	38,3	40,2	39,3	38,7
CaO	0,358	0,351	0,319	0,382	2,18	3,26	2,01	2,66	2,69
MnO	0,118	0,118	0,119	0,121	0,125	0,129	0,124	0,132	0,130
NiO	0,296	0,298	0,299	0,292	0,260	0,243	0,284	0,240	0,260
Na2O	0,048	0,040	0,045	0,058	0,219	0,290	0,185	0,216	0,210
TiO2	0,010	0,012	0,016	0,017	0,124	0,153	0,082	0,131	0,130
LOI	4,81	5,23	4,49	4,10	0,68	0,35	1,23	1,75	2,62
TOTAL	99,1	99,4	99,1	99,7	99,7	97,9	95,1	100,1	100,0
total-LOI	94,3	94,1	94,6	95,6	99,0	97,6	93,9	98,3	97,4
recalculated without LOI									
SiO2	43,8	44,1	43,8	43,8	44,4	44,9	43,5	45,0	45,2
Al2O3	0,465	0,478	0,470	0,564	2,12	3,48	1,99	3,21	3,07
Cr2O3	0,305	0,268	0,235	0,286	0,466	0,365	0,582	0,383	0,351
FeO	8,16	8,19	8,33	8,23	7,73	7,76	8,22	8,00	8,12
MgO	46,4	46,1	46,3	46,2	42,4	39,3	42,9	39,9	39,7
CaO	0,380	0,373	0,337	0,400	2,20	3,34	2,14	2,71	2,76
MnO	0,125	0,126	0,126	0,127	0,126	0,133	0,132	0,134	0,133
NiO	0,314	0,316	0,316	0,306	0,263	0,249	0,303	0,244	0,267
Na2O	0,051	0,042	0,047	0,061	0,221	0,297	0,197	0,220	0,216
TiO2	0,011	0,012	0,017	0,017	0,125	0,157	0,087	0,134	0,133
total	100,0	100,0	100,0	100,0	100,0	100,0	100,0	100,0	100,0

Table 3 - continued

Sample	06LF27	06LF16	06LF25	06LF20	06LF15	06LF14	06LD6	06LF11	06LE6	06LE6W	06LE7	06LF28L	06LF17	06LF8
	harz.	lherz.	lherz.	webst.	lherz.	lherz.	harz.	lherz.	harz.	lherz.	lherz.	lherz.	webst.	webst.
SiO2	44,1	45,2	44,7	47,3	44,4	45,6	43,0	44,2	41,3	45,3	45,5	43,8	44,6	48,9
Al2O3	1,11	3,19	3,14	12,80	2,95	3,88	3,39	0,750	1,28	2,79	3,37	3,57	5,64	6,04
Cr2O3	0,313	0,373	0,325	0,596	0,377	0,357	0,294	0,356	0,690	1,05	1,04	0,359	0,583	0,544
FeO	7,29	6,90	7,99	5,44	7,82	8,00	7,25	7,73	7,21	6,46	6,39	7,31	7,16	6,16
MgO	43,6	37,9	39,6	24,7	39,8	37,5	37,3	45,0	41,7	38,1	37,7	37,9	35,2	31,3
CaO	0,810	3,04	2,35	8,38	2,77	3,21	2,80	0,680	0,800	4,00	3,28	2,91	4,74	5,82
MnO	0,120	0,120	0,130	0,130	0,130	0,130	0,130	0,120	0,120	0,110	0,110	0,130	0,120	0,120
Na2O	0,080	0,240	0,200	0,640	0,220	0,270	0,210	0,060	0,050	0,300	0,270	0,190	0,350	0,500
TiO2	0,050	0,130	0,140	0,300	0,110	0,160	0,150	0,000	0,040	0,100	0,140	0,120	0,180	0,280
LOI	3,31	3,43	1,83	1,01	1,78	1,09	5,81	1,80	6,58	3,22	2,40	3,60	1,67	1,15
TOTAL	100,7	100,5	100,3	101,3	100,3	100,2	100,3	100,7	99,8	101,4	100,2	99,9	100,2	100,8
total-LOI	97,4	97,0	98,5	100,3	98,6	99,1	94,5	98,9	93,2	98,2	97,8	96,3	98,5	99,6
recalculated without LOI														
SiO2	45,2	46,6	45,3	47,2	45,0	46,0	45,5	44,7	44,3	46,1	46,5	45,5	45,3	49,1
Al2O3	1,14	3,29	3,19	12,76	2,99	3,92	3,59	0,758	1,37	2,84	3,45	3,71	5,72	6,06
Cr2O3	0,322	0,384	0,330	0,594	0,383	0,360	0,311	0,360	0,740	1,07	1,07	0,373	0,592	0,546
FeO	7,48	7,11	8,11	5,42	7,94	8,07	7,68	7,81	7,74	6,58	6,53	7,59	7,26	6,18
MgO	44,7	39,0	40,2	24,6	40,4	37,9	39,5	45,5	44,8	38,8	38,5	39,3	35,7	31,4
CaO	0,832	3,13	2,39	8,36	2,81	3,24	2,96	0,687	0,858	4,07	3,35	3,02	4,81	5,84
MnO	0,123	0,124	0,132	0,130	0,132	0,131	0,138	0,121	0,129	0,112	0,112	0,135	0,122	0,120
Na2O	0,082	0,247	0,203	0,638	0,223	0,272	0,222	0,061	0,054	0,306	0,276	0,197	0,355	0,502
TiO2	0,051	0,134	0,142	0,299	0,112	0,161	0,159	0,000	0,043	0,102	0,143	0,125	0,183	0,281
total	100,0	100,0	100,0	100,0	100,0	100,0	100,0	100,0	100,0	100,0	100,0	100,0	100,0	100,0

Table 3 - continued

Sample	06LF26W	06LF9	06LD8	06LF13	06LA17	06LF26L	06LF3W	06LE5	06LF4	06LF23	06LF28W	06LF3L
	webst.	lherz.	harz.	webst.	lherz.	lherz.	webst.	lherz.	harz.	lherz.	webst.	lherz.
SiO2	46,9	44,8	43,1	48,5	46,0	43,9	46,0	44,3	42,6	44,5	45,2	45,0
Al2O3	10,2	3,82	0,78	8,59	5,09	2,69	4,48	3,70	1,57	5,13	4,85	4,00
Cr2O3	0,651	0,394	0,414	0,350	1,00	0,407	0,393	0,377	0,381	0,403	0,524	0,363
FeO	5,64	7,63	7,33	5,75	5,93	8,26	7,07	8,57	7,17	6,98	6,53	7,47
MgO	25,5	37,3	44,1	27,4	33,9	39,7	34,8	39,1	40,4	34,0	34,1	36,8
CaO	9,66	3,27	0,500	8,68	5,07	2,51	4,28	3,27	1,28	4,39	5,03	3,47
MnO	0,120	0,130	0,120	0,120	0,110	0,140	0,130	0,140	0,120	0,120	0,120	0,130
Na2O	0,780	0,270	0,050	0,600	0,310	0,200	0,340	0,260	0,090	0,320	0,320	0,290
TiO2	0,330	0,170	0,040	0,300	0,250	0,090	0,210	0,160	0,070	0,200	0,170	0,180
LOI	0,930	1,96	4,08	0,940	2,47	2,70	2,30	0,260	5,36	3,58	3,39	2,60
TOTAL	100,7	99,8	100,4	101,2	100,1	100,5	100,0	100,0	99,1	99,6	100,2	100,2
total-LOI	99,8	97,8	96,3	100,3	97,6	97,8	97,7	99,8	93,7	96,0	96,8	97,6
recalculated without LOI												
SiO2	47,0	45,8	44,7	48,3	47,1	44,8	47,1	44,3	45,5	46,3	46,7	46,1
Al2O3	10,18	3,91	0,81	8,57	5,21	2,75	4,59	3,71	1,68	5,34	5,01	4,10
Cr2O3	0,653	0,402	0,430	0,350	1,02	0,416	0,402	0,377	0,407	0,420	0,541	0,372
FeO	5,66	7,80	7,60	5,74	6,08	8,44	7,23	8,59	7,65	7,27	6,74	7,65
MgO	25,6	38,2	45,7	27,3	34,7	40,5	35,6	39,1	43,1	35,4	35,2	37,7
CaO	9,68	3,34	0,519	8,66	5,19	2,57	4,38	3,28	1,37	4,57	5,20	3,55
MnO	0,120	0,133	0,125	0,120	0,113	0,143	0,133	0,140	0,128	0,125	0,124	0,133
Na2O	0,782	0,276	0,052	0,598	0,318	0,204	0,348	0,261	0,096	0,333	0,331	0,297
TiO2	0,331	0,174	0,042	0,299	0,256	0,092	0,215	0,160	0,075	0,208	0,176	0,184
total	100,0	100,0	100,0	100,0	100,0	100,0	100,0	100,0	100,0	100,0	100,0	100,0

Table 3: Major and minor elements compositions of whole-rocks harzburgites (harz.), lherzolites (lherz.) and websterites (webst.) from the Lherz massif. Analyses were performed on whole-rocks powders (obtained in Geosciences Montpellier) by GEOLABS, Canada.

Table 4 - Whole-rocks chemical compositions – trace elements (ppm)

	05LA1	05LA2	05LA3	05LA4	05LA5	05LA6	05LA8	05LA9	05LA12	05LA15	05LA16	05LD1	05LD4	05L3	05LE3
Cs	0,001	0,003	0,008	0,003	0,004	0,003	0,005	0,003	0,003	0,004	0,002	0,000	0,004	0,005	0,002
Rb	0,018	0,039	0,027	0,027	0,109	0,062	0,083	0,029	0,046	0,128	0,018	0,007	0,045	0,072	0,052
Ba	0,136	0,304	1,612	1,009	0,430	0,894	0,912	1,026	0,401	0,820	0,418	0,069	0,560	0,326	0,437
Th	0,002	0,002	0,040	0,003	0,002	0,026	0,009	0,004	0,007	0,012	0,019	0,005	0,009	0,006	0,003
U	0,001	0,001	0,001	0,001	0,001	0,005	0,003	0,001	0,003	0,006	0,002	0,002	0,003	0,003	0,091
La	0,012	0,014	0,431	0,025	0,154	0,191	0,204	0,027	0,199	0,208	0,101	0,020	0,027	0,105	0,104
Ce	0,026	0,040	0,799	0,075	0,651	0,624	0,745	0,074	0,486	0,669	0,207	0,042	0,055	0,408	0,380
Pr	0,005	0,007	0,095	0,012	0,133	0,105	0,134	0,010	0,067	0,122	0,023	0,006	0,007	0,075	0,070
Sr	0,861	1,014	3,214	2,051	14,737	8,455	14,420	1,098	11,376	13,458	1,778	0,921	1,100	8,728	8,090
Nd	0,031	0,044	0,415	0,091	0,927	0,632	0,836	0,042	0,403	0,724	0,118	0,027	0,036	0,516	0,473
Zr	0,511	0,243	0,716	0,710	8,027	4,520	7,293	0,167	2,669	6,137	0,750	0,087	0,204	4,610	4,499
Hf	0,009	0,004	0,019	0,019	0,220	0,113	0,196	0,003	0,057	0,168	0,020	0,002	0,007	0,131	0,120
Sm	0,017	0,018	0,084	0,033	0,381	0,211	0,319	0,010	0,126	0,268	0,027	0,009	0,011	0,205	0,189
Eu	0,008	0,007	0,022	0,012	0,166	0,083	0,136	0,003	0,051	0,114	0,008	0,002	0,003	0,089	0,076
Gd	0,029	0,025	0,078	0,043	0,662	0,324	0,527	0,010	0,178	0,445	0,032	0,007	0,011	0,362	0,317
Tb	0,006	0,005	0,011	0,007	0,126	0,059	0,097	0,002	0,032	0,081	0,005	0,001	0,002	0,068	0,061
Dy	0,056	0,046	0,061	0,057	0,945	0,441	0,715	0,017	0,215	0,611	0,044	0,007	0,013	0,512	0,447
Y	0,344	0,303	0,278	0,275	4,949	2,288	3,868	0,122	1,050	3,191	0,206	0,025	0,061	2,669	2,502
Ho	0,015	0,012	0,012	0,013	0,204	0,096	0,160	0,005	0,045	0,132	0,009	0,001	0,003	0,111	0,101
Er	0,048	0,046	0,037	0,038	0,637	0,307	0,469	0,017	0,134	0,415	0,032	0,004	0,009	0,338	0,310
Yb	0,067	0,070	0,047	0,045	0,584	0,297	0,464	0,034	0,131	0,404	0,037	0,008	0,020	0,335	0,308
Lu	0,013	0,014	0,009	0,009	0,097	0,052	0,080	0,007	0,023	0,070	0,008	0,002	0,004	0,059	0,056

Table 4 - continued

	06Li10a	06Li5a	06Li8	06Li2	06Li4	06Li1	06Li9	06Li5b	06Li3 (dup)	06Li15	06Li3	06Li16	06Li6	06Li17	06Li7	06Li12
Cs	0,005	0,002	0,001	0,004	0,001	0,009	0,002	0,002	0,002	0,001	0,002	0,001	0,006	0,004	0,002	0,003
Rb	0,053	0,021	0,011	0,032	0,015	0,128	0,024	0,020	0,027	0,008	0,037	0,014	0,044	0,056	0,019	0,062
Ba	1,174	0,525	0,495	0,790	0,553	1,909	2,029	0,581	1,071	0,149	0,507	0,251	0,993	0,625	1,051	2,159
Th	0,015	0,015	0,008	0,030	0,009	0,013	0,009	0,015	0,008	0,002	0,006	0,008	0,017	0,003	0,016	0,004
U	0,006	0,004	0,003	0,009	0,003	0,005	0,003	0,004	0,003	0,001	0,003	0,003	0,005	0,002	0,004	0,002
Nb	0,072	0,063	0,020	0,080	0,027	0,065	0,021	0,047	0,021	0,019	0,020	0,028	0,097	0,033	0,070	0,044
Ta	0,013	0,016	0,001	0,006	0,011	0,006	0,002	0,014	0,001	0,000	0,018	0,004	0,015	0,003	0,005	0,001
La	0,170	0,165	0,058	0,213	0,067	0,131	0,074	0,162	0,061	0,008	0,055	0,081	0,151	0,112	0,073	0,058
Ce	0,367	0,343	0,166	0,720	0,197	0,610	0,236	0,357	0,191	0,015	0,179	0,226	0,282	0,430	0,107	0,275
Pr	0,046	0,039	0,028	0,147	0,033	0,150	0,041	0,042	0,034	0,002	0,031	0,036	0,032	0,090	0,011	0,072
Sr	2,183	2,416	1,819	11,091	2,271	12,252	2,583	2,468	2,992	0,912	2,767	4,390	2,236	7,780	1,575	6,772
Nd	0,178	0,164	0,147	0,867	0,171	1,019	0,226	0,154	0,187	0,011	0,164	0,167	0,122	0,551	0,046	0,482
Zr	1,091	0,811	0,747	6,940	1,302	8,167	1,794	0,933	1,556	0,097	1,425	0,567	0,668	4,545	0,322	5,368
Hf	0,018	0,017	0,011	0,220	0,032	0,282	0,049	0,014	0,044	0,003	0,041	0,009	0,018	0,142	0,007	0,175
Sm	0,031	0,026	0,036	0,351	0,053	0,454	0,068	0,028	0,061	0,004	0,051	0,038	0,028	0,232	0,014	0,231
Eu	0,011	0,009	0,013	0,134	0,019	0,186	0,023	0,009	0,021	0,001	0,020	0,014	0,009	0,093	0,004	0,092
Gd	0,030	0,029	0,039	0,517	0,061	0,750	0,079	0,029	0,076	0,004	0,069	0,039	0,028	0,369	0,014	0,368
Tb	0,004	0,005	0,007	0,091	0,010	0,137	0,013	0,005	0,014	0,001	0,012	0,006	0,005	0,068	0,002	0,068
Dy	0,027	0,031	0,042	0,602	0,065	0,965	0,086	0,032	0,090	0,005	0,082	0,034	0,027	0,478	0,016	0,482
Y	0,178	0,217	0,243	3,306	0,385	5,671	0,506	0,208	0,568	0,045	0,497	0,190	0,170	2,940	0,107	2,893
Ho	0,006	0,008	0,009	0,131	0,015	0,220	0,019	0,008	0,020	0,002	0,019	0,007	0,006	0,111	0,004	0,107
Er	0,020	0,028	0,029	0,367	0,045	0,644	0,060	0,027	0,064	0,008	0,062	0,022	0,020	0,331	0,014	0,326
Yb	0,027	0,039	0,038	0,326	0,057	0,596	0,069	0,038	0,082	0,017	0,072	0,029	0,028	0,323	0,020	0,318
Lu	0,005	0,007	0,007	0,048	0,010	0,089	0,012	0,007	0,014	0,004	0,013	0,005	0,005	0,051	0,004	0,048

Table 4: Trace elements concentrations (ppm) in Lherz peridotites obtained by ICPMS at Geosciences Montpellier (05LA series) and GEMOC ARC National Key Centre (06Li series).

Table 5 - Whole-rocks chemical compositions – trace elements normalized to primitive mantle

	05LA1	05LA2	05LA3	05LA4	05LA5	05LA6	05LA8	05LA9	05LA12	05LA15	05LA16	05LD1	05LD4	05L3	05LE3
Cs	0,012	0,046	0,120	0,038	0,057	0,039	0,066	0,036	0,040	0,058	0,023	0,005	0,055	0,071	0,034
Rb	0,028	0,061	0,043	0,042	0,171	0,098	0,131	0,046	0,073	0,201	0,028	0,010	0,071	0,113	0,081
Ba	0,020	0,043	0,231	0,144	0,061	0,128	0,130	0,147	0,057	0,117	0,060	0,010	0,080	0,047	0,063
Th	0,019	0,020	0,468	0,033	0,024	0,305	0,103	0,041	0,078	0,146	0,220	0,058	0,107	0,074	0,033
U	0,028	0,033	0,028	0,046	0,043	0,245	0,123	0,069	0,127	0,284	0,078	0,082	0,141	0,122	4,355
La	0,018	0,020	0,628	0,037	0,224	0,278	0,297	0,040	0,290	0,303	0,148	0,029	0,040	0,152	0,151
Ce	0,015	0,023	0,450	0,042	0,367	0,351	0,419	0,042	0,274	0,377	0,117	0,023	0,031	0,230	0,214
Pr	0,018	0,026	0,345	0,042	0,483	0,380	0,487	0,036	0,242	0,440	0,082	0,020	0,026	0,272	0,253
Sr	0,041	0,048	0,152	0,097	0,698	0,401	0,683	0,052	0,539	0,638	0,084	0,044	0,052	0,414	0,383
Nd	0,023	0,033	0,307	0,067	0,685	0,467	0,618	0,031	0,298	0,535	0,087	0,020	0,026	0,381	0,349
Zr	0,046	0,022	0,064	0,063	0,717	0,404	0,651	0,015	0,238	0,548	0,067	0,008	0,018	0,412	0,402
Hf	0,030	0,014	0,061	0,060	0,712	0,366	0,634	0,011	0,185	0,543	0,065	0,007	0,023	0,424	0,388
Sm	0,039	0,040	0,189	0,074	0,858	0,475	0,718	0,021	0,284	0,604	0,061	0,021	0,025	0,462	0,425
Eu	0,045	0,041	0,132	0,074	0,990	0,491	0,810	0,018	0,306	0,680	0,050	0,013	0,019	0,531	0,450
Gd	0,049	0,041	0,131	0,073	1,111	0,544	0,884	0,017	0,299	0,747	0,054	0,013	0,018	0,608	0,532
Tb	0,060	0,047	0,098	0,069	1,167	0,549	0,897	0,018	0,292	0,751	0,051	0,010	0,016	0,628	0,569
Dy	0,076	0,062	0,083	0,078	1,282	0,598	0,971	0,023	0,292	0,829	0,059	0,009	0,017	0,695	0,606
Y	0,076	0,067	0,061	0,060	1,088	0,503	0,850	0,027	0,231	0,701	0,045	0,005	0,013	0,587	0,550
Ho	0,089	0,072	0,073	0,076	1,247	0,586	0,978	0,031	0,273	0,806	0,056	0,008	0,016	0,677	0,615
Er	0,100	0,095	0,077	0,079	1,328	0,639	0,978	0,036	0,279	0,866	0,066	0,009	0,020	0,705	0,646
Yb	0,136	0,142	0,095	0,092	1,184	0,602	0,941	0,069	0,266	0,820	0,075	0,016	0,040	0,679	0,624
Lu	0,175	0,192	0,123	0,117	1,309	0,704	1,081	0,095	0,305	0,951	0,107	0,025	0,060	0,793	0,752

Table 5 - continued

	06Li10a	06Li5a	06Li8	06Li2	06Li4	06Li1	06Li9	06Li5b	06Li3 (dup)	06Li15	06Li3 (1)	06Li16	06Li6	06Li17	06Li7	06Li12
Cs	0,065	0,028	0,015	0,049	0,020	0,129	0,029	0,034	0,032	0,007	0,031	0,016	0,085	0,053	0,026	0,040
Rb	0,083	0,033	0,017	0,051	0,024	0,202	0,039	0,032	0,042	0,012	0,058	0,022	0,069	0,089	0,030	0,098
Ba	0,168	0,075	0,071	0,113	0,079	0,273	0,290	0,083	0,153	0,021	0,073	0,036	0,142	0,089	0,150	0,309
Th	0,173	0,173	0,097	0,358	0,110	0,156	0,101	0,173	0,090	0,024	0,067	0,094	0,198	0,033	0,190	0,045
U	0,282	0,209	0,124	0,414	0,124	0,241	0,138	0,205	0,134	0,047	0,145	0,122	0,219	0,075	0,209	0,105
Nb	0,101	0,089	0,027	0,112	0,038	0,091	0,029	0,066	0,030	0,026	0,028	0,039	0,136	0,046	0,098	0,061
Ta	0,321	0,393	0,027	0,158	0,272	0,151	0,060	0,331	0,017		0,428	0,092	0,378	0,071	0,124	0,027
La	0,247	0,240	0,085	0,310	0,097	0,190	0,107	0,236	0,089	0,011	0,081	0,118	0,220	0,163	0,106	0,084
Ce	0,207	0,193	0,093	0,406	0,111	0,344	0,133	0,201	0,107	0,008	0,101	0,127	0,159	0,242	0,060	0,155
Pr	0,165	0,141	0,101	0,532	0,121	0,542	0,147	0,150	0,124	0,008	0,112	0,129	0,114	0,328	0,041	0,261
Sr	0,103	0,115	0,086	0,526	0,108	0,581	0,122	0,117	0,142	0,043	0,131	0,208	0,106	0,369	0,075	0,321
Nd	0,131	0,121	0,108	0,640	0,126	0,752	0,167	0,114	0,138	0,008	0,121	0,123	0,090	0,407	0,034	0,356
Zr	0,097	0,072	0,067	0,620	0,116	0,729	0,160	0,083	0,139	0,009	0,127	0,051	0,060	0,406	0,029	0,479
Hf	0,059	0,055	0,036	0,711	0,105	0,913	0,157	0,045	0,143	0,010	0,133	0,029	0,059	0,459	0,023	0,565
Sm	0,071	0,059	0,082	0,791	0,118	1,021	0,153	0,063	0,137	0,009	0,115	0,086	0,064	0,523	0,032	0,521
Eu	0,066	0,053	0,076	0,798	0,115	1,105	0,138	0,056	0,128	0,007	0,120	0,081	0,052	0,555	0,024	0,546
Gd	0,051	0,049	0,066	0,868	0,102	1,259	0,133	0,049	0,128	0,006	0,116	0,066	0,047	0,620	0,024	0,618
Tb	0,039	0,045	0,062	0,840	0,094	1,270	0,121	0,044	0,128	0,006	0,110	0,056	0,042	0,626	0,023	0,628
Dy	0,036	0,043	0,057	0,816	0,088	1,309	0,117	0,043	0,122	0,007	0,111	0,046	0,036	0,649	0,022	0,654
Y	0,039	0,048	0,053	0,727	0,085	1,246	0,111	0,046	0,125	0,010	0,109	0,042	0,037	0,646	0,024	0,636
Ho	0,039	0,047	0,054	0,797	0,091	1,343	0,116	0,046	0,124	0,010	0,118	0,044	0,039	0,679	0,023	0,655
Er	0,043	0,057	0,059	0,765	0,094	1,341	0,125	0,056	0,134	0,016	0,129	0,046	0,042	0,690	0,029	0,680
Yb	0,055	0,079	0,077	0,661	0,115	1,210	0,139	0,076	0,166	0,034	0,146	0,058	0,056	0,655	0,042	0,646
Lu	0,072	0,098	0,088	0,653	0,132	1,203	0,162	0,098	0,186	0,051	0,173	0,067	0,069	0,684	0,056	0,651

Table 5: trace elements concentrations (ppm) normalized to primitive mantle (McDonough and Sun, 1995) in Lherz peridotites obtained by ICPMS at Geosciences Montpellier (05LA series) and GEMOC ARC National Key Centre (06Li series).

Figure 2 - Whole-rocks trace elements normalized to primitive mantle

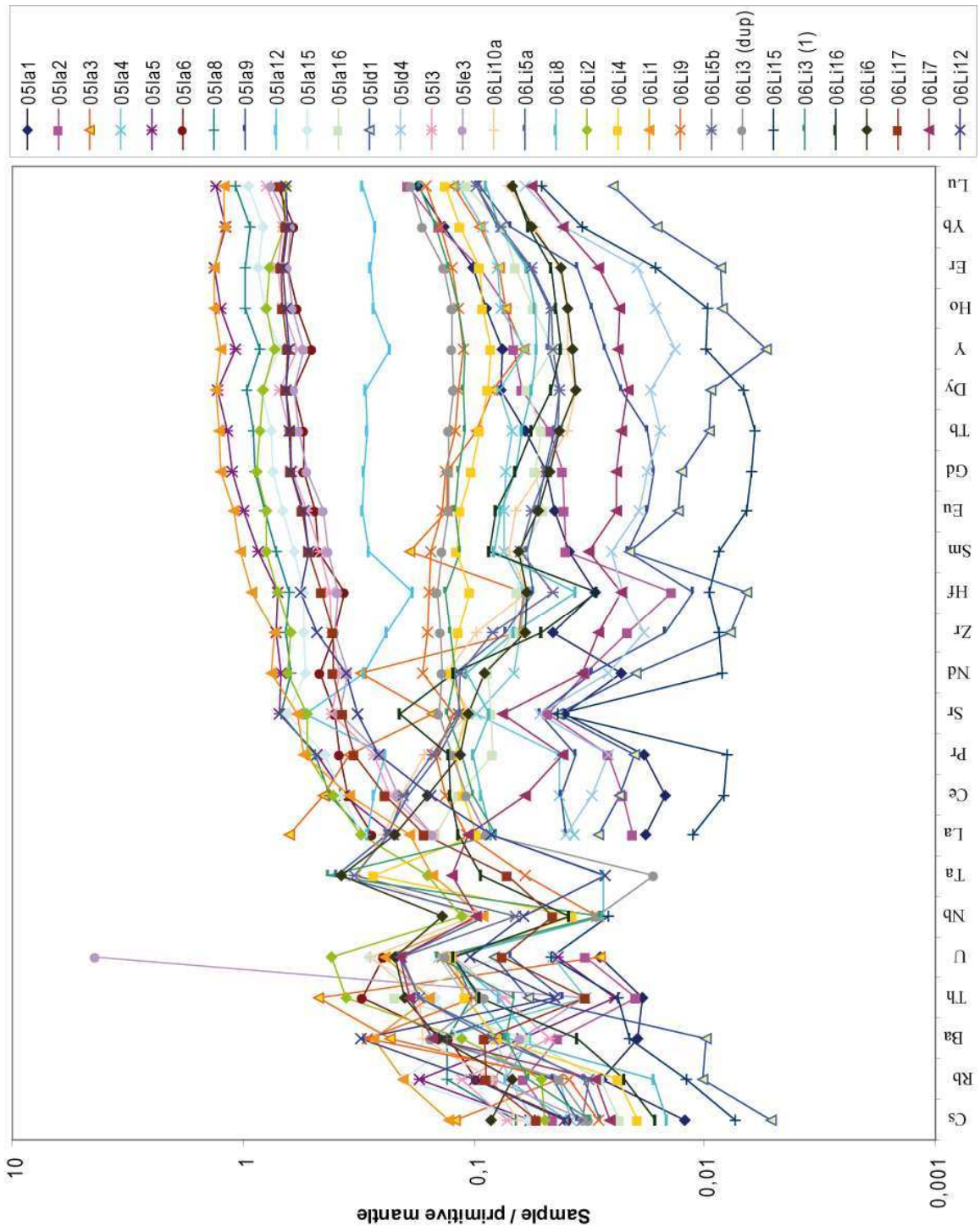

Table 6 - Modal compositions of Lherz peridotites

	04LH04	04LH815	04LH07	04LH08	04LH11	04LH14	04LH12	04LH13	04LH39	04LH37	04LH35	04LH33	05LA1	05LA2
	lherzolite	lherzolite	lherzolite	lherzolite	harzburgite	harzburgite	harzburgite	harzburgite	lherzolite	lherzolite	harzburgite	harzburgite	harzburgite	harzburgite
% olivine	59,9	61,6	72,6	68,8	80,4	84,1	82,9	82	53,5	51,5	78,8	77,6	76,9	66,8
% Opx	26,3	20,8	16,2	19,9	17,6	14,1	15,3	16	23,5	27,3	18,1	18,6	20,3	27,7
% Cpx	11,7	14,9	9,3	9,7	1,5	1,4	1,4	1,4	19,5	18,1	2,3	2,6	2,1	3,1
% Spl	2,1	2,7	1,9	1,6	0,5	0,4	0,4	0,6	3,5	3,1	0,8	1,2	0,7	2,5
error	*2,1*	*2,0*	*1,8*	*2,2*	*1,9*	*1,6*	*1,7*	*1,9*	*1,6*	*1,6*	*1,9*	*1,5*	*2,1*	*2,1*

	05LA3	05LA4	05LA5	05LA6	05LA8	05LA9	05LA12	05LA15	05LA16	05LD1	05LD4	05L3	05LE3	06LF-27
	harzburgite	harzburgite	lherzolite	lherzolite	lherzolite	harzburgite	harzburgite	lherzolite	harzburgite	harzburgite	harzburgite	lherzolite	lherzolite	harzburgite
% olivine	75,3	79,6	45,5	57,3	54,4	71,4	69,1	47,1	79,5	94,0	79,5	63,6	60,9	70,0
% Opx	20,8	17,9	28,5	29,5	28,4	25,7	16,7	34,4	18,4	4,6	16,8	22,7	25,6	25,0
% Cpx	2,2	1,9	22,7	10,9	15,2	2,3	10,7	15,7	1,5	1,2	2,4	12,0	11,3	3,0
% Spl	1,7	0,6	3,3	2,3	2,0	0,6	3,5	2,8	0,6	0,2	1,2	1,7	2,2	2,0
error	*2,1*	*2,0*	*2,1*	*2,1*	*2,2*	*2,1*	*2,0*	*2,0*	*1,9*	*1,1*	*1,8*	*2,2*	*2,0*	*1,5*

	06LF-16	06LF-25	06LF-20	06LF-15	06LF-11	06LF-28L	06LF-17	06LF-8	06LF26W	06LF-9	06LF-26L	06LF-3W	06LF-4	06LF-23
	lherzolite	lherzolite	websterite	lherzolite	lherzolite	lherzolite	websterite	websterite	websterite	lherzolite	lherzolite	websterite	harzburgite	lherzolite
% olivine	51,0	65,5	5,0	60,0	78,0	53,0	45,0	30,0	12,0	48,0	61,0	46,0	75,0	46,0
% Opx	31,0	19,0	46,5	25,0	16,0	29,0	28,0	39,0	34,0	35,0	25,0	32,0	16,5	29,0
% Cpx	15,0	13,0	38,5	12,5	5,0	14,0	22,5	27,0	45,0	15,0	11,5	20,0	7,0	20,0
% Spl	3,0	2,5	10,0	2,5	1,0	4,0	4,5	4,0	9,0	2,0	2,5	2,0	1,5	5,0
error	*1,7*	*1,9*	*1,6*	*1,6*	*2,0*	*2,1*	*1,2*	*1,1*	*2,1*	*1,8*	*1,7*	*1,7*	*1,9*	*2,1*

	06LF-3L	06LD6	06LD8	06LE5
	lherzolite	harzburgite	harzburgite	lherzolite
% olivine	50,0	78,0	76,0	63,0
% Opx	31,0	19,0	21,0	19,0
% Cpx	16,0	2,0	2,0	15,0
% Spl	3,0	1,0	1,0	3,0
error	*1,5*	*1,5*	*1,8*	*1,6*

Table 7 - REE clinopyroxenes concentrations (ppm)

Sample	05ld1	05ld4	05la2	05la1	05la16	05la9	05la12	05la3	05la4	05la5	05la6	05la8	05la15	05l3	05le1	05le2	05le3
	harz	harz	harz	harz	harz	harz	harz	harz	harz	lherz	lherz	lherz	lherz	lherz	lherz	lherz	lherz
dist. from c	>15m	>15m	4.5m	3.5m	1m	1m	10cm	10cm	5cm	1.5m	3m	5m	5m	150m	150m	150m	150m
Li			5.36	2.52		7.14		2.66	2.00	1.48	0.796	1.47					
Ca	164095	166668	151874	150359	117783	159164	118283	118855	147800	147872	144870	145299	149730	150445	148872	152875	150087
Sc	118,1	75,7	76,6	67,8	76,4	63,9	89,2	65,9	93,4	61,9	68,4	64,6	66,8	74,6	66,3	70,4	66,4
Ti	367,9	322,7	381,1	1555,3	1303,4	228,1	1967,9	1397,7	2217,1	4235,2	4511,5	4131,7	4275,9	3846,3	4137,6	3918,8	3821,6
V	227,9	199,9	228,2	200,8	181,7	217,4	244,1	183,3	251,6	265,4	259,4	250,4	250,5	268,1	263,7	275,7	258,5
Cr	7397,6	7132,7	11049,8	9220,7	9610,4	9534,0	9235,9	9117,4	10609,7	4602,2	5337,2	5469,0	5221,3	6130,8	5549,3	5983,9	5918,9
Co	19,4	19,6	20,3	18,0	17,2	19,3	22,3	13,7	33,1	18,5	16,8	17,2	17,6	17,7	17,2	17,4	16,6
Rb	0,057	0,027	0,127	0,036	0,029	0,056	0,043	0,017	0,050	0,050	0,065	0,020	0,036	0,037	0,053	0,036	0,021
Sr	59,6	33,1	19,7	62,8	82,3	15,3	74,9	60,6	85,4	61,9	78,4	79,4	86,2	60,5	56,9	61,3	61,3
Y	2,06	1,56	7,21	13,08	9,51	2,43	9,51	8,39	11,3	20,5	20,7	20,0	20,2	20,5	20,3	19,2	19,0
Zr	4,58	4,63	6,35	19,74	39,29	3,52	21,8	19,8	25,8	25,5	33,4	31,4	32,0	30,5	30,1	27,4	28,7
Nb	0,159	0,164	0,182	0,181	0,266	0,341	0,488	0,207	0,297	0,040	0,199	0,126	0,162	0,116	0,150	0,152	0,106
Cs	0,044	0,014	0,097	0,091	-	0,077	-	0,006	0,030	0,051	0,061	-	0,027	-	0,024	-	0,033
Ba	0,051	0,038	0,148	1,09	0,093	0,049	0,420	0,020	0,067	0,054	0,046	0,050	0,043	0,053	0,082	0,063	0,069
La	1,29	0,595	0,379	0,402	4,90	0,761	1,53	0,625	0,913	0,655	1,73	1,17	1,41	0,745	0,649	0,902	0,915
Ce	3,12	1,49	1,22	1,450	10,780	2,27	4,03	2,33	3,36	2,92	5,67	4,29	4,83	3,03	2,74	3,33	3,51
Pr	0,396	0,244	0,232	0,285	1,41	0,303	0,598	0,461	0,642	0,592	0,971	0,751	0,867	0,631	0,604	0,65	0,64
Nd	1,728	1,265	1,40	1,82	6,35	1,12	3,50	2,98	3,97	3,80	5,49	4,42	5,01	3,82	3,97	3,89	3,93
Sm	0,414	0,353	0,515	0,897	1,45	0,195	1,14	1,134	1,37	1,70	1,93	1,751	1,84	1,64	1,76	1,61	1,64
Eu	0,143	0,104	0,214	0,384	0,433	0,070	0,459	0,437	0,591	0,725	0,777	0,733	0,785	0,676	0,728	0,684	0,700
Gd	0,369	0,345	0,691	1,503	1,59	0,210	1,57	1,39	1,84	2,63	2,87	2,67	2,64	2,59	2,65	2,53	2,47
Tb	0,052	0,043	0,132	0,300	0,262	0,040	0,252	0,232	0,309	0,497	0,499	0,477	0,487	0,475	0,478	0,462	0,450
Dy	0,350	0,300	1,12	2,23	1,78	0,329	1,81	1,59	2,19	3,71	3,81	3,60	3,66	3,50	3,65	3,58	3,43
Ho	0,075	0,061	0,249	0,470	0,375	0,091	0,384	0,330	0,453	0,798	0,818	0,783	0,795	0,777	0,782	0,752	0,727
Er	0,263	0,219	0,892	1,44	1,06	0,346	1,11	0,924	1,29	2,37	2,36	2,31	2,29	2,31	2,27	2,17	2,26
Tm	0,055	0,041	0,143	0,199	0,151	0,057	0,169	0,126	0,186	0,342	0,355	0,340	0,334	0,333	0,335	0,327	0,321
Yb	0,430	0,307	0,978	1,23	0,999	0,467	1,09	0,875	1,21	2,30	2,35	2,22	2,26	2,33	2,28	2,12	2,19
Lu	0,069	0,050	0,147	0,175	0,139	0,074	0,159	0,120	0,175	0,327	0,337	0,325	0,322	0,323	0,301	0,309	0,295
Hf	0,049	0,133	0,103	0,553	0,875	0,111	0,520	0,590	0,699	0,852	1,01	1,04	1,01	1,01	1,01	0,958	0,985
Ta	0,030	0,023	0,012	0,012	0,063	0,044	0,059	0,052	0,063	0,004	0,034	0,017	0,024	0,009	0,011	0,018	0,014
Pb	0,229	0,089	0,217	0,292	0,442	0,193	0,158	0,216	0,262	0,198	0,232	0,369	0,164	0,127	0,136	0,265	0,206
Th	0,038	0,059	0,015	0,014	0,293	0,138	0,051	0,006	0,013	0,005	0,192	0,052	0,079	0,024	0,030	0,020	0,021
U	0,034	0,054	0,042	0,067	0,034	0,093	0,086	0,012	0,037	0,054	0,055	0,067	0,029	0,111	0,041	-	0,042

Table 7 - continued

Sample	04LH12	04LH11	04LH09	04LH08	04LH07	04LH04
	harz	harz	lherz	lherz	lherz	lherz
dist. from c	1.5m	1m	10cm	10cm	80cm	1.5m
Li	3,67	2,29	0,930	0,985	1,10	1,69
Be	0,168	0,169	0,190	0,172	0,124	0,077
B	1,38	1,13	1,26	1,34	1,50	1,72
Mg	150721	114975	108290	116185	102884	118125
Si	260954	239749	233712	229384	224733	240954
P	36,4	39,6	55,3	52,7	52,7	56,4
K	14,8	-	-	-	-	-
Ca	149780	150294	149558	150945	151631	153589
Sc	139,4	120,8	107,9	90,5	87,9	73,5
Ti	747,1	1319,4	4042,2	5125,4	4308,8	5078,6
V	297,6	282,6	293,6	249,4	273,2	258,1
Cr	12595,8	12741,5	10389,8	8803,6	7761,5	5095,5
Ni	630,8	240,6	290,4	351,3	265,3	335,7
Cu	4,61	0,410	0,427	1,54	0,385	0,380
Cu	4,99	0,330	0,404	1,61	0,356	0,431
Zn	13,1	6,1	5,8	8,5	8,5	7,9
Rb	-	-	0,010	0,006	0,007	0,020
Sr	106,8	111,3	97,6	90,8	70,5	50,3
Y	6,73	9,69	16,5	18,3	21,2	25,8
Zr	25,1	44,1	47,9	51,1	40,8	39,2
Nb	1,67	2,04	0,307	0,233	1,00	0,275
Mo	0,069	0,055	-	-	0,026	0,025
Cs	-	-	-	-	-	0,002
Ba	0,055	0,035	0,433	0,045	0,032	0,123
La	6,78	6,99	2,33	1,59	1,45	0,653
Ce	11,3	13,4	7,6	5,6	3,8	2,7
Pr	1,25	1,41	1,28	1,14	0,766	0,673
Nd	5,47	5,52	6,98	7,24	5,16	5,02
Sm	1,36	1,31	2,27	2,71	2,17	2,29
Eu	0,431	0,456	0,887	1,037	0,852	0,911
Gd	1,37	1,50	2,72	3,49	3,20	3,66
Tb	0,203	0,245	0,454	0,560	0,553	0,649
Dy	1,33	1,74	3,14	3,75	3,99	4,75
Ho	0,262	0,369	0,642	0,729	0,824	1,000
Er	0,768	1,11	1,83	1,99	2,33	2,89
Yb	0,827	1,17	1,77	1,76	2,14	2,71
Lu	0,125	0,175	0,255	0,246	0,299	0,378
Hf	0,439	0,868	1,50	1,601	1,33	1,36
Ta	0,541	0,629	0,055	0,040	0,027	0,013
Pb	0,525	0,197	0,224	0,152	0,159	0,089
Th	0,339	0,254	0,081	0,113	0,131	0,091
U	0,071	0,067	0,026	0,030	0,046	0,023

Table 7 - continued

Sample	06LD6	06LI16	06LI15	06LI8	06LI7	06LI13	06LI6	06LI10b	06LI10a	06LI5b	06LI5a	06LI4	06LI9	06LI11	06LI3	06LI2	06LI1
	harz	harz	harz	harz	harz	harz	harz	harz	harz	harz	harz	harz	lherz	lherz	lherz	lherz	lherz
dist. from c	>15m	15m	15m	2,5m	2m	1,9m	1,8m	1,3m	1m	1,5m	1,3m	30cm	30cm	70cm	1m	1,3m	1,5m
Li	8,82	2,16	4,75	4,65	5.20	5.21	34,3	1,04	6,10	2,52	2,60	1,59	2,00	0,520	0,890	0,653	1,99
Al	11045	14976	11026	18928	16312	15603	19187	21631	16102	22623	23177	27101	25992	31109	27457	29116	36378
Si	250076	243609	226829	258075	265013	249039	260484	305504	264702	267013	275531	263315	266457	251858	267915	257280	250656
Ca42	143787	151520	150892	149828	150296	150025	149198	150416	149684	149341	149234	149377	149726	150410	150056	149989	150299
Ca43	150087	150087	150087	21	21	150087	150087	150087	150087	150087	150087	150087	21	150087	21	21	21
Sc	68,9	71,5	58,4	111,3	104,7	112,6	109,8	150,1	115,3	106,1	120,3	85,9	98,0	94,8	80,8	81,0	60,1
Ti	112,6	454,6	126,9	615,3	397,6	403,2	760,0	812,9	403,3	1060,2	1224,6	2300,3	2340,6	3894,7	3131,4	3360,2	4102,9
V	198,0	231,5	180,2	286,2	290,7	287,1	296,9	391,6	302,7	319,2	349,2	295,8	320,1	309,3	321,9	306,8	302,9
Cr	6388,2	8015,8	5911,2	10766,5	10640,1	9914,2	10337,0	11348,7	10716,0	11896,7	11696,2	10756,6	10277,4	6917,6	9884,6	8224,4	3292,4
Co	20,8	17,5	18,7	15,8	17,9	17,1	18,7	28,9	18,4	18,4	19,9	16,2	17,2	14,6	18,2	15,7	18,1
Ni	313,6	266,5	296,9	245,9	262,7	257,0	252,8	484,7	272,2	292,6	292,8	242,5	263,7	241,2	253,5	262,1	334,5
Ga69	1,10	1,75	1,09	3,06	2,16	1,90	2,39	2,47	2,07	2,80	2,74	3,87	3,68	3,92	4,00	3,48	4,24
Ga71	1,17	1,79	1,11	3,15	2,23	2,00	2,43	2,67	2,09	2,96	2,88	4,09	3,87	4,13	4,13	3,53	4,37
Rb	-	-	-	-	-	-	-	0,045	-	-	-	-	0,026	-	0,024	-	-
Sr86	16,3	180,8	14,4	126,5	77,3	71,5	126,8	174,4	62,7	165,2	144,1	128,8	112,2	78,4	104,1	80,1	54,6
Sr88	16,8	181,5	14,6	127,4	77,9	72,4	132,3	174,8	62,4	168,2	144,6	128,6	113,3	79,5	105,6	81,7	55,2
Y	0,918	4,90	0,936	9,877	4,01	3,92	6,72	6,93	4,04	7,85	8,45	16,5	15,1	23,5	14,9	17,9	21,4
Zr	0,713	16,1	1,177	32,1	14,6	13,7	30,0	61,6	14,5	41,8	35,3	54,2	49,6	114,2	43,6	45,2	27,4
Nb	0,073	0,350	0,091	0,226	1,63	1,43	1,99	1,90	1,52	1,32	1,69	0,539	0,363	0,188	0,363	0,396	0,117
Cs	-	-	-	-	-	-	-	-	-	-	-	-	-	-	-	-	0,008
Ba	0,147	0,038	0,046	0,071	0,090	0,055	0,135	0,137	-	0,068	0,054	0,066	-	-	0,249	0,088	0,161
La	0,112	2,92	0,228	3,03	4,66	4,39	7,18	10,8	3,73	8,66	8,23	3,81	2,97	2,58	2,29	1,37	0,561
Ce	0,326	9,98	0,522	10,2	6,98	7,03	14,6	27,2	5,73	22,7	19,1	13,9	11,0	11,3	8,94	4,79	3,19
Pr	0,057	1,54	0,066	1,68	0,633	0,608	1,60	3,31	0,508	2,66	2,09	2,36	1,84	2,22	1,53	0,929	0,730
Nd	0,254	6,97	0,286	7,97	2,51	2,17	6,30	11,9	2,03	8,94	6,81	11,1	8,87	12,2	7,61	5,34	4,68
Sm	0,062	1,63	0,077	2,06	0,646	0,544	1,51	1,88	0,625	1,46	1,24	2,92	2,45	3,88	2,25	2,09	1,97
Eu	0,025	0,594	0,031	0,768	0,257	0,215	0,481	0,621	0,220	0,516	0,466	1,06	0,930	1,37	0,950	0,855	0,887
Gd	0,058	1,39	0,080	1,91	0,725	0,589	1,36	1,46	0,644	1,29	1,21	2,91	2,49	4,15	2,49	2,75	2,85
Tb	0,015	0,184	0,016	0,287	0,111	0,094	0,206	0,189	0,102	0,196	0,202	0,471	0,407	0,687	0,417	0,478	0,532
Dy	0,107	1,05	0,128	1,84	0,697	0,669	1,28	1,30	0,683	1,34	1,42	3,00	2,69	4,54	2,79	3,29	3,92
Ho	0,029	0,193	0,035	0,378	0,147	0,152	0,260	0,250	0,148	0,304	0,318	0,636	0,576	0,939	0,581	0,701	0,850
Er	0,142	0,478	0,138	0,993	0,455	0,451	0,700	0,742	0,449	0,876	0,963	1,73	1,65	2,55	1,60	1,92	2,40
Tm	0,028	0,065	0,028	0,149	0,069	0,071	0,106	0,111	0,075	0,135	0,149	0,247	0,236	0,368	0,225	0,266	0,340
Yb	0,260	0,452	0,256	1,03	0,540	0,551	0,733	0,843	0,540	0,966	1,05	1,69	1,59	2,46	1,57	1,72	2,26
Lu	0,043	0,068	0,043	0,147	0,086	0,086	0,112	0,128	0,081	0,144	0,160	0,240	0,229	0,340	0,216	0,238	0,315
Hf	0,013	0,112	0,030	0,367	0,318	0,280	0,626	1,17	0,283	0,601	0,566	1,30	1,23	3,50	1,34	1,49	0,951
Ta	0,030	0,129	0,010	0,050	0,396	0,382	0,564	0,824	0,372	0,837	0,782	0,114	0,083	0,146	0,049	0,029	0,007
Pb	0,103	0,097	0,098	0,360	0,202	0,240	0,555	0,464	0,206	0,370	0,207	0,119	0,140	0,158	0,152	0,211	0,104
Th	0,019	0,097	0,007	0,075	0,238	0,187	0,428	0,317	0,184	0,253	0,348	0,183	0,135	0,080	0,110	0,135	0,037
U	0,152	0,041	0,007	0,034	0,066	0,054	0,109	0,097	0,057	0,089	0,102	0,072	0,053	0,039	0,049	0,053	0,021

Table 7 -continued

Sample	06LI14	06LI12	06LI17	06LF4	06LF27	06LF3L	06LF25	06LF26L	06LF26W	06LF9	06LF23	06LF11	06LF15	06LF16	06LF3W	06LF8	06LF17	06LF20
	lherz	lherz	lherz	harz	harz	lherz	lherz	lherz	webst	lherz	lherz	lherz	lherz	lherz	webst	webst	webst	webst
dist. from c	1,8	2m	>15m	3m	4m	4m	20m	30m	30m	50m	70m	80m	80m	80m	10m	30m	100m	100m
Li	0,87	1,10	1,12	2,45	2,80	1,43	1,24	1,25	1,69	1,04	2,32	0,81	1,01	1,70	1,59	2,76	2,76	4,18
Al	31868	36236	30332	21199	19696	35890	34373	33479	35569	38799	40778	34709	32244	33178	35274	34185	35475	37724
Si	236339	255182	250149	260273	245177	253847	253478	256857	247809	251719	251641	241748	249164	251381	253422	258813	245761	252842
Ca42	150921	149986	150300	141740	143913	142731	143231	144178	141680	144842	145323	144492	151291	151236	143241	143170	143657	144142
Ca43	150087	150087	150087	150087	150087	150087	150087	150087	150087	150087	150087	150087	21	21	150087	150087	150087	150087
Sc	63,4	62,9	58,8	71,2	75,7	59,5	60,9	70,4	58,7	60,4	60,4	62,9	59,1	56,2	58,5	57,3	58,5	70,1
Ti	4032,8	4416,0	3332,3	1458,4	1920,0	4120,3	3648,3	3267,1	3237,7	3508,3	3422,9	3805,0	2863,3	3196,1	3600,7	3913,7	2939,4	3023,2
V	298,8	284,2	282,0	266,0	246,7	286,1	286,0	288,6	295,8	266,8	300,9	266,3	270,1	266,0	284,9	278,5	260,0	270,9
Cr	4463,2	5686,9	4836,7	7985,3	7717,3	4095,7	5122,6	6161,1	2591,2	4803,4	3289,0	4358,9	5699,7	5630,5	3983,3	4368,3	4288,9	2265,9
Co	15,6	17,0	16,8	19,4	16,2	16,2	15,7	17,3	15,2	16,4	19,7	15,3	18,0	15,6	15,4	17,5	14,9	16,0
Ni	245,8	258,8	263,9	290,6	287,9	257,8	244,5	244,4	279,3	255,8	317,0	229,2	275,0	259,0	300,7	304,9	247,9	264,7
Ga69	3,72	4,20	3,43	2,28	1,98	4,01	3,73	3,67	3,97	4,12	4,76	3,50	3,62	3,48	4,32	4,22	3,59	3,63
Ga71	3,93	4,22	3,51	2,36	1,93	4,20	3,88	3,67	4,10	4,26	4,94	3,51	3,71	3,55	4,28	4,38	3,62	3,73
Rb	-	-	0,028	-	-	-	0,031	-	0,033	-	0,057	-	-	-	-	0,048	0,276	0,072
Sr86	70,3	49,7	52,3	49,0	46,4	67,9	63,7	66,4	99,9	89,8	61,9	66,0	64,6	101,5	68,2	43,3	80,9	73,8
Sr88	70,8	50,1	52,9	49,8	47,6	69,4	64,4	67,1	101,3	92,2	63,1	68,7	63,9	101,3	69,0	43,6	82,0	75,1
Y	19,5	22,6	16,9	11,1	14,0	20,9	18,9	18,8	19,2	21,0	23,4	21,4	16,2	17,4	20,7	22,3	15,0	16,4
Zr	28,9	42,2	28,8	20,8	24,6	33,8	31,8	33,6	24,8	39,7	28,0	35,5	25,6	29,8	36,3	28,6	21,2	20,5
Nb	0,457	0,110	0,078	0,157	0,348	0,082	0,193	0,233	0,868	0,308	0,065	0,093	0,117	0,498	0,103	0,074	0,071	0,058
Cs	-	-	-	-	-	-	0,006	-	-	-	0,025	-	-	0,015	-	0,011	0,027	0,015
Ba	-	-	0,051	-	0,040	-	-	-	0,123	0,032	0,201	-	-	0,315	-	0,262	1,050	0,328
La	1,75	0,460	0,847	0,522	0,734	0,931	0,653	0,961	4,94	3,22	0,972	0,825	0,736	1,65	0,896	0,508	0,946	0,798
Ce	5,89	2,67	3,79	2,20	1,87	4,06	3,09	3,59	8,44	10,05	3,90	3,74	3,20	5,75	4,18	2,50	3,78	3,35
Pr	0,927	0,674	0,732	0,465	0,407	0,842	0,667	0,676	0,961	1,63	0,751	0,782	0,648	0,976	0,866	0,525	0,728	0,635
Nd	5,16	4,61	3,21	2,80	3,04	4,84	4,13	3,97	4,22	7,62	4,09	4,56	3,77	5,03	5,10	3,14	4,11	3,65
Sm	2,03	2,09	1,65	1,16	1,52	1,91	1,77	1,50	1,46	2,25	1,61	1,83	1,52	1,76	2,05	1,65	1,48	1,46
Eu	0,934	0,875	0,734	0,497	0,643	0,847	0,779	0,658	0,678	0,864	0,727	0,801	0,659	0,772	0,863	0,757	0,666	0,685
Gd	2,60	3,09	2,25	1,46	2,12	2,70	2,47	2,12	2,16	2,78	2,50	2,74	2,11	2,33	2,89	2,57	1,98	2,17
Tb	0,519	0,563	0,411	0,275	0,390	0,493	0,471	0,400	0,427	0,503	0,502	0,510	0,400	0,428	0,515	0,526	0,366	0,402
Dy	3,54	4,050	3,055	1,972	2,659	3,627	3,330	3,090	3,227	3,633	3,930	3,683	2,875	3,123	3,710	3,960	2,607	2,997
Ho	0,779	0,879	0,662	0,430	0,564	0,804	0,743	0,715	0,756	0,817	0,898	0,815	0,649	0,683	0,807	0,888	0,579	0,653
Er	2,18	2,43	1,87	1,22	1,53	2,28	2,11	2,05	2,22	2,30	2,68	2,29	1,78	1,92	2,29	2,47	1,62	1,81
Tm	0,317	0,339	0,272	0,175	0,201	0,323	0,301	0,321	0,321	0,333	0,388	0,334	0,259	0,269	0,320	0,355	0,239	0,265
Yb	2,31	2,32	1,87	1,16	1,21	2,22	2,07	2,20	2,23	2,17	2,64	2,18	1,76	1,84	2,19	2,34	1,62	1,80
Lu	0,317	0,329	0,265	0,161	0,160	0,310	0,292	0,307	0,319	0,314	0,369	0,319	0,245	0,257	0,313	0,317	0,234	0,238
Hf	0,961	1,41	0,904	0,432	1,00	1,07	1,03	1,06	0,630	1,04	0,881	1,09	0,797	0,929	1,22	1,02	0,648	0,660
Ta	0,053	-	0,011	0,018	0,026	0,014	0,005	0,028	0,034	0,048	0,012	0,009	0,014	0,028	0,018	0,009	0,015	0,010
Pb	0,117	0,155	0,201	0,065	0,169	0,122	0,168	0,077	0,219	0,271	0,099	0,101	0,134	0,230	0,184	0,128	0,212	0,090
Th	0,068	0,011	0,011	0,008	0,029	0,013	0,039	0,029	0,775	0,331	0,014	0,007	0,020	0,069	0,017	0,008	0,013	0,010
U	0,036	0,008	0,006	0,005	0,014	0,006	0,013	0,014	0,092	0,059	0,004	0,006	0,007	0,033	0,179	0,049	0,012	0,003

Table 7: REE clinopyroxenes concentrations (ppm). At least 5 clinopyroxenes have been measured in every thin section. The table presents the average of REE concentrations in every thin section.

Table 8 - REE clinopyroxenes concentrations normalized to chondrites

Sample	05ld1	05ld4	05la2	05la1	05la16	05la9	05la12	05la3	05la4	05la5	05la6	05la8	05la15	05l3	05le1	05le2	05le3
	harz	harz	harz	harz	harz	harz	harz	harz	harz	lherz	lherz	lherz	lherz	lherz	lherz	lherz	lherz
dist. from contact	>15m	>15m	4.5m	3.5m	1m	1m	10cm	10cm	5cm	1.5m	3m	5m	5m	150m	150m	150m	150m
La	3,52	1,62	1,03	1,09	13,34	2,07	4,18	1,70	2,49	1,78	4,73	3,19	3,84	1,93	1,77	2,46	2,49
Ce	3,26	1,56	1,27	1,52	11,26	2,37	4,21	2,43	3,51	3,05	5,93	4,49	5,04	3,02	2,86	3,48	3,67
Pr	2,89	1,78	1,69	2,08	10,32	2,21	4,36	3,36	4,69	4,32	7,08	5,48	6,33	4,31	4,41	4,74	4,67
Nd	2,43	1,78	1,97	2,56	8,93	1,57	4,92	4,20	5,58	5,34	7,72	6,22	7,05	5,33	5,58	5,47	5,53
Sm	1,79	1,53	2,23	3,89	6,26	0,85	4,93	4,91	5,94	7,34	8,33	7,58	7,97	7,01	7,63	6,96	7,10
Eu	1,64	1,19	2,46	4,41	4,97	0,81	5,28	5,02	6,80	8,33	8,93	8,42	9,02	7,66	8,37	7,86	8,04
Gd	1,21	1,13	2,26	4,92	5,21	0,69	5,12	4,54	6,03	8,59	9,39	8,73	8,64	8,29	8,67	8,26	8,07
Tb	0,89	0,75	2,28	5,18	4,52	0,69	4,35	4,00	5,33	8,57	8,60	8,23	8,39	8,02	8,25	7,96	7,76
Dy	0,92	0,79	2,95	5,84	4,66	0,86	4,75	4,17	5,75	9,74	9,99	9,44	9,59	8,24	9,58	9,40	9,01
Ho	0,88	0,72	2,93	5,54	4,40	1,07	4,51	3,88	5,33	9,37	9,62	9,20	9,34	9,08	9,19	8,83	8,54
Er	1,06	0,88	3,58	5,80	4,25	1,39	4,46	3,71	5,18	9,50	9,45	9,27	9,21	9,31	9,13	8,74	9,07
Tm	1,55	1,14	4,03	5,60	4,24	1,59	4,75	3,53	5,22	9,60	9,96	9,56	9,37	9,29	9,41	9,17	9,00
Yb	1,73	1,24	3,95	4,97	4,03	1,88	4,38	3,53	4,89	9,26	9,46	8,97	9,10	9,09	9,22	8,56	8,83
Lu	1,82	1,30	3,87	4,60	3,64	1,95	4,18	3,15	4,59	8,59	8,85	8,53	8,45	8,39	7,89	8,10	7,73

Sample	04LH12	04LH11	04LH09	04LH08	04LH07	04LH04	06LD6	06LI16	06LI15	06LI8	06LI7	06LI13	06LI6	06LI10B	06LI10A	06LI5B	06LI5A
	harz	harz	lherz	lherz	lherz	lherz	harz	harz	harz	harz	harz	harz	harz	harz	harz	harz	harz
dist. from contact	1.5m	1m	10cm	10cm	80cm	1.5m	>15m	15m	15m	2.5m	2m	1.9m	1.8m	1.3m	1m	1.5m	1.3m
La	16,07	19,04	7,03	4,34	3,96	1,78	0,30	7,96	0,51	8,67	12,68	11,96	19,56	29,45	10,17	21,31	22,42
Ce	10,62	13,97	8,48	5,84	3,98	2,82	0,34	10,42	0,53	11,00	7,29	7,34	15,22	28,47	5,98	22,05	19,97
Pr	8,25	10,31	10,13	8,29	5,59	4,91	0,42	11,23	0,38	12,65	4,63	4,44	11,65	24,14	3,71	18,15	15,25
Nd	7,01	7,76	11,03	10,18	7,26	7,05	0,36	9,80	0,36	11,50	3,53	3,04	8,86	16,68	2,86	11,91	9,58
Sm	5,57	5,65	11,27	11,73	9,39	9,89	0,27	7,04	0,25	9,16	2,80	2,35	6,53	8,16	2,70	6,10	5,38
Eu	4,67	5,25	11,60	11,91	9,79	10,47	0,29	6,82	0,27	8,92	2,95	2,48	5,53	7,14	2,53	5,70	5,35
Gd	4,17	4,88	9,80	11,42	10,45	11,96	0,19	4,53	0,21	6,31	2,37	1,92	4,44	4,78	2,10	4,10	3,97
Tb	3,28	4,22	8,36	9,64	9,53	11,19	0,26	3,17	0,19	5,01	1,92	1,61	3,54	3,27	1,76	3,33	3,49
Dy	3,29	4,56	8,42	9,85	10,47	12,48	0,28	2,77	0,28	4,80	1,83	1,76	3,36	3,42	1,79	3,52	3,74
Ho	2,99	4,33	7,56	8,56	9,69	11,75	0,34	2,27	0,32	4,47	1,72	1,79	3,06	2,94	1,74	3,63	3,74
Er	2,97	4,45	6,99	7,99	9,33	11,58	0,57	1,92	0,44	3,93	1,83	1,81	2,81	2,98	1,80	3,58	3,87
Tm	-	-	-	-	-	-	0,79	1,82	0,60	4,16	1,94	2,00	2,97	3,12	2,10	3,82	4,18
Yb	3,20	4,71	6,61	7,09	8,62	10,89	1,05	1,82	0,84	4,22	2,18	2,22	2,95	3,40	2,18	3,94	4,25
Lu	3,11	4,61	6,22	6,47	7,86	9,93	1,13	1,80	0,88	3,98	2,27	2,25	2,95	3,36	2,11	3,86	4,20

Sample	06LI4	06LI9	06LI11	06LI3	06LI2	06LI1	06LI14	06LI12	06LI17	06LF4	06LF27	06LF3L	06LF25	06LF26L	06LF26W	06LF9	06LF23
	harz	lherz	lherz	lherz	lherz	lherz	lherz	lherz	lherz	harz	harz	lherz	lherz	lherz	webst	lherz	lherz
dist. from contact	30cm	30cm	70cm	1m	1,3m	1,5m	1,8	2m	>15m	3m	4m	4m	20m	30m	30m	50m	70m
La	10,37	5,80	7,03	6,25	3,74	1,49	3,70	1,25	2,31	1,42	2,00	2,54	1,78	2,62	13,47	8,78	2,65
Ce	14,55	7,98	11,77	9,34	5,01	3,26	4,77	2,79	3,96	2,30	1,96	4,24	3,23	3,75	8,82	10,50	4,07
Pr	17,23	9,74	16,22	11,15	6,78	5,24	5,20	4,92	5,34	3,40	2,97	6,15	4,87	4,94	7,02	11,87	5,48
Nd	15,63	9,44	17,15	10,70	7,51	6,51	5,54	6,48	5,93	3,94	4,28	6,81	5,81	5,59	5,93	10,72	5,75
Sm	12,64	9,61	16,80	9,71	9,06	8,49	6,67	9,05	7,14	5,02	6,60	8,27	7,65	6,48	6,30	9,74	6,98
Eu	12,22	9,80	15,70	10,91	9,83	10,08	8,19	10,06	8,44	5,71	7,39	9,73	8,96	7,56	7,79	9,93	8,36
Gd	9,48	8,47	13,57	8,15	8,98	9,25	6,33	10,09	7,37	4,76	6,91	8,82	8,07	6,92	7,06	9,10	8,18
Tb	8,12	7,61	11,84	7,18	8,25	9,04	6,70	9,70	7,08	4,74	6,72	8,50	8,11	6,90	7,35	8,67	8,65
Dy	7,88	7,81	11,90	7,33	8,64	10,23	6,92	10,63	8,01	5,17	6,98	9,52	8,74	8,11	8,47	9,53	10,32
Ho	7,48	7,52	11,03	6,83	8,23	9,89	6,82	10,33	7,78	5,05	6,63	9,45	8,73	8,40	8,88	9,60	10,55
Er	6,96	7,16	10,23	6,41	7,70	9,45	6,59	9,77	7,50	4,89	6,12	9,16	8,46	8,25	8,90	9,24	10,79
Tm	6,93	7,28	10,35	6,33	7,48	9,38	6,68	9,52	7,63	4,92	5,64	9,08	8,44	9,02	9,03	9,34	10,90
Yb	6,82	6,80	9,91	6,31	6,95	9,00	7,11	9,35	7,55	4,66	4,89	8,94	8,36	8,86	8,99	8,75	10,66
Lu	6,30	6,27	8,93	5,67	6,26	8,11	6,33	8,63	6,96	4,22	4,19	8,12	7,67	8,05	8,38	8,25	9,68

Table 8 - continued

Sample	06LF11	06LF15	06LF16	06LF3W	06LF8	06LF17	06LF20
	lherz	lherz	lherz	websT	websT	websT	websT
dist. from contact	80m	80m	80m	10m	30m	100m	100m
La	2,25	2,00	4,49	2,44	1,38	2,58	2,17
Ce	3,90	3,35	6,01	4,37	2,61	3,95	3,50
Pr	5,71	4,73	7,13	6,32	3,83	5,31	4,64
Nd	6,41	5,30	7,07	7,17	4,43	5,77	5,13
Sm	7,90	6,60	7,61	8,89	7,16	6,39	6,32
Eu	9,21	7,57	8,87	9,92	8,70	7,65	7,87
Gd	8,95	6,90	7,64	9,45	8,41	6,47	7,11
Tb	8,79	6,90	7,39	8,88	9,06	6,31	6,94
Dy	9,66	7,55	8,20	9,74	10,39	6,84	7,86
Ho	9,58	7,62	8,03	9,48	10,44	6,81	7,67
Er	9,19	7,13	7,73	9,21	9,91	6,50	7,25
Tm	9,38	7,26	7,55	8,98	9,96	6,70	7,46
Yb	8,81	7,08	7,43	8,84	9,41	6,52	7,28
Lu	8,38	6,42	6,74	8,23	8,32	6,15	6,23

Table 8: REE clinopyroxenes concentrations normalized to chondrites after Sun and McDonough (1989). At least 5 clinopyroxenes have been measured in every thin section. The table presents the average of REE concentrations normalized to chondrites in every thin section

Figure 3 - REE clinopyroxenes concentrations normalized to chondrites

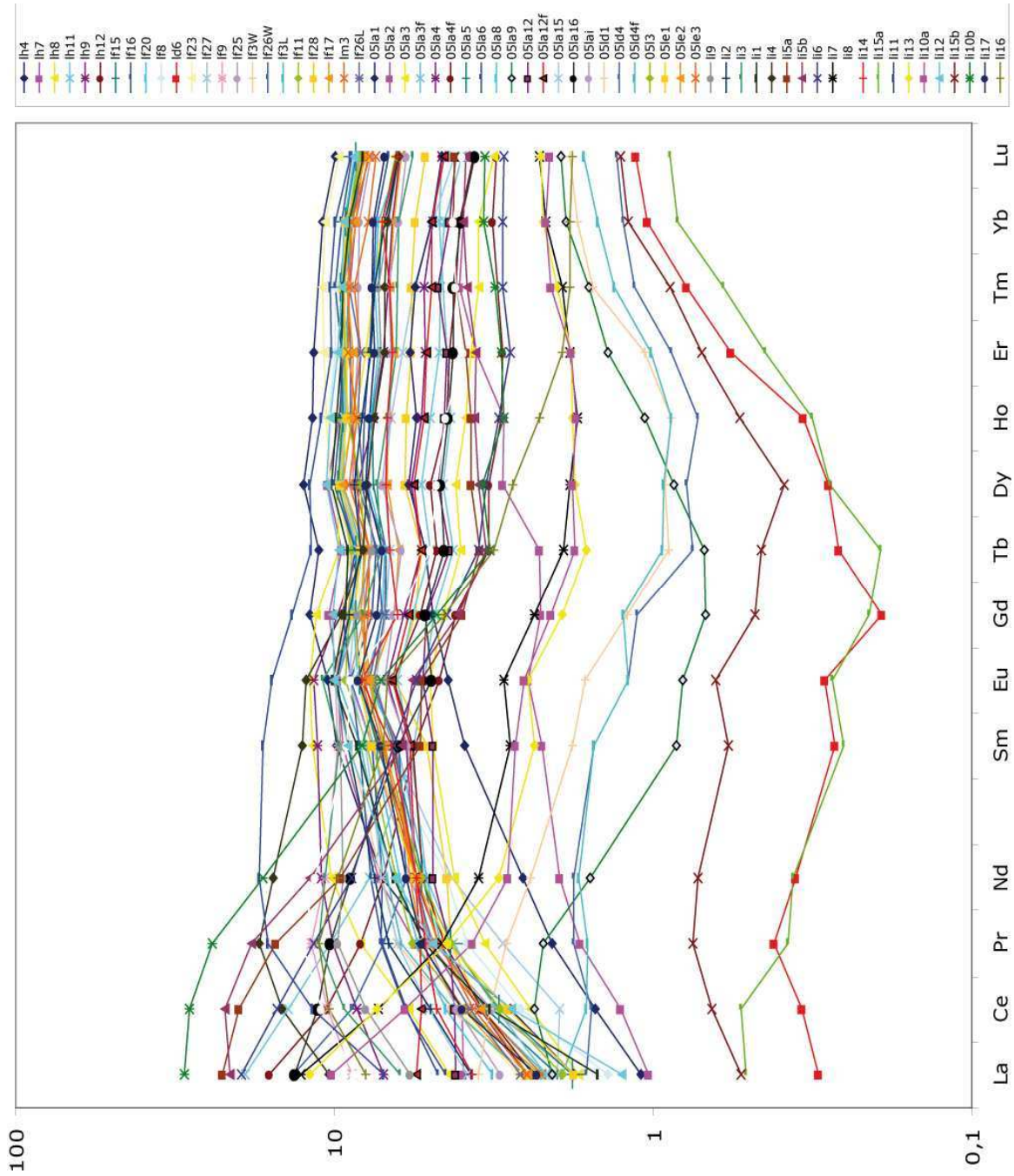

Table 9 - Hf, Nd and Sr isotopic ratios of the Lherz peridotites

CPX	dist.	Rb	Sr	$^{87}Rb/^{86}Sr$	$^{87}Sr/^{86}Sr$		Sm	Nd	$^{147}Sm/^{144}Nd$	$^{143}Nd/^{144}Nd$		Lu	Hf	$^{176}Lu/^{177}Hf$	$^{176}Hf/^{177}Hf$	
Spinel lherzolites																
06LI1	1,5	0,0713	55,22	0,0037	0,702809	± *7,6E-06*	1,973	4,675	0,2526	0,51278	± *1,1E-05*	0,3153	0,951	0,0471	0,283029	± *2,6E-06*
06LI2	2	0,0297	81,72	0,0011	0,703176	± *6,0E-06*	2,094	5,340	0,2348	0,512796	± *8,8E-06*	0,2383	1,491	0,0227	0,282996	± *3,2E-06*
06LI3	1	0,0482	105,60	0,0013	0,70297	± *1,2E-05*	2,245	7,605	0,1768	0,512854	± *6,3E-06*	0,2160	1,337	0,0229	0,282996	± *4,2E-06*
06LI9	0,3	0,0260	113,31	0,0007	0,703133	± *6,7E-06*	2,451	8,873	0,1654	0,512802	± *7,0E-06*	0,2287	1,230	0,0264	0,283019	± *2,1E-06*
06LI112	2	0,0966	50,11	0,0056	0,70280	± *1,8E-05*	2,091	4,605	0,2719	0,512822	± *5,7E-06*	0,3288	1,410	0,0331	0,282926	± *5,2E-06*
06LI117	50	0,0344	62,85	0,0016	0,702562	± *9,0E-06*	1,649	4,213	0,2344	0,513087	± *6,0E-06*	0,2653	0,904	0,0417	0,283289	± *7,8E-06*
Harzburgites																
06LI4	0,3	0,0286	128,63	0,0006	0,702981	± *2,5E-06*	2,920	11,115	0,1573	0,512847	± *7,2E-06*	0,2400	1,296	0,0263	0,283159	± *6,4E-06*
06LI5a	1,3	0,0207	144,63	0,0004	0,702950	± *3,2E-06*	1,243	6,810	0,1093	0,512706	± *6,6E-06*	0,1599	0,566	0,0401	0,282832	± *7,7E-06*
06LI5b	1,5	0,0171	168,24	0,0003	0,702901	± *3,0E-06*	1,457	8,943	0,0976	0,512724	± *2,9E-06*	0,1436	0,601	0,0339	0,283492	± *5,6E-06*
06LI6	1,8	0,0184	132,29	0,0004	0,703276	± *3,0E-06*	1,508	6,298	0,1434	0,512551	± *2,4E-06*	0,1122	0,626	0,0254	0,283051	± *4,3E-06*
06LI7	2	0,0236	77,92	0,0009	0,702875	± *3,0E-06*	0,646	2,511	0,1540	0,512818	± *3,1E-06*	0,0864	0,318	0,0386	0,284067	± *8,7E-06*
06LI8	2,5	0,0265	127,40	0,0006	0,703024	± *2,8E-06*	2,064	7,973	0,1550	0,512788	± *2,9E-06*	0,1469	0,367	0,0569	0,283434	± *3,3E-06*
06LI10a	1	0,0160	62,36	0,0007	0,702923	± *3,9E-06*	0,625	2,034	0,1839	0,512665	± *2,5E-06*	0,0805	0,283	0,0405	0,283323	± *3,6E-06*
06LI10b	1,3	0,0396	174,77	0,0007	0,702963	± *5,2E-06*	1,884	11,863	0,0951	0,512715	± *2,7E-06*	0,1280	1,172	0,0155	0,283108	± *3,4E-06*
06LI15	15	0,0330	14,63	0,0065	0,703046	± *2,6E-06*	0,134	0,516	0,2805	0,512643	± *8,7E-06*	0,0484	0,080	0,0862	0,28883	± *6,3E-05*
06LI16	15	0,0585	181,54	0,0009	0,702944	± *3,0E-06*	1,627	6,965	0,1398	0,512763	± *3,5E-06*	0,0683	0,112	0,0866	0,28546	± *1,6E-05*

WR	dist.	Rb	Sr	$^{87}Rb/^{86}Sr$	$^{87}Sr/^{86}Sr$		Sm	Nd	$^{147}Sm/^{144}Nd$	$^{143}Nd/^{144}Nd$		Lu	Hf	$^{176}Lu/^{177}Hf$	$^{176}Hf/^{177}Hf$	
Spinel lherzolites																
06LI1	1,5	0,13	12,14	0,0305	0,70355	± *1,0E-05*	0,45	1,02	0,2666	0,513040	± *6,4E-06*	0,09	0,28	0,0448	0,28307	± *1,3E-05*
06LI2	2	0,03	10,99	0,0085	0,703610	± *3,0E-06*	0,35	0,87	0,2426	0,512907	± *7,4E-06*	0,05	0,22	0,0312	0,28295	± *1,4E-05*
06LI3	1					±					±					±
06LI9	0,3	0,02	2,59	0,0273	0,704837	± *2,9E-06*	0,07	0,23	0,18	0,51283	± *2,0E-05*	0,01	0,05	0,0351	0,28304	± *2,5E-05*
06LI12	2	0,06	6,81	0,0265	0,704055	± *2,3E-06*	0,23	0,48	0,2874	0,51294	± *1,4E-05*					±
06LI17	50	0,06	7,79	0,0209	0,702768	± *3,5E-06*	0,23	0,55	0,2525	0,5129	± *1,5E-04*					±
Harzburgites																
06LI4	0,3	0,02	2,27	0,0192	0,70403	± *4,1E-05*					±	0,01	0,03	0,0428	0,28295	± *3,8E-05*
06LI5a	1,3	0,02	2,42	0,0253	0,70515	± *1,4E-05*					±					±
06LI5b	1,5					±					±					±
06LI6	1,8	0,04	2,25	0,056	0,704973	± *9,0E-06*	0,03	0,12	0,1395	0,5126	± *1,0E-04*					±
06LI7	2					±					±					±
06LI8	2,5					±					±					±
06LI10a	1	0,05	2,20	0,0691	0,704825	± *8,9E-06*					±					±
06LI15	15					±					±					±
06LI16	15	0,01	4,43	0,0092	0,703638	± *6,4E-06*					±					±

Summary of chemical techniques and methods

Preparation of Clinopyroxenes separates

We sampled 16 peridotites in the Lherz massif (Pyrenees, France) from where clinopyroxenes were separated. The rocks have been cut using diamond saw. Once the rims had been removed, the interiors were crushed in a steel crusher, carefully cleaned after each sample to avoid cross-contamination. Aliquots of the crushed samples were ground in agate mortars to produce whole-rocks powders. Another aliquot was sieved. Only fractions of < 200µm, < 250µm and < 350µm were used later on. These fractions have been washed with pure water to remove dust and dried in an oven. Then the minerals were passed through a Frantz magnetic separator, which allows the separation of clinopyroxene from orthopyroxene, olivine and spinel (from the less to the most magnetic mineral). The resulting clinopyroxene-enriched fraction was still mixed with some orthopyroxenes and clinopyroxene-orthopyroxene aggregates. Pure clinopyroxenes grains, devoid of inclusion and joint grains were carefully handpicked under a binocular microscope. The final 16 clinopyroxenes fractions have been leached in diluted HCl prior to dissolution to remove possible contamination from grain surfaces and cracks. The individual weights of these fractions range between 102 to 222mg.

Hf, Nd, Sr chemical separation

*Weight the clinopyroxene separates in clean beakers, or weight between 150 to 200mg of the sample, if whole-rock powder. Add diluted HNO_3 to the powder to avoid static electricity. Put on the hot plate, lids open.

* Sample dissolution
All acids are Teflon distilled except Hydrofluoric acid where the cleanest grade is purchased.

- Samples were then initially dissolved in 2ml of 27N HF (merck, suprapur grade) and 2ml of HNO_3 (Ajax) . The beakers were closed and placed on the hotplate at150°C overnight. The samples were then dried down and the above step was repeated.
- When dry, add 10-15 drops of $HCLO_4$ (merck suprapur grade) to the samples. The $HCLO_4$ was then dried down at 150°C for a few hours and then the temperature was slowly increased to 200°C. Once all of the $HCLO_4$ evaporated, 4ml of 6N HCl (merck) and 200µl of H_2O_2 was added and refluxed for 2 hours at 150°C. This step reduces the Cr^{6+} to Cr^{3+}. The Cr^{3+} passes through independently of Hf whereas Cr^{6+} does not. Also, Cr^{6+} sticks to the anion exchange resin and causes a large amount of the Hf to be lost as it damages the resin and competes with complexation sites[52].

The samples are then dried down at 150°C and then one more dissolution in 6N HCl is carried out, the samples are then dried and 1.4ml of 2.5N HCl / 0.1N HF is added to the samples. Samples are transferred to 2ml microcentrifuge tubes and centrifuged to remove and precipitate prior to column separation.

*Columns (1) – Collect Hf, Sr, Nd

*Hf collection – 5.4ml.

- Samples were loaded into Teflon columns containing Biorad® AG50W-X8 (200-400mesh) cation exchange resin with a bed height of 18cm and an I.D of 6.4mm.
- Once the sample eluted, 1ml of 2.5N HCl/ 0.1N HF was added. This step was carried out a total of 4 times.
- The samples were then dried down and prepared for the second Hf separation column as the Hf in this step was eluted with the bulk of the sample matrix.
- Before Sr could be collected, 21.5ml of 2.5N HCl was added, to remove elements such as Rb and Ca.

*Sr collection – 8ml.

- Strontium was then collected by adding 8ml of 2.5N HCl.
Samples were then dried and had a drop of concentrated HNO_3 added to remove any organics from the resin.
- The dried sample was then ready for analysis on the TIMS instrument.
- Before Nd could be collected, 7ml of 6N HCl was added to elute Lu.

*Nd collection –
Nd was then eluted by adding a 6-7ml of 6N HCl.
- Samples are then dried at 150°C and then a drop of concentrated HNO_3 is added to remove organics derived from the resin.

This fraction also contains many other REE such as Ce and Sm which then need to be removed by a subsequent column.

* Cleaning columns (1)

- 15ml of 4N HF.
- Backflush with 25ml MQ water.
- 10ml of 6N HCl.
- 15ml of 2.5NHCl/0.1N HF. To recondition the columns.
- 5ml of 2.5N HCl/0.1N HF before loading next sample.

*Columns (2) – Further purification of the Hf fraction.

- The H_2O_2 and 6NHCl step as described above is repeated to reduce chromium.

- The dried down samples then had 1.4ml of 0.5N HCl/0.5N HF ready for the column.

*Cleaning columns (2)

- Full reservoir of 4N HF.
- Full reservoir of 6N HCl.
- Full reservoir of 0.5N HCl/0.5N HF.
- 4ml 0.5N HCl/0.5N HF before loading.

*Washing columns

- Load the 1.4ml samples Biorad® AG1-X8 (100-200 mesh) anion exchange resin.
- 4cm Biorad plastic poly prep columns are used. 2.7ml of resin (wet) is added.
- Add 1ml of 0.5N HCl/0.5N HF in the column and wait until passed through the column. Repeat 2 times.
- Add 16ml of 0.5N HCl/0.5N HF.

*Hf is then collected by adding 10ml of 6N HCl.

- A few drops of $HCLO_4$ are added to the cut and the samples are put on the hotplate at 170°C until all of the $HCLO_4$ has dried down. This step is repeated 2 times and then 1.4ml 2.5N HCl is added, ready for the 3rd Hf column.

*Column: 3rd Hf separation column.

- Add some drops of H_2O_2 before loading. (Ti indicator).

- Load the 1.4ml samples in Teflon columns (13cm with 6.4mm ID) with 4.2 ml AG50W-X8 cation exchange resin.
- Add 1ml of 2.5N HCl in the column and wait until passed through the column. Repeat 2 times. A total of 5ml of 2.5N HCl (enough to elute all of the Ti) is added before the Hf is collected.

*Hf collection – 12ml of 2.5N HCl/ 0.1N HF.

- Put 12ml of 2.5N HCl/0.1N HF to collect Hf. Dry on the hot plate at 150°C. Samples are then made up into 2% HNO_3 ready for analysis by MC-ICPMS.

*Cleaning columns (3)

- 10ml of 4N HF.
- Backflushing with 25ml MQ water.
- 15ml of 6N HCl.
- 25ml of 2.5N HCl to recondition columns
- 5 ml of 2.5N HCl before loading.

* Nd specific column (2) –This column will remove the Ba, La, Ce, Pr, and Sm from the samples. Method used is adapted from Pin et al.[53]. Glass biorad columns (5cm in length) are used. Approximately 5cm of resin (Eichrom® Ln Spec resin) is added (approx. 300mg). The resin is turned into a slurry with 1N HCl and then added to the column.

*Cleaning columns

- Full reservoir of 1N HCl. Repeat 2 times.
- Full reservoir of 0.25N HCl.

*Loading

-The dried fraction from the first column is redissolved in 0.7ml 0.05M HNO_3 and then loaded onto a column containing Eichrom® Ln Spec resin. The sample is loaded stepwise in 3x 0.2ml + 1x 0.1ml increments.

- Add 3x0.1ml of 0.25N HCl to wash sample onto resin.
- Add 0.75ml of 0.25N HCl (remove Ba)
- Add 0.75ml of 0.25N HCl (remove La)
- Add 1.25ml of 0.25N HCl (remove Ce)
- Add 0.6ml of 0.25N HCl (remove Pr)

*Nd collection

- 3ml of 0.25N HCl. Dry overnight at 120°C. Sample beakers may be wrapped in aluminium foil to prevent static electricity once the sample has been dried down.

References:

[52] Blichert-Toft, J., *Geostandards Newsletter* **25** (1), 41-56 (2001).
[53] Pin, C. and Zalduegui, J. F. S., *Analytica Chimica Acta* **339**, 79-89 (1997).

Résumé

La différenciation du manteau lithosphérique s'est principalement effectuée par fusion partielle et extraction de magmas. Les harzburgites sont généralement considérées comme des résidus de fusion tandis que les lherzolites représentent un manteau originel peu affecté par la fusion. Cependant, certaines péridotites orogéniques montrent des évidences de refertilisation magmatique. Dans ce contexte, ce travail remet en cause la nature primitive des lherzolites de Lherz (Pyrénées), lithotype de la lherzolite.

Les données structurales et géochimiques montrent que ces lherzolites ne représentent pas du manteau préservé mais qu'elles se sont formées par une réaction de refertilisation entre un liquide de type MORB et une lithosphère réfractaire. De plus, les orientations préférentielles de réseau (OPR) des minéraux montrent une forte interdépendance entre la percolation magmatique et la déformation finie observée dans les roches percolées. Les variations d'OPR semblent contrôlées par un équilibre subtil entre fraction de liquide instantanée et taux de déformation local.

Ce travail a également abordé les effets de la percolation magmatique sur la variabilité isotopique des roches mantelliques. Les résultats montrent qu'un fort découplage isotopique peut s'observer dans un front de percolation. Les modèles suggèrent que le découplage des signatures isotopiques se produit pendant la percolation, gouverné par le rapport des concentrations en éléments (magma/matrice), la diffusivité et le processus d'homogénéisation isotopique. Les réactions magma/roche peuvent générer des signatures isotopiques de type intraplaque. Ceci suggère qu'une part des signatures isotopiques des roches ou laves dérivées du manteau pourrait être produite par des processus diffusionnels associés à du transport de magma.

Mots-clés : Massif de Lherz ; refertilisation ; réaction magma/roche ; érosion du manteau lithosphérique ; ségrégation de magmas ; localisation de la déformation ; diffusion ; découplage isotopique ; transport de magmas.

Melt-rock interactions and melt-assisted deformation in the Lherz peridotite, with implications for the structural, chemical and isotopic evolution of the lithospheric mantle

Differentiation of the lithospheric mantle occurred principally through partial melting and extraction of melts. Harzburgites are generally considered as melting residues whereas lherzolites are regarded as pristine mantle weakly affected by melting. However, some orogenic peridotites show evidence of igneous refertilization. In this context, this work re-investigates the nature of the Lherz lherzolites (Pyrenees), type-locality of lherzolites, described as a piece of preserved fertile mantle.

Structural and geochemical data show that these lherzolites are not pristine but formed through a refertilization reaction between MORB-like melts and refractory lithosphere. Moreover, the Lherz peridotites were partly used to infer the composition of the primitive upper mantle and these results may have important implications for the nature of the late veneer.

Additionally, crystal-preferred orientations of minerals (CPO) highlight a strong feedback between melt percolation and finite strain in the percolated rocks. CPO variations are ruled by a subtle balance between instantaneous melt fraction and local strain rate.

This work also investigated the effect of melt percolation on Hf, Nd and Sr isotopes. Isotope systematics in Lherz shows that strong isotopic decoupling may arise in a percolation front. The modelling suggests that decoupled isotopic signatures are generated during porous flow and governed by the melt/matrix elements concentrations, chemical diffusivities or efficiency of isotopic homogenization. Melt-rock interactions can generate "intraplate-like" isotopic signatures. This suggests that a part of isotopic signatures of mantle-related rocks could be generated by diffusional processes associated with melt transport.

Keywords: Lherz massif; refertilization; melt-rock reaction; erosion of lithospheric mantle; melt segregation; strain localization; diffusion; isotopic decoupling; melt transport.

Discipline : Sciences de la Terre
Laboratoire : Géosciences Montpellier (UMR 5243). Place Eugène Bataillon 34095 MONTPELLIER cedex 5. FRANCE